



Energy Systems Research Unit
Aerospace and Mechanical Engineering Department
Faculty of Applied Sciences
University of Liège

Modulation strategies of integrated HVAC systems used in residential buildings for demand-side management at different scales

Dissertation presented in partial fulfillment of the requirements for the degree of
Doctor in Engineering Sciences

by

Emeline Georges

April 2017

Members of the Examination Committee:

Prof. Dr. Ir. V. Lemort, *Supervisor*
(Université de Liège, Belgium)

Prof. Dr. Ir. J.E. Braun
(Purdue University, USA)

Prof. Dr. Ir. L. Helsen
(KU Leuven, Belgium)

Prof. Dr. Ir. P. André
(Université de Liège, Belgium)

Assistant Prof. Dr. Ir. B. Cornélusse
(Université de Liège, Belgium)

Dr. Ir. S. Quoilin
(Université de Liège (Belgium), European Commission)

Dr. Ir. C. Crunelle
(Laborelec, Belgium)

À ma famille et mes proches...

*Tout le monde veut vivre au sommet de la montagne,
sans soupçonner que le vrai bonheur est dans la manière de gravir la pente.*

— Gabriel García Márquez

Acknowledgements

The achievement of a PhD dissertation cannot be reached alone, and I would like to thank all the people who have contributed to make it happen.

I would like to start with acknowledging my advisor, Vincent Lemort, for his guidance, open-mindedness, optimism and trust. I am also very grateful to Professor J. Braun and Professor E. Groll for hosting my stay at Herrick Laboratories (Purdue University) and for the time spent on advising me in my research. This has been a very enriching experience. I would also like to thank the members of the "Smart Grids team" of University of Liège and, in particular, Sébastien Matthieu, Prof. Cornélusse and Prof. Ernst for the great collaborative research work in the course of this project.

I would like to express my deepest gratitude to my family for their unwavering support. A very special acknowledgment goes to my partner, Abhinav, for his encouragement and compassion during all those years, and particularly, for his great support during the very last steps. You all have been my unfailing source of motivation.

It would not have been possible to achieve this work without the amazing and unique atmosphere of the Thermodynamics Laboratory. I would like to thank all my wonderful colleagues for their support and the great times spent together: Sam, Bertrand, Randy, Monsieur Declaye, Rémi, Oli, Ludo, Adriano, Sylvain, Ioannis, Fred, Kévin, Damien, J-F, Thomas, Roberto, Long, Richard, petit Bernard, José, Isabelle and Papa. You have made this lab my second home! I would also like to thank Sylvain for his many inputs on my work.

Many thanks to my friends Thibaut and Vincent – we were all in the same boat and that was our biggest strength!

Finally, I would like to thank F.R.S - FNRS for funding this research work.

Abstract

The integration of renewable energy sources in the electricity production mix has an important impact on the management of the electricity grid, due to their intermittency. In particular, to ensure grid balancing, there is a rising need for flexibility, both on the supply and demand side.

A possible solution to help achieve grid balancing is the smart modulation of the electrical load in a "demand following supply" scheme through demand-side management. In this context, the objective of this work is to assess the amount of flexibility that can be harvested from the management of residential thermostatically-controlled loads and, in particular, through the use of heat pumps and storage. To that end, a modeling and control framework is developed to define efficient and scalable optimal load modulation strategies, in order to unlock the flexibility in different contexts.

The first part of this work focuses on the development of load management schemes at the scale of a building. A first approach investigates the potential of flexible loads to reduce day-ahead procurement costs by shifting load from peak to off-peak periods with different storage options. A second approach proposes a general methodology for optimal load management with distributed renewable energy generation and storage. The third approach defines a flexibility service that consists in upward and downward modulations with a constrained and parametrized rebound effect. Then, the performance of these three methods are compared in an example case-study of load matching with distributed solar production and different storage options.

In the second part of this work, an aggregation method to model large sets of loads is proposed. The resulting models are used in combined optimization problems for the large-scale assessment of the flexibility of domestic heat pumps. On the one hand, the impact of large-scale activation of flexible loads on day-ahead market clearing prices is investigated. On the other hand, the potential of such flexible loads to provide secondary reserve is studied.

Results show promising outcome of residential demand-side flexibility for use in the frame of operational planning and real-time balancing by system operators. Key findings include:

- procurement costs reduction ranging from 1 to 44%, depending on the type of load shifting incentive, storage and house insulation level. However, this entails overconsumption of up to 23%. In terms of cost savings, optimal control-based strategies outperform conventional rule-based strategies by up to 19%.
- surplus electricity production by PV delivered to the grid can be reduced by 10 to 30% without any additional storage through optimal load matching control. Results depend on the geographical

location and size of the PV system. Overconsumption of 3 to 9% is observed but still allows for significant CO₂ reduction. For heating-dominated climates, optimal load management allows for an increase of 30 to 80% in the optimal size of the PV system.

- constraining and mitigating the rebound effect following a direct load activation affects the average achievable modulation potential. Indeed, the potential decreases by up to 61% but yields up to 36% additional costs savings. A rebound effect constrained within one hour and 15 minutes proves to be a good compromise between achievable modulation amplitude and mitigation of deviations from baseline consumption.
- in the frame of secondary reserve, a case-study in the Belgian context reveals that the provision of up to 70% of the current contracted amount of winter upward reserve (140 MW) can be achieved with 40000 heat pump units at 44% of historical costs. The provision of downward reserve is more challenging as it entails substantial overconsumption.

Keywords: Heat pump, storage, flexibility, optimal control, demand-side management, overconsumption, rebound effect, aggregation, electricity markets, power systems

Résumé

En raison de leur production intermittente, l'intégration de sources d'énergies renouvelables dans le parc de production électrique a un impact important sur la gestion du réseau. En particulier, pour assurer l'équilibre du réseau, on observe un besoin croissant de flexibilité, tant du côté de la production que de la demande.

La gestion intelligente de la demande, sous forme de modulation de la charge électrique, constitue une solution possible pour assurer l'équilibre du réseau. Dans ce contexte, l'objectif de ce travail est d'évaluer le degré de flexibilité qui peut être obtenu par la gestion des charges résidentielles et, en particulier, par l'utilisation de pompes à chaleur et systèmes de stockage associés. Une méthode de modélisation et de contrôle des charges est proposée, afin de définir des stratégies optimales de modulation de la demande électrique, et ce dans différents contextes.

La première partie de ce travail se concentre sur le développement de lois de gestion de la charge à l'échelle d'un bâtiment. Une première approche étudie le potentiel des charges flexibles dans le cadre de la réduction des coûts d'approvisionnement journaliers en électricité. Elle se base sur le déplacement de la demande des périodes de pointe aux périodes creuses grâce à différentes options de stockage. La deuxième approche propose une méthode générale de gestion optimale de la demande, ainsi que des systèmes de stockage, en présence de sources de production d'électricité distribuées. La troisième approche définit un service de flexibilité qui consiste en des modulations de puissance à la hausse et à la baisse, avec un effet de rebond restreint et paramétré. Enfin, les performances de ces trois méthodes sont comparées dans un exemple d'autoconsommation de la production solaire décentralisée avec différentes options de stockage thermique.

Dans la seconde partie de ce travail, une méthode d'agrégation des charges est proposée afin de modéliser de grands ensembles de charges. Les modèles qui en découlent sont utilisés dans des problèmes d'optimisation dont l'objectif est d'évaluer la flexibilité à grande échelle des pompes à chaleur domestiques. On étudie d'une part l'impact de l'activation d'un grand nombre de charges flexibles sur les prix du marché de l'électricité et, d'autre part, le potentiel de ces dernières dans le contexte de la réserve secondaire.

Les différents cas d'étude montrent des résultats prometteurs dans le cadre de la gestion opérationnelle du réseau électrique et de son équilibrage en temps réel. Les conclusions principales sont les suivantes :

- une réduction des coûts d'approvisionnement allant de 1% à 44%, selon le type d'incitation au déplacement de charge, de stockage et de niveau d'isolation des maisons. Cela entraîne toutefois

une surconsommation pouvant atteindre jusqu'à 23%. Les stratégies basées sur un contrôle optimal permettent jusqu'à 19% d'économies supplémentaires par rapport aux stratégies de contrôle dites conventionnelles.

- la production d'électricité excédentaire injectée sur le réseau par les panneaux photovoltaïques peut être réduite de 10 à 30% sans aucun stockage supplémentaire grâce à une stratégie optimale d'autoconsommation. Les résultats dépendent cependant de la localisation géographique et de la taille des systèmes photovoltaïques. Une surconsommation de 3 à 9% est observée, mais permet néanmoins une réduction significative des émissions de CO₂. Pour les climats froids, la gestion optimale de la charge permet une augmentation de 30 à 80% de la taille optimale du système de production décentralisé.
- limiter l'effet de rebond suivant l'activation à la hausse ou à la baisse de la charge électrique affecte directement le potentiel de modulation moyen réalisable. En effet, ce dernier diminue jusqu'à 61%, mais est accompagné d'une réduction de coûts pouvant atteindre 36% en moyenne. Un effet de rebond restreint à une heure et 15 minutes s'avère être un bon compromis entre la maximisation de l'amplitude de modulation réalisable et l'atténuation des déviations par rapport à la consommation de base.
- dans le cadre de la réserve secondaire, une étude de cas dans le contexte belge révèle que la fourniture de jusqu'à 70% de la réserve contractuelle hivernale (140 MW) à la hausse peut être obtenue avec 40000 pompes à chaleur pour seulement 44% du coût disponible actuellement sur le marché. Le potentiel de réserve à la baisse est plus limité en raison de la surconsommation entraînée par son activation.

Mots clés : Pompe à chaleur, stockage, flexibilité, control optimal, demand-side management, surconsommation, effet rebond, agrégation, marchés de l'électricité, réseaux électriques

Contents

I	Context	1
1	Introduction	3
1.1	General problem statement	3
1.2	Concepts	4
1.2.1	Flexibility and Demand-Side Management	4
1.2.2	Recall on European electricity system and market	4
1.3	General literature survey	6
1.3.1	Challenges related to the integration of decentralized renewable energy sources	6
1.3.2	Demand-side management options	7
1.3.3	Demand-side management with domestic TCLs	8
1.4	Contributions of the present dissertation	10
1.4.1	Research objectives	10
1.4.2	Methods	11
1.4.3	Structure of the document	11
2	Assessment of the need for DSM at the national scale	13
2.1	Bottom-up modeling of the Belgian residential building stock	13
2.1.1	Building stock description	13
2.1.2	Load profiles	15
2.2	Aggregated results at the national scale	16
2.2.1	Validation of the load profiles	17
2.2.2	All electric evolution scenarios	18
2.2.3	Resulting research questions	21
II	Modeling	23
3	Tools for DSM modeling	25
3.1	Constructive characteristics of buildings	25
3.2	Thermal models	26
3.2.1	Buildings	26
3.2.2	Heat pumps	35
3.2.3	Water tanks	38
3.2.4	Exogenous electrical consumption and DHW consumption profiles	38
3.3	Control strategies	38

3.3.1	Heuristic control laws	38
3.3.2	Optimal control laws	39
3.3.3	Model predictive control	40
3.3.4	Linearization of heat pump performance model	41
III	Load modulation strategies at the building scale	43
4	Optimal management of price-responsive heat pumps for load shifting	45
4.1	Motivations	45
4.2	Electricity price profile	46
4.3	Case-study buildings and systems	47
4.4	Control strategies	49
4.4.1	Optimal predictive control in response to price incentive	49
4.4.2	Rule-based control	51
4.5	Flexibility metrics	54
4.6	Results and analyses	55
4.6.1	Optimal load shifting	55
4.6.2	Rule-based load shifting	61
4.7	Model mismatch and uncertainties	64
4.7.1	"On-line" simulation scheme	64
4.7.2	State observation	65
4.7.3	Application	66
4.8	Research outcome	68
5	Optimal management of HVAC systems for load matching	71
5.1	Motivations	71
5.2	Billing mechanisms in the U.S.	73
5.3	Methodology	73
5.3.1	Optimization problem for load management	73
5.3.2	Modeling	74
5.3.3	State-space formulation and linearization	77
5.3.4	Solver	80
5.3.5	Impact indicators	80
5.3.6	System right-sizing	81
5.4	Results and discussion	81
5.4.1	Influence of metering programs	81
5.4.2	Influence of thermal storage	87
5.4.3	Additional electrical storage	89
5.4.4	Guidelines for system right-sizing	90
5.5	Parametric studies	93
5.6	Research outcome	93

6 Residential heat pump as flexible load for direct control service	95
6.1 Introduction	95
6.2 Load modulation service	96
6.3 Buildings and heat pumps	98
6.4 Optimization problems	99
6.4.1 Baseline electricity consumption profile	100
6.4.2 Achievable modulation amplitude	100
6.5 Generation of the test cases	102
6.6 Results	103
6.6.1 Illustration on a single house	103
6.6.2 Choice of aggregated set of houses	105
6.6.3 Impact of power deviation amplitude limitation	107
6.6.4 Time constants of the modulation service	109
6.6.5 Deviations and overconsumption	114
6.6.6 Impact of state constraint relaxation	115
6.6.7 Influence of the tariff structure	116
6.6.8 Illustration with the balancing market	116
6.7 Research outcome	118
7 A comparison of control strategies and thermal storage options	121
7.1 Motivations	121
7.2 Load modulation strategies	121
7.3 Buildings and systems	123
7.3.1 Case-study buildings	123
7.3.2 Storage options and sizing	123
7.4 Problem constraints	125
7.5 Case studies	126
7.5.1 Ranking of thermal storage options	126
7.5.2 Application to a semi-urban feeder	131
7.6 Research outcome	135
IV Load modulation strategies: large-scale investigation	137
8 Large-scale assessment of the flexibility of residential heat pumps	139
8.1 Motivations	139
8.1.1 Centralized and decentralized control of thermostatically-controlled loads	139
8.1.2 Aggregation of thermostatically-controlled loads	140
8.1.3 Research objectives	142
8.2 Load aggregation model	142
8.2.1 Aggregation of space-heating demand	142
8.2.2 Aggregation of domestic hot water demand	145
8.2.3 Aggregation of both space-heating and domestic hot water demands	148
8.2.4 Validation	150
8.2.5 Generation of test-cases	151

8.3	Assessment of the impact of flexible heat pumps on day-ahead market prices	152
8.3.1	Day-ahead market clearing	152
8.3.2	Optimization problem for the participation of heat pump aggregators in the day-ahead market	154
8.3.3	Case-studies in the Belgian context	156
8.4	Application of load aggregation to the provision of ancillary services	159
8.4.1	Reserve mechanisms	159
8.4.2	Demand-side provision of reserve	160
8.4.3	Optimization problem for the provision of reserve	160
8.4.4	Illustration on a single house	162
8.4.5	Application in the Belgian context	163
8.5	Research outcome	171
 V Conclusions		 173
C.1	Modeling and control framework	175
C.2	Price-based load shifting and analysis of overconsumption	176
C.3	Direct load control and characterization of the rebound effect	177
C.4	Choice of storage option	178
C.5	Large-scale applications	178
C.6	General conclusions	179
 List of Symbols		 181
 Bibliography		 189
 Annexes		 199
A.1	Chapter 2 - Additional material	199
A.2	Chapter 3 - Model Identification	201
A.3	Chapter 4	202
A.3.1	2030 cost scenario - Energy mix and RES share	202
A.3.2	Dialog Matlab – Dymola	203
A.4	Chapter 5 - Parametric studies for the U.S.	204
A.5	Chapter 6 - additional results	209
A.6	Recall on linear programming	211
A.6.1	Duality in linear programming	211
A.6.2	Solving linear programs	212
A.7	Electronic annex	213

Context Part I

1 Introduction

1.1 General problem statement

Over the last century, economic development in many areas has entailed tremendous growth in energy consumption through the intensification of the industrial sector, increase in domestic consumption and growth of the automobile industry. The buildings sector, in particular, is the most energy intensive sector and accounts for over one-third of the global final energy consumption (International Energy Agency (2013)), out of which 70% is due to residential buildings. Thus far, this increase in energy demand has been mainly met by a massive use of fossil fuels, leading to the depletion of their reserves and to atmospheric pollution. Recent concerns regarding energy supply security and climate change mitigation have encouraged the development of alternative energy sources and better management and efficiency of energy systems.

The rapid spread of distributed power generation through the integration of renewable energy sources, and in particular, the increased use of solar photovoltaic (PV) collectors and wind turbines, represent additional challenges for the management of the electricity grid. One main objective of this management is to ensure the balancing between electricity consumption and production. The intermittency of these renewable energies makes such balancing more difficult. Conventional power modulations on the supply-side are no longer enough to ensure security of supply.

A possible solution to help achieve balancing is the smart modulation of electrical loads in a "demand following supply" scheme, referred to as demand-side management (DSM). So far, the flexibility of industrial loads has been mostly considered, but it appears that buildings can also become key systems for smart energy management at the distribution grid level. Indeed, in the coming years, a substantial electrification of this sector is expected with increased use of electric/plug-in hybrid vehicles or space conditioning systems such as high efficiency heat pumps. The electrical load of such end-users can be modulated by

- the time-shift of the use of certain devices such as heating and cooling systems as well as large electric appliances (dishwashers, clothes driers, washing machines,...).
- the emergence of prosumers, i.e. consumers who have their own production of electricity (PV collectors, micro-CHP units,...) and can either auto-consume the electricity produced or supply it to the grid,
- the use of storage systems: so far, the high cost of electrical storage systems has prevented their

widespread use at the residential scale. However, thermal storage systems, when coupled to building-integrated electricity-based heating, ventilating or air-conditioning (HVAC) systems, are a promising alternative.

To manage all these flexible loads, a new entity, called *aggregator*, is being developed. This aggregator pools the flexibility of electricity consumers and can either trade it on the electricity market, or offer it as a service to electricity grid management entities. In order to assess the flexibility potential offered by these consumers, reliable demand-side models and load modulation strategies are required. Indeed, a significant part of the success of demand-side management lies in the determination of suitable incentives that encourage end-consumers to participate in such service and to change their consumption patterns.

In this regard, the objective of this work is to assess the flexibility offered by residential end-users equipped with electricity-driven HVAC systems through different load modulation strategies in the changing electricity supply context.

1.2 Concepts

This section defines the main concepts that form the basis of the topic treated in this document. In addition, a brief summary of the structure of European electricity markets is provided.

1.2.1 Flexibility and Demand-Side Management

Flexibility is defined as "*the ability to quickly adapt power generation and demand in response to varying electricity prices, electricity market conditions, transmission and distribution system conditions, and of regulation*" (Kärkkäinen (2008)).

Demand-side management is defined as "(...) *those electric utility activities designed to influence customer uses of electricity (...) that will produce desired changes in the utility's load shape*" (Gellings (1985)). The concept of DSM can be further divided in the following two categories, differentiated by the time frame of application (Palensky and Dietrich (2011)):

- *energy efficiency*, which includes all permanent changes in systems or users' behavior that yield energy savings,
- *demand-response*, which gathers all types of dynamic incentives that influence the users' behavior in order to correct predicted or existing problems in the energy grid.

1.2.2 Recall on European electricity system and market

1.2.2.1 Main actors

Historically, electricity systems were organized in a vertically integrated manner, including *generating companies*, *transmission and distribution system operators*, and *end-consumers*. The transmission system operator (TSO) is responsible for overall grid balancing. Along with the distribution system operator (DSO), they transport electricity from the production sites to the end-consumers and ensure

system reliability and security of supply. With the liberalization of the electricity market, additional actors have emerged. New actors include (Cornélusse and Ernst (2014)):

- *large and small consumers*: as opposed to small consumers, large consumers can interact directly with generation companies and operators.
- *energy retailers*: they buy electricity to sell it to end-consumers.
- *balance responsible parties (BRPs)*: they are responsible for the quarter-hourly balance between production and consumption within a delimited perimeter. This role can be held by producers, retailers or large consumers.
- *load aggregators*: they pool, manage and trade the flexibility of decentralized consumers. This role can be held by BRPs, retailers or separate entities.
- *market operators*: they operate the power exchange spot market and allocate cross-border capacity.
- *regulators*: they ensure transparent and competitive markets, determine transmission and distribution tariffs and defend consumers' interest.

The general structure of European electrical power systems is summarized in Figure 1.1.

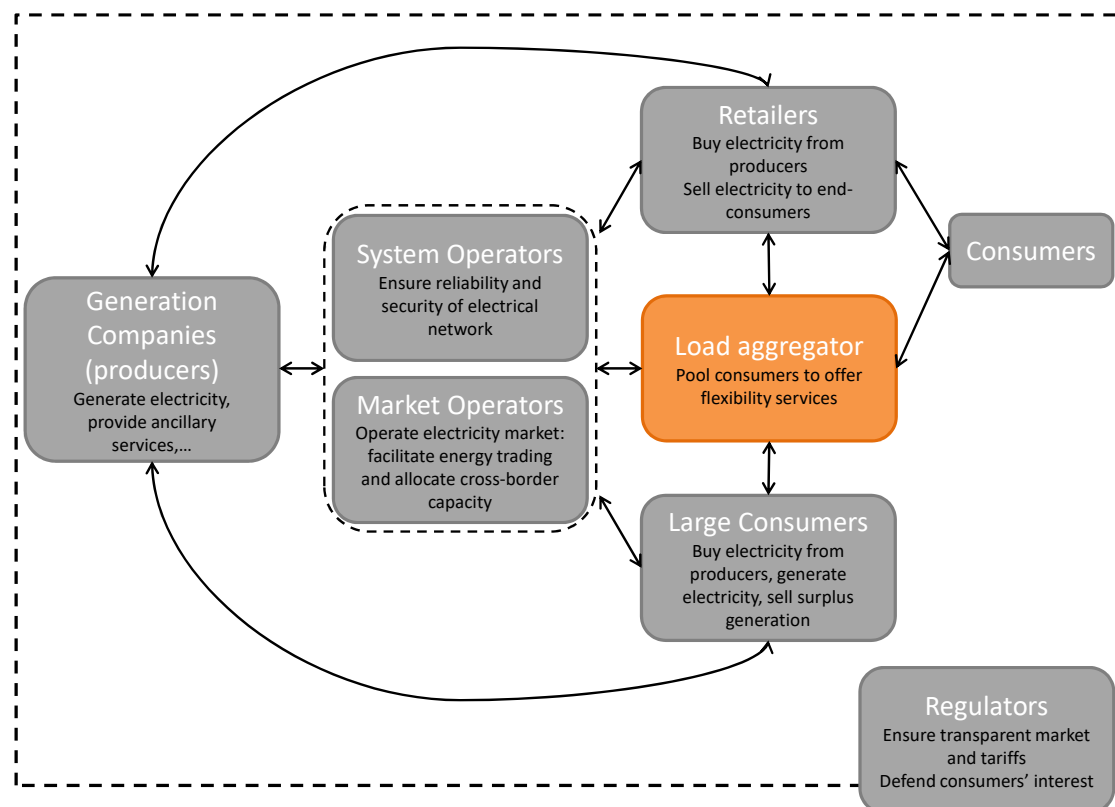


Figure 1.1 – Structure of European electrical power systems (modified from the original version proposed by Cornélusse and Ernst (2014))

1.2.2.2 Electricity market segments

The electricity market is composed of different time-related segments. One can distinguish long-term bilateral contracts, also referred to as "futures", day-ahead, intra-day and real-time segments.

In day-ahead, BRPs make consumption and production forecasts, optimize available flexibility, state their positions to the transmission system operator and place bids on the *day-ahead* spot market. Day-ahead spot market prices are established on an hourly basis, following a "pay as clear" clearing strategy. Clearing prices are set once per day, hence the reference to a fixed-gate auction.

On the *intra-day* segment, new forecasts and adjustments are performed to reduce the system imbalance. In this market segment, participants submit orders at any time, and each possible match is validated. It is referred to as a continuous-time auction.

The *real-time* market corresponds to real-time balancing of the system. To ensure grid balancing and stability, TSOs have developed power reserves called *ancillary services*. Among those services, one distinguishes the primary, secondary and tertiary reserves, further discussed in Chapter 8. Power reserves can be contracted or traded on dedicated market segments. The residual system imbalance is penalized at the *imbalance tariff*.

1.3 General literature survey

The literature review proposed in this section is a general survey of existing studies illustrating the problem introduced in Section 1.1. The objective is to gather studies relevant to the definition of the research objectives of this work. Detailed literature reviews are then added in each chapter.

1.3.1 Challenges related to the integration of decentralized renewable energy sources

As pointed out in Section 1.1, the integration of decentralized and renewable energy sources entails additional challenges for the management of the electricity system. At the overall power system level, power fluctuations entailed by their intermittency complicate grid balancing and affect system performance and efficiency (Vittal (2010)), increasing the need for flexibility and storage capacity (Denholm and Hand (2011), MIT Energy Initiative Symposium (2012)). At distribution level, decentralized energy sources also threaten system reliability. Existing distribution networks present a radial structure where the electricity flows from the medium voltage network towards the low voltage end-consumer. Initially, they are not designed for bidirectional energy flows caused by a significant introduction of decentralized production systems at the low to mid voltage levels (Lopes et al. (2007)). The massive introduction of such units can cause voltage rise effects, power quality disturbance, line and transformer congestion, as well as unplanned changes in flow direction. In the case of back-feeding to the transmission network, the latter may interfere with the planning of centralized production units and cause stability issues. Options that yield optimal use of existing lines, congestion management and improvement of overall system efficiency belong to the field of *smart grids* (Fischer and Madani (2017)).

Regarding the need for flexibility, one solution consists in adjusting the power output of existing generating units. However, ramping abilities are limited by technical constraints inherent to each technology (Kumar et al. (2012)). In the case of a large penetration of renewable energy sources, the

flexibility potential available on the supply-side may not be sufficient anymore (Weitemeyer et al. (2015)), hence the rising interest in storage and management of demand-side power consumption. Indeed, demand-side management offers competitive solutions to those challenges by improving system efficiency and reducing grid reinforcement needs (Strbac (2008)).

1.3.2 Demand-side management options

Among consumers, the flexibility of large industrial consumers, such as manufacturing plants, is already used in ancillary services for the provision of power reserve (Hirst (1999), Kirby and Hirst (1999)). With the electrification of heating systems in buildings and of the transportation sector, smaller consumers can also become key players for demand-side management. Several studies illustrate the interest of active demand side management programs, in terms of peak demand and power flow management. Vinter (2008) presented a study with improved communication between all decentralized units in a mid-voltage network in Sweden and showed that limitation of annual peak load demand by demand-response theoretically allows to reduce network reinforcement costs by up to 80%. Strbac et al. (2010) quantified the reduction in grid reinforcement costs brought by smart management programs of heat pumps and electrical vehicles at the scale of a country (UK). Investment cost reduction of up to 60% are reached for the low-voltage grid, when switching from a business as usual control scenario to a smart management of the loads.

The large share of buildings in the total final energy consumption has triggered interest in the use of HVAC systems as flexible loads. In particular, the use of heat pumps for space conditioning and domestic hot water production combined with different thermal storage strategies is investigated in several studies. The flexibility brought by heat pumps and thermal energy storage comes from their ability to decouple electricity consumption and heat demand in buildings (Fischer and Madani (2017)). The electrical consumption can therefore be shifted in time, which is referred to as *load shifting*. Such loads are identified as thermostatically-controlled loads (TCLs). Both office and residential buildings offer flexibility potential, but in the frame of this work, only the literature regarding residential buildings is presented. In light of the challenges raised by the integration of decentralized energy production units, there are two ways for buildings equipped with such systems to interact with the electricity grid:

- they can improve system-level efficiency by offering flexibility for operational planning and system balancing. Improvement in overall system efficiency is quantified in terms of reduction in total operational costs (Patteeuw et al. (2015a), Arteconi et al. (2016)), CO_2 -abatement costs (Patteeuw et al. (2015b)) and renewable power curtailment (Barth et al. (2006), Meibom et al. (2007)). Provision of balancing power as part of ancillary services is investigated for spinning (Wang et al. (2013)) and non-spinning reserves (Biegel et al. (2014)).
- they can improve system reliability by eliminating local bottlenecks through voltage control (Wang et al. (2012)) and congestion management (Csetvei et al. (2011), Baetens et al. (2012), Baetens (2015)).

Flexibility can be initiated in response to different triggers: signals from the grid such as power exchange (Miara et al. (2014)), voltage level (De Coninck et al. (2014)) and price signals (Halvgaard et al. (2012)). This is rendered possible by improved communication and metering technologies (Wang et al. (2011)).

1.3.3 Demand-side management with domestic TCLs

There is a flourishing number of studies on demand-side management with domestic TCLs. Studies differ by the modeling approach, level of details of demand-side models and control strategies implemented. A detailed review of the use of heat pumps in the smart grid context is proposed by Fischer and Madani (2017). Key studies in the context of the present work are summarized hereafter, along with additional relevant studies.

1.3.3.1 Modeling approach

Among the studies focusing on demand-side management with domestic TCLs, one distinguishes five types of approaches:

- integrated models of supply and demand sides,
- market-oriented models for demand-side management,
- aggregated models of demand-side,
- district-level models of demand-side,
- building-level models.

The study of Patteeuw et al. (2015a) presents an **integrated modeling approach** of active demand response with heat pumps. The purpose is to compare the ability of different couplings of supply and demand-side models to investigate the potential reduction in total operational system costs brought by active demand-response with heat pumps. The paper highlights the need for integrated modeling and concludes that a merit-order based model of the supply-side coupled to detailed thermodynamic models of the demand-side offers a good compromise between accuracy and computational requirements. In a complementary study by Arteconi et al. (2016), the share of renewable energy sources in the electricity mix is varied along with the percentage of active demand response. It is concluded that operational costs reduction by active demand response increase with the share of renewable energy sources.

The studies of Barth et al. (2006) and Meibom et al. (2007) present a stochastic unit-commitment model for the evaluation of the impact of wind power. The study considers five different **markets segments** of the Nordic System. The method is used to illustrate the value of electric boilers and heat pumps to help wind integration with a large share of combined heat and power plants. Results show that the use of heat pumps increases the value of wind power by reducing curtailment, regulating power price and market prices. The model does not include a detailed modeling of demand-side consumption.

Nielsen et al. (2013) present an algorithm that redistributes the energy bought on the day-ahead market in real-time within a portfolio of buildings equipped with heat pumps. The objective is to limit the imbalance that could arise due to uncertainty in the prediction of domestic consumption, while maintaining thermal comfort for the occupants. The method focuses on demand-side modeling and relies on a scheduling technique that attributes different states to each heat pump. Each house is modeled separately. In a companion paper (Biegel et al. (2013)), house models are **aggregated** in a first-order model in order to optimize their flexibility in day-ahead and reserve markets context.

At the **district** level, Baetens et al. (2012) developed a tool to model grid-connected buildings. The

tool includes detailed transient modeling of both buildings and distribution grid. It is used to assess electrical bottlenecks, i.e. voltage fluctuations and transformer overload, in a residential nearly-zero-energy neighborhood with building-integrated photovoltaic systems. The fraction of local PV supply wasted by inverter curtailment and peak transformer loads was estimated to be between 14% and 47%. Dallmer-Zerbe et al. (2016) proposed a control algorithm for voltage control in a district with heat pumps and PV panels. Domestic electricity use is modeled by stochastic load profiles. Thermal loads of buildings and storages are modeled using non-trained grey-box linear models. A detailed model of the distribution grid is included. All models are coupled into a probabilistic load flow analysis. Csetvei et al. (2011) used a low voltage radial system with two nodes to investigate overload elimination with price-responsive heat pumps. Demand-side models are based on non-trained models based on an equivalent RC network with two thermal capacities.

Studies investigating demand-side management at the **building** level rely on both detailed (De Coninck et al. (2010)) and reduced-order building models (Reynders et al. (2013b)). They differ by the type of flexible loads (Gottwalt et al. (2011)), storage options (Hedegaard et al. (2012)), incentives used to trigger load modulation and control strategies.

Domestic thermostatically controlled loads investigated in the literature include heat pumps, water heaters and cooling appliances. In the case of heat pumps, different storage options and heat emitters are investigated in the following studies. De Coninck et al. (2010) investigated the potential of peak demand management brought by the use of an additional storage tank in a single-family house equipped with a heat pumps, hydraulic radiators and PV panels. It was shown that with a 1m³ buffer tank, up to 50% of the peaks could be reduced. Six et al. (2011a) investigated the potential in consumption delay offered by residential houses with heat pumps and both space-heating (SH) and domestic hot water (DHW) storage tanks. A flexibility of 0.5 to 1 hour was determined for the investigated case-study. Miara et al. (2014) studied the load shifting potential of a single-family building equipped with a heat pump connected to a water tank and a floor heating system. Two scenarios of penetration of renewable energy sources for year 2012 and 2030 were investigated. Results showed that load shifting brings significant reduction in residual load for larger storage tank sizes, but entails overconsumption of up to 19%. Reynders et al. (2013a) investigated the potential of building thermal mass as storage option for peak demand reduction and self-consumption in dwellings equipped with PV panels. A study of the influence of building structure, thermal insulation level and heat emission system was performed.

Load modulation of domestic HVAC systems can be triggered by direct load control from system operators (Kim et al. (2015)) or by an external signal. The signal can be reflective either of the state of the whole electrical system or of local bottlenecks (Csetvei et al. (2011)). For example, Miara et al. (2014) proposed to use the daily normalized residual load¹ as a time-of-use (TOU) incentive to shift load. Other incentives rely on variable retail electricity tariffs. One distinguishes TOU pricing, which consists in dividing the day in a number of periods characterized by different prices, critical peak pricing, limited to periods of the day characterized by high demand and real-time pricing, for which the price is reflective of actual market costs (Newsham and Bowker (2010)).

To perform the load modulation, two types of control strategies are implemented: rule-based and model predictive control. Rule-based control constitutes the current standard implementation of

¹The residual load is the load that remains after subtracting renewable energy production.

energy management in buildings (Vrettos et al. (2013)). It can be extended to the context of demand-side load management by adapting temperature set points of HVAC systems in response to incentive signals (Yoon et al. (2014), De Coninck et al. (2014)). However, as emphasized by De Coninck et al. (2014), the benefits retrieved are limited, compared to advanced control methods such as predictive control. Nevertheless, it is used as reference to compare additional benefits brought by predictive methods (Vrettos et al. (2013)). Model predictive control has been implemented by Candanedo and Athienitis (2009) for load management in a net-zero-energy solar house. Simulation results indicated potential reduction of heat pump electricity consumption of up to 23.4% with optimal use of the building-integrated PV/T roof system. Verhelst et al. (2012) studied the optimal control problem formulation of a residential air-to-water heat pump connected to a floor-heating system. In particular, the impact of different objective function formulations on cost savings was investigated. An economic model predictive control problem was formulated by Halvgaard et al. (2012) for indoor climate control in the context of a smart grid, showing 25 to 35% cost savings.

1.4 Contributions of the present dissertation

1.4.1 Research objectives

The literature review confirms the potential offered by domestic TCLs, and in particular heat pumps and thermal storage, to help solve the rising need in flexibility in the energy transition context. Flexibility needs arise either from system-level grid management or for local bottleneck elimination, and require proper modulation strategies of flexible loads. In that regard, results presented in available studies focusing on single buildings tend to be case-study dependent and are not straightforward to generalize to other types of buildings and systems for large-scale applications. In contrast, studies based on integrated modeling of supply and demand allow a better understanding of the flexibility needs at system-level. However, they consider the electricity grid as a copper plate and do not take into account interaction models between market actors. Finally, studies that investigate market-based approaches rely on simplified models of the loads. These models do not take into account the overconsumption and the rebound effect inherent to load modulation with TLCs.

In light of the above, the main research objectives of this work are:

- to propose general methods for optimal load management of flexible residential loads: the proposed load modulation strategies rely on advanced control methods that easily adapt to accommodate different types of systems and can be applied to harvest flexibility in response to both system-level and local needs.
- to perform a detailed analysis of the overconsumption entailed by load shifting and its effect on the economics of different market actors.
- to study the rebound effect inherent to direct load control with TCLs and emphasize its impact in the context of the definition and implementation of flexibility services for operational planning or real-time balancing.
- to develop stand-alone physics-based aggregated model of residential buildings equipped with heat pumps and thermal energy storage for large-scale assessment of the flexibility.
- to identify the bases behind the allocation costs for the provision of ancillary services with flexible heat pumps.

1.4.2 Methods

The methodology follows two main axes. On the one hand, a modeling framework for the assessment of load flexibility is developed based on a bottom-up modeling approach of systems, including:

- detailed thermal models of building,
- reliable reduced-order dynamic building models obtained through model reduction and system identification/observation techniques,
- empirical models of HVAC system performance,
- reduced-order models of water storage tanks,
- stochastic modeling of the use of hot water, lighting and appliances and of occupancy patterns,

On the other hand, two types of control approaches are implemented to develop load modulation strategies: rule-based and model-based predictive control. In the case of optimal control, decentralized and centralized optimization problems are formulated to propose general load management schemes to answer the above research questions.

Example of the simulation codes developed in the frame of this thesis will be made available in an electronic annex (Annex A.7).

1.4.3 Structure of the document

The document is organized in five main parts.

The first part focuses on the context of the study. It is divided in an introduction gathering problem statement, general literature review and research objectives (Chapter 1) and an large-scale illustration of the need for demand-side management (Chapter 2). The results presented in Chapter 2 set the bases of the following research work.

The second part presents the modeling tools developed in this work and used throughout the document (Chapter 3).

The third part investigates advanced load modulation strategies at the building scale. It is divided in four chapters. Chapter 4 focuses on forward-price-induced load shifting. New flexibility indicators are proposed and the flexibility potential of buildings with different insulation levels, emission systems and thermal storage options are compared. Overconsumption and its impact on consumers and electricity retailers' economics is discussed. Both rule-based and optimal control strategies are investigated. Chapter 5 proposes a general methodology for optimal load management with distributed renewable energy generation and storage in residential housing. The method is based on evolving billing mechanisms that encourage on-site consumption of local renewable production. The proposed optimal control formulation is very flexible, and can be applied to any type of storage systems (thermal or electrical) and of decentralized electricity production unit, such as PV panels or μ -CHP units. It also considers storage/resale considerations that arise with the use of electrical storage. Chapter 6 addresses the problem of an aggregator controlling residential flexible loads to offer a direct control flexibility service. The proposed service consists of a power modulation, upward or downward, directly followed by a parametrized constrained rebound effect. The impact of the constrained rebound effect on achievable modulation amplitude and costs is studied thoroughly. Finally, Chapter 7 proposes

1.4. Contributions of the present dissertation

a comparison of the modulation strategies presented in the three previous chapters with different thermal storage options. The objective is to homogenize the findings in terms of interactions between load modulation strategies and thermal characteristics of buildings and storage.

The fourth part assesses the flexibility potential offered by large sets of residential buildings equipped with heat pumps. To that end, aggregated models are developed and used to solve two centralized optimization problems (Chapter 8). The first application aims at quantifying the impact of unlocking the flexibility of large numbers of consumer on day-ahead market clearing prices. The second application investigates the potential of heat pumps to provide secondary reserve and focuses on the determination of allocation costs.

Finally, the fifth part provides concluding remarks and perspectives.

2 Assessment of the need for DSM at the national scale

The purpose of this chapter is to summarize the study that set the bases of the research questions investigated in this thesis. The objective of the study was to develop a versatile modeling framework to simulate the gas and electricity demand profiles of the Belgian residential building stock. It was articulated around two major steps: the development of a description of the Belgian residential building typologies (Gendebien et al. (2015)) and its coupling to models of energy systems in order to obtain energy demand profiles (Georges et al. (2013)). The resulting tool allows a quantitative analysis of the need for demand-side management and suitable load modulation strategies in the context of an increasing use of electricity-driven HVAC systems and renewable energy sources. The modeling framework is further developed in this thesis and detailed in Chapter 3.

2.1 Bottom-up modeling of the Belgian residential building stock

2.1.1 Building stock description

The methodology followed for the building stock description is based on a forward bottom-up approach. It is presented in details in Gendebien et al. (2015) and applied to the case-study of the Belgian residential housing stock. The first step consists in defining a tree-structure with a set of buildings able to capture the diversity of the entire building stock. According to Cyx et al. (2011), a distinction can be made between a set of representative buildings and a set of typical buildings. Representative buildings are fictional buildings whose characteristics are based on average values. Those values can be tuned to meet available data regarding the energy consumption of the total building stock. Typical buildings, contrariwise, are existing buildings chosen to represent a set of similar buildings among the examined stock. The use of typical buildings is more flexible, as it allows the use of the building stock description to investigate different scenarios of retrofit measures for example. The approach proposed in this work can be qualified as *hybrid*. It combines the strength of both approaches, as follows:

- from the typical approach: the geometric characteristics of existing buildings have been chosen to characterize buildings from a same age class.
- from the representative approach: for a same geometry and age class, different insulation levels envelope components and different types of energy vectors and HVAC systems are considered. This leads to a set of fictitious buildings.

2.1. Bottom-up modeling of the Belgian residential building stock

The hybrid approach is therefore more versatile, as it allows considering different envelope characteristics and HVAC systems for a same typical building geometry.

In a very diverse building stock such as in Belgium, decisions made to reduce the set of representative buildings to a reasonable and manageable number while preserving a sufficient level of diversity and accuracy are of major importance. Further details regarding the assumptions behind those simplifications can be found in Gendebien et al. (2015). The different buildings were finally grouped as follows:

- type of buildings: apartment, freestanding, terraced and semi-detached,
- age class (before 1945, 1946-1970, 1971-1990, 1991-2007 and after 2007),
- insulation level of envelope components: walls, windows, ground floor and roof,
- energy vectors (oil, natural gas, electricity and others) and systems characteristics for space-heating and domestic hot water production.

The final tree-structure contains 992 cases. One branch is illustrated in Figure 2.1.

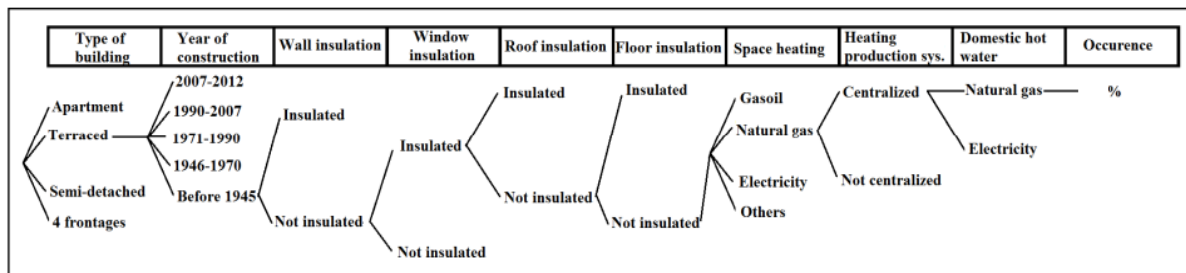


Figure 2.1 – Illustration of the proposed tree-structure for the Belgian residential building stock.

The typical building geometries come from the work of Allacker (2010). Each building is divided in six thermal zones: living room, bedrooms, kitchen, bathrooms, unheated zone and corridor. For each zone, dimensions are provided for walls, floor, windows, roof, doors, adjacent and internal walls.

Existing residential buildings composing the Belgian building stock typically present a heavy structure composed of bricks and concrete or local stones. The wall composition for each age class, together with tabulated U-values, thermal capacitances, equivalent thermal bridging U-values and infiltration rates can be found in Annex A.1. An illustration of the repartition of U-values for walls and windows in the building stock for year 2012 is provided in Figure 2.2.

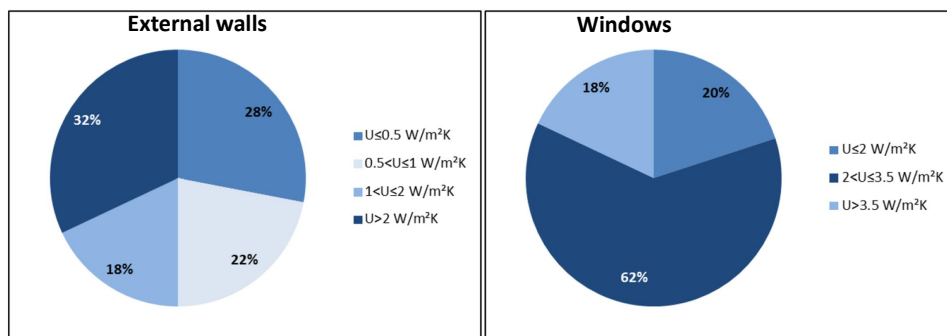


Figure 2.2 – Repartition of U-values for walls (left) and windows (right) in the building stock.

2.1. Bottom-up modeling of the Belgian residential building stock

The proposed tree-structure has been established for year 2012, and can be automatically updated to simulate different evolution scenarios of the building stock for horizon 2030. This horizon is particularly relevant for electricity and gas suppliers in their mid-term evaluation of aggregated energy demand. It can also provide an insight for HVAC manufacturers regarding potential introduction of innovative systems in the market. Finally, this horizon is also suitable for the determination of energy policies at the national level.

2.1.2 Load profiles

The final energy use of a building can be evaluated based on the sequential approach depicted in Figure 2.3. Several inputs, namely the outdoor climate conditions, occupancy profiles of the building, domestic appliances and lighting use and water draw-off events, are provided to the building model. The latter includes a modeling of thermal zones and of emission, distribution and production systems. The model determines the thermal loads associated to space heating or air-conditioning and domestic hot water needs, and the electricity consumption profiles for appliances and lighting.

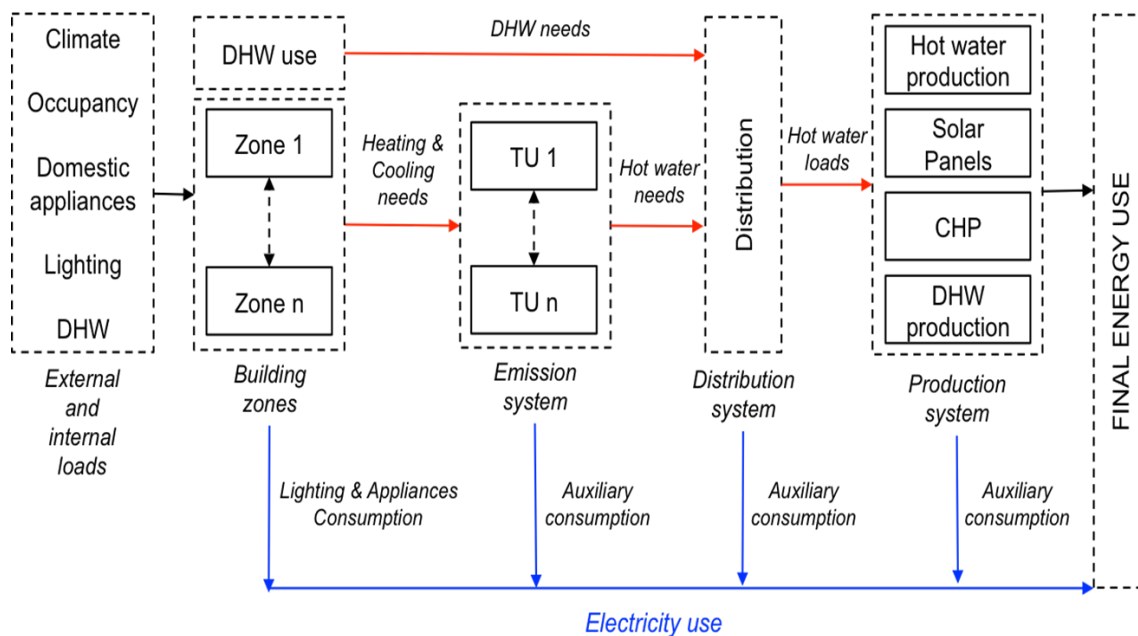


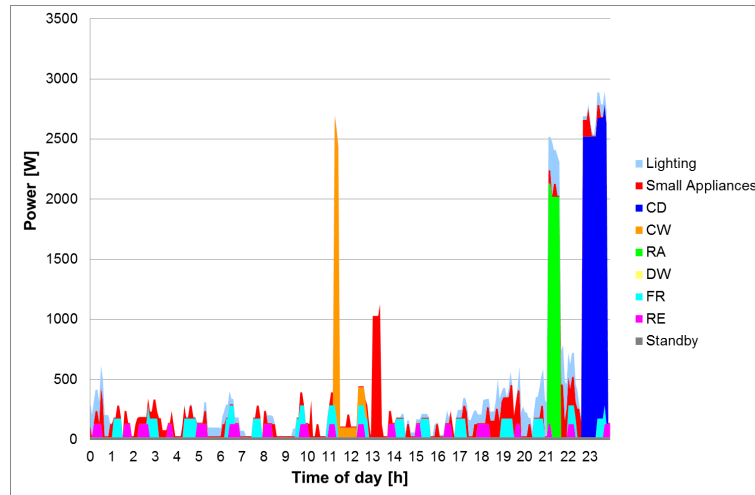
Figure 2.3 – Schematic description of the determination of final energy use in buildings.

The thermal model of the building is the multi-zone quasi steady-state model described in both RT-2012 (Centre Scientifique et Technique du Bâtiment (CSTB) (2012)) and ISO13790-2007 (Comité Européen de Normalisation (2008)). This model is based on a 1C-5R equivalent thermal network of thermal zones. Its structure and accuracy are discussed in Chapter 3. This model allows a high flexibility regarding the level of details taken into account in the model at reduced computational costs. The model takes into account solar gains, internal gains due to occupants and appliances, infiltrations and ventilation.

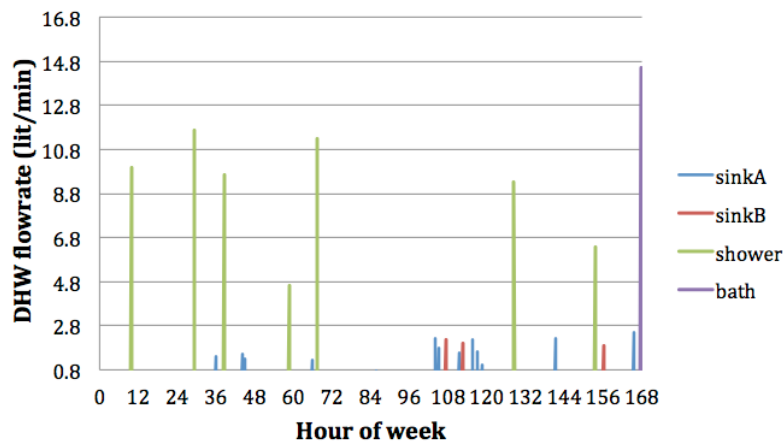
The development of electric appliances and lighting profiles relies on the use of predefined time-of-use probability curves available in the literature. They are adapted to the Belgian context in the work of Georges et al. (2013). They determine switch-on and switch-off times of the devices. A probability

2.2. Aggregated results at the national scale

adjustment process is performed to attain the annual total and specific consumption targets of each category of appliances. Similarly, DHW draw-off events are determined based on probability curves, adjusted to reach an average daily use of around 50 liters per occupant at 50°C. For further details, the reader is referred to Georges et al. (2013). Sample results of the profiles obtained are provided in Figure 2.4.



(a) Appliances - example daily power profile (CD: clothes drier, CW: clothes washer, RA: range, DW: dishwasher, FR: freezer, RE: refrigerator)



(b) DHW draw-off events - example weekly profile

Figure 2.4 – Example results for appliances and DHW draw-off event profiles.

2.2 Aggregated results at the national scale

The above tree-structure description of the residential building stock, building simulation tool and load profiles are combined to perform dynamic simulations for each type of building. The simulation time step is set to 15 minutes.

2.2.1 Validation of the load profiles

Gas

First thermal models of the buildings were validated following the *BESTEST* procedure (Judkoff et al. (2011)). Then, annual gas consumption for space-heating and domestic hot water consumption obtained when simulating the whole building stock were compared to historical data. Results showed agreement within 12% error on an annual basis.

Electricity

In Belgium, electricity meters of residential end-consumers are only monitored on a yearly basis. In order to allocate their consumption for grid management purposes, such consumers are associated to synthetic load profiles (SLPs - Synergrid (2012)) defined on a quarter-hourly basis. These profiles are built based on the monitoring of 2500 dwellings chosen statistically to represent the Belgian residential building stock. Depending on the day/night electricity use ratio, residential consumers can be associated to two different types of SLPs: S21 and S22.

These synthetic profiles can be compared the load profiles obtained with the present simulation tool. To obtain electrical load profiles per average building, simulation results were aggregated based on the percentage of each building in the tree-structure as follows:

- let x_i be the share of houses of type i in the building stock \mathcal{S} ,
- let $P_i^{app,light}$ be the corresponding electric load profile for appliances and lighting,
- let y_i^s be a Boolean variable equal to one if electricity is used as energy source for space heating, and let P_i^s be the associated load profile,
- let y_i^w be a Boolean variable equal to one if electricity is used as energy source for DHW, and let P_i^w be the associated load profile,

The electric power consumption profile per average building, P^{tot} , is then given by

$$P^{tot} = \sum_{i \in \mathcal{S}} x_i (P_i^{app,light} + y_i^s P_i^s + y_i^w P_i^w) \quad (2.1)$$

Agreements within 4.5% error were obtained on the annual electricity use between simulated and synthetic profiles. However, the normalized root-mean-squared error reaches 19%. Two major limitations may account for the differences observed in terms of quarter-hourly comparison of the profiles:

- the synthetic profiles are built based on historical monitoring data over several years and are therefore very smooth, compared to the profiles obtained with the present simulation tool.
- neither the repartition of houses between each type of synthetic profiles (S21 and S22), nor the percentage of houses equipped with electric radiators and boilers associated to those profiles is known exactly.

In light of these comments, a quarter-hourly comparison based on average daily profile may be a more suitable approach. Both synthetic and simulated profiles are therefore illustrated in Figure 2.5 for an average day.

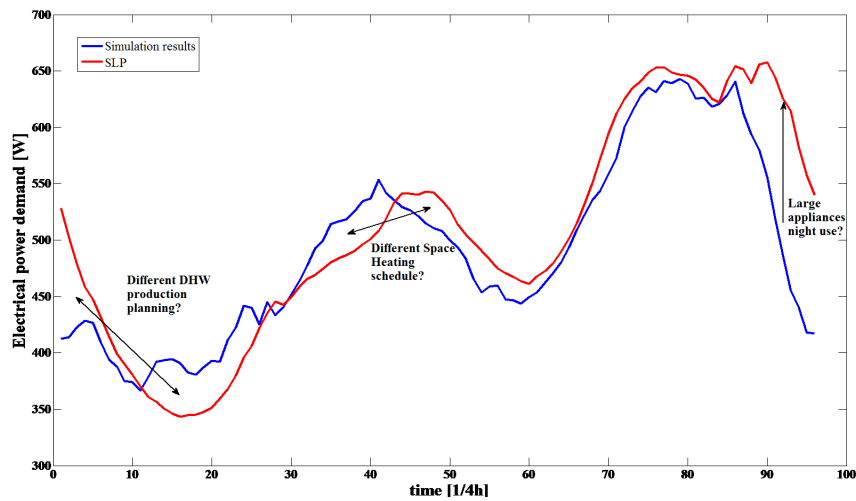


Figure 2.5 – Comparison between synthetic profile (SLP) and simulation results for an average day.

2.2.2 All electric evolution scenarios

The versatility of the developed tool allows the investigation of different evolution scenarios of the building envelopes and HVAC systems by horizon 2030. In particular, the increasing trend towards the electrification of HVAC systems through the use of heat pumps can be simulated. To that end, the following modeling assumptions are made:

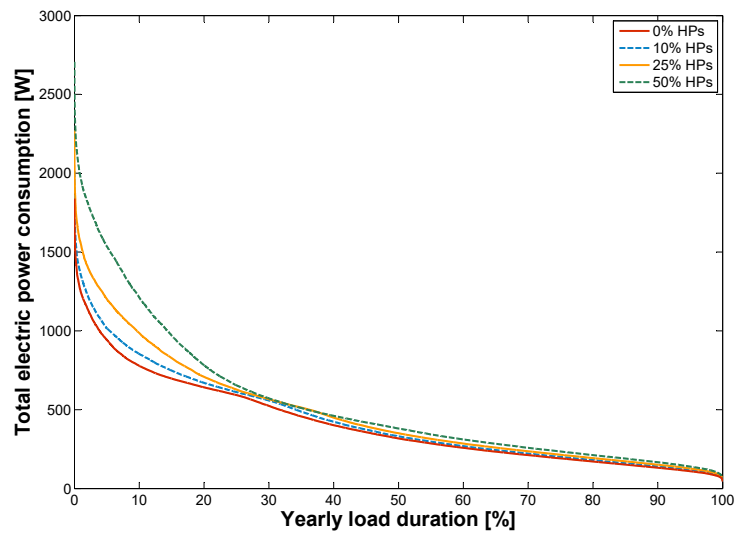
- a «business as usual» evolution of the building stock in terms of demolition, construction and retrofit rates, set respectively to 0.075%, 0.9% and 0.5% per year,
- an evolution of lighting and appliances consumption following the “best available technology”,
- air-to-water heat pumps are installed only in houses that meet minimum insulation requirements, and the maximum installed thermal capacity is limited to that of the largest residential heat pump commercially available,
- the electricity grid is assumed to behave as a copper plate, and no congestions are considered.

The ability to model such evolution scenarios of the building stock is of interest in the context of the operational planning of centralized electricity production generators. Three metrics directly influence the operation costs of such generation units (Palacio et al. (2014)):

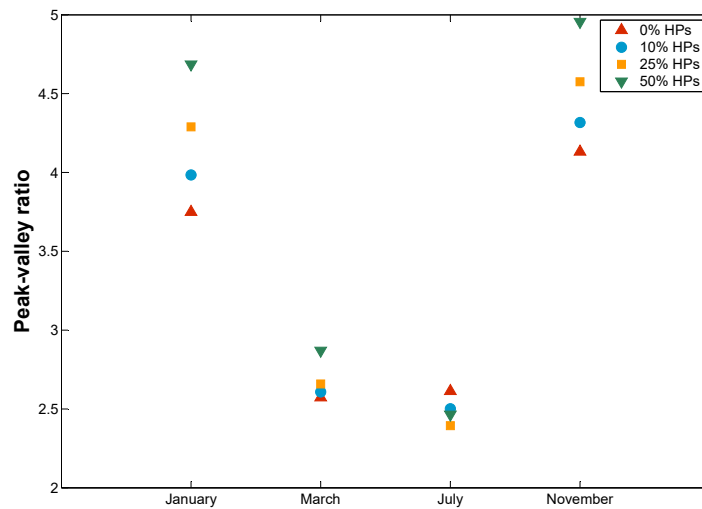
- the *load factor*, which refers to the ratio between the average load and the peak load,
- the *peak-valley ratio*, which refers to the ratio between maximum and minimum values,
- the *ramping*, which characterizes the adjustment of power production by generators to adjust to short-term changes in load consumption. It is defined by the sum of the difference in power between successive time steps over a defined period of time.

In a first scenario, changes in those metrics entailed by an increased use of heat pumps in the building stock is illustrated in Figure 2.6. Peak demand increases of 9%, 23% and 47% respectively are observed for 10%, 25% and 50% penetration rates of heat pumps, respectively. The influence on peak-valley ratio is illustrated for four representative months of the year. This metric is most impacted in the winter and in the fall, with up to 27% increase.

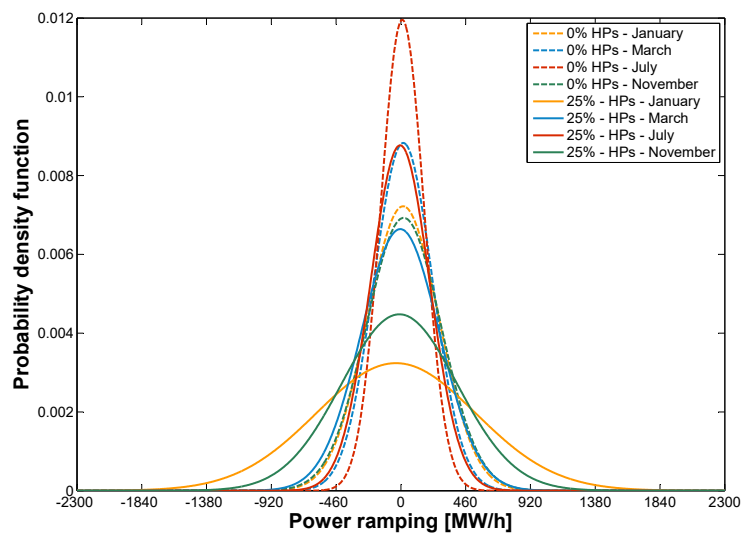
2.2. Aggregated results at the national scale



(a) Total electric power load duration curve per average house (Equation (2.1)) with 0 to 50% penetration rates of heat pumps.



(b) Average peak-valley ratio for January, March, July and November with 0 to 50% penetration rates of heat pumps.



(c) Total power ramping density probability function for the residential building stock.

Figure 2.6 – Illustration of the impact of increasing penetration rate of heat pumps in the residential building stock.

2.2. Aggregated results at the national scale

The power ramping is calculated for a one-hour period. In the absence of heat pumps, maximum power ramping ranges between 600MW/h and 800MW/h for the overall residential building stock, depending on the season. As the use of heat pump increases, the range extends up to around 1800MW/h. In normal system operation, increasing these three metrics results in a rise in operation costs, due to the commitment of additional expensive fast-moving generation units. In order to lower system costs, load management for peak shaving and valley filling becomes essential.

In a second scenario, PV panels are installed in addition to the heat pumps. A new metric, the *surplus production*, is introduced. It is defined as the share of PV production that cannot be consumed simultaneously by the average electrical demand defined by Equation (2.1). The average daily profiles resulting from the installation of 25% of PV panels and 25% of heat pumps are illustrated in Figure 2.7 for four months of the year for an average house.

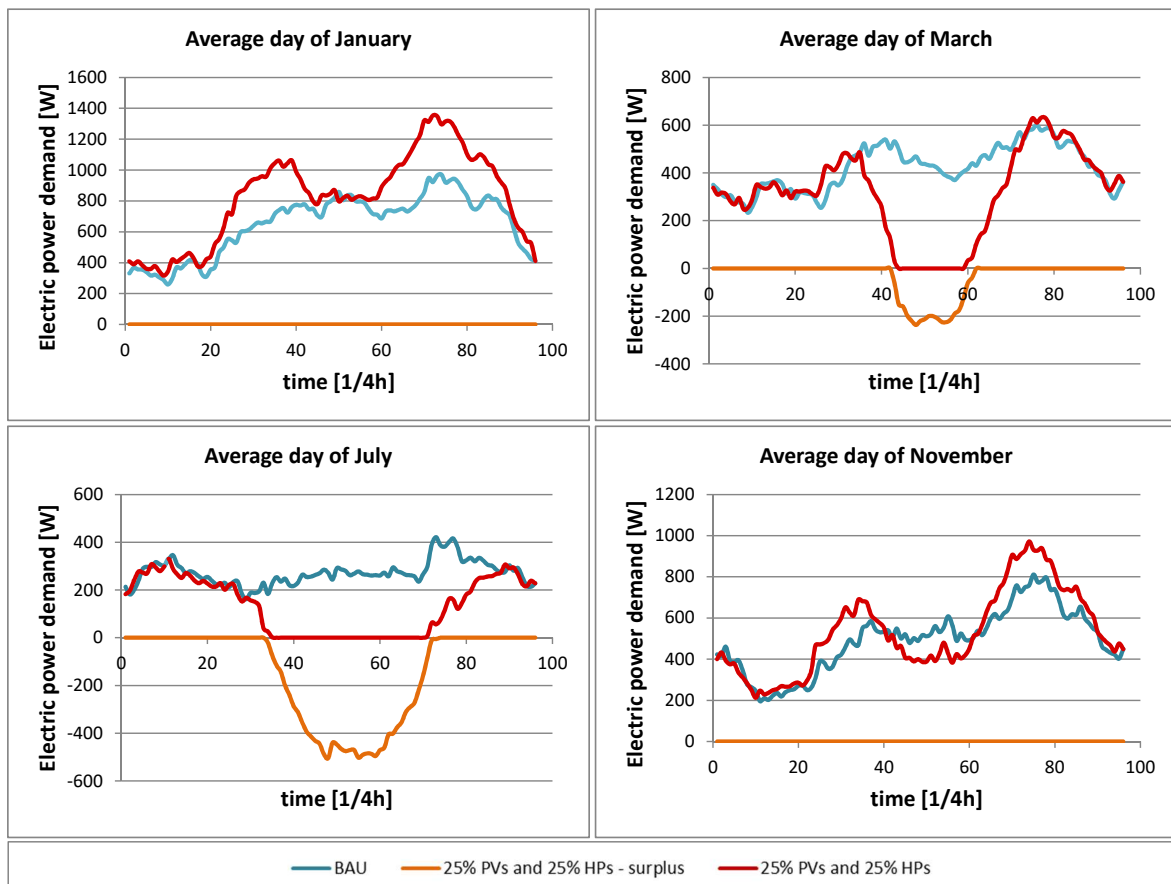


Figure 2.7 – Average daily electricity consumption profiles per average house for the months of January, March, July and November. Comparison of two scenarios: a business-as-usual scenario with no heat pumps and no PV panels (BAU), and a prospective scenario with 25% penetration of heat pumps and PV panels. In the second case, the surplus electricity production by PV panels is also illustrated.

In the winter and in the fall, the entire PV production can be consumed simultaneously and there is no surplus electricity production. In the spring and summer, contrariwise, the average electricity demand is lower and significant surplus production is observed in the middle of the day. Such excess power

production can jeopardize the system stability, by increasing the risks of transformer overloading and over-voltage. Moreover, as illustrated in Figure 2.8, the combined use of heat pumps and PV panels modifies the needs for power ramping of centralized generation units. Maximum downward ramping needs increase in the morning, whereas the need for upward ramping increases in the evening. Depending on the forecast uncertainty, those changes may require the commitment of costly fast-moving generation units. For the above reasons, load matching of decentralized PV production through load shifting can contribute to system safety and reduction of operation costs.

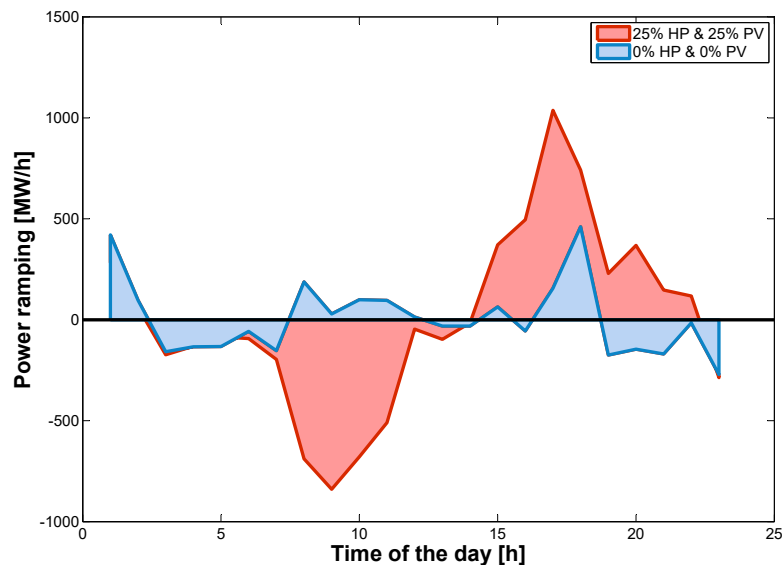


Figure 2.8 – Average daily power ramping for the month of July for the overall residential building stock. Two scenarios are considered: a business-as-usual scenario (0% HPs and 0% PVs) and a scenario with 25% heat pumps (mostly used to cover DHW needs) and 25% PV panels.

2.2.3 Resulting research questions

The above scenarios highlight the need for modulation of the electrical domestic load and raise the following research questions:

- what kind of load modulation strategies are suitable to limit the impact of an increased use of electrically-driven systems and of decentralized electricity production units? What incentive can encourage end-consumers to become "flexible"? The answers to these questions are developed in Chapters 4 and 5.
- what storage options provide the most flexibility? This is partly discussed in Chapters 4 and 5 and thoroughly investigated in Chapter 7.
- how can this flexibility be harvested by a load aggregator? A flexibility service is proposed in Chapter 6 and illustrated for different applications in Chapter 8.
- what is the impact of the scale considered? Load modulation strategies are developed at the scale of a building in Chapters 4 through 7, and extended to large-scale simulations in Chapter 8.

Modeling Part II

3 Tools for DSM modeling

The purpose of this chapter is to set the bases of a framework to investigate modulation strategies of flexible residential electrical loads. It includes a brief description of typical building typologies, a comparison of reduced-order thermal models of buildings, models of storage and HVAC systems, and a general recall on control strategies. Different load modulation strategies are then further developed in the following chapters. In those chapters, additional models specific to the application studied in the chapter are also detailed.

3.1 Constructive characteristics of buildings

As presented in Section 2.1.1, a methodology that defines building typologies to describe a building stock at the national scale was proposed. The methodology is applied to the Belgian residential building stock as case-study. The resulting building stock description is illustrated in Figure 2.1. Typical house typologies from this set are used for detailed investigation of load modulation strategies in the following chapters.

Amongst others, retrofitted and new freestanding houses built after 1971 are studied extensively. The first type of house is a two-story building representative of freestanding houses built after 1991. The house has a total heated volume of 457 m³. It is divided into four zones: a living zone, a staircase, a sleeping zone, and a bathroom, as shown in Figure 3.1. The house presents a typical heavy concrete structure. Vertical walls are composed of 20 cm hollow concrete blocks, rigid insulation panels, and brick as finishing material on the external side. Ground and upper floors are made of precast concrete, while the roof is a wooden insulated structure. Two insulation levels are considered:

- K45-level, which corresponds to the Belgian standard for newly built houses before 2014. The overall U-value is 0.46 W/m²K, with an air change rate n_{50} equal to 6 ACH. This house is used as test case-study to compare the performance of reduced-order building models in Section 3.2.1.
- K30-level, which corresponds to an overall U-value of 0.305 W/m²K, with an air change rate n_{50} of 3 ACH.

The second type of houses are representative of freestanding houses built between 1971 and 1990. They are characterized by a single-story geometry. The building structure is made of heavy concrete, similarly to the two-story house. At that time, buildings were often poorly insulated. In the frame of

this work, two retrofit options are considered: a light retrofit of roof and windows, and a heavy retrofit that also includes external walls and floors. Characteristics of the four houses are summarized in Table 3.1.

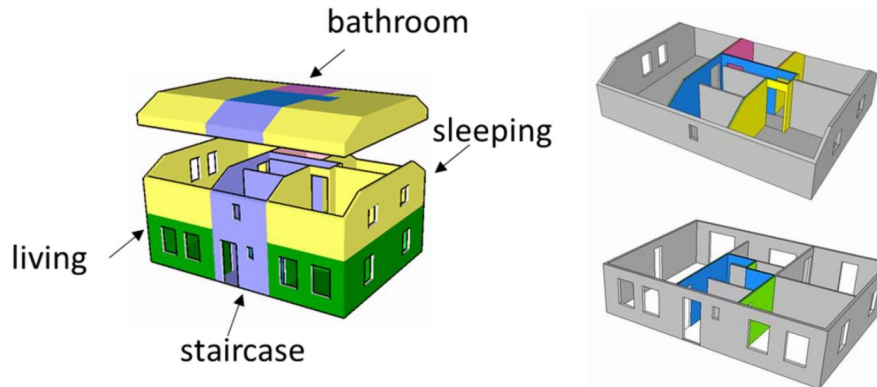


Figure 3.1 – Illustration of the geometry of the K45 test house: division of the heated volume into four thermal zones (left) and layout of the ground and first floors showing zone separating walls (Masy (2008)).

Table 3.1 – Characteristics of four typical buildings.

Year of construction	Number of floors []	Heated volume [m ³]	Ground floor area [m ²]	Average U-value [W/m ² K]
≥ 2007	2	457	75	0.31
1991-2006	2	457	75	0.46
1971-1990 <i>Heavy retrofit</i>	1	423	148.5	0.77
1971-1990 <i>Light retrofit</i>	1	423	148.5	1.24

3.2 Thermal models

3.2.1 Buildings

Models for dynamic simulation of building energy demand are commonly classified as white-box, grey-box or black-box models (Bohlin (1995), Bacher and Madsen (2010) and De Coninck et al. (2016)). Those models differ by their level of details and computational complexity. White box models compute the building heating and cooling loads based on a purely physical description of the building envelope characteristics. They provide the highest level of details, but require a full prior knowledge of all building parameters. Such models are traditionally implemented in available building simulation software. Grey-box models are reduced-order models whose structure is based on the thermal network analogy. The model parameters, consisting of thermal resistances, R in K/W, and lumped thermal capacitances, C in J/K, are identified from white-box model simulation results or real data. They provide an accurate representation of the thermal response of the building at significantly reduced computational requirements and allow for extrapolation to other climate conditions. Black-box models

are fully empirical models derived from statistical data analysis. Although computationally efficient, they don't allow the extrapolation to other building characteristics or external conditions.

In this chapter, three types of grey-box models of different complexities are presented and compared. Their structure and performance are illustrated for the K45 example house in the following sections. Those models are then compared to black-box models.

3.2.1.1 Grey-box models

Multi-zone model (Masy (2008))

A simplified multi-zone dynamic building model has been proposed by Masy (2008). The model is an extension of the zone model with RC analogy introduced by Laret (1981). In this model, each external capacitive wall is represented by a 2R-1C network, as illustrated in Figure 3.2a. Two additional parameters, ϕ and θ , are introduced. They are adjusted based on a frequency analysis for a 24h-period sinusoidal solicitation (Ngendakumana and Liebecq (1986)) and define respectively the proportion of the wall capacity accessible over the solicitation period and the position of that capacity in the wall. Further details regarding the identification method are provided in Annex A.2, and can be found in the work of Masy (2008) and Ngendakumana and Liebecq (1986).

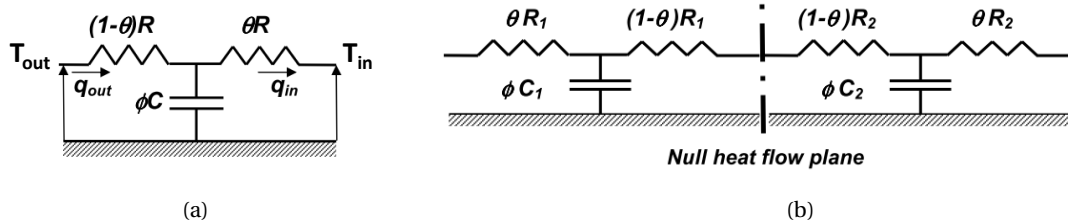


Figure 3.2 – 2R-1C network for external wall with isothermal boundary condition (left) and 3R-2C network for a partition wall (right) (Masy (2008)).

Capacitive partition walls, are modeled by connecting two 2R-1C networks. Each 2R-1C network is assumed to have an adiabatic boundary condition, resulting in a "null heat flux plane", as illustrated in Figure 3.2b. Windows and doors are assumed to behave as purely resistive components. Ventilation heat losses are also modeled by an equivalent thermal resistance. The full single-zone model is illustrated in Figure 3.3. Adjacent zones are connected through partition walls. Solar heat gains, internal gains due to occupants, appliances and lighting as well as heat input from HVAC systems are injected on the zone temperature node.

The model has been validated for the K45 house against a reference convolution model based on response factors. Root-mean-square (RMS) errors on indoor temperature for a whole year were less than 0.2 K for a single-zone model and less than 0.3K for a multi-zone model. The model has also been validated against experimental data for another house typology in Masy et al. (2015b). This multi-zone model is chosen as reference to compare the performance of the following reduced-order models.

Single-zone model with parameter identification

Two trends are observed in the literature to determine the appropriate structure of single-zone grey-

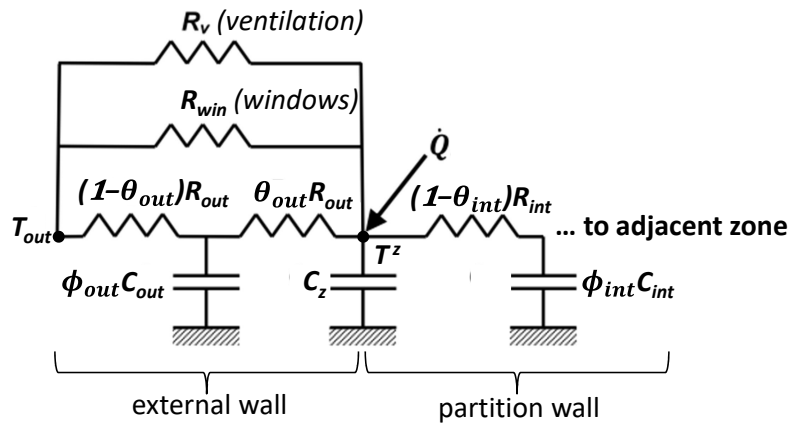
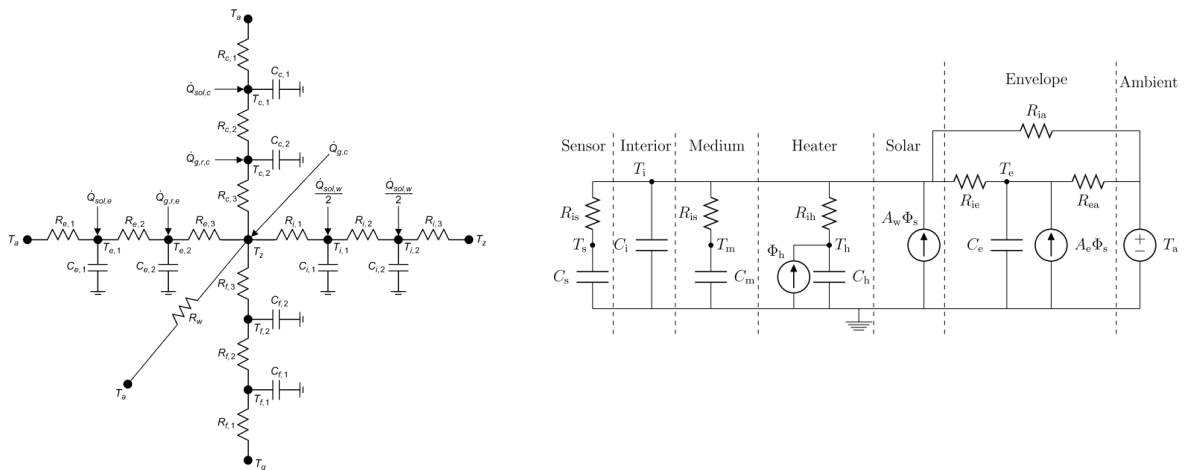


Figure 3.3 – Equivalent thermal network for a single zone proposed by Masy (2008).

box models: physics-based and statistics-based approaches. In the physics-based approach, the RC structure is determined from the knowledge of the characteristics of the building. Braun and Chaturvedi (2002) proposed a general thermal network model for a single zone building. It is illustrated in Figure 3.4a. In this model, external walls, floor, ceiling and internal walls are represented by different 3R-2C branches. An additional purely resistive branch is added to represent light walls. From this general model, simplifications can be made based on the knowledge of the building structure, in order to obtain a simplified yet suitable RC structure. Parameter identification is carried by minimizing the RMS error on zone temperature or zone thermal power input.



(a) General single zone thermal network proposed by Braun and Chaturvedi (2002).

(b) General single zone thermal network proposed by Bacher and Madsen (2010).

Figure 3.4 – General single-zone thermal networks for physics-based (left) and statistics-based (right) approaches.

The statistics-based approach determines the suitable model structure based on statistics indicators, such as the maximum likelihood estimator (Bacher and Madsen (2010)). The procedure consists in

increasing the model complexity from a 2R-1C structure to a more detailed one so as to maximize the likelihood estimator while minimizing the number of parameters. The level of complexity of the model is considered sufficient to capture the thermal behavior of the building if the resulting error after identification can be assimilated to Gaussian noise. The most complex model structure is illustrated in Figure 3.4b.

The procedure followed in this work is similar to the one proposed by Cai and Braun (2012), and based on the physics-based approach. The obtained RC structure for the case-study building is represented in Figure 3.5a. Parameters identification relies on the constrained minimization of the RMS error on the predicted zone temperature, T^z , i.e.,

$$RMSE = \sqrt{\frac{\sum_{i=1}^n (\hat{T}_i^z - T_i^z)^2}{n}} \quad (3.1)$$

Initial guess values for the lumped parameters are imposed based on thermal and geometrical characteristics provided for the real building. Intervals of variation of the parameters are constrained around the initial guess values. In order to avoid local minima, a "multi-start" procedure that generates random sets of initial values comprised within the allowed variation intervals is used.

The identification is performed on a yearly basis with a set of training data consisting of outdoor conditions of year 2012 and a random heating power signal illustrated in Figure 3.6c. A yearly RMSE on indoor zone temperature of 0.55 K is obtained. The model is validated with a cross-validation data set illustrated in Figure 3.6d. A yearly RMSE of 0.58 K is found. Identified parameters are provided in Figure 3.5b. Temperature profiles obtained with the trained model are illustrated for both the training and cross-validation data sets in Figure 3.6a and Figure 3.6b.

As explained in the work of De Coninck et al. (2016), the validity of the identified model requires:

- a) *"the parameters not to lie in the specified minimum and maximum bounds,*
- b) *their value to be physically reasonable,*
- c) *the confidence intervals to be within reasonable bounds. This provides information regarding the accuracy of the identification and the influence of the parameters on the model output prediction. The confidence interval is obtained from the distribution of the standard deviation of each parameter. The standard deviation is the square root of the diagonal elements of the covariance matrix*

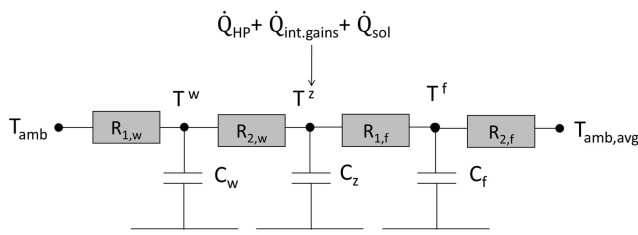
$$cov(\mathbf{p}) = var(\mathbf{e})(\mathbf{J}^T \mathbf{J})^{-1} \quad (3.2)$$

where $var(\mathbf{e})$ is the expected variance of the output deviation \mathbf{e} , and \mathbf{J} contains the sensitivities of the model outputs with respect to the estimated parameters."

Parameters and normalized covariance for the identified model are provided in Figure 3.6b. The parameters do not lie in their imposed bounds.

Single-zone model with semi-empirical parameters

Detailed models or monitoring campaign data are not always available, hampering the identification of the grey-box model parameters. Other grey-box model structures exist for which parameters are imposed by semi-empirical laws (Centre Scientifique et Technique du Bâtiment (CSTB) (2012), Comité Européen de Normalisation (2008)). The structure of the model proposed by Comité Européen de

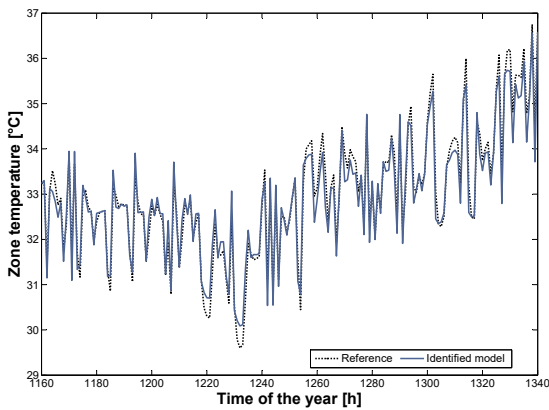


(a) Single zone thermal network structure.

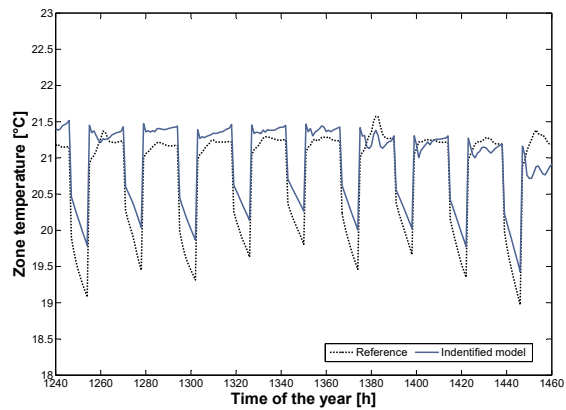
Parameters	Values	95% Confidence interval
C_f	$1.3 \cdot 10^8$ J/K	0.34%
C_w	$1.03 \cdot 10^8$ J/K	2.48%
C_z	$1.86 \cdot 10^6$ J/K	2.48%
$R_{1,w}$	0.006 K/W	0.18%
$R_{2,w}$	$2.7 \cdot 10^{-4}$ K/W	0.09%
$R_{1,f}$	0.093 K/W	0.10%
$R_{2,f}$	0.0458 K/W	0.27%
gA	4.61 m^2	0.27%

(b) Identified parameters and normalized confidence intervals.

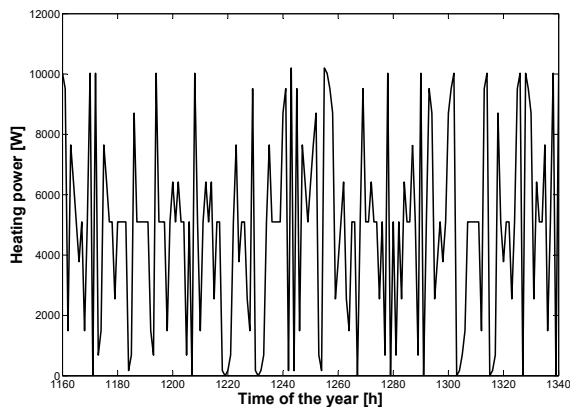
Figure 3.5 – Single zone thermal network structure and parameters for K45 case-study based on physics-based approach.



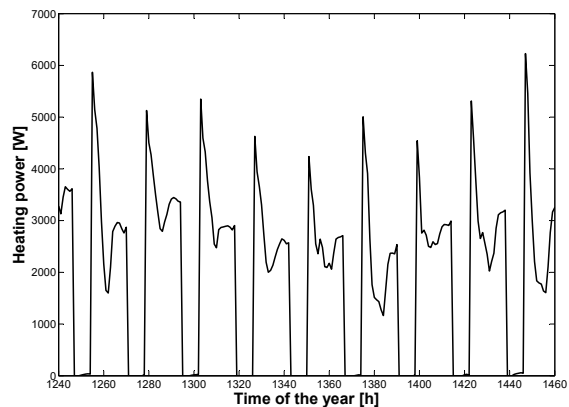
(a) Zone temperature - training data set.



(b) Zone temperature - cross-validation data set.



(c) Heating power - training data set.



(d) Heating power - cross-validation data set.

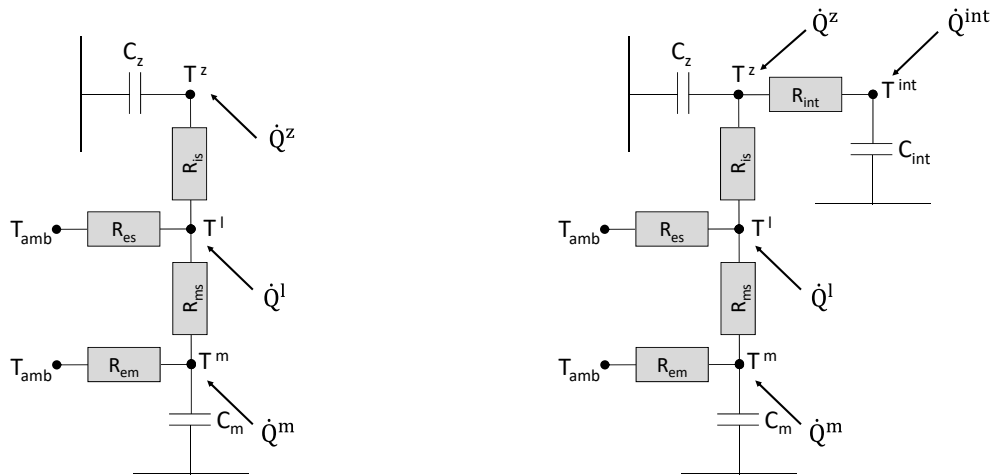
Figure 3.6 – Illustration of temperature profiles obtained with both reference and identified grey-box models.

Normalisation (2008) is illustrated in Figure 3.7a. In this model, a single lumped thermal capacitance, C_m , is used to represent the thermal capacity of all heavy components of the building structure. The

associated temperature node, T^m , is connected to the temperature node of massless components, T^l . The latter is then connected to the zone air temperature node T^z . Heat gains due to the heating system, internal gains and solar gains are distributed among the three nodes (\dot{Q}^m , \dot{Q}^l , \dot{Q}^z), depending on their respective convective and radiative shares.

Due to the use of a single lumped thermal capacitance for all external massive components, and to the fact that this capacitance is by-passed by a branch representing massless envelope components (R_{es}), the dynamic response of heavyweight buildings is not well captured by this model. In the present section, a modification of the model structure is proposed in order to better capture the dynamic response of such buildings.

For this, the thermal mass associated to internal walls and floors (C_{int}), as well as the influence of the stratification of the air in the zone (C_z) are modeled separately from the lumped thermal capacitance C_m , as illustrated in Figure 3.7b.



(a) Standard ISO13790 model proposed by Comité Européen de Normalisation (2008). (b) Modification of the standard model (ISO13790 – modified).

Figure 3.7 – ISO13790 single zone thermal network and proposed modifications.

For this new model, parameters and heat flow distribution are defined as follows (all variables are detailed in the Nomenclature section):

- thermal resistances are given by

$$R_{es} = \left(A_{lopw} \frac{1}{\frac{1}{U_{lopw}} - \frac{1}{h_{i,lopw}}} + A_{gl} \frac{1}{\frac{1}{U_{gl}} - \frac{1}{h_{i,gl}}} \right)^{-1} \quad (3.3)$$

$$R_{is} = \left(A_w \frac{1}{\frac{1}{h_{ci}} - \frac{1}{h_{is}}} \right)^{-1} \quad (3.4)$$

$$R_{ms} = (h_{is} A_m)^{-1} \quad (3.5)$$

$$R_{op} = \left(\sum_k A_{hopw,k} \frac{1}{\frac{1}{U_k} - \frac{1}{h_{i,k}}} \right)^{-1} \quad (3.6)$$

$$R_{em} = R_{op} - R_{ms} \quad (3.7)$$

$$R_{int} = (2h_{is}A_{int})^{-1} \quad (3.8)$$

where h_{ci} and h_{is} are respectively the indoor air convective coefficient and the combined radiative and convective coefficient, U in W/m^2K , A in m^2 and C in J/K are respectively the U-value, surface area and thermal capacity of a wall, and where

$$A_w = A_{hopw,tot} + A_{lopw} + A_{gl} \quad (3.9)$$

$$C_m = \sum_k \kappa_{hopw,k} A_{hopw,k} \quad (3.10)$$

$$A_m = \frac{C_m^2}{\sum_k \kappa_{hopw,k}^2 A_{hopw,k}} \quad (3.11)$$

where κ is the thermal capacity per surface area in J/m^2K and the subscripts *hopw*, *lopw* and *gl* stand for heavy and light opaque wall and glazing, respectively.

- heat flows are distributed on the temperature nodes as follows

$$\dot{Q}^z = f_{sol,c} \dot{Q}^{sol} + f_{int,c} \dot{Q}^{int,gains} + f_{h,c} \dot{Q}^h \quad (3.12)$$

$$\dot{Q}^l = P_{rl} (1 - f_{sol,c}) \dot{Q}^{sol} + P_{rl} \left((1 - f_{int,c}) \dot{Q}^{int,gains} + (1 - f_{h,c}) \dot{Q}^h \right) \quad (3.13)$$

$$\dot{Q}^m = P_{rm} (1 - f_{sol,c}) \dot{Q}^{sol} + P_{rm} \left((1 - f_{int,c}) \dot{Q}^{int,gains} + (1 - f_{h,c}) \dot{Q}^h \right) \quad (3.14)$$

$$\dot{Q}^{int} = P_{rint} (1 - f_{sol,c}) \dot{Q}^{sol} + P_{rint} \left((1 - f_{int,c}) \dot{Q}^{int,gains} + (1 - f_{h,c}) \dot{Q}^h \right) \quad (3.15)$$

where $f_{sol,c}$, $f_{int,c}$ and $f_{h,c}$ are respectively the convective share of the solar heat gains (\dot{Q}^{sol}), the internal heat gains ($\dot{Q}^{int,gains}$) and the heating power (\dot{Q}^h), and where

$$A_{tot} = A_{hopw,tot} + A_{lopw} + A_{gl} + A_{int} \quad (3.16)$$

$$P_{rm} = \frac{A_m}{A_{tot}} \quad (3.17)$$

$$P_{rint} = \frac{A_{int}}{A_{tot}} \quad (3.18)$$

$$P_{rl} = 1 - P_{rm} - P_{rint} \quad (3.19)$$

$$P_{rmd} = \frac{A_m}{A_{tot} - A_{gl}} \quad (3.20)$$

$$P_{rintd} = \frac{A_{int}}{A_{tot} - A_{gl}} \quad (3.21)$$

$$P_{rld} = 1 - P_{rmd} - P_{rintd} \quad (3.22)$$

Both initial and modified versions of the model have been tested on the case-study house. RMSE on the indoor temperature of 1.06 K and 0.23 K were found, respectively with the initial model and the proposed modifications. Cross-validation with another set of data led to a RMSE of 0.50 K with the new model, hereby highlighting the suitability of the proposed model improvement. A comparison of zone temperature profiles obtained with both the reference multi-zone model and the proposed grey-box model is illustrated in Figure 3.8 for three days during winter and summer periods.

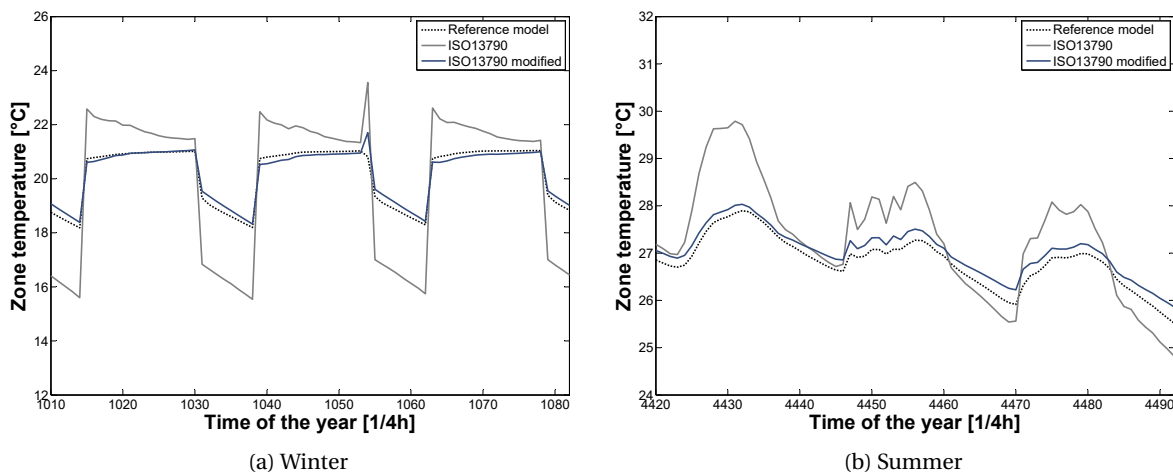


Figure 3.8 – Comparison of indoor temperature profiles obtained with the initial ISO13790 model and the proposed modifications (ISO13790-modified).

Although less accurate than trained grey-box models, this model can be useful to simulate large sets of diverse buildings. However, its ability to accurately represent the thermal behavior of different buildings must be verified. To that end, the model is tested with different fictitious buildings, derived from the test case-study as follows:

- a) The overall U value of the test-case building is divided by 2.
- b) The overall U value of the test-case building is multiplied by 2.
- c) The floor area of the test-case building is divided by 4.
- d) The floor area of the test-case building is multiplied by 4.

Table 3.2 – RMS error on indoor temperature prediction with the initial ISO13790 model and the proposed modification compared to the reference model for 4 cases: a) U-value divided by 2, b) U-value multiplied by 2, c) Floor area divided by 4, d) Floor area multiplied by 4.

	ISO13790	ISO13790 – modified
Case a)	0.82 K	0.51 K
Case b)	2.39 K	0.76 K
Case c)	1.16 K	0.72 K
Case d)	1.02 K	0.28 K

Results in terms of RMS errors on indoor temperature predictions are illustrated in Table 3.2 for both the ISO1390 model and its improved version, for annual simulations with a one-hour time step. In all cases, the modified version allows a significant reduction of the prediction errors, with values comprised between 0.28 K and 0.76 K. The model is therefore considered valid for use with heavyweight buildings of different geometries and insulation levels.

Finally, it can be noted that, if the parameters of the proposed modified model structure were identified, the RMSE for the K45 case-study house could only be reduced from 0.23 K to 0.22 K.

3.2.1.2 Black box models

Purely empirical models can also be used to model the thermal response of buildings. These models rely purely on data regression. In this section, auto-regressive models are investigated. The general formulation of auto-regressive exogenous models with moving average (ARMAX) can be summarized by

$$A(q)y_t = \sum_i B_i(q)u_t^i + C(q)\epsilon_t \quad (3.23a)$$

where y is the system output, u the system input, and

$$A(q) = 1 + a_1q^{-1} + a_2q^{-2} + \dots + a_{n_a}q^{-n_a} \quad (3.23b)$$

$$B_i(q) = b_{i,0} + b_{i,1}q^{-1} + b_{i,2}q^{-2} + \dots + b_{i,m_b}q^{-m_b} \quad (3.23c)$$

$$C(q) = 1 + c_1q^{-1} + \dots + c_{n_c}q^{-n_c} \quad (3.23d)$$

and q^{-k} is the back shift operator, such that $q^{-k}x_t = x_{t-k}$. The prediction error is the difference between the measured output y and the predictor \hat{y} :

$$\epsilon(t, \theta) = y_t - \hat{y}(t, \theta) \quad (3.23e)$$

where

$$\theta = [a_1 \dots a_{n_a} \quad b_{i,0} \dots b_{i,n_b} \quad c_1 \dots c_{n_c}] \quad (3.23f)$$

are the adjustable parameters, and where the predictor is given by

$$\hat{y}(t, \theta) = [1 - A(q)]y_t + B(q)u_t + C(q)\epsilon_t \quad (3.23g)$$

Similarly, the auto-regressive exogenous (ARX) model is expressed as

$$A(q)y_t = \sum_i B_i(q)u_t^i + \epsilon_t \quad (3.24)$$

Bacher and Delff (2014) proposed a methodology to identify the orders, n_a , n_b and n_c , based on the auto-correlation of the prediction error and its cross-correlation with the different inputs. The objective is to obtain white noise identification residuals. In this section, a similar method is applied

to identify orders and parameters of the following regression:

$$A(q)T_t^z = B_1(q)\dot{Q}_t^h + B_2(q)T_t^{amb} + B_3(q)I_t^{glob,h} + \epsilon_t \quad (3.25)$$

where \dot{Q}^h is the heat input, T^{amb} is the ambient temperature and $I^{glob,h}$ is the global solar irradiation on a horizontal surface.

Both ARX and ARMAX models are investigated on a 20-day period and for annual simulations. Results obtained with identification and cross-validation data sets are summarized in Table 3.3. Several conclusions can be drawn from these results. First, for a regression over a limited period of time with similar boundary conditions, such as several consecutive days during a given season of the year, both ARX and ARMAX regressions yield good results. The ARMAX model tends to slightly outperform the ARX model. For extended regression data including data with varied boundary conditions, such as yearly data, the ARMAX model is able to provide a better fit than the ARX model for the training data set. However, both models yield similar RMSE on the cross-validation data set.

Table 3.3 – RMSE on indoor zone temperature with ARX and ARMAX models for the K45 case-study house.

	20 days		yearly	
	ARX $n_a = 3, n_b = 2$	ARMAX $n_a = 2, n_b = 1, n_c = 1$	ARX $n_a = 4, n_b = 3$	ARMAX $n_a = 2, n_b = 1, n_c = 1$
Identification	0.15 K	0.11 K	0.51 K	0.27 K
Cross-validation	0.51 K	0.42 K	0.91 K	0.96 K

It is known that black-box models are not suitable for use with input data sets that differ from the identification set, and that they do not allow for extrapolation to other system characteristics. Nevertheless, they could be suitable for "on-line" identification schemes, in which model parameters are continuously updated based on new measurement data. In the remainder of this document, however, grey-box models are used instead.

3.2.2 Heat pumps

3.2.2.1 Heat sources/heat sinks and market trends in Belgium

Depending on the type of heat source/sink, heat pump technologies may be used for both heating and cooling applications. In Belgium, the most common types of heat pumps are ground-source and air-water heat pumps or heat pump water-heaters, as illustrated in Figure 3.9a. Heat pumps are typically used in new constructions or as retrofit option (Figure 3.9b).

3.2.2.2 Capacity control

Two main heat pump technologies are available on the market: fixed- and variable-speed heat pumps. Fixed-speed heat pumps are equipped with a single-speed compressor. Such systems are characterized by a simple regulation, which reduces the investment cost for the consumer. However, this implies that the heat pump always provides its full capacity. Therefore, if directly connected to the heat

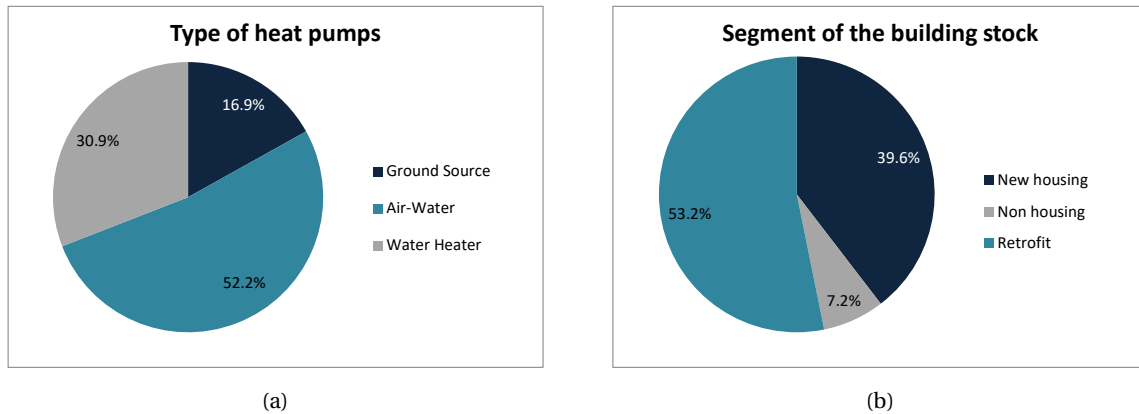


Figure 3.9 – Heat pump types (left) and segment of the building stock in 2012 in Belgium based on the number of units (right) (BRG Building Solutions (2013)).

emission system, the heat pump has to perform ON/OFF cycles over a period of time in order to meet the house heating requirements. Heat pump cycling significantly impacts the system performance through start-up losses, and reduces the lifetime of the system. To tackle this, such heat pumps are commonly installed with buffer tanks that reduce cycling. However, the latter tend to increase the average condensing temperature of the heat pump and hence the overall system losses as further discussed in Section 4.6.1.3. Variable-speed heat pumps, contrariwise, are equipped with variable-speed compressors whose frequency is adjusted by power electronics. This enables the heat pump to adjust the heating capacity by varying the compressor mass flow rate. This results in greater indoor comfort, enhanced life time and reduced energy consumption due to better performance at part-load (Karlsson (2007)). However, under a given part-load ratio (typically for 20-30% of full-load capacity), the control of the heat pump becomes similar to ON/OFF regulation. Consequently, variable-speed heat pumps are usually preferred over fixed-speed ones when providing heat directly to the hydraulic circuit of the heat emitters.

3.2.2.3 Performance modeling of air-to-water heat pumps

In this work, minimum simulation and control decision time steps are set to 900 seconds. The transient behavior of heat pumps is typically comprised within 30-90 seconds, and their dynamics is significantly faster than that of buildings. Therefore, only steady-state performance of heat pumps is modeled.

As proposed by Rivière (2004), the degradation in coefficient of performance (COP) of single-speed heat pumps due to cycling can be correlated to the external part-load ratio (PLR) as follows:

$$PLR = \frac{\dot{Q}}{\dot{Q}^{fl}} \quad (3.26)$$

$$\frac{COP}{COP^{fl}} = \frac{PLR}{aPLR + b} \quad (3.27)$$

where \dot{Q} is the building heat demand, \dot{Q}^{fl} is the heat pump full-load capacity, $a = 0.7701$ and $b = 0.2299$.

Steady-state performance of variable-speed heat pumps can be modeled using an empirical model proposed by Bolher et al. (1999). Full load performance is obtained based on the ambient and water supply temperatures (T^{amb} and T^{su}), expressed in K, in both rated and real conditions, and based on the rated heating capacity (\dot{Q}^{rat}). Equations (3.28a) to (3.28c) first determine the heat pump capacity (\dot{Q}^{fl}) and COP at full-load (COP^{fl}). The electrical consumption of the compressor at full-load is then given by Equation (3.28d).

$$\dot{Q}_t^{fl} = \left(d_0 + d_1 \left(T_t^{amb} - T^{amb, rat} \right) + d_2 \left(T_t^{su} - T^{su, rat} \right) \right) \dot{Q}^{rat} \quad (3.28a)$$

$$\Delta T_t = \frac{T_t^{amb}}{T_t^{su}} - \frac{T^{amb, rat}}{T^{su, rat}} \quad (3.28b)$$

$$COP_t^{fl} = \frac{COP^{rat}}{c_0 + c_1 \Delta T_t + c_2 \Delta T_t^2} \quad (3.28c)$$

$$\dot{W}_t^{fl} = \frac{\dot{Q}_t^{fl}}{COP_t^{fl}} \quad (3.28d)$$

In Bolher et al. (1999), the part-load electrical consumption of the variable-speed compressor, \dot{W}_t , is a quadratic function of the part-load heat ratio, given by

$$\dot{W}_t = (f_1 PLR + (f_2 - f_1) PLR + (1 - f_2) PLR^2) \dot{W}_t^{fl} \quad (3.29)$$

For part-load ratios below 20 or 30%, referred to as PLR_{ONOFF} , the compressor switches to ON/OFF capacity control, and a performance degradation law similar to Equation (3.27) is used:

$$\frac{COP}{COP_{ONOFF}} = \frac{\frac{PLR}{PLR_{ONOFF}}}{a \frac{PLR}{PLR_{ONOFF}} + b} \quad (3.30)$$

Parameters of the heat pump model, c_i , d_i and f_i , used in Equations (3.28) and (3.29) are calibrated based on manufacturer data.

Performance curves for both technologies are illustrated in Figure 3.10. They compare the ratio of part-load COP to full-load COP as a function of the part-load ratio.

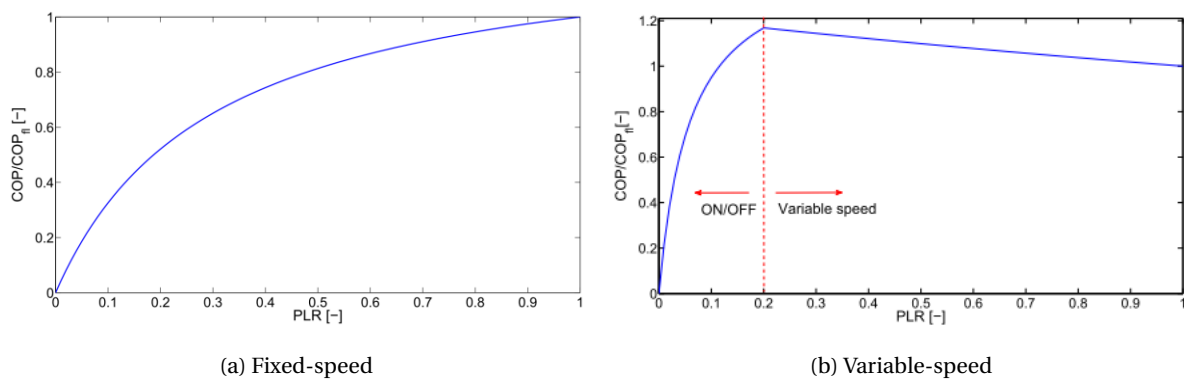


Figure 3.10 – Heat pump part-load performance as a function of the technology.

Technical constraints prevent the heat pump from working simultaneously to supply heat to the domestic hot water tank and for space heating. Moreover, to prevent the damage of mechanical components, decisions to start or stop the heat pumps should not occur more than eight times an hour. This precaution is ensured by decision time steps greater than 15 minutes.

3.2.3 Water tanks

In their review of modeling techniques for domestic hot water tanks, Dumont et al. (2016) propose a methodology to determine the suitable modeling approach depending on the application. CFD-based models provide the most accurate representation of all physical phenomena, but require large computational resources which make them unusable for real-time control applications. To tackle this, methods commonly used in the literature rely on fully-mixed tank models. The governing differential equation is

$$m_w c_w \frac{dT^w}{dt} = \dot{Q}^h - AU_{loss}(T^w - T^{surr}) - \dot{Q}_w \quad (3.31)$$

where T^w is the water temperature, m_w is the mass of water in the tank, c_w is the thermal capacity of water, \dot{Q}^h is the amount of heat supplied to the tank, \dot{Q}_w is the amount of heat withdrawn from the tank by DHW draw-off events, AU_{loss} is the heat transfer coefficient to the surrounding environment and T^{surr} is the temperature of the surrounding environment.

As emphasized by Baeten et al. (2016), one drawback of such simplified models is that they tend to underestimate the effective storage capacity. This hereby causes the heat pump to start more frequently than with stratified or moving-boundary tank models.

3.2.4 Exogenous electrical consumption and DHW consumption profiles

Load profiles for electrical consumption of appliances and lighting as well as domestic hot water draw-off events presented in Section 2.1.2 are used in the remainder of the document.

3.3 Control strategies

To manage energy use of buildings and systems, different control strategies can be implemented. The main underlying principles are recalled hereafter.

3.3.1 Heuristic control laws

Rule-based control (RBC) strategies, also known as heuristic control laws, are based on the definition of control rules that aim at achieving a given objective in a sufficient but sub-optimal manner. In building applications, heuristic laws are commonly used to reduce energy consumption while maintaining thermal comfort for the occupants. Given a set of inputs, such as ambient conditions and occupancy schedules, control rules are determined and applied to the different systems. Such control strategies rely on past experience or good practice. If the number of systems increases, or if the level of complexity of the systems increases, they become more challenging to define. In addition, due to the absence of

model of the controlled system, such control strategies are unable to adapt to unpredicted changes in boundary conditions.

Example of rule-based control strategies include:

- the implementation of temperature set backs, that consist in a reduction in zone temperature set point during unoccupied hours,
- the adjustment of water supply temperature of heat emitters according to outdoor conditions following a heating curve.

Additional rule-based control strategies are proposed in Chapter 4 in the context of load modulation with price-responsive heat pumps.

3.3.2 Optimal control laws

Optimal control of a system aims at finding a control sequence that satisfies an optimality criterion over a time horizon $\{0 : T\}$. The general formulation of the resulting constrained optimization problem can be written as

$$\min J(\mathbf{x}_0, \mathbf{u}(t), \mathbf{w}(t), t) = \int_0^T F(\mathbf{x}(t), \mathbf{u}(t), \mathbf{w}(t), t) dt \quad (3.32a)$$

subject to

$$\dot{\mathbf{x}} = f(\mathbf{x}(t), \mathbf{u}(t), \mathbf{w}(t)) \quad (3.32b)$$

$$\mathbf{x}_0 = \mathbf{x}(0) \quad (3.32c)$$

$$\mathbf{g}(\mathbf{x}(t)) \leq 0 \quad (3.32d)$$

$$\mathbf{h}(\mathbf{x}(t)) = 0 \quad (3.32e)$$

where \mathbf{x} are the state variables, \mathbf{u} the control variables and \mathbf{w} the disturbances. Equation (3.32b) represents the system dynamics. Equation (3.32d) stands for the set of inequality constraints and Equation (3.32e) for the equality constraints.

One can distinguish two categories of problems: convex and non-convex problems. The convexity of an optimization problem is verified if the cost function J is convex¹, and if the solution space is convex². Convexity guarantees the existence of a global optimum to the problem. Efficient solvers for such problems are readily available. Non-convex problems can be further divided into non-linear problems and mixed-integer problems (MIP). The latter are characterized by both continuous and integer variables which typically yield the feasible set to be non-convex. They can be linear (MILP) or non linear (MINLP). Although more difficult to handle than linear problems, efficient solvers are available to solve nonlinear problems. For mixed-integer problems, computationally-efficient solvers exist to solve linear problems, but very few are available for mixed-integer nonlinear problems.

¹A continuous, twice differentiable function of several variables is convex on a convex set if and only if its Hessian matrix is symmetric positive semidefinite on the interior of the convex set.

²A convex space is such that two points of the space can be joined by a line that does not exit the space. This requires all inequality constraints to be convex.

3.3.3 Model predictive control

Model predictive control (MPC) consists in solving a sequence of optimal control problems on a finite optimization horizon \mathcal{H} , also referred to as prediction horizon. As opposed to heuristic control, predictions of future system behavior are based on models of the systems embedded in the optimizer (Equation (3.32b)). The resulting control inputs are applied over a control horizon \mathcal{M} , with the number of periods M less than or equal to H . The prediction horizon is then shifted forward in time to the end of the control horizon, following a receding horizon control scheme. The receding horizon principle is illustrated in Figure 3.11.

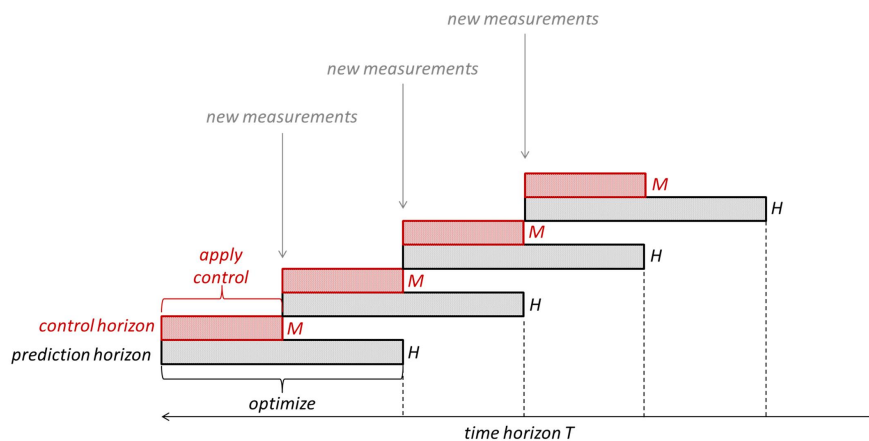


Figure 3.11 – Receding horizon control scheme.

Compared to other control mechanism, such as PID controllers, model predictive control allows (Maciejowski (2002), Kvasnica (2014))

- taking into account constraints on both state and control variables,
- the optimization of a performance objective on the prediction horizon,
- a good approximation of the optimal "infinite" horizon trajectory at reduced computational cost,
- taking into account possible disturbances,
- tackling systems with multiple inputs/outputs (MIMO).

One distinguishes conventional or tracking MPC, for which the objective is to steer the system to the economically optimal steady-state operation (Ellis et al. (2014)), and economic MPC (EMPC) that optimizes the process economics over the prediction horizon and performs a time-varying operation of the system (Tran et al. (2014)). The general EMPC scheme is depicted in Figure 3.12.

Control and prediction horizons are such that $M \leq H$. This condition allows avoiding the use of terminal constraints on the states. Their choice influences the ability of the MPC scheme to approximate the optimal control trajectory over the entire horizon $\{0, T\}$. Short control and prediction horizons lead to aggressive control strategies. The larger the prediction horizon, the closer the control inputs to the optimal control trajectory on an "infinite" horizon. In practice, control and prediction horizon lengths are dictated by the time constants of the disturbances and system, respectively. For example, for heavy-weight insulated residential buildings, the settling time of the system can reach several days. Weather conditions, such as solar irradiation, contrariwise, present daily fluctuation patterns. In this case, a

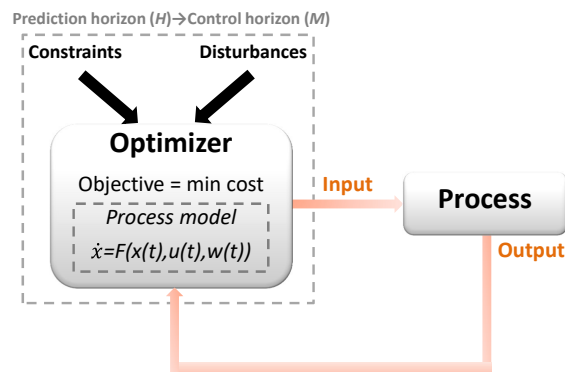


Figure 3.12 – General economic model predictive control scheme.

good approximation of the "infinite" horizon solution is obtained by setting the prediction horizon to the time constant of the building and the control horizon to the period of external disturbances.

Three EMPC strategies are further investigated in Chapters 4 to 6. All resulting optimization problems are linear or MILP problems. They are solved using Cplex solver (ILOG (2013)).

3.3.4 Linearization of heat pump performance model

In general, the water supply temperature and part-load ratio have an effect on the coefficient of performance of an air-to-water heat pump. As pointed out by Verhelst et al. (2012), this dependency turns optimization problems aiming at the minimization of electricity consumption/cost into non-linear and non-convex problems.

In the case of direct space-heating, one solution consists in considering a constant coefficient of performance or in modeling its dependency on ambient conditions only. According to Verhelst et al. (2012), the first solution shows the best approximation of the optimal non-convex problem. Another solution consists in setting the water supply temperature according to a heating curve adapted to the outdoor temperature. As demonstrated by Verhelst et al. (2012) however, this may also yield a suboptimal control of the heat pump in the context of demand-side management, due to the imposed limitation in heating capacity. Nevertheless, this allows to model changes in performance at part-load. In the case of variable-speed heat pumps, the electrical power consumption is a convex function of the part-load ratio, as illustrated in Figure 3.13. The heat pump performance tends to increase at part-load. For part-load ratios below a certain threshold (20 - 30 %) however, heat pump performance degradation due to cycling and auxiliary consumption becomes significant (Figure 3.13 - left).

In practice, when used to supply both space-heating and domestic hot water, the heat pump can only work in one mode at a time. For the optimization problem formulation, this is translated by the use of a Boolean variable (Chapter 6). In this case, the fact that the compressor power is different from zero at a no-load ratio cannot be taken into account anymore. Therefore, the performance curve illustrated in Figure 3.13 (right) is used instead.

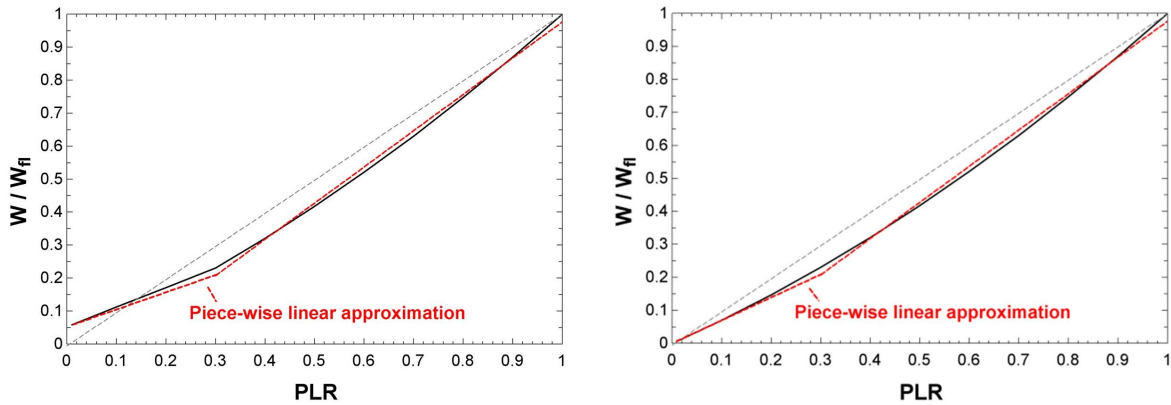


Figure 3.13 – Illustration of part-load performance of variable-speed heat pump: with auxiliary consumption (left) and without auxiliary consumption (right).

The quadratic function can be replaced by a piecewise-linear approximation, as follows:

$$\dot{W} = (X_1 + X_2)\dot{W}^{fl} \quad (3.33a)$$

where

$$PLR = PLR_1 + PLR_2 \quad (3.33b)$$

$$X_1 = f_1 PLR_1 \quad (3.33c)$$

$$X_2 = f_2 PLR_2 \quad (3.33d)$$

$$0 \leq PLR_1 \leq PLR_1^{max} \quad (3.33e)$$

$$0 \leq PLR_2 \leq PLR_2^{max} \quad (3.33f)$$

In this example, PLR_1^{max} and PLR_2^{max} are set to 0.3 and 0.7, respectively. This linearization method is used in Chapters 4 and 6.

When the heat pump is connected to a water tank, taking into account heat pump performance degradation with the water tank temperature level turns the optimization problem into a non-convex problem as well. Two options arise:

- one can assume the COP as constant, or to be only dependent on outdoor temperature. This assumption is chosen in Chapters 6 and 8.
- in the case of space-heating, the water temperature in the tank is constrained to be greater than the heating curve by an increment ΔT (see Section 4.4.1). In the case of domestic hot water production, a minimum temperature of 50°C is needed to meet health and safety requirements. Finally, due to technical limits, the maximum temperature level is set to 65°C. In light of this, the heat pump full-load capacity can be approximated by taking the average between those temperature levels. This assumption allows to model changes in heat pump performance at part-load, as illustrated in Figure 3.13 (right). This assumption is chosen in Chapters 4 and 7.

Load modulation strategies at the building scale **Part III**

4 Optimal management of price-responsive heat pumps for load shifting

4.1 Motivations

As explained in Section 1.2.2, the management of electricity grids requires the supply and demand of electricity to be in balance at any point in time. To ensure grid balancing, several levels of action take place at different times. On the day-ahead electricity market, electricity retailers have to nominate their electricity bids such that forecasted supply and demand are in balance. At the intraday-level, mismatches between forecasted and actual supply and demand can be compensated for by reserve capacity or by real-time demand response.

Smart Grid Energy ready Buildings¹ can help minimizing the cost of electricity supply at the distribution grid level in three different ways. A first one is to predict electricity demand profiles associated to local consumers equipped with smart metering devices as accurately as possible. A second one is to minimize the procurement costs of electricity by shifting flexible loads from peak to off-peak hours. A third one is to minimize the imbalance costs resulting from mismatches between forecasted supply and demand, by real-time demand response.

On the day-ahead, one incentive to support demand-side participation consists in offering consumers time varying electricity tariffs that reflect those procurement costs (Faruqui et al. (2012)). Price-responsive domestic systems include large appliances, such as dishwashers, washing machines and tumble dryers, as investigated by EnergyVille (2014), electric DHW heaters and electricity-driven heating and cooling systems. In particular, heat pumps coupled to thermal energy storage systems offer great load shifting potential (Arteconi et al. (2013)). Sensible storage options commonly investigated include building thermal mass (Braun (1990)) and water tanks (Miara et al. (2014)). Two questions then arise:

- *what type of control strategy responds best to the price incentive?*
- *how does it influence flexibility potential and retailers and consumers' economics?*

As emphasized by Braun (1990), conventional heuristic control laws do not unlock the potential of thermal storage in the building structure to reduce system operation costs. However, optimal control of building thermal mass storage allows for significant energy cost reduction through load shifting and

¹The contributions of Gabrielle Masy, Clara Verhelst and the members of the FLEXIPAC Consortium for this chapter are gratefully acknowledged. For further information, the reader is referred to the study of Masy et al. (2015a).

peak shaving. Embedded model predictive control has been identified as an appropriate methodology for optimal load shifting in response to electricity price signals in several studies (Halvgaard et al. (2012), Ma et al. (2012)). However, De Coninck et al. (2014) warn that the extra benefits retrieved from such control strategy might not be worth the extra computational requirements, compared to suitable rule-based control laws. In terms of storage options, most studies focus on using building thermal mass or DHW tanks. Although less widespread in practice, some heat pump systems include a separate storage tank either for heating (Miara et al. (2014), Floss and Hofmann (2015)) or for cooling (Palacio et al. (2014)). The study of Miara et al. (2014) is limited to rule-based control strategies for demand-side management. The study of Floss and Hofmann (2015) proposes different hydraulic configurations of the storage tanks. The impact of these configurations on the potential for demand-side management is studied in detail in Chapter 7.

In the present chapter, the objective for the electricity retailer is to minimize his electricity procurement costs on the day-ahead market. Since the control of flexible loads belongs to end-users, the retailer chooses to use real-time pricing as an incentive to promote load shifting from peak to off-peak hours. The objective for the end-user is to minimize his electricity cost, while satisfying thermal comfort in the house. In light of the literature survey, this chapter proposes the following contributions:

- a throughout investigation of rule-based versus optimal control strategies of price-responsive heat pumps used for space heating, and coupled to different thermal storage options: building thermal mass and extra space-heating water tank,
- the definition of new demand flexibility indexes,
- the addition of a feedback loop to the optimal controller to take into account model mismatch and prediction uncertainties.

The methodology is illustrated with case-studies of buildings in the Belgian context.

4.2 Electricity price profile

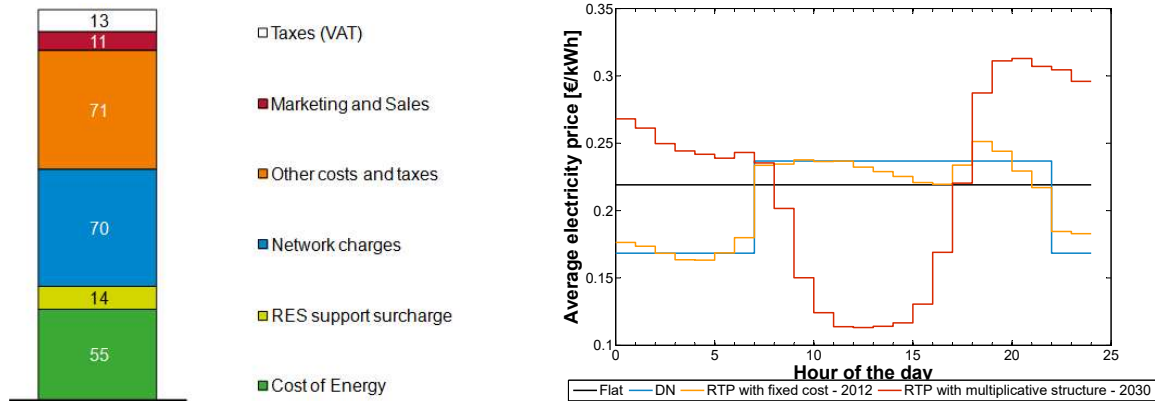
In Belgium, different tariff structures are already implemented for residential customers, following flat and day-night (DN) pricing schemes. Historically, the DN pricing scheme has been introduced as an incentive to promote energy consumption during off-peak hours. So far, residential consumers are therefore exposed to retail tariffs with a very low time-varying character. In order to support demand participation and efficient use of distributed energy resources, it is recommended to move away from fixed rates by making them more time varying (Faruqui et al. (2012)).

Since the liberalization of the electricity market, Belpex, a power exchange for short-term trading, has been launched and provides the market with transparent prices. One of its segments, the Belpex Day-Ahead Market, focuses on day-ahead trading. Real-Time Pricing (RTP) tariffs aligned on day-ahead market prices constitute the best available signal to reflect the marginal value of electricity. Retail tariffs, however, are not only based on spot prices but also include fixed “residual network costs”, as illustrated in Figure 4.1a for a residential retail tariff. Therefore, two types of dynamic tariff structures can be investigated. The first tariff structure follows a RTP scheme with fixed “residual network costs”. The part related to the energy cost is the only time-varying component. It is illustrated for year 2012 in Figure 4.1b. The second structure is a multiplicative dynamic tariff proposed by Stratmann (2014).

This structure is based on the assumption that the “residual network costs” are, on the one hand, recovered on a volumetric basis, and, on the other hand, also aligned on the day-ahead market prices. This solution, compared to RTP with fixed costs, enables a much stronger market signal with a better emphasis of peak and off-peak hours. In this approach, the final retail price is calculated by multiplying the day-ahead spot price by a multiplicative factor. The multiplicative factor is such that the average consumer’s bill is the same under both multiplicative and flat-rate structures. As proposed by CEEME (2015), synthetic load profiles (SLP) representing the consumption profile of an average consumer and provided by the system operator (Synergrid (2012)) can be used. The multiplicative factor, β , is then given by

$$\beta = \frac{\sum_t SLP_t \pi^{flat}}{\sum_t SLP_t \pi^{DA}} \quad (4.1)$$

where π^{flat} is the flat retail tariff and π^{DA} is the day-ahead spot market price. CEEME (2015) proposed a prospective evolution scenario of spot market prices by year 2030 with 43% renewable energy sources. The resulting dynamic tariff structure is illustrated in Figure 4.1b for an average day over the year. Further information regarding the prospective energy mix used to establish this tariff can be found in Annex A.3.1.



(a) Example retail tariff breakdown in Belgium in 2012. Values provided are in euro per MWh. The total is 234 €/MWh.

(b) Daily average tariff structures.

Figure 4.1 – Retail tariff breakdown and structures.

It should be noted that the electricity price profiles used for the retailer correspond to day-ahead market prices and therefore differ from those of residential end-users, which include all other charges and taxes (Figure 4.1a).

4.3 Case-study buildings and systems

The case-study building used in this chapter is a typical concrete-structure freestanding house described in Section 3.1. Two different insulation levels are considered,

- the K45 level, which corresponds to the Belgian standards for newly built houses before 2014. The overall U-value is 0.46 W/m²K, with an air change rate n_{50} equal to 6,

- the K30 level, which corresponds to an overall U-value of 0.305 W/m²K, with an air change rate n_{50} of 3 ACR.

Buildings are modeled using trained grey-box models whose structure differs slightly to accommodate two heating emission system options: hydronic radiators and floor-heating system. For example, the RC networks are illustrated in Figure 4.2 for the K30 building. The procedure to identify the model parameters follows the method presented in Section 3.2.1.1. Annual RMS errors on zone temperature of 0.55 K and 0.49 K were found respectively for the K45 and K30 houses with radiators, and of 0.43 K and 0.42 K for the K45 and K30 houses with floor heating, respectively.

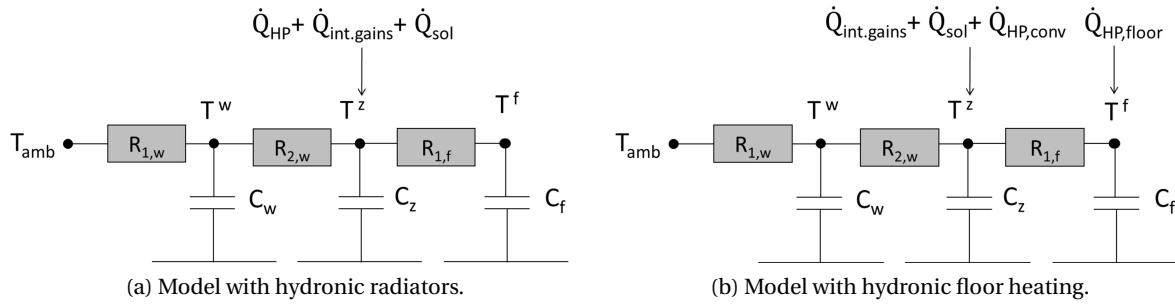


Figure 4.2 – Grey-box models for the K30 building equipped either with radiators or with floor heating.

Each house is equipped with an air-to-water heat pump sized to cover 80% of the space-heating demand in design conditions, i.e. for an outdoor temperature of -10°C. In this chapter, the heat pump is used to provide space heating only. Three thermal storage options are investigated for space heating:

- storage in the building envelope with conventional radiators,
- storage in the building envelope with floor heating system,
- storage in a water tank following a parallel four-pipe configuration: the heat pump is connected to the water tank, which in turn, is used to supply the house, as illustrated in Figure 4.3.

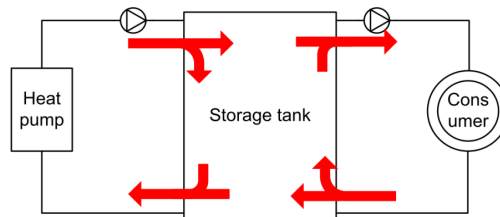


Figure 4.3 – Parallel four-pipe configuration for SH water tank storage.

When directly supplying the heat emission system, the heat pump used is a variable-frequency technology, whereas when connected to the water tank, both variable-frequency and single-speed technologies are considered. Their performance is modeled using the empirical laws presented in Section 3.2.2. The water supply temperature, $T^{w,su}$, is adapted to the house insulation level and adjusted as a function of the ambient temperature, T^{amb} , following a heating curve, such that

$$T^{w,su} = T^{w,su,max} - \frac{\Delta T^{w,su,rat}}{\Delta T^{amb,rat}} (T^{amb} - T^{amb,min}) \quad (4.2)$$

The heat supplied by the heat emission system is modeled using empirical emission laws functions of the difference between the average water temperature in the emitter, \bar{T}^w , and the room temperature, T^z . For conventional radiators, the emission law is given by²

$$\dot{Q}^{rad,max} = \left(\frac{\bar{T}^w - T^z}{(\bar{T}^w - T^z)_{rat}} \right)^{1.3} \dot{Q}^{rad,rat} \quad (4.3)$$

The average emitter surface temperature is replaced by the average water temperature, expressed as the average of the supply temperature, dictated by the heating curve, and the return temperature. The latter is assumed to be 10K lower than the supply temperature. Olesen (2009) proposed the following correlation to model the heat emission by heating floors³

$$\dot{Q}^{hf,max} = 8.92 A_{floor} (\bar{T}^w - T^z)^{1.1} \quad (4.4)$$

where A_{floor} is the floor surface area.

4.4 Control strategies

The building and tank models allow the use of a discrete linear state-space representation of the system summarized by

$$\mathbf{x}_{t+1} = \mathbf{A}\mathbf{x}_t + \mathbf{B}\mathbf{u}_t + \mathbf{E}\mathbf{w}_t \quad (4.5)$$

where \mathbf{x} is the state space variable vector composed of the zone, wall, floor temperatures and of the space heating water tank temperature when the latter is used as storage,

$$\mathbf{x}_t^T = [T^z, T^w, T^f, T^{SH,tank}] \quad (4.6)$$

\mathbf{u} is the vector of control variables, namely the heating rate provided by the heat pump directly to the heat emitters, $\dot{Q}^{HP,hem}$, or to the water tank, $\dot{Q}^{HP,tank}$, depending on the storage option. When connected to the water tank, a second control variable representing the amount of heat withdrawn from the water tank to supply the radiators, \dot{Q}^{tank} , is added. \mathbf{w} is the vector of disturbances, i.e., outdoor air temperature, internal gains due to occupants, appliances and lighting, and solar gains.

$$\mathbf{w}_t^T = [T^{amb}, \dot{Q}^{int.gains}, \dot{Q}^{sol}] \quad (4.7)$$

The total electricity consumption of the consumer at time t , P_t^{cons} , is composed of the consumption of the heat pump, \dot{W}_t^{HP} , and of the backup electric heater, P_t^{bh} .

4.4.1 Optimal predictive control in response to price incentive

The objective of the optimal predictive control (OPC) scheme is to minimize the electricity cost for the consumer in response to incentive retail tariffs on a prediction horizon \mathcal{H} , assuming perfect foresight.

²Source: Architecture et Climat and Service public de Wallonie.

³The correlation uses the temperature difference between the average floor surface temperature and the room design operative temperature. In this chapter, these are approximated by the average water temperature and room temperature.

The cost function is

$$\min \sum_{t \in \mathcal{H}} P_t^{cons} \pi_t \quad (4.8)$$

with respect to the decision variables, and subject to

$$x_t^{min} \leq x_t \leq x_t^{max} \quad \forall t \in \mathcal{H} \quad (4.9)$$

$$u_t^{min} \leq u_t \leq u_t^{max} \quad \forall t \in \mathcal{H} \quad (4.10)$$

where π_t is the retail electricity price, and Constraints (4.9) and (4.10) depend on the considered storage option.

The storage potential in the building thermal mass can be unlocked by allowing the zone temperature to vary around the reference set point, as expressed by Constraint (4.9). However, occupants' thermal comfort should be satisfied at all times. ASHRAE standard 55 (American Society of Heating, Refrigerating and Air-Conditioning Engineers (ASHRAE (1992))) defines acceptable indoor air temperature variation rates that respect occupants' comfort. In this standard, the temperature variation should not exceed 2.2 K during a one-hour period, and 1.1 K during any quarter of that period. With a one-hour time step, comfort requirements can be met by allowing a 1 K temperature range around the reference set point in the winter. In the summer, the upper limit of Constraints (4.9) can vary, since no cooling system is considered in this chapter.

For the thermal power supplied by the heat pump, Constraint (4.10) translates as

$$0 \leq Q_t^{HP,hem} \leq \min(\dot{Q}_t^{HP,fl} + P^{bh}, \dot{Q}_t^{rad,max}) \quad (4.11)$$

for conventional radiators, and as

$$0 \leq \dot{Q}_t^{HP,hem} \leq \min(\dot{Q}_t^{HP,fl} + P^{bh}, \dot{Q}_t^{hf,max}) \quad (4.12)$$

for floor heating.

When using a water tank as storage option, the indoor temperature is set to strictly follow the set point, and the flexibility potential is unlocked by increasing temperature levels in the tank. Constraints (4.9) and (4.10) become

$$T_t^{w,su} + \Delta T \leq T_t^{SH,tank} \leq T^{SH,tank,max} \quad (4.13a)$$

$$\begin{bmatrix} 0 \\ 0 \end{bmatrix} \leq \begin{bmatrix} \dot{Q}_t^{tank} \\ \dot{Q}_t^{HP,tank} \end{bmatrix} \leq \begin{bmatrix} \dot{Q}_t^{rad,max} \\ \dot{Q}_t^{HP,fl} + P^{bh} \end{bmatrix} \quad (4.13b)$$

where ΔT is used to ensure that the temperature of water supplied to the emission systems meets comfort requirements and to reduce heat pump cycling. Perfect predictions of the electricity retail tariff, internal gains and weather conditions are assumed for the purpose of evaluating the load shifting opportunities. Based on the known future inputs, the optimizer determines an optimal control response that minimizes the objective function of Equation (4.8) over the prediction horizon \mathcal{H} and then applies the control inputs over a defined control horizon \mathcal{M} , with \mathcal{M} less than \mathcal{H} . The prediction

horizon is then shifted forward in time to the end of the control horizon, following a receding horizon control scheme. The condition \mathcal{M} less than \mathcal{H} replaces the use of terminal constraints on the states.

4.4.2 Rule-based control

4.4.2.1 Reference consumption profile

To compare different control strategies, a reference consumption profile is defined. The reference profile corresponds to the electricity consumption that satisfies thermal comfort in the absence of price incentive. For thermal storage in the building thermal mass, the consumption profile is obtained by forcing the zone temperature in Equation (4.5) to follow a given set point schedule. The heat pump power is constrained to be the minimum between the heat pump capacity at full load with auxiliary heater and the maximum amount of heat that can be supplied by the emission system, i.e.,

$$T_t^z = \mathbf{C}\mathbf{x}_t = \begin{bmatrix} 1 & 0 & 0 \end{bmatrix} \mathbf{x}_t \quad (4.14a)$$

$$\dot{Q}_t^{HP,hem} = \min \left((\mathbf{CB})^{-1} (T_{t+1}^{sp} - \mathbf{C}\mathbf{A}\mathbf{x}_t - \mathbf{C}\mathbf{E}\mathbf{w}_t), \min \left(\dot{Q}_t^{rad/hf,max}, \dot{Q}_t^{HP,fl} + P^{bh} \right) \right) \quad (4.14b)$$

For storage in a space heating water tank, the amount of heat that can be withdrawn from the water tank is dictated by the emission law of radiators. Water temperature lower and upper bounds are respectively 5 K above the heating curve and 65°C, the latter corresponding to the technical limit of the heat pump. To prevent the heat pump from cycling, the tank is heated exclusively when the temperature drops below the lower bound, and up until the upper temperature bound is reached.

$$\begin{bmatrix} T_t^z \\ T_t^{SH,tank} \end{bmatrix} = \mathbf{C}\mathbf{x}_t = \begin{bmatrix} 1 & 0 & 0 & 0 \\ 0 & 0 & 0 & 1 \end{bmatrix} \mathbf{x}_t \quad (4.15a)$$

$$T_t^{w,su} + \Delta T \leq T_t^{SH,tank} \leq T_t^{SH,tank,max} \quad (4.15b)$$

$$\begin{bmatrix} \dot{Q}_t^{tank} \\ \dot{Q}_t^{HP,tank} \end{bmatrix} = \min \left((\mathbf{CB})^{-1} \left(\begin{bmatrix} T_{t+1}^{sp} \\ T_t^{h,tank,max} \end{bmatrix} - \mathbf{C}\mathbf{A}\mathbf{x}_t - \mathbf{C}\mathbf{E}\mathbf{w}_t \right), \begin{bmatrix} \dot{Q}_t^{rad,max} \\ \dot{Q}_t^{HP,fl} + P^{bh} \end{bmatrix} \right) \quad (4.15c)$$

4.4.2.2 Rule-based control response to price incentive

The optimal control scheme is computationally expensive, and assumes perfect prediction of all disturbances. In practice, the optimal trajectory can be approximated by heuristic laws, also referred to as rule-based control (RBC). To that end, the objective function (4.8) can be translated into the definition of price thresholds to trigger load shifting⁴. For storage in the building thermal mass, a low price threshold can be introduced as follows

$$\pi_d^{low} = \pi_d^{min} + p(\pi_d^{max} - \pi_d^{min}) \quad (4.16)$$

It is defined on a daily basis. π_d^{min} and π_d^{max} are respectively the daily minimum and maximum day-ahead prices. The adjustment of parameter p is discussed in Section 4.6.2.

The control strategy then consists in storing energy when the electricity retail price is below the low

⁴The author would like to acknowledge the contribution of Pierre Garsoux to this section (for more information: Georges et al. (2016).)

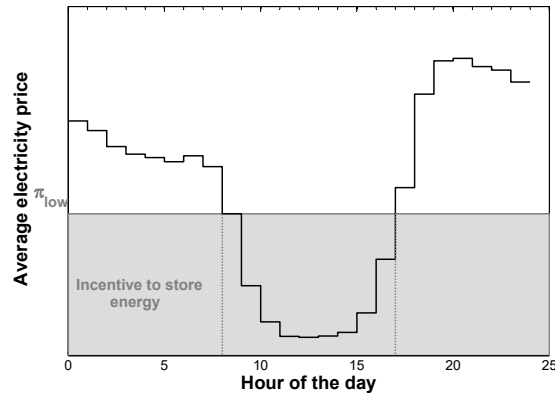
threshold π_d^{low} . This can be performed by raising the temperature set point to its upper limit, i.e.,

$$T_t^{sp} = T^{sp,max} \quad (4.17)$$

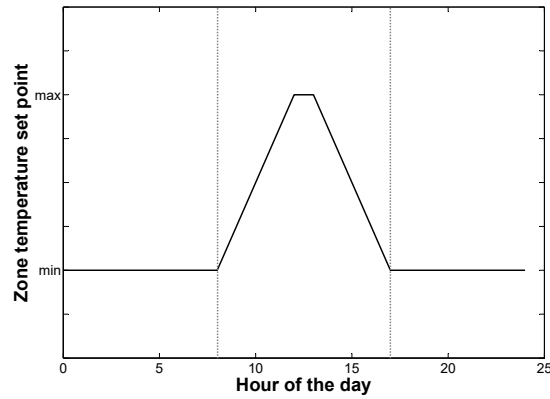
However, as discussed in Section 4.6.2, such control strategy is too reactive, and leads to significant overconsumption that limits consumer's cost savings. A more suitable strategy consists in adjusting the temperature set point proportionally to the difference between the current electricity price, π_t , and the daily minimum value

$$T_t^{sp} = T^{sp,max} - \frac{T^{sp,max} - T^{sp,min}}{\pi_d^{low} - \pi_d^{min}} (\pi_t - \pi_d^{min}) \quad (4.18)$$

This approach is illustrated in Figure 4.4.



(a) Price threshold.



(b) Corresponding temperature set point.

Figure 4.4 – Illustration of RBC strategy for storage in the building thermal mass.

For storage in a space-heating water tank, the study of Miara et al. (2014) proposed rule-based control strategies for the adjustment of the temperature level in the tank. The approach consists in dividing the electricity price reflecting the daily residual load in different zones. Below the low threshold, set to 25% of the daily normalized residual load in the study, the temperature set point is increased by 10 K. The high threshold is set to 50%. Between the low and high thresholds, the temperature set point is increased by 5 K.

A similar control strategy can be implemented based on price levels, as proposed for the storage in the building thermal mass. Two different approaches are investigated. In a first approach, it is proposed to follow the temperature adjustment proposed by Miara et al. (2014) and to quantify the impact of the chosen low and high thresholds. To that end, those thresholds are defined based on adjustable parameters, p_1 and p_2 , such that

$$\pi_d^{low} = \pi_d^{min} + p_1(\pi_d^{max} - \pi_d^{min}) \quad (4.19a)$$

$$\pi_d^{high} = \pi_d^{max} - p_2(\pi_d^{max} - \pi_d^{min}) \quad (4.19b)$$

Parameters p_1 and p_2 can be tuned to approximate the optimal solution, as discussed in Section 4.6.2. In a second approach, the maximum temperature level is adjusted linearly with the electricity price as follows

$$T_t^{tank,high} = T^{tank,max} - \frac{T^{tank,max} - T_t^{tank,min}}{\pi_d^{low} - \pi_d^{min}} (\pi_t - \pi_d^{min}) \quad (4.20)$$

In this formulation, only the low price threshold of Equation (4.19) is used. The control strategy consists in storing energy when the electricity retail price is below the low threshold, π_d^{low} . Parameter p_1 can be tuned to approximate the optimal solution, as discussed in Section 4.6.2. Both control approaches are illustrated in Figure 4.5.

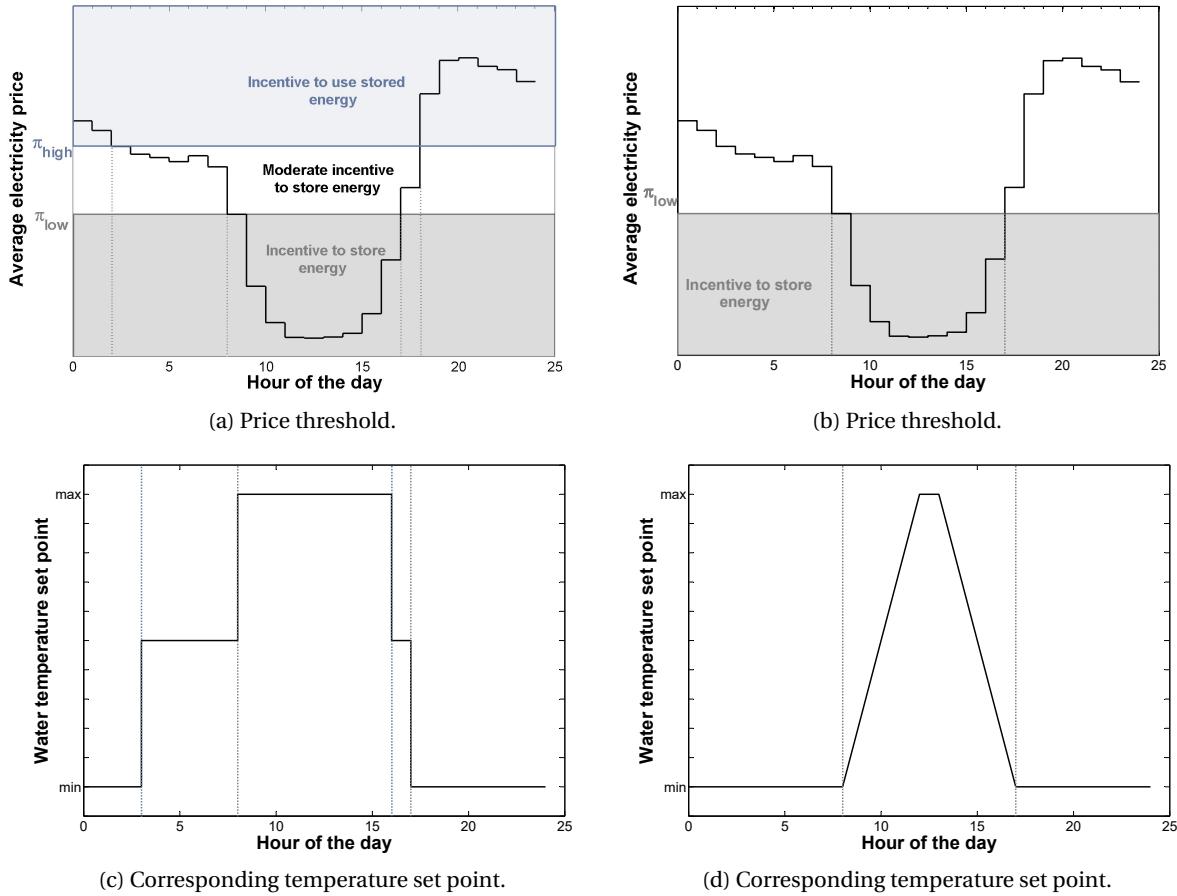


Figure 4.5 – Illustration of RBC strategy for storage in water tanks: based on Miara et al. (2014) (left) and proposed modification (right).

4.5 Flexibility metrics

In his review of metrics describing grid interaction and flexibility of buildings, Klein (2016) highlighted different flexibility indexes including demand price-elasticities (Bruninx et al. (2013) and Venkatesan et al. (2012)), flexibility indexes based on duration-based (Six et al. (2011b) and Stinner et al. (2015)) and price-based load shifting indexes (Dar et al. (2014) and Masy et al. (2015a)). In particular, Dar et al. (2014) and Masy et al. (2015a) propose two similar metrics to determine the ability of control strategies to shift loads in response to incentive retail prices. The index proposed in Masy et al. (2015a) is defined as follows

$$FI = \frac{\sum_t P_t \pi_{d,t}^{max} - \sum_t P_t \pi_t}{\sum_t P_t \pi_{d,t}^{max} - \sum_t P_t \pi_{d,t}^{min}} \quad (4.21)$$

where $\pi_{d,t}^{max}$ and $\pi_{d,t}^{min}$ are respectively the maximum and minimum daily retail tariffs.

The main drawback of these indexes is that they do not penalize the overconsumption in the calculation of the flexibility potential. This implies that an inefficient control strategy that would increase the consumption during low price periods without decreasing it later on could lead to an increase in flexibility index. This would cause pure overconsumption without providing any actual load shifting. This case is unprofitable from both the consumer's and the electricity retailer's standpoints.

To overcome this issue, the consumption profile resulting from a price-based control strategy, P_t , must be compared to a reference scenario with no load shifting incentive, P_t^{ref} . Equation (4.21) is modified as follows:

$$FI = \frac{\sum_t P_t^{ref} \pi_{d,t}^{max} - \sum_t P_t \pi_t}{\sum_t P_t^{ref} \pi_{d,t}^{max} - \sum_t P_t^{ref} \pi_{d,t}^{min}} \quad (4.22)$$

This definition should however only be used with positive prices. Indeed, negative prices could also lead to pure overconsumption, while still resulting in an increase of the flexibility index.

Two other metrics arise from the definition of the flexibility index. The average electricity price, which represents the price at which the average consumption occurs, is defined by

$$\pi^{avg} = \frac{\sum_t P_t \pi_t}{\sum_t P_t} \quad (4.23)$$

The effective volume shifted in time is then defined by (Masy et al. (2015a))

$$VS = \frac{FI - FI^{ref}}{FI^{ref}} \quad (4.24)$$

where

$$FI^{ref} = \frac{\sum_t P_t^{ref} \pi_{d,t}^{max} - \sum_t P_t^{ref} \pi_t}{\sum_t P_t^{ref} \pi_{d,t}^{max} - \sum_t P_t^{ref} \pi_{d,t}^{min}} \quad (4.25)$$

Load shifting may yield overconsumption, which is defined as the increase in electricity consumption,

compared to the consumption in the absence of incentive tariff.

$$OC = \frac{E - E^{ref}}{E^{ref}} \quad (4.26a)$$

where

$$E = \sum_t P_t \Delta t \quad (4.26b)$$

Cost saving entailed by price-induced load shifting is given by

$$CS = \sum_t P_t \pi_t - \sum_t P_t^{ref} \pi_t \quad (4.27)$$

4.6 Results and analyses

The method is applied to both K30 and K45 buildings for climatic year 2012. The simulation time step is one hour. For the optimal control strategy, the control and prediction horizons are set respectively to 24 and 72 hours.

4.6.1 Optimal load shifting

4.6.1.1 Definition of a reference load profile

To compare different control strategies, a reference consumption profile is needed. The reference profile corresponds to the electricity consumption that satisfies thermal comfort in the absence of price incentive, or equivalently, for a flat retail tariff. A question arises regarding the definition of the reference set point temperature, and its corresponding lower and upper bounds defined in Constraint (4.9). A first option would consist in imposing the minimum and maximum bounds symmetrically around the set point. A second option would consist in defining the reference set point as the lower bound of Constraint (4.9). The two options and their implications are illustrated on the K45 building with thermal mass as storage option. Two tariff structures are compared: a flat and a sinusoidal time-varying price profile. In the first case, a constant reference set point of 21°C is chosen, and maximum temperature deviations of 1 K around the set point are allowed. In the second case, a constant reference set point of 20°C is chosen, and maximum temperature deviations of 2 K above the set point are allowed. The resulting load profiles are presented in Figure 4.6 for an average winter day.

With the flat tariff, the optimal control strategy results in a zone temperature that tends to strictly follow the set point. The slight temperature overshoot observed after 4pm is due to the limited heat pump capacity. In order to avoid using the backup resistance heater, the optimal controller slightly preheats the room by raising the temperature above the set point. With the time varying tariff, the optimal control drives the room temperature towards its lowest bound when the electricity price is high, and towards its highest bound when the latter is low. If the reference temperature set point is set to 21°C, the load shifting strategy with optimal control and sinusoidal tariff results in an average daily room temperature 0.47 K lower than with the flat tariff. The total cost saving for the consumer reaches 17%, out of which 41% is brought by load shifting and 59% is due to the lower temperature level and

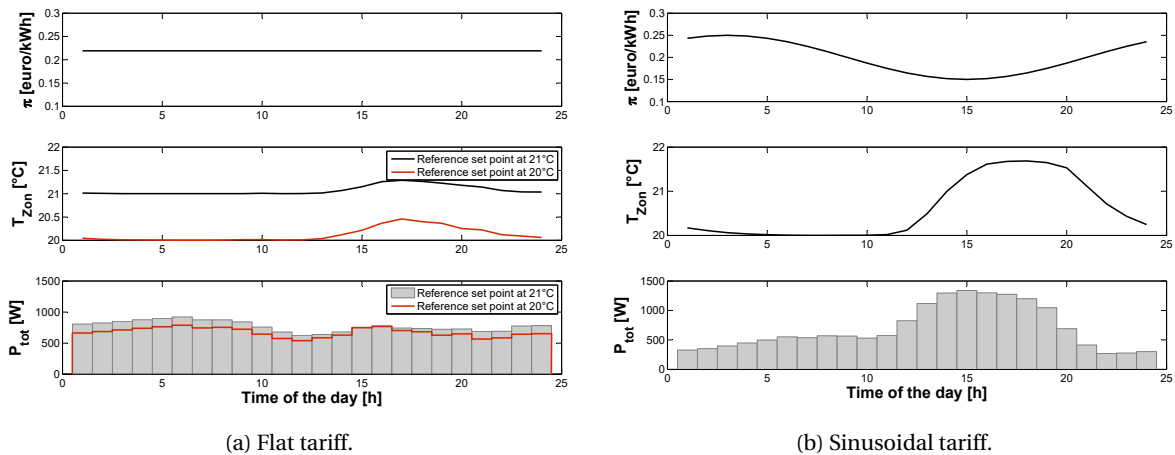


Figure 4.6 – Illustration of load shifting with price-responsive heat pump and storage in the building envelope thermal mass for an average winter day.

different heat pump performance. Contrariwise, if the reference temperature set point is set to 20°C, the average temperature reached with load shifting is 0.47 K higher than for the reference profile. The total electricity consumption is 4% larger, but cost savings reach 7%. In light of the above results, it is decided to chose the second option as reference in the remainder of the document. Indeed, lowering the average set point constitutes an option in itself to reduce the electricity bill, independently from time-varying price incentives and load shifting. It is therefore assumed that the occupants are not willing to compromise their thermal comfort to reduce their electricity bill, but rather to adjust its level to be able to increase the potential for load shifting.

4.6.1.2 Heat storage in building thermal mass

For heat storage in building thermal mass with conventional radiators, three heating schedules are simulated:

- a continuous heating schedule: the temperature set point is set to 20°C,
- a night set-back heating schedule: the temperature is set to 18°C between 10pm and 7am and to 20°C from 7am to 10pm,
- an intermittent heating schedule: the set point is set to 18°C from 10pm to 7am and from 10am to 5pm, and to 20°C between 7am and 10 am and from 5pm to 10pm.

Simulations are performed for K45 and K30 case-study buildings, for each of the above heating schedules, and with the retail tariff structures presented in Section 4.2. Results are illustrated in Figure 4.7. In terms of flexibility, the impact of the building envelope is straightforward: the flexibility index increases with the insulation level of the building envelope. The flexibility index tends to increase for variable tariff structures compared to the reference flat tariff. Results obtained with the RTP and DN tariffs for year 2012 are comparable, due to the similarity of the average electricity profiles. The reason for such similarity is two-fold. Firstly, the type of power plants used in 2012 in Belgium are nuclear plants and CCGTs as base load and gas turbines as marginal power plants. With such unit commitment, the day-ahead market price profile is on average close to the DN pricing, though more volatile on a



(a) Retailer's stand point.

(b) Consumer's stand point

Figure 4.7 – Results of optimal control for load shifting with price-responsive heat pumps, radiators and storage in building thermal mass for annual simulations. Two envelope insulation levels, three heating schedules and three retail tariffs are considered.

day-to-day basis, as illustrated in Figure 4.1. Secondly, the RTP 2012 structure is based on fixed costs, which limits the variability of the retail tariff. Nevertheless, the RTP 2012 tariff brings higher benefits for the energy retailer, whereas its equivalent DN structure is better suited to maximize the consumer's benefits. The flexibility potential reached with the RTP 2030 tariff structure is significantly larger than with the fixed-costs RTP 2012 structure (83.5 to 95.2% compared to 53.7 to 68.0%). Therefore, the larger the average ratio of peak to minimum values in the price profile, the larger the increase in flexibility. With such a tariff structure, both consumer's and retailer's cost savings are identical. From a consumer's standpoint, in all cases, cost savings overcome overconsumption. The latter reaches 2.8 to 19.9% of the reference consumption. Finally, the impact of the heating strategy strongly depends on the pricing structure. In all cases, the continuous heating strategy offers the lowest potential of volume shifted. For a day-night tariff structure, a day-night heating strategy allows 2.4 to 4.7% additional volume shifted compared to the intermittent heating schedule. The latter allows to shift up to 57.7% more energy towards low retail prices with the RTP 2030 structure, but also yields up to 7.9% more overconsumption than the other heating strategies.

To increase thermal inertia, radiators can be replaced by a heavy radiant floor heating system. Based

on the results obtained for radiators only, two heating strategies are simulated: continuous and intermittent heating. Simulation results for the K30 house are illustrated in Figure 4.8 for an average winter day with the prospective RTP 2030 tariff. Both electricity demand profiles with radiators and floor heating present similar trends. However, the floor heating system confers a larger thermal inertia to the overall system, which decreases both temperature fluctuations and peak power demand for optimal control with and without price incentives. Performance for load shifting are compared in terms

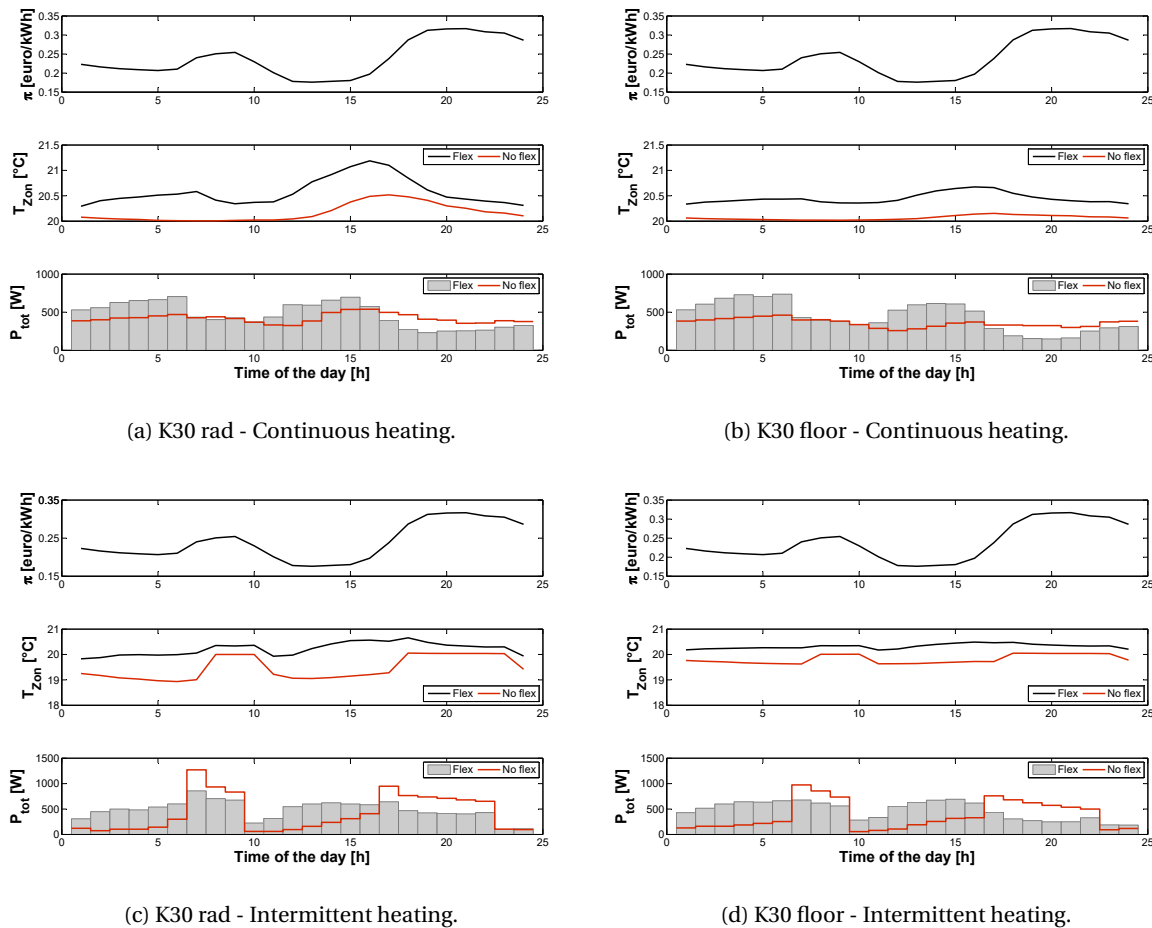


Figure 4.8 – Influence of the heat emission system on temperature and load profiles for load shifting with optimal control ("Flex") and without price incentive ("No flex") for an average winter day.

of shifted volume for the electricity retailer and average electricity price for the consumer in Figure 4.9. From an electricity retailer's standpoint, the intermittent heating strategy yields 13% to 57% additional shifted volumes compared to continuous heating, both with radiators and floor heating. With floor heating systems however, an intermittent strategy results in 4.4% to 8.8% additional overconsumption compared to conventional radiators, hence reducing the relative increase in shifted volume compared to continuous heating. From a consumer's standpoint, the intermittent heating strategy therefore tends to increase the average electricity price (Equation (4.23)) in the absence of price incentive. With optimal control for load shifting, a reverse trend is observed, and the combination of an intermittent heating strategy with a floor heating system yields the highest cost savings.

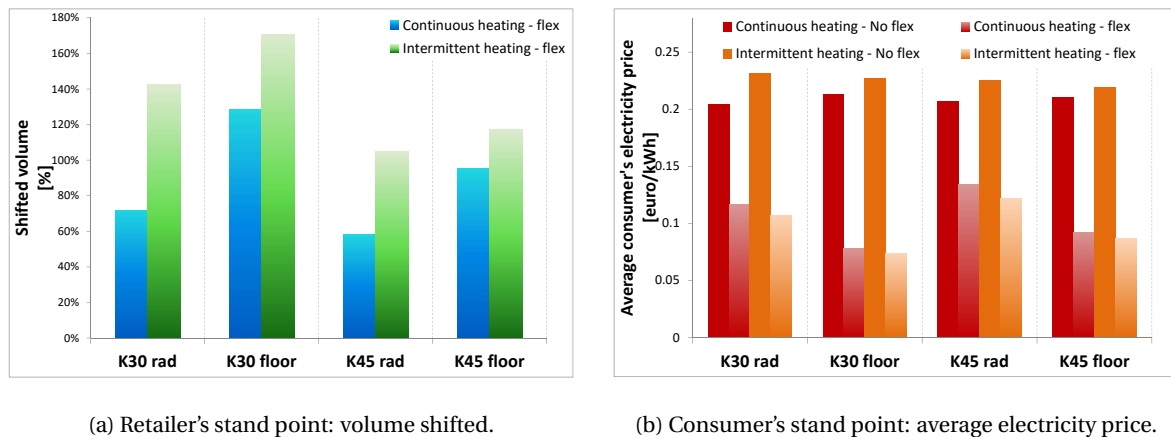


Figure 4.9 – Influence of heat emission system and heating strategy on reference load profiles ("No flex") and optimal control results for load shifting ("flex") for annual simulations with the prospective RTP 2030 tariff.

4.6.1.3 Heat storage in water tank

If no modification of indoor thermal comfort is allowed, or if the building envelope insulation is not sufficient enough to allow efficient load shifting, a water storage tank can be added in order to increase the system flexibility. The K45 house with radiators is used as case-study for this section.

Single- or variable-speed heat pump technology?

Water storage tanks are usually installed with single-speed heat pump technology to limit heat pump degradation due to cycling with conventional control ("No flex"). Control strategies resulting from price-incentives ("Flex") tend to bring the heat pump to work at part-load more frequently. In this context, it might become more profitable to install a variable-speed (inverter) heat pump, as shown in Figure 4.10. Depending on the heating strategy, cycling losses account for 12 to 21% of the annual consumption. A variable-speed heat pump allows a reduction in electricity cost of 31 to 36%. This technology is considered in the remainder of the document.

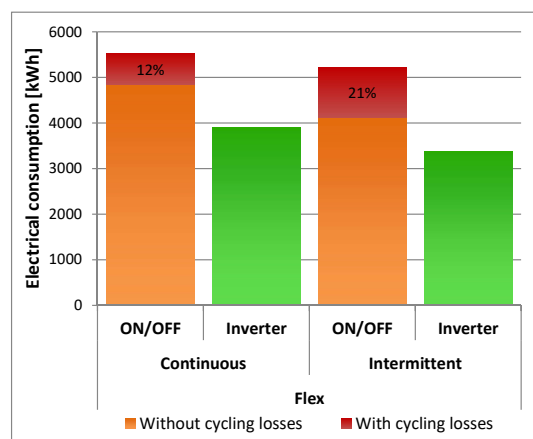


Figure 4.10 – Performance comparison of variable-speed (inverter) and fixed-speed (ON/OFF) heat pumps.

Sizing of water tank

Proper sizing of the tank is required to limit overconsumption and to accommodate seasonal differences. To perform load shifting, a larger tank volume is needed in order to limit temperature increase in the tank and related heat pump performance degradation. To that end, the optimization scheme has been run for 10 consecutive days in the winter, spring and fall, for a continuous heating strategy and a sinusoidal price signal, and for different tank sizes ranging from 300 to 900 liters. The additional electricity cost due to overconsumption as a function of the additional tank volume is illustrated in Figure 4.11. The reference volume is set to 300 liters. The optimum additional volume clearly depends on the season. However, increasing the tank size by 300 liters offers a good compromise by limiting the additional cost in the absence of load shifting incentive ("No flex"), and allowing a near-optimum cost reduction for all seasons for load shifting with optimal control ("flex"). The following simulations are therefore performed with a 600 liters tank.

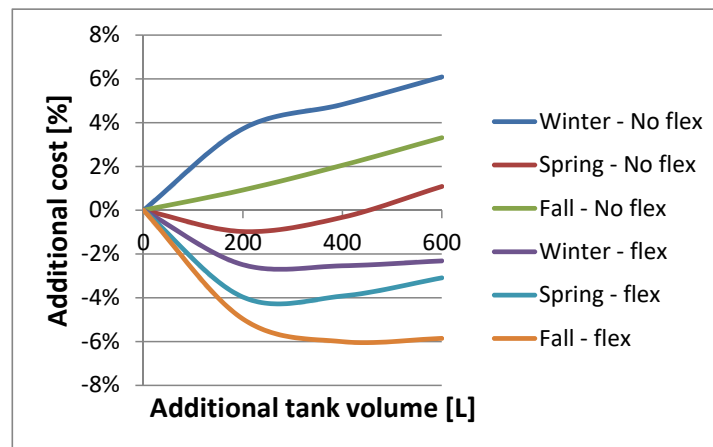


Figure 4.11 – Sizing of water storage tank with ("flex") and without ("No flex") incentive for load shifting.

Results

Results are presented in Table 4.1 and compare the annual electricity consumption, overconsumption, average electricity price and shifted volume for continuous and intermittent heating, with and without load shifting incentive.

Table 4.1 – Annual results of optimal control for load shifting for K45 building. Comparison of storage in the building thermal mass with radiators and storage in a water tank.

		Continuous heating				Intermittent heating			
		Elec. cons. [kWh/yr]	OC [%]	CS [%]	VS [%]	Elec. cons. [kWh/yr]	OC [%]	CS [%]	VS [%]
Envelope & radiators	No flex	2779.5	/	/	/	2630.1	/	/	/
	Flex	3063.7	10%	29%	58%	3107.3	18%	36%	105%
Water tank & radiators	No flex	3732.1	/	/	/	3339.0	/	/	/
	Flex	3811.7	2%	16%	32%	3462.1	4%	22%	57%

Compared to the reference profile, load shifting with storage in a water tank allows an increase in cost savings for the consumer by 16 to 22% and shifted volumes of 32 to 57% depending on the heating

schedule. Compared to storage in the thermal envelope of the building, the total annual electricity consumption is 24% larger for continuous heating and 11% greater for intermittent heating. Due to the larger shifted volume, cost savings for the consumer are the highest with radiators and storage in the building thermal mass. The main advantage of using a water tank storage lies in its ability to provide flexibility while ensuring the same thermal comfort for the occupants as the reference control without load shifting. Other storage options and hydronic configurations with water tanks are further discussed in Chapters 5 and 7.

4.6.2 Rule-based load shifting

4.6.2.1 Storage in the building thermal mass

The rule-based control strategies presented in Section 4.4.2.2 are simulated for both K45 and K30 buildings with radiators. Price threshold parameter p is varied between 0 and 1 and tested with three tariffs structures, namely the prospective RTP 2030 tariff, and two sinusoidal tariffs shown in Figure 4.12.

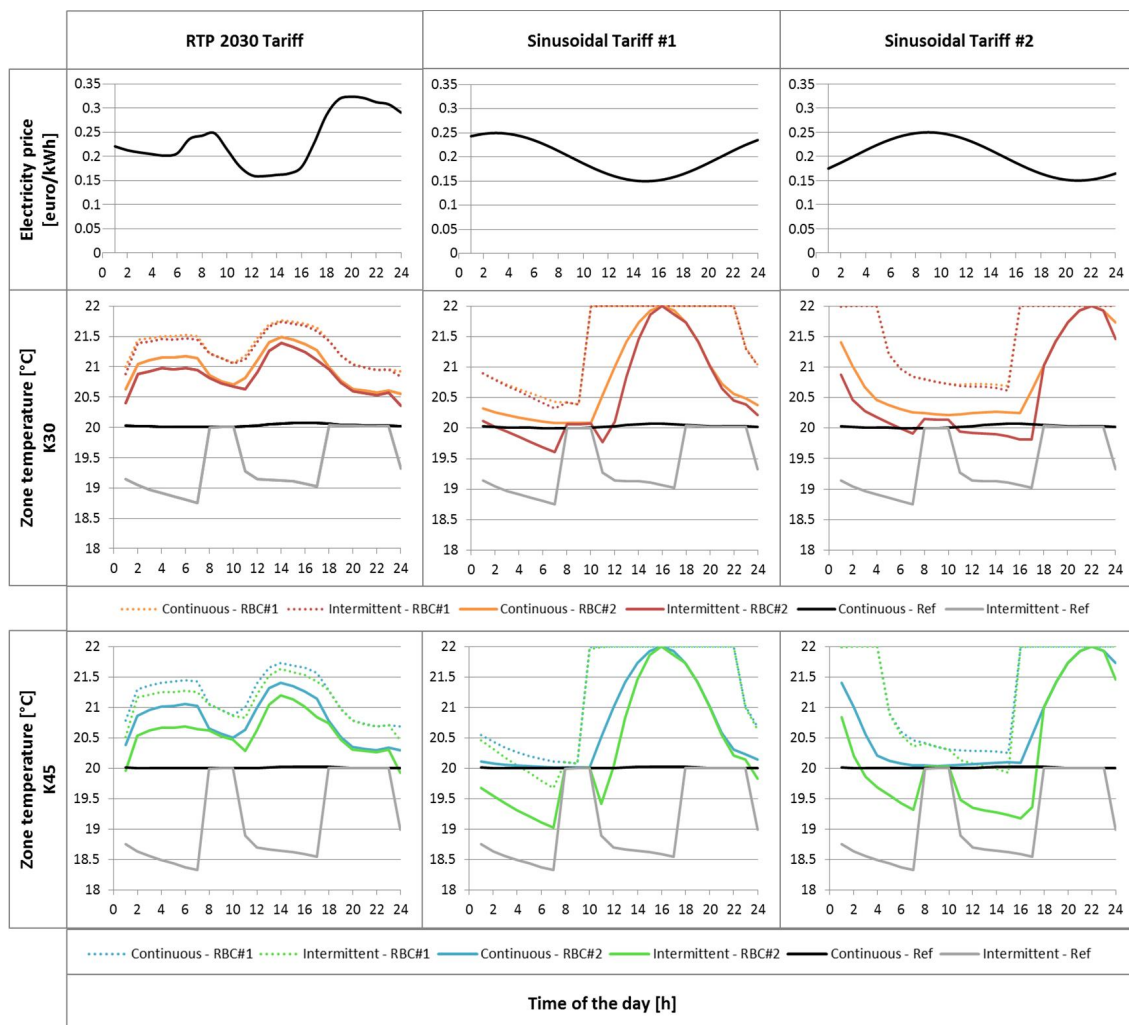


Figure 4.12 – Illustration of rule-based control strategies for load shifting with different tariff structures (parameter p is arbitrarily set to 0.5).

This figure shows the influence of RBC strategies on zone temperature control. Both strategies defined by Equations (4.16) and (4.17), and Equations (4.16) and (4.18), are compared for a value of parameter p arbitrarily set to 0.5. They are referred to as RBC#1 and RBC#2, respectively. As expected, RBC#1 leads to a more aggressive temperature control than RBC#2. The average zone temperature is higher with RBC#1, which yields overconsumption, especially when the building insulation level decreases. With a continuous heating schedule, load shifting may be beneficial for all three tariffs. With an intermittent heating schedule, both RTP 2030 tariff and the first sinusoidal tariff drive the heat pump to preheat the zone during unoccupied hours, which correspond to low retail electricity prices. For the second sinusoidal tariff, contrariwise, the zone temperature peaks during the evening occupancy period, which is likely to yield no financial benefits.

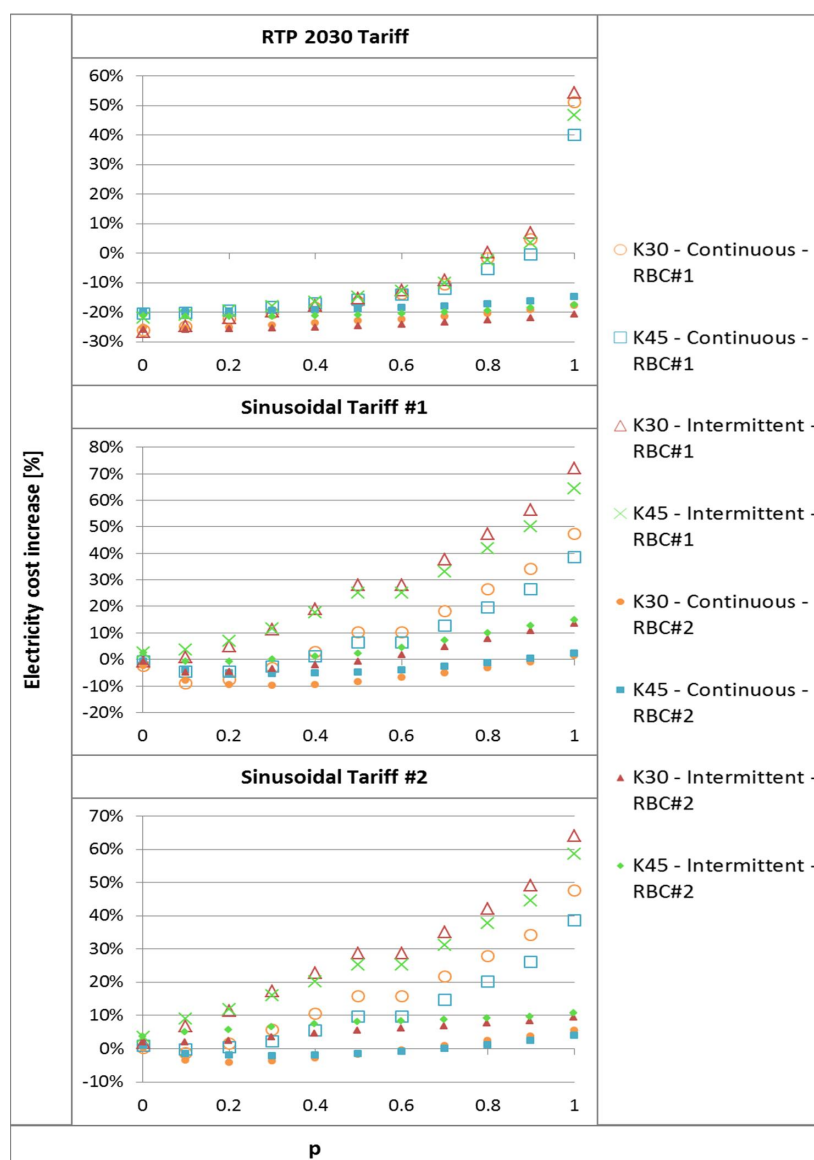


Figure 4.13 – Illustration of the influence of price threshold p on consumer’s annual electricity costs in the case of thermal storage in the building envelope. RBC#1 corresponds to Equations (4.16) and (4.17), and RBC#2 to Equations (4.16) and (4.18).

These observations are confirmed by Figure 4.13, which illustrates the influence of price threshold parameter p on the annual electricity cost for the consumer. Regardless of the tariff structure, house insulation level or heating schedule, the electricity cost is much more sensitive to the price threshold with RBC#1 than with RBC#2. For the prospective RTP 2030 tariff, the largest cost savings occur for a price threshold parameter of 0.01. This is inherent to the structure of the tariff, and is due to the large share of renewable energy sources. Indeed, the latter entails extended periods of time during which the retail tariff remains close to the minimum daily value, which allows to store energy during several consecutive hours at the lowest price. For the sinusoidal tariffs, a minimum arises for p equal to 0.2. Below this value, the time period available to store energy is too short, and no substantial load shifting occurs. Above this value, most of the energy is stored at a price that is higher than the minimum value. As already mentioned, the second sinusoidal tariff is only profitable with a continuous heating schedule. In general, a reasonable sub-optimal control is obtained with RBC#2 for a value of p equal to 0.5.

4.6.2.2 Storage in space-heating water tank

For storage in water tank with 4-pipe hydraulic configuration, a mapping of the influence of parameters p_1 and p_2 on the consumer's cost savings is shown in Figure 4.14. Compared to the reference control strategy, cost savings are brought both by a reduction in consumption due to better temperature management in the tank, and by load shifting. For both continuous and intermittent heating strategies, the largest cost savings occur for the smallest values of parameter p_1 and the largest values of parameter p_2 , such that low and high price thresholds coincide. Indeed, the intermediate tank temperature level adjustment tends to increase the consumption, without significantly increasing load shifting capabilities. For a fixed value of parameter p_1 , decreasing p_2 increases the electricity consumption by up to 3%.

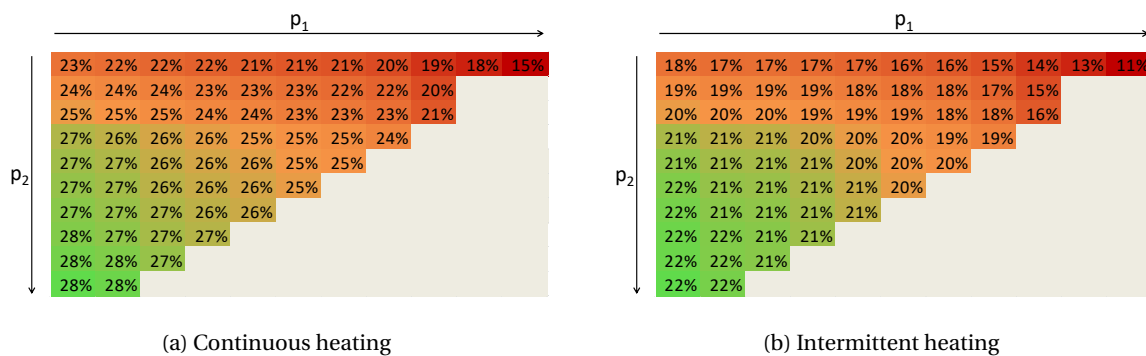


Figure 4.14 – Influence of price threshold parameters p_1 and p_2 on consumer's cost savings for thermal storage in a water tank.

In light of these results, a strategy based on the definition of a low price threshold only, as proposed for storage in the building thermal mass, leads to the most efficient load shifting. Temperature adjustment is performed following Equation (4.20) and yields 29% cost savings for continuous heating and 23% for intermittent heating.

4.6.2.3 Rule-based control or optimal predictive control?

Table 4.2 summarizes the results obtained with rule-based control and optimal control for the K45 house equipped with radiators. Results are compared for two storage options: storage in the thermal envelope and storage in a separate water tank. Results show that, compared to RBC, OPC allows to reduce the average electricity price by an additional 6 to 19%. In the case of thermal storage in building envelope with radiators, OPC tends to decrease the annual consumption, which combined with lower average electricity prices, increases the shifted volume by 12 to 35%. When coupled to a storage tank, additional cost savings for the consumer and shifted volumes reach up to 19% and 39%, respectively.

Table 4.2 – Comparison of results for K45 house obtained with rule-based control and optimal control for RTP2030 electricity retail tariff structure.

		Continuous heating		Intermittent heating			
		Elec. cons. [kWh/yr]	π^{avg} [€/kWh]	VS [%]	Elec. cons. [kWh/yr]	π^{avg} [€/kWh]	VS [%]
Envelope & radiators	RBC	3315.1	0.143	46%	3315.6	0.134	70%
	OPC	3063.7	0.134	58%	3107.3	0.122	105%
		-8%	-6%	+12%	-6%	-10%	+35%
Water tank	RBC	3901.5	0.187	18%	3384.7	0.201	18%
	OPC	3811.7	0.166	32%	3462.1	0.161	57%
		-2%	-11%	+14%	+2%	-19%	+39%

4.7 Model mismatch and uncertainties

The above results were obtained by assuming perfect prediction of all data inputs, and no mismatch between the optimizer model and the behavior of the real building, also referred to as the "plant". This represents the best prediction that can be achieved on a day-ahead basis. In real-time however, discrepancies may arise between predicted and real system responses, due to

- differences in building thermal response due to the use of a simplified building model,
- temperature measurement errors,
- weather forecast errors,
- unpredicted changes in occupants' behavior.

In that case, simulation results may lead to significant deviations in time, compared to real data.

4.7.1 "On-line" simulation scheme

In order to mitigate those deviations, an "on-line" scheme, illustrated in Figure 4.15, is implemented. In this scheme, the first control decision of the optimal electricity demand profile determined by the optimizer is applied to the real building. A feedback loop with temperature measurements from the real building to the optimizer is added. A state observer is used to update the states of the optimizer model based on the temperature measurements in the zone.

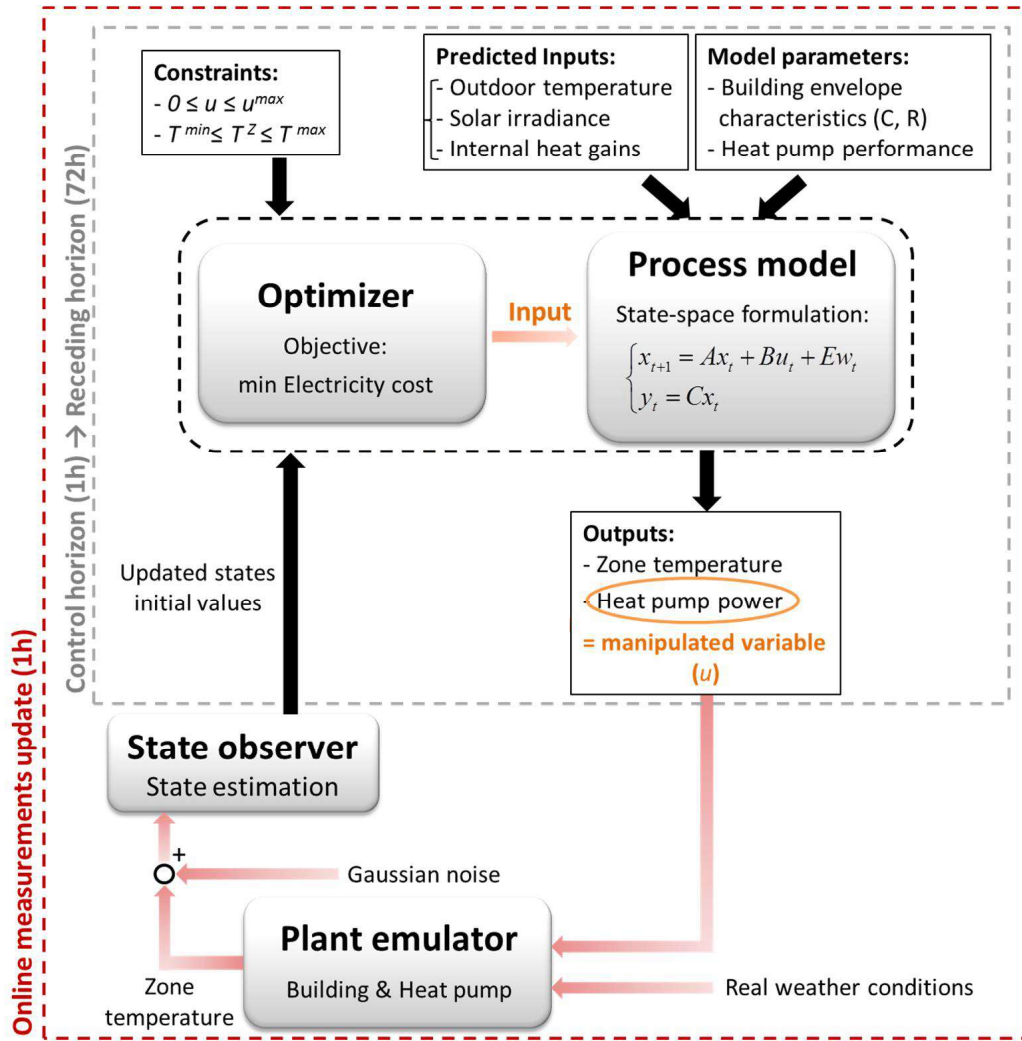


Figure 4.15 – On-line optimal predictive control scheme with emulator feedback and Kalman filter.

4.7.2 State observation

State observation can be carried out by Kalman filtering. The steady-state Kalman filter is implemented as follows:

Kalman Filter Implementation.

$$\text{Estimation: } \hat{x}_{t+1|t} = Ax_t + Bu_t + Ew_t$$

$$\text{Covariance: } P_{t+1|t} = AP_{t|t}A^T + Q$$

$$\text{Innovation: } e = y_{t+1} - C\hat{x}_{t+1|t}$$

$$\text{Innovation covariance: } S = R + CP_{t+1|t}C^T$$

$$\text{Gain: } K = P_{t+1|t}C^T S^{-1}$$

$$\text{Updated estimation: } \hat{x}_{t+1|t+1} = \hat{x}_{t+1|t} + Ke$$

$$\text{Updated covariance: } P_{t+1|t+1} = P_{t+1|t} - KSK^T$$

where R and Q are respectively the measurement noise and the process noise, P is the covariance matrix and K is the Kalman gain. Matrices A , B and E are identical to those used in the model-based optimal controller.

The implementation of a state observer requires the system to be observable. The observability of a system is defined as the ability to describe the behavior of the system based on its outputs. For LTI systems, observability is verified if the observability matrix is full rank, i.e. if

$$\text{rank} \begin{bmatrix} C \\ CA \\ CA^2 \\ \vdots \\ CA^{n-1} \end{bmatrix} = n \quad (4.28)$$

with n the state-space model order.

4.7.3 Application

The method is illustrated with the K45 case-study house equipped with radiators. The real building is replaced by a plant emulator consisting of a more detailed model of the building dynamics and a model of the heat pump with slightly different parameters. The detailed building model is the multi-zone model presented in Section 3.2.1.1 and implemented in *Modelica* language in *Dymola*. A dialog framework is set up between *Matlab* and *Dymola* (Annex A.3.2). To mimic monitoring data from a real building, Gaussian measurement noise is added to the emulated zone temperature, which serves as feedback signal to the optimizer.

The state-space model of Equation (4.5) is observable and the state observer parameters are tuned to filter measurement noise added to the temperature signal. The parameter R , is imposed to the accuracy of the sensors, i.e. to the standard deviation of the Gaussian noise. The process noise, Q , is tuned to obtain the best identification results. The influence of the process noise is illustrated in Figure 4.16. If the process noise is too large ($Q \gg$), the filter does not trust the model predictions and follows only the measurements. A properly tuned filter, contrariwise, allows a better filtering of the measurement noise and estimation of the state space variables.

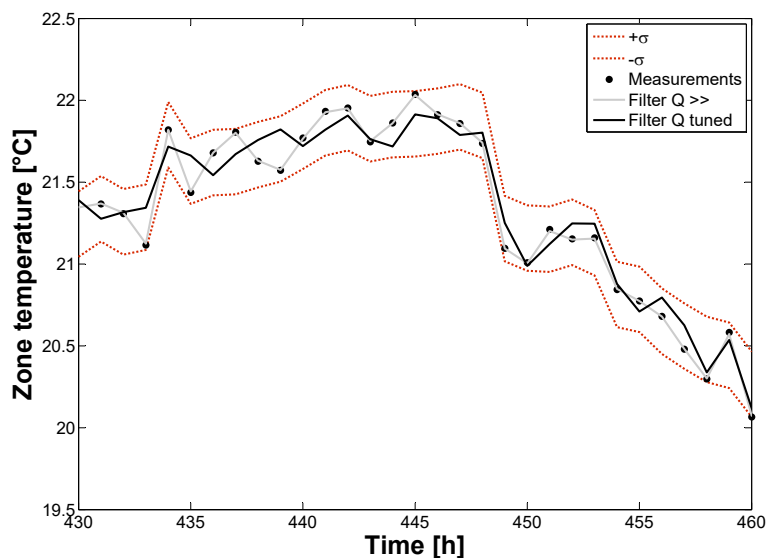
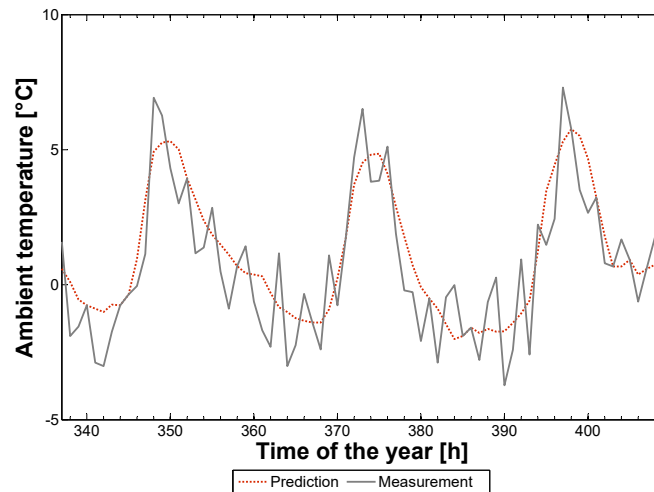
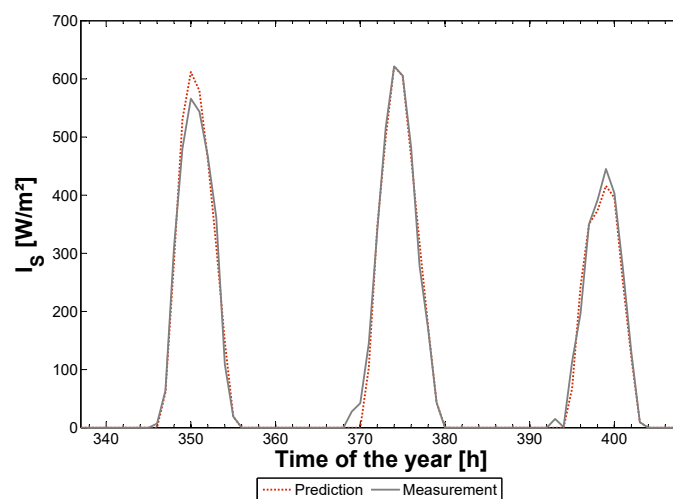


Figure 4.16 – Tuning of Kalman filter process noise (Q).

The "on-line" scheme is simulated for the month of January. Figure 4.18 illustrates the correction of temperature and electricity consumption operated by the closed-loop scheme to take into account the thermal response of the real building, different heat pump performance and prediction errors on the ambient temperature and solar irradiation (Figure 4.17). In open-loop, the day-ahead optimization zone temperature deviations of the emulator compared to the optimizer tend to increase in time. Indeed, in this case, the heat pump performance are over-estimated by the optimizer model and perfect weather forecast is assumed. Due to those mismatches, the comfort requirements in the real building are no longer met. The closed-loop schemes allows to reduce the temperature difference between the real building and the optimizer down to the accuracy of the measurement sensor. The heat pump electrical power is corrected accordingly. In this specific case, the prediction error on the total electrical power consumption with the open-loop scheme can reach 30%. From an electricity supplier standpoint, who can potentially be a balance-responsible party, this uncertainty can strongly impact the balancing between electricity injections and off-takes in a control area. It should be included in the day-ahead prediction.

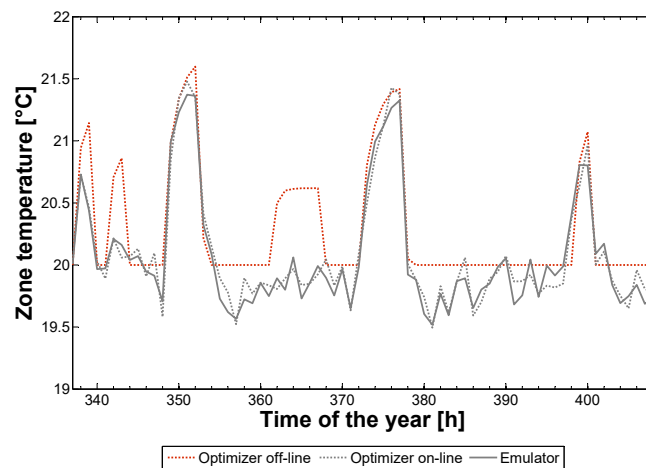


(a) Ambient temperature.

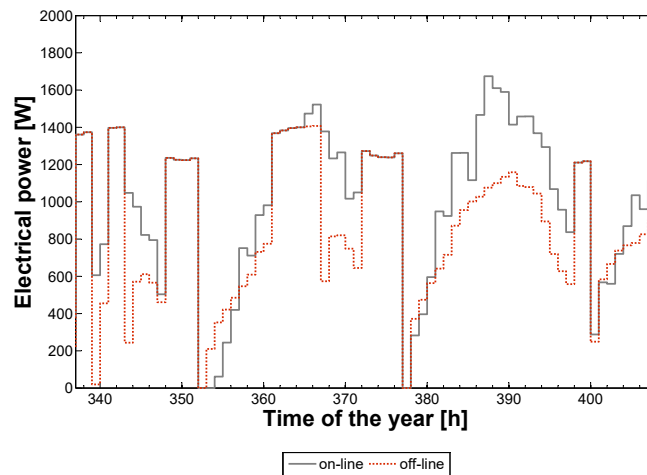


(b) Solar irradiation on South-oriented vertical pane.

Figure 4.17 – Illustration of uncertainty on weather conditions for 3 days in January.



(a) Zone temperature.



(b) Heat pump electrical power.

Figure 4.18 – Illustration of optimal control with off-line and on-line schemes for 3 days in January and a continuous heating strategy.

In order to reduce model mismatch, model parameters could also be identified from real-time measurements and added to the above control scheme. This aspect is investigated in the work of De Coninck (2015).

4.8 Research outcome

The analysis proposed in this chapter yields the following research outcome:

- the ability of heat pumps to activate the flexibility potential of residential buildings in response to price incentives has been demonstrated.
- new metrics to quantify the flexibility have been introduced and consider both the consumer's and retailer's standpoints.
- different control strategies have been compared, including optimal predictive and rule-based

control. In both cases, it has been shown that the performance of the load modulation is directly related to the ability of the control strategy to limit the overconsumption entailed by load shifting. OPC yields up to 19% additional cost savings compared to RBC and up to 39% additional shifted volume.

- the obtained results strongly depend on the house insulation level, heating schedule, storage option and electricity tariff structure. However, general guidelines can be formulated:
 - the flexibility potential offered by storage in the building envelope increases with the house insulation level. An intermittent heating strategy yields larger flexibility than a continuous heating strategy.
 - with a water tank storage, there is an optimal tank size that limits overconsumption. Compared to storage in the thermal envelope, the use of a water tank significantly reduces the flexibility potential, but yields no modification of the thermal comfort. The use of a water tank is particularly suited for poorly insulated houses, as further developed in Chapter 7.
 - RTP tariffs with multiplicative costs allow the largest load shifting potential but also yield the largest overconsumption.
- uncertainty in weather predictions, occupants behavior and system performance, as well as model mismatch, can cause the real-time electricity consumption profile to differ strongly from the day-ahead prediction. This can in turn decrease the cost savings of the retailer. This is tackled in an "on-line" control scheme including measurement updates and state observation with Kalman filtering.

5 Optimal management of HVAC systems for load matching

This chapter is adapted from:

E. Georges, J. E. Braun and V. Lemort, "A general methodology for optimal load management with distributed renewable energy generation and storage in residential housing", *Journal of Building Performance Simulation*, Vol. 10 (2), 2017.

5.1 Motivations

As pointed out in Section 1.1, depletion of fossil fuel reserves and atmospheric pollution concerns have encouraged the development of alternative energy sources. Incentive programs have emerged to promote the installation of on-site renewable energy sources, such as tax incentives, low-interest loans and net energy metering. As illustrated in Chapter 2, surplus production by decentralized units entails additional challenges for the management of the electricity grid.

In that regard, two mainstream approaches are presented in the literature to investigate the potential benefits of decentralized power units: a centralized approach and a decentralized approach. In the centralized approach, the problem is studied across a portfolio of buildings with different consumption load profiles, PV orientations, system sizes and often include a model of the electricity grid (Strbac et al. (2010), Csetvei et al. (2011), Baetens et al. (2012), Nykamp et al. (2012)). As load profiles differ for each end-user, the surplus electricity produced by a decentralized unit can be consumed by another end-user (International Energy Agency (IEA) (2014)). To maximize the utility's benefits, end-users consumption load profiles can be shaped through active demand response based on a global optimization for the set of connected end-users, regardless of local self-consumption. In the decentralized approach, most studies have focused on the maximization of load matching indicators at the scale of a single building (Vanhoudt (2012) and Dar et al. (2014)). Widén et al. (2009) proposed three options to improve load matching: PV array orientation, optimal load management and additional electrical storage. The two last options were identified as the most effective.

The implementation of demand response programs raises the question of the economic viability for end-users. Indeed, financial benefits are seen as a driving force for residential building owners to invest in new technologies (International Energy Agency (IEA) (2014)). In current net metering programs, for which the resale price is equal to the retail price, the global optimization of the centralized approach

does not harm the economic returns of the end-users as long as their surplus production is not curtailed. However, the cost savings for the utility entailed by a large penetration rate of decentralized production is often lower than the cost of compensating this surplus production, and the market model for PV panels is moving towards less attractive surplus resale tariffs (European Commission (2015)). In this context, the optimum electrical load management for the end-user may differ in the centralized and decentralized approaches as metering programs evolve. In the decentralized approach, to attain grid parity under less attractive economic conditions, the objective for the end-user is no longer to maximize the surplus electricity delivered to the grid, but to maximize its self-consumption (Mondol et al. (2009)). Kamyar and Peet (2015) carried out a global analysis including utility and customer welfare to determine optimal electricity rates in the presence of demand response programs. Simulations showed that a reduction of electricity bills by up to 20% could be achieved with passive thermal storage and optimal thermostat programming. This entails the need for appropriate load control and right sizing of the PV panels. Zhang and Augenbroe (2014) presented a method to determine optimal PV sizing for a residential U.S. house under different demand response programs and for different locations in the U.S. The method is based on the determination of the maximum net present value based on the influence on curtailing losses of different metering programs.

The method proposed in the present chapter is a general methodology for assessing opportunities associated with optimal load management in response to different utility incentives for residential buildings that employ renewable energy sources and energy storage. In light of the above literature survey, the chosen approach is a decentralized optimization to maximize the consumer's benefit through an appropriate control of existing electrical systems, as an incentive to continue promoting the integration of renewable sources in response to changing metering programs. Net metering allows customers with decentralized electricity production units to supply their excess local electricity production to the electricity grid. A general optimal control solution is proposed to assess the potential of load matching with decentralized production and to study the effects of different buy-back prices on customer economics. The method is illustrated with a case-study of a typical American house equipped with PV panels, an air-to-air heat pump, a water heater and an electrical storage for different buy-back prices. The potential for load matching is characterized in terms of percentage of the electricity production consumed on-site and the proportion of the demand covered by decentralized electricity generation (Baetens et al. (2012) and Van Roy et al. (2013)). Guidelines for optimal control of the electrical load and for right-sizing of PV panels are proposed. The price signals used can either be reflective of centralized optimization results maximizing the electricity grid utility's benefits, or can be an image of the congestion level in the distribution grid as in the study of Csetvei et al. (2011). It is assumed that the price signal is established in a fair way by the electricity grid utility. Action on the grid (e.g. grid reinforcement) is not considered in the optimization process. The objective is to reduce the burden on the electricity grid while ensuring grid parity for residential prosumers.

The primary uniqueness of this study resides in the general optimal problem formulation to assess the influence of metering programs on load matching potential. The proposed formulation is very flexible and can be applied to any decentralized power unit and storage system. Moreover, the focus is on the influence of feed in prices rather than forward price signals as in most of the aforementioned studies. The study presents a complimentary approach to the work of Zhang and Augenbroe (2014), for which load shifting and storage were not considered for optimal sizing of the PV system.

5.2 Billing mechanisms in the U.S.

To promote the integration of renewable energy sources, agreements exist between utilities and consumers with grid-connected PV systems. Such consumers are allowed to deliver surplus electricity generated on-site to the local distribution grid following two different existing billing mechanisms. The first mechanism, referred to as net metering, only requires one meter that counts the net power flow to or from the grid. The second option, less widespread in the U.S., meters separately the instantaneous electricity consumption and production. In this case, the electricity is sold back to the utilities at a resale tariff that can differ from the retail tariff. In the U.S., metering policies vary according to the states: so far, the excess power generation supplied to the grid is either “bought” at retail or at wholesale price tariffs (U.S. Energy Information Administration (EIA) (2012)). Currently, the retail tariff is applied in most states with net metering programs. From a customer’s standpoint, this implies the same economic benefit whether the electricity produced by the PV system is instantaneously consumed on-site or delivered to the grid. There is therefore no incentive to shift the electricity consumption in time to match the local production. With the increase in the number of prosumers, electricity grid congestion and PV curtailment become more frequent, which restricts the amount of distributed power supplied to the grid and tends to modify the economics of surplus electricity sale to the grid. In this work, a different metering program is proposed that would promote better load matching between production and consumption. The net electricity flow, i.e. the instantaneous difference between the power consumed and produced on site is determined. If positive, the billing tariff is the retail tariff, π_{ret} . If negative, the excess production is bought back at a buy-back tariff, π_{bb} . One can therefore define the buy-back ratio as

$$\alpha = \frac{\pi_{bb}}{\pi_{ret}} \quad (5.1)$$

In the following section, the retail tariff chosen as the reference is a flat tariff. The definition easily extends to time-of-use tariffs.

5.3 Methodology

5.3.1 Optimization problem for load management

In this section, the general optimal load management problem is specified. The discrete state space representation of the system is summarized by

$$\mathbf{x}_{t+1} = f(\mathbf{x}_t, \mathbf{u}_t, \mathbf{w}_t) \quad (5.2)$$

where \mathbf{x} is the state space variable vector, \mathbf{u} is the vector of decision variables, i.e. the modular electric power, and \mathbf{w} is a vector of disturbances. The total electricity consumption of the consumer at time t , P_t , is composed of modular components, $u_{i,t}$, i.e., the consumption of systems that can be adjusted by the optimal load management scheme, and the exogenous consumption, Γ_t , i.e. the share of the electricity consumption that cannot be controlled through load management,

$$P_t^{cons} = \sum_i u_{i,t} + \Gamma_t \quad (5.3)$$

The net power flow is the difference between the consumption, including storage, and the local electricity production, P_t^{prod} , including storage discharge and decentralized power unit production,

$$P_t^{net} = P_t^{cons} - P_t^{prod} \quad (5.4)$$

The objective is to minimize the electricity cost for the end-user for a given metering buy-back ratio, α , which can be expressed as

$$\min \sum_{t \in \mathcal{H}} (\max(P_t^{net}, 0) + \min(P_t^{net}, 0)\alpha) dt \quad (5.5a)$$

with respect to the decision variables and subject to

$$\mathbf{x}_t^{min} \leq \mathbf{x}_t \leq \mathbf{x}_t^{max} \quad \forall t \in \mathcal{H} \quad (5.5b)$$

$$\mathbf{u}_t^{min} \leq \mathbf{u}_t \leq \mathbf{u}_t^{max} \quad \forall t \in \mathcal{H} \quad (5.5c)$$

$$u_{i,t} + u_{j,t} \leq \max(u_{i,t}, u_{j,t}) \quad \forall t \in \mathcal{H}, i \neq j \quad (5.5d)$$

where Equation (5.5c) specifies the upper and lower limits for power modulation of the modular components and Equation (5.5d) ensures that two related decision variables are not activated simultaneously, as further explained in Section 5.3.3. Perfect predictions of the electricity generation by decentralized units and use profiles are assumed (Section 5.3.2.4) for the purpose of evaluating the load management opportunities. Based on the known future inputs, the optimizer determines an optimal control response that minimizes the objective function of Equation (5.5a) over the prediction horizon \mathcal{H} and then applies the control inputs over a defined control horizon \mathcal{M} , with \mathcal{M} less than \mathcal{H} . The prediction horizon is then shifted forward in time to the end of the control horizon, following a so-called “receding horizon” control scheme. The condition \mathcal{M} less than \mathcal{H} replaces the use of terminal constraints on the states and allows for an anticipation of the decentralized electricity production.

5.3.2 Modeling

5.3.2.1 Case study

The optimal problem presented in Section 5.3.1 was applied to a typical 4-bedroom single-story ranch-type American house built in the 1990’s. Building characteristics have been detailed by Holloway (2013). The building structure consists of a 2-by-4 insulated wood frame on a concrete ground floor. The heated volume is 408m³. The building is equipped with a reversible single speed air-to-air heat pump for space conditioning and an electric water heater for domestic hot water, which constitute the flexible thermostatically-controlled loads. High efficiency photovoltaic panels are installed on the roof. An additional electrical storage can be added optionally as flexible load.

5.3.2.2 Thermal models

A detailed dynamic model of the house is available in TRNSYS (Holloway (2013)). The model is detailed regarding the building envelope, but not the equipment (heat pump), as the available data are performance curves from the manufacturer. For the purpose of this work, the heating and cooling demands of the building are determined using a grey-box model trained with yearly simulation results

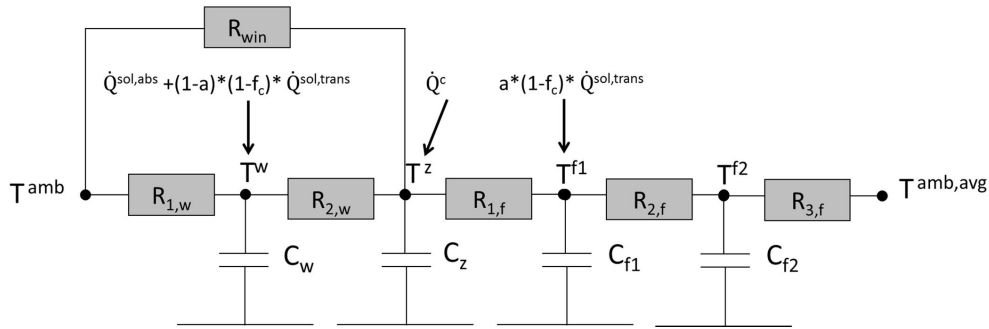


Figure 5.1 – Grey-box model structure.

from the detailed TRNSYS model. The grey-box model provides an accurate representation of the thermal response of the house at significantly reduced computational requirements. Root mean square error in free-floating zone temperature prediction was below 0.25°C over a year. Yearly error on total cooling and heating needs is 2.3%. The structure of the model is illustrated in Figure 5.1. The ground temperature is set to the average annual ambient temperature, $T^{amb,avg}$. The convective thermal power, \dot{Q}^c , is the sum of the heating (or cooling) power, the internal heat gains due to lighting and occupants, and the convective share of solar gains. No solar protection and no night ventilation in the summer is considered when performing thermal simulation. The reversible single speed air-to-air heat pump is modeled according to the ASHRAE toolkit model (Brandemuehl et al. (1993)) in which capacity and coefficient of performance, symbolized by Y in the following equations, are defined as functions of their values at rated conditions (Air-conditioning, Heating and Refrigeration Institute (AHRI) (2008)) and correction coefficients, f_{Y_T} and f_{Y_m} , taking into account the dependency on the indoor air temperature and humidity, outdoor air temperature, and mass flow rates. Equations in cooling mode are given here below.

$$Y = Y^{rat} f_{Y_T} f_{Y_m} \quad (5.6a)$$

with

$$f_{Y_T} = a_0 + a_1 T^{amb} + a_2 (T^{amb})^2 + a_3 T^{z,wb} + a_4 (T^{z,wb})^2 + a_5 T^{z,wb} T^{amb} \quad (5.6b)$$

$$f_{Y_m} = b_1 + b_2 \dot{m} / \dot{m}_{rat} \quad (5.6c)$$

In heating mode, the zone wet bulb temperature is replaced by the dry bulb temperature in Equations (5.6b) and (5.6c). All the coefficients for both COP and capacity were derived from performance maps for commercially available heat pumps (Holloway (2013)).

The dependency of the unit performance in cooling mode on the indoor wet bulb temperature has two impacts. First, it introduces a nonlinearity in the system, since the wet bulb temperature is a nonlinear non convex function of the dry bulb temperature and relative humidity. This is further developed in Section 5.3.3. Secondly, it requires the addition of a moisture model to the building thermal model. A lumped moisture capacitance model is adopted, assuming constant dry air mass in the room, and ten times the air mass capacitance (Rudd (2013)). The continuity equation for water is expressed by the

following mass balance

$$m_a \frac{dw_{in}}{dt} = \dot{m}_{a,inf} w_{amb} + \dot{m}_{w,occ} - \dot{m}_{w,cond} - \dot{m}_{a,inf} w_z \quad (5.7)$$

where the infiltration and exfiltration rates are assumed to be equal ($\dot{m}_{a,inf}$), $\dot{m}_{w,occ}$ is the amount of water released by the occupants and $\dot{m}_{w,cond}$ is the mass flow rate of water condensing in the cooling coil and given by

$$\dot{m}_{w,cond} = \frac{\dot{Q}^l}{h_{fg}} \quad (5.8)$$

where h_{fg} is the enthalpy of vaporization. The latent heat transfer rate, \dot{Q}^l , depends on the sensible heat ratio (SHR) of the cooling unit. Two different methods are compared: constant SHR and the by-pass model proposed by Brandemuehl et al. (1993). In the second method, the SHR is defined as a function of the by-pass factor, f_{bp} , as follows

$$SHR = \frac{\dot{Q}^s}{\dot{Q}^s + \dot{Q}^l} = \frac{h(T = T_{in}, w = w_{out}) - h_{out}}{h_{in} - h_{out}} \quad (5.9)$$

where T_{in} is the temperature of the air at the inlet of the cooling coil, w_{out} is the humidity ratio of the air exiting the coil and

$$h_{out} = (1 - f_{bp})h_{adp} + f_{bp}h_{in} \quad (5.10)$$

The dependency of the SHR on indoor humidity ratio also introduces a nonlinearity and is further developed in Section 5.3.3. Domestic hot water production is provided by an electric water heater equipped with two thermostats and two heating elements located in the upper third and in the lower two-thirds of the tank. Both heating elements cannot be switched on simultaneously, and priority is given to the upper element. Hot water is drawn from the top of the tank and cold water is supplied at the bottom. The water in each part of the tank is assumed to be homogeneously mixed.

5.3.2.3 Electrical storage model

In addition to the systems traditionally installed in residential buildings, such as electrically-driven heating systems and domestic hot water production systems, an electrical storage can be added. The electricity that flows between the battery and the decentralized power production unit or the electricity grid is modeled by a round-trip efficiency composed of the input efficiency, η_i , which depends on the supply source (AC/DC), the internal battery efficiency, η_{bat} , and the output efficiency, η_o , which corresponds to the efficiency of the inverter. Performance degradation with increased number of cycles is not modeled. The battery state of charge (SOC) is given by

$$SOC_t = SOC_{t-1} + P_t^{supply} \eta_i \Delta t - \frac{P_t^{discharge}}{\eta_o} \Delta t - L^{bat} \quad (5.11)$$

where the battery losses, L^{bat} , are given by

$$L_{bat} = \frac{P_t^{discharge}}{\eta_o} \left(\frac{1}{\eta_{bat}} - 1 \right) \Delta t \quad (5.12)$$

and the internal battery efficiency is assumed constant.

5.3.2.4 Load profiles

The total building energy demand includes the building space heating (SH) and cooling (AC) loads, the domestic hot water needs and the electricity consumption of appliances and lighting. Water draw-off events as well as appliances and lighting use are modeled by predefined load profiles. Realistically, it is not likely for the controller to have an exact prediction of the DHW, appliances and lighting events, since they directly relate to unpredictable occupants' behavior. However, typical average load profiles are available and are used for the prediction of the optimal response. In the "Building America House Simulation Protocols", Wilson et al. (2014) provide a set of data including consumption and typical daily use profiles for an average American dwelling. Profiles for a four-bedroom/two-bathroom dwelling are illustrated in Figure 5.2. The DHW consumption includes hot water for baths, showers and sinks as well as a dishwasher and a clothes washer. The hot water daily consumption is 265 liters for weekdays and 290 liters on weekends at a supply temperature of about 52°C. For lighting, a seasonal effect is taken into account. The annual electricity consumption for appliances and lighting is 6936 kWh.

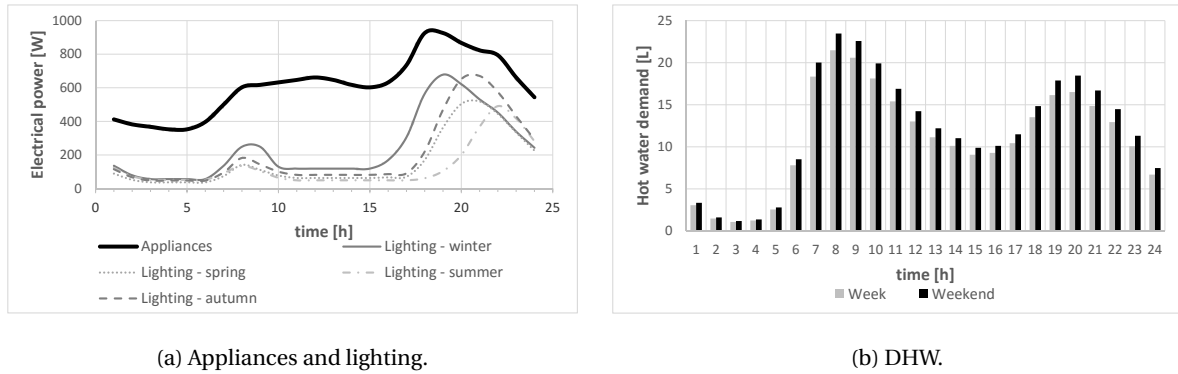


Figure 5.2 – Average daily load profiles.

5.3.3 State-space formulation and linearization

The water heater, battery and grey-box building models allow a straightforward state-space formulation of the governing differential equations as follows

$$\mathbf{x}_{t+1} = \mathbf{A}\mathbf{x}_t + \mathbf{B}\mathbf{u}_t + \mathbf{E}\mathbf{w}_t \quad (5.13)$$

where \mathbf{x} is the state space variable vector composed of the zone, wall, first and second floor node temperatures, top and bottom water tank node temperatures, indoor humidity ratio, and battery

state-of-charge,

$$\mathbf{x}^T = [T^z, T^w, T^{f1}, T^{f2}, T^{tank,tp}, T^{tank,bt}, w_z, SOC] \quad (5.14)$$

\mathbf{u} is the vector of decision variables, namely the sensible cooling or heating rate provided by the heat pump to the house (\dot{Q}^s), the electric power supplied to the top and bottom parts of the water heater ($P^{WH,tp}$ and $P^{WH,bt}$), the latent thermal cooling rate in the case of cooling (\dot{Q}^l), and the battery charging or discharging rate (P^{bat})

$$\mathbf{u}^T = [\dot{Q}^s, P^{WH,tp}, P^{WH,bt}, \dot{Q}^l, P^{bat}] \quad (5.15)$$

Sign conventions are such that \dot{Q}^s is defined as positive in heating mode and negative in cooling mode, and P^{bat} is taken positive when the battery is charging and negative when discharging. \mathbf{w} is the vector of disturbances, i.e., the outdoor air temperature and humidity ratio, the occupants, lighting and solar gains, the mains water temperature and the rate of hot water used by occupants. The power consumption expressed in Equation (5.3) is composed of the power consumed by the heat pump unit, the auxiliary heater, the water heater, the electrical storage and the exogenous consumption corresponding to the consumption of appliances and lighting. Simulations are performed assuming perfect prediction of the electricity consumption profiles of the house. Constraints (5.5b) to (5.5d) translate as follows:

- The building zone temperature should remain within a predefined dead band

$$T^{sp,low} \leq T^z \leq T^{sp,high} \quad (5.16)$$

A night set-back strategy is chosen. Over the heating season, $T^{sp,low}$ is set to 18°C during the night and 20°C during the day, while $T^{sp,high}$ is set to 22°C. For the cooling season, the low set point limit is set to 20°C, whereas the high set point limit is set to 24°C during the night and 22°C during the day.

- The water tank temperature in the upper and lower parts should remain within an imposed dead band:

$$T^{sp,low,DHW} \leq T^{tank,bt}, T^{tank,tp} \leq T^{sp,high,DHW} \quad (5.17)$$

with $T^{sp,low,DHW}$ and $T^{sp,high,DHW}$ set respectively to 35°C and 50°C in the bottom part and 50°C and 60°C in the top part of the tank.

- The heat delivered to/retrieved from the house should not exceed the full load capacity of the heat pump and auxiliary heater combined in heating mode or of the air-conditioning unit in cooling mode.
- The power supplied to the water tank should remain below the maximum value of each heating element.
- Both hot water tank heaters cannot work simultaneously, which introduces Boolean variables in the optimization problem (Equation (5.5d)) and turns the optimization problem into a mixed-integer problem.
- The battery state of charge should remain within a predefined dead-band to avoid deterioration

$$SOC^{min} \leq SOC \leq SOC^{max} \quad (5.18)$$

with SOC^{min} and SOC^{max} set respectively to 15% and 95% of the battery capacity.

- The charging and discharging rates of the electrical storage are limited by maximum values specified by the manufacturer.

Feedback control of the HVAC systems is carried out following an “energy rate approach”, which considers that the system is allowed to cycle freely to meet the energy requirement for a given simulation time step. Performance degradation due to cycling is taken into account following the method from ASHRAE Standard 116 (American society of heating, refrigerating and air-conditioning engineers (ASHRAE) (1983)) and is expressed as a function of the fraction of simulation time step during which the unit is working. The energy rate approach was chosen in order to avoid the use of small time steps that would be needed to explicitly model the dynamic response associated with feedback control.

In the case where no detailed humidity model is included, and constant SHR is assumed, formulation (5.13) is linear. However, when taking into account the dependency of SHR and unit performance on the indoor humidity ratio, w_{in} , the model becomes nonlinear. Although more difficult to handle, efficient solvers are available to solve nonlinear problems. However, few computationally efficient solvers exist to solve mixed-integer nonlinear problems (MINLP). One solution would require the linearization of all thermodynamics properties of moist air, which is very time-consuming but would be required for real-time application of the proposed method. Since the purpose of this study is to analyse yearly results and parameters of influence, another solution is proposed to linearize the problem. The method consists in considering the error of the indoor humidity estimation as an unpredictable disturbance. The method supposes that the disturbance term is white noise and small (Ljung, 1987) and that the trajectory of the disturbance-free system corresponds to an input sequence w_{in}^* of the indoor humidity ratio, to which corresponds a state trajectory x^* . The linearized form of the system is then

$$\Delta x(k+1) = F\Delta x(k) + G\Delta u(k) + \bar{v}(k) \quad (5.19a)$$

where

$$\Delta x = x - x^* \quad (5.19b)$$

$$\Delta u = u - u^* \quad (5.19c)$$

and \bar{v} is a white noise disturbance. In the proposed method, w_{in}^* is obtained based on the estimation of a potential sensible cooling demand. The potential sensible cooling demand, \dot{Q}^{s*} , is a fraction of the full-load sensible capacity. This fraction is assumed to be the ratio of the indoor/outdoor temperature difference over the same difference in rated conditions.

$$\dot{Q}^{s*} = \min \left(\dot{Q}^{s,fl} \frac{T^{amb} - T^{sp}}{T^{amb,c,rat} - T^{sp}}, \dot{Q}^{s,fl} \right) \quad (5.20)$$

where $\dot{Q}^{s,fl}$ is the sensible cooling capacity at full load, T^{sp} is the room temperature set point, T^{amb} is the ambient temperature and $T^{amb,c,rat}$ is the ambient temperature at rated conditions. As a consequence, an approximation of w_{in} , w_{in}^* , is obtained from Equation (5.7) with a condensing water

flow rate given by

$$\dot{m}_{w,cond}^* = \frac{\dot{Q}^{l,fl}}{h_{fg}} \frac{T^{amb} - T^{sp}}{T^{amb,c,rat} - T^{sp}} \quad (5.21)$$

The variable w_{in}^* is initialized to the real value of w_{in} after each control horizon of 12 hours.

Three modeling assumptions are investigated to approximate w_{in} . The first method consists of imposing constant humidity ratio and SHR. The second option considers the indoor humidity model proposed in Equations (5.20) and (5.21) with constant SHR, and the last method adds the determination of the SHR with the by-pass model (Section 5.3.2.2). The three methods are compared to a reference scenario based on a conventional tracking of a prescribed indoor set point. This scenario is simulated over four months during the cooling season to obtain a reference profile for w_{in} . The same prescribed control strategy is used to simulate the three modeling approaches. Prediction errors for indoor humidity ratio, full load cooling capacity and full load sensible cooling capacity are summarized in Table 5.1. Since the optimal load management for space conditioning is based on indoor temperature control, the accurate prediction of the available sensible capacity is of major importance, as it appears as a lower limit in Constraint (5.5c). The third method significantly improves the model accuracy in predicting the maximum sensible capacity and is used in the following sections.

Table 5.1 – Mean prediction error for indoor humidity ratio, full load cooling capacity and full load sensible capacity with 1) constant humidity ratio and SHR, 2) indoor humidity modelled by Equations (5.20)-(5.21) and constant SHR, 3) indoor humidity modelled by Equations (5.20)-(5.21) and SHR from by-pass model.

Method	Prediction error		
	w_{in}	$\dot{Q}^{tot,fl}$	$\dot{Q}^{s,fl}$
$w_{in}^* = 0.009424 \text{ kg/kg dry air}$ and $SHR = 0.6$	24.1%	6.7%	13.9%
w_{in} approximated by w_{in}^* and $SHR = 0.6$	14.0%	3.9%	24.3%
w_{in} approximated by w_{in}^* and by-pass model	8.9%	2.5%	5.6%

5.3.4 Solver

The resulting minimization problem is a convex mixed integer linear programming problem (MILP) solved with the open-source MATLAB compatible toolbox YALMIP (Lofberg (2004)) coupled to the CPLEX solver (ILOG (2013)). Simulations are performed with a one-hour time step, a prediction horizon of 24 hours and a control horizon of 12 hours for a year of simulation.

5.3.5 Impact indicators

The following grid-impact indicators, first introduced by Baetens et al. (Baetens et al. (2012)), are used to quantify the improvement in load matching brought by the proposed optimal load management scheme. The supply cover factor, γ_S , represents the percentage of local electricity production

consumed on-site

$$\gamma_S = \frac{\sum \min(P^{cons,net}, P^{PV})}{\sum P^{PV}} \quad (5.22)$$

where $P^{cons,net}$ represents the net power consumed including net power exchange with the electrical storage (charging and discharging). The demand cover factor, γ_D , represents the percentage of electricity consumption covered by on-site generation

$$\gamma_D = \frac{\sum \min(P^{cons,net}, P^{PV})}{\sum P^{cons,net}} \quad (5.23)$$

Results are also analyzed in terms of overconsumption due to load shifting, and CO₂ emissions.

5.3.6 System right-sizing

The pay-back time of the system, PB , is defined by Equation (5.24), and is a function of the net investment costs, C , including tax credit incentives, the retail electricity price, π^{ret} , the interest rate, r , the annual energy consumption, E^{cons} , and the percentage of annual cost savings, S .

$$PB = \frac{C}{\sum_{i=1}^{PB} S(\alpha, P_{PV}) E^{cons} \pi^{ret} (1+r)^i} \quad (5.24)$$

For the system to be profitable, it should be sized so that the pay-back time does not exceed the expected system lifetime (L), i.e.

$$PB \leq L \quad (5.25)$$

For a given installed PV capacity, buy-back ratios less than unity tend to decrease the cost savings for the end-user. This increases the pay-back time of the system and reduces the maximum area that can be installed. The optimal control strategy investigated here helps mitigate this pay-back time increase, which, for a given buy-back ratio, allows for the installation of larger systems, compared to a conventional control. To propose guidelines for right-sizing of PV systems, the optimal control strategy is simulated for a set of buy-back ratios, installed PV capacities and storage. The optimal results are then interpolated to determine the largest system size that satisfies Equation (5.25), for each buy-back ratio.

5.4 Results and discussion

5.4.1 Influence of metering programs

As mentioned in Section 5.3.2.1, the building investigated is a typical 4-bedroom single-story ranch-type American house built in the 1990's (Figure 5.3). The envelope insulation levels meet standard efficiency code (International Code Council (ICC) (2003)) for the climate zone associated with the city of Indianapolis in the Midwest (zone number 5, International Code Council (ICC) (2009)). Overall

air-to-air heat transfer coefficients (U values) for walls, roof and windows and a breakdown of the annual electricity consumption are given in Figure 5.3. High efficiency photovoltaic panels are installed on the west slope of the roof of the house. The choice of orientation can be justified by the interest of a mid-afternoon peak PV production in the case of high peak electricity consumption in the evening and in the absence of additional electrical storage. For the following results, a total surface of PV panels of 30m², equivalent to 50% annual load coverage is considered. Table 5.2 summarizes the characteristics of each system. The weather data used in the simulations are hourly values of solar irradiation and meteorological elements for Indianapolis, IN for a one-year period based on the National Solar Radiation Data Base updated for years 1991 to 2005.

Five metering tariffs are investigated, out of which four are flat tariffs with buy-back ratios set respectively to 1, 0.75, 0.25 and 0.01. A fifth tariff following a predefined daily profile is used where the buy-back ratio is equal to one during peak demand hours (7 to 9 am and 6 to 8 pm) and to 0.1 during off-peak hours. Results are presented in terms of annual demand and supply cover factors (Section 5.3.5), total annual electricity consumption, and cost savings for the consumer compared to the costs without PV collectors. Results for the different cases are summarized in Table 5.3. It should be noted that these results constitute an upper limit on the load matching potential, and that in practice, buy-back tariffs of less than 1 might only be applied during time-periods of grid congestion.

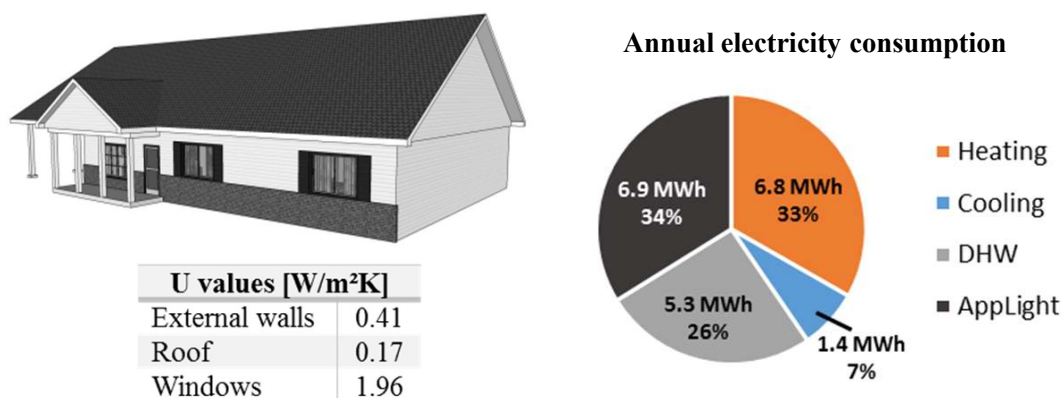


Figure 5.3 – Ranch house (reproduced from Holloway (2013)) – Building envelope characteristics and breakdown of annual electricity consumption.

For a control strategy without optimal load management, which consists in the tracking of a prescribed temperature set point, the demand and supply cover factors have no dependence on buy-back ratio. Conversely, for optimal load management that decreases surplus PV production, both demand and supply cover factors increase with decreasing buy-back ratio. When the electricity surplus sale price is reduced from 100% to 75% of the retail price, demand and supply cover factors increase by about 3% and 6%, respectively, with optimal control. A less significant improvement (3% and 5%) is observed when reducing the tariff from 75% to 25%. The total cost savings for the consumer diminishes by 4% and 10.9% when the PV production buy-back price is reduced respectively from 100% to 75% and from 100% to 25%. The results in terms of cover factors obtained with the variable tariff for peak and off-peak periods (predefined daily profile) are very similar to those obtained for a flat buy-back price of 25% of the retail price. For the present case study, with limited storage capacity, the values for the demand

Table 5.2 – Systems characteristics summary for ranch-type house.

Systems characteristics - Ranch house		
Heat pump	Heating capacity / COP (rated conditions for heating)	11.7 kW / 3.7 (47°F / 70°F)
	Cooling capacity / COP (rated conditions for cooling)	11.3 kW / 3.9 (95°F / 80°F)
	Back up electric heater	5 kW
Water heater	Volume	0.189 m ³
	Lower / upper element heating power	4.5 kW / 4.5 kW
PV panel	Annual load coverage (surface)	10 – 100% (6 – 60 m ²)
	Efficiency	21.5% (PV manufacturer, 2014)

and supply cover factors approach 0.34 and 0.75, respectively, for a buy-back tariff approaching zero. A monthly analysis of the cover factors is summarized in Table 5.4. As expected, the demand cover factors are higher in the summer, whereas the supply cover factors are higher in the winter.

Table 5.3 – Supply/demand cover factors, total electricity demand and cost savings for five metering tariffs. Cost savings are compared to a case without PV collectors. The control strategy with "No optimization" consists in a conventional tracking of a prescribed indoor temperature set point.

α	<i>Optimal</i>				<i>No optimization</i>			<i>Comparison</i>
	γ_D []	γ_S []	P_{cons} [MWh/y]	Cost saving [%]	γ_D []	γ_S []	Cost saving [%]	Cost saving increase
1	0.27	0.59	18.80	50.3%	0.28	0.64	43.9%	6.4%
0.75	0.30	0.65	18.82	46.3%	0.28	0.64	40.0%	6.4%
0.25	0.33	0.70	19.02	39.4%	0.28	0.64	32.1%	7.3%
profile	0.32	0.69	19.19	39.6%	0.28	0.64	31.3%	8.3%
0.01	0.34	0.75	19.41	36.4%	0.28	0.64	28.3%	8.1%

Table 5.4 – Supply and demand cover factors – monthly analysis.

α	Demand cover factor γ_D			Supply cover factor γ_S		
	Mean	Min (month)	Max (month)	Mean	Min (month)	Max (month)
1	0.27	0.11 (12)	0.57 (7)	0.59	0.47 (4)	0.89 (1)
0.75	0.30	0.12 (12)	0.62 (7)	0.65	0.53 (5)	0.98 (1)
0.25	0.33	0.13 (12)	0.66 (7)	0.70	0.58 (5)	0.99 (1)
profile	0.32	0.13 (12)	0.63 (7)	0.69	0.57 (5)	0.99 (1)
0.01	0.34	0.13 (12)	0.68 (7)	0.75	0.63 (5)	0.99 (1)

Despite the increase in on-site consumption of local electricity production with lower buy-back ratios, the total electricity consumption cost for the consumer seems to increase (Table 5.3). However, the cost savings should not be compared between the different tariffs. For the same tariff enforced by the electricity supplier, optimizing the consumer's load profile to match PV production brings up to about 8.3% additional cost savings compared to results without optimization.

Figure 5.4 and Figure 5.5 compare example optimal responses obtained for two buy-back tariffs: 100% and 25% of the retail price.

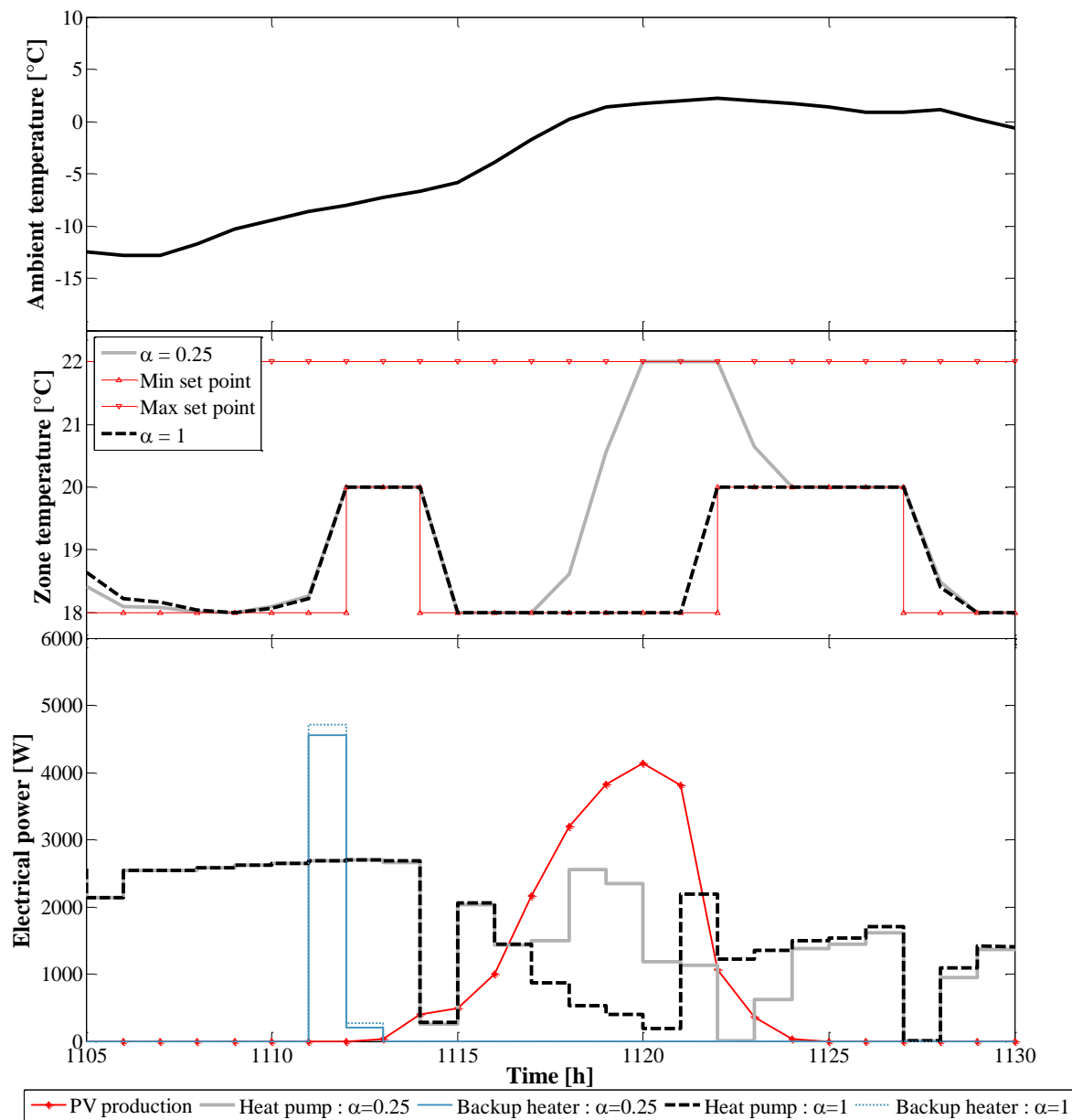


Figure 5.4 – Bottom - Electrical power consumption for space heating for $\alpha=1$ and $\alpha=0.25$ and PV production for February 15th. Top - Corresponding zone and ambient temperatures.

As can be observed in Figure 5.4, for lower net-metering tariffs, the optimal control tends to shift the heat pump electrical demand to periods of time with simultaneous PV production. The building zone is preheated in order to lower the electricity consumption during periods of time with the absence of sun. For the example shown in Figure 5.4, preheating the indoor air allows the heat pump to remain off for the next hour, and to work for shorter time periods the following hours. An analogous trend is observed in Figure 5.5 for the electric water heater. Preheating the water typically allows for up to a three-hour slowdown of the system. The amount of load shifted by using the DHW heaters and the heat pump varies with the buy-back ratio and the period of the year. Figure 5.6 shows the monthly additional load shifted by each system towards periods with PV production, for buy-back ratios of 0.75

and 0.01 compared to a buy-back ratio equal to unity. For a buy-back ratio of 0.75, the incentive to shift the load is not very strong and the amount of load shifted is relatively homogeneous throughout the year. During the summer, most of the load shifted is ensured by the water heaters. Indeed, shifting the heat pump demand to periods of the day with warmer ambient temperatures increases the heat pump consumption, which in turn may be less profitable than selling the excess PV production at a reduced resale price. In contrast, for a buy-back ratio of 0.01, contrariwise, the monthly evolution of the load shifting potential is directly correlated to the amount of PV production. The amount of load shifted using the building structure as thermal storage is about two times larger than with the water heater. It should be noted that the values obtained are strongly dependent on temperature dead bands set as constraints, and would differ for a building with higher thermal inertia.

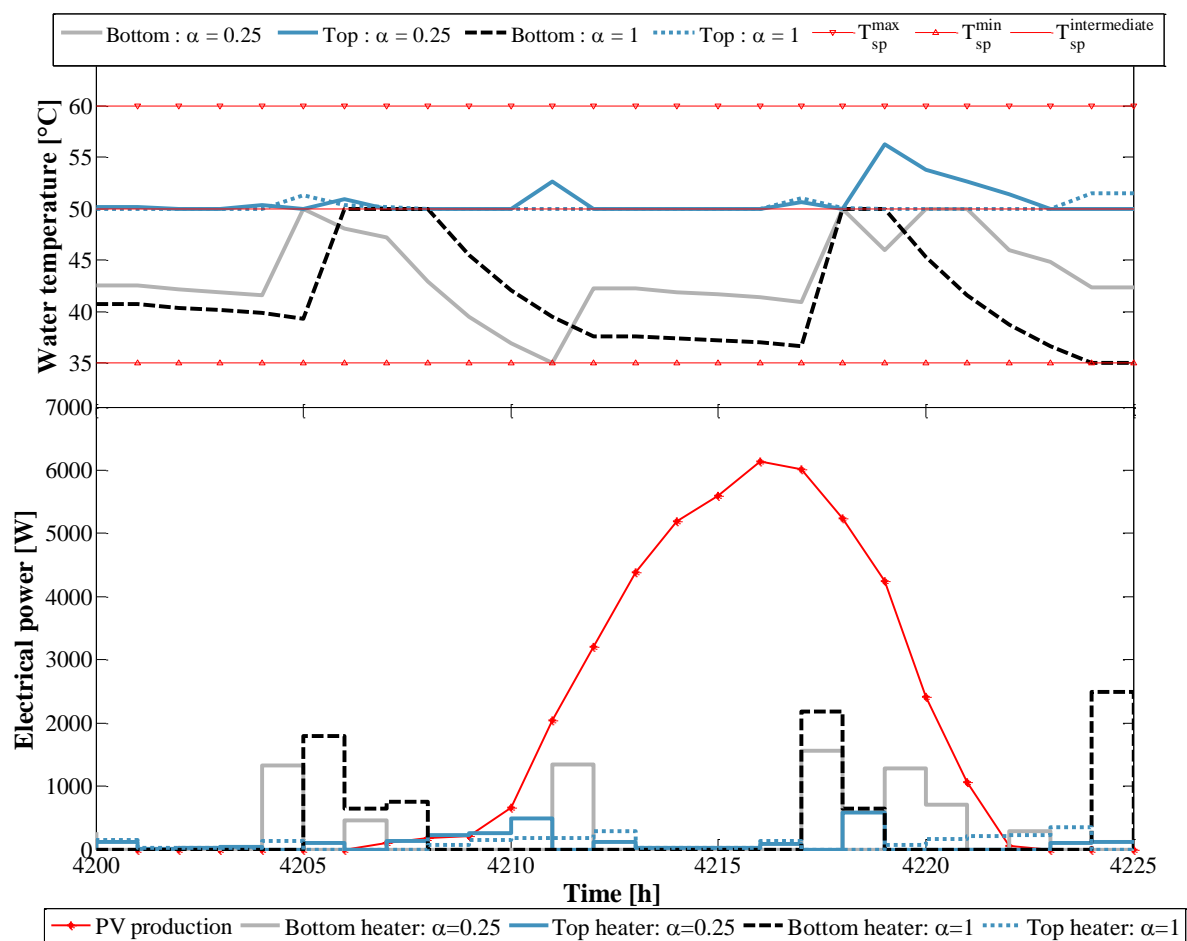


Figure 5.5 – Bottom - Electrical power consumption for DHW for $\alpha=1$ and $\alpha=0.25$ and PV production for June 24th. Top - Corresponding water tank lower and upper thermostat temperatures.

Finally, the optimal total electricity demand profile obtained with the time-varying net-metering pricing is illustrated in Figure 5.7. Load matching is enforced during off-peak hours, typically in the afternoon when the PV production is maximum. This also tends to shift part of the morning and night consumption peaks to off-peak periods, but not as significantly as for constant tariffs. Indeed, since surplus electricity production can be sold at a higher price during these periods, it remains interesting for the consumer to deliver electricity back to the grid. Therefore, flat tariffs seem more suitable as an

incentive for load matching.

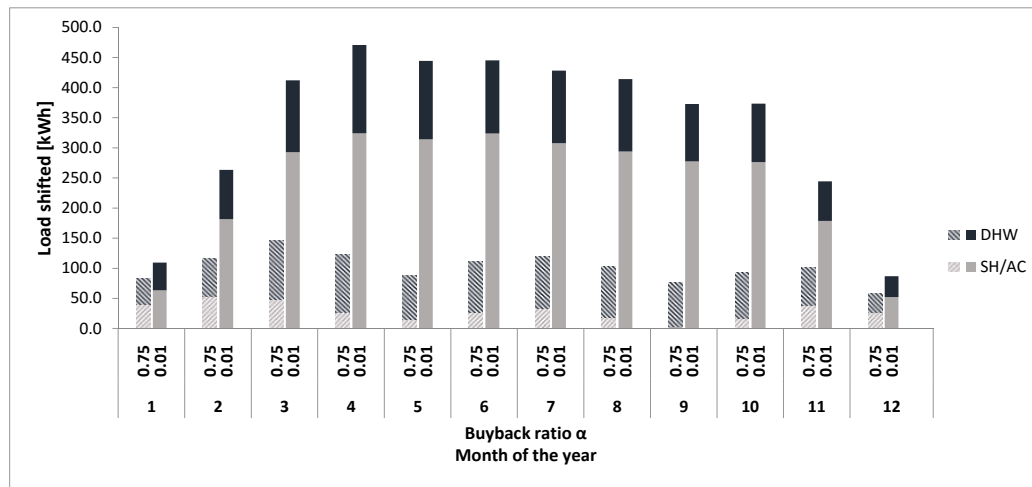


Figure 5.6 – Thermal load shifted to match PV production per month for DHW and space heating or air-conditioning (SH/AC).

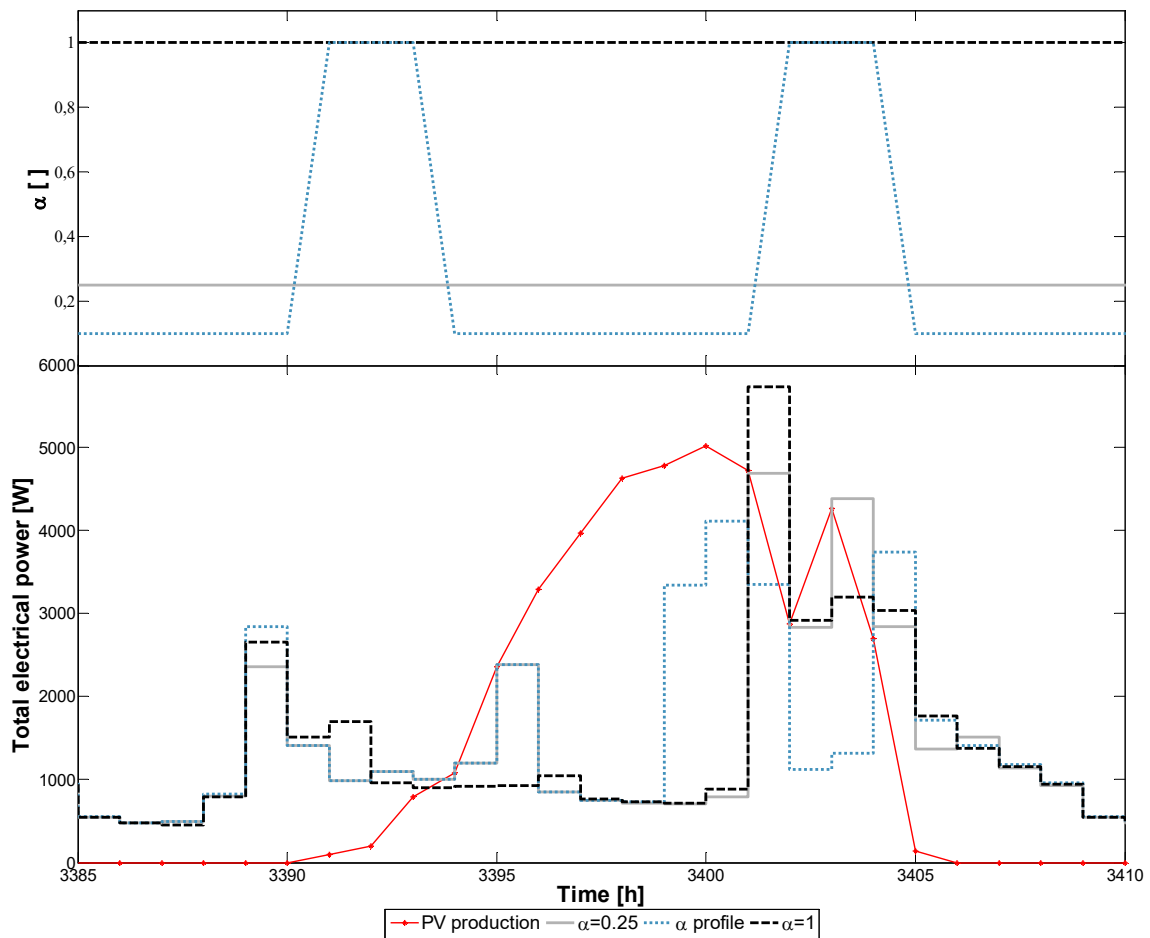


Figure 5.7 – Comparison of total electricity consumption and PV production for α following a daily profile (1 during peak hours and 0.1 during off-peak hours), $\alpha=0.25$ and $\alpha=1$.

Load shifting to increase load matching also leads to an increase in the total annual electricity consumption of up to 3.3% (Table 5.3) compared to a buy-back ratio of unity. Figure 5.8 identifies the sources of overconsumption. During the heating season, as the buy-back ratio decreases, the slightly higher set points achieved tend to increase the ambient heat losses and can slightly deteriorate the COP of the heat pump. In cooling mode, the heat transfer through the building envelope increases due to lower set points. The average COP tends to improve for a buy-back ratio of 0.75, as the unit works closer to full load which reduces performance degradation due to cycling losses. For lower buy-back ratios however, this effect is counterbalanced by the performance degradation due to greater operation of the unit during time periods with high ambient temperatures. The relative share of heat losses from the water tank tends to diminish with decreasing buy-back ratios, but the absolute value of energy wasted increases. One could argue that overconsumption could counter-balance the benefits retrieved from using on-site renewable electricity production in terms of CO₂ emissions. This is discussed in Section 5.4.4.

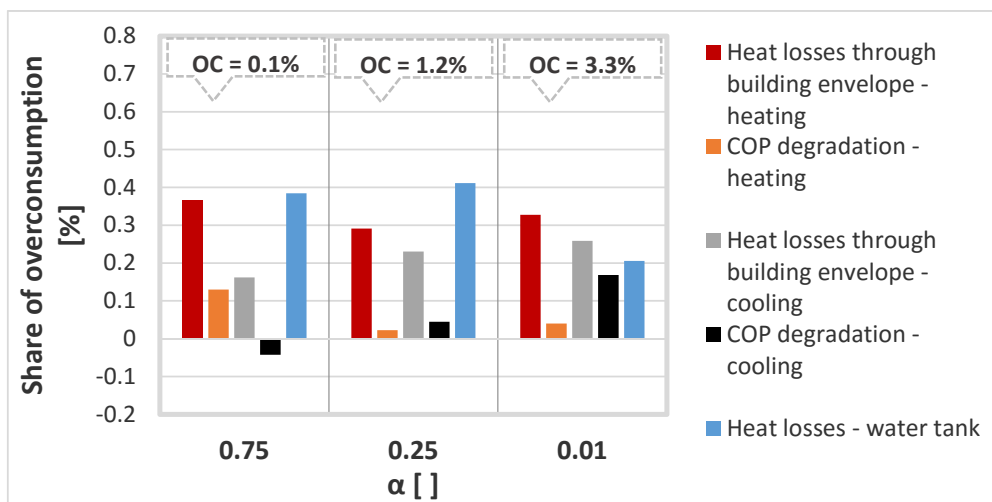


Figure 5.8 – Sources of overconsumption compared to buy-back ratio of unity.

5.4.2 Influence of thermal storage

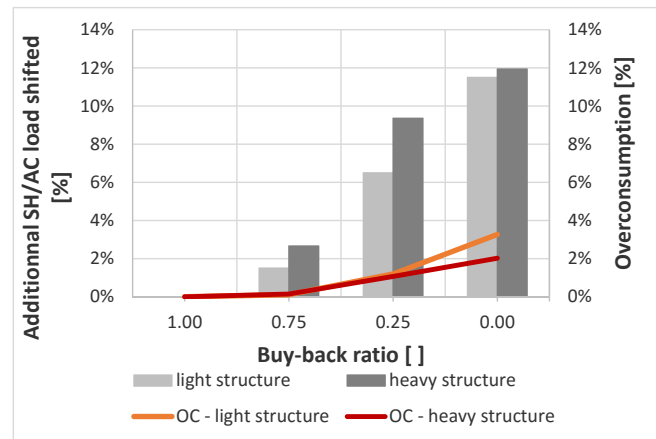
The building considered in the above sections is a typical light wooden structure for residential construction in the U.S. Similarly, the volume of the water tank is set to the average value for a 4-bedroom house, i.e. 189 liters, which is less than the average daily DHW use (Section 5.3.2.4). The storage capacity for load shifting is therefore limited, and it is worth investigating the load matching potential attained with additional thermal storage. Two options are considered here. In the first case, the thermal inertia of the building is increased by replacing the light wooden structure by heavy concrete walls. The overall U-value remains unchanged.

Figure 5.9a shows the additional percentage of load shifted for space conditioning as a function of the buy-back ratio. The additional percentage of load shifted is greater with the heavy structure, but the increase becomes less significant as the buy-back ratio decreases. The heavy structure also allows for slightly more efficient load shifting with less overconsumption and increased cost savings (Table 5.5 – left). The second option consists in increasing the size of the DHW tank. Other standard DHW tank sizes available on the market are 300 liters and 450 liters. When decreasing the buy-back ratio

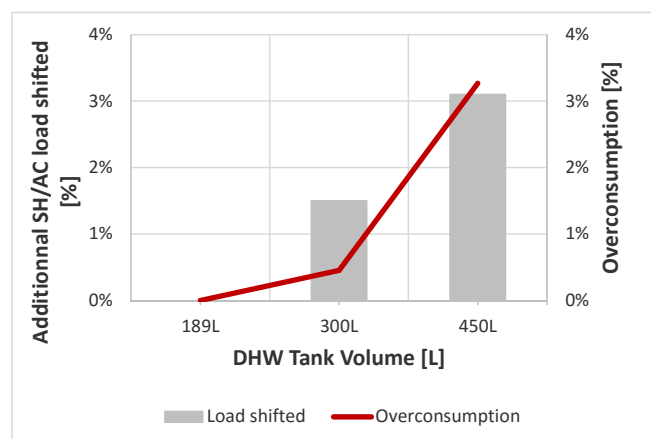
from one to zero, up to 3.1% additional DHW electricity consumption can be shifted to match PV production, compared to results with the baseline tank volume, as shown in Figure 5.9b. However, additional overconsumption of up to 3.3% is observed. The additional cost savings, without taking into account the extra investment for a larger water heater, reach up to 5.2% (Table 5.5 – right).

Table 5.5 – Cost savings increase – Left: heavy vs light structures – Right: DHW tank volume. Cost savings increase are determined compared to a case without optimal control.

α	Cost saving increase		Volume	Cost saving increase	
	Light	Heavy		$\alpha=1$	$\alpha=0.01$
1	6.4%	7.2%			
0.75	6.4%	7.3%	0.189 m ³	6.4%	8.1%
0.25	7.3%	8.9%	0.300 m ³	6.4%	11.4%
0.01	8.1%	10.1%	0.450 m ³	6.3%	13.3%



(a) SH/AC: Light and heavy building structures.



(b) DHW: impact of increasing water heater tank volume with a buy-back ratio of 0.01, compared to a tank volume of 189 liters and a buy-back ratio equal to unity.

Figure 5.9 – Additional load shifted and overconsumption (OC).

Other options exist, such as replacing the ducted heating system by a radiant floor heating with additional water storage tank. This requires significant changes and is better suited for new construction rather than as a retrofit option. They are worth investigating in future work.

5.4.3 Additional electrical storage

An additional electricity storage system was added to the systems used in Section 5.4.1 and additional simulations were performed. The characteristics are provided in Table 5.6. It was found that with a flat electricity tariff, buy-back ratio of one, and round trip efficiency less than 100%, then optimal control leads to no utilization of the battery regardless of the battery capacity and PV system sizing. In other words, it makes no sense to utilize a battery if the utilities will buy back electricity at the same rate they sell it, except for ensuring security of supply in the case of power outage. However, as the buy-back ratio decreases from one to zero, the use of the battery helps increase cost savings and load cover factors, as shown in Table 5.7 for fifty percent load coverage by west-oriented PVs and a battery size of 7kWh. The maximum additional cost savings for a buy-back ratio 0.01 are only about 5%, resulting from increased demand and supply cover factors. The use of south-oriented PV panels led to an additional cost savings of 4% compared to west-orientated ones. However, overconsumption resulting from load shifting went up by 17% in that case.

Table 5.6 – Battery characteristics (manufacturer data, 2015).

Systems characteristics - Ranch house		
Battery	Capacity	7 kWh - 10.5 kWh - 14 kWh
	Maximum charge/discharge rate	3.3 kW
	DC/DC roundtrip efficiency	0.92
	Battery cost	429\$/kWh
	Inverter and installation cost	1500\$

Table 5.7 – Results for west-oriented PVs with 50% load coverage: comparison between thermal storage only and an additional battery of 7kWh.

Thermal storage				Thermal + electrical storages			Comparison
α	γ_S []	γ_D []	Cost saving [%]	γ_S []	γ_D []	Cost saving [%]	Cost saving increase
1	0.59	0.27	50.3%	0.59	0.27	50.3%	0.0%
0.75	0.65	0.30	46.3%	0.80	0.37	47.1%	0.8%
0.25	0.70	0.33	39.4%	0.83	0.38	43.0%	3.6%
0.01	0.75	0.34	36.4%	0.87	0.39	41.3%	4.9%

With a flat retail tariff and a constant buy-back ratio, the optimal control stores the excess PV production in the battery, but never supplies it back to the electricity grid. To consider the possibility of resale of the electricity stored in the battery to the grid, the buy-back ratio profile presented in Section 5.4.1 was used and is illustrated in Figure 5.10 (top). This profile encourages the sale of excess PV production or the resale of electricity stored in the battery to the grid during time periods with high buy-back ratios. Electrical power management is illustrated in Figure 5.10 (bottom) for an area of south-oriented PV-panels ensuring 100% annual load coverage and a battery capacity of 14kWh for three days of the

spring season. The optimal control stores surplus electricity produced by PVs when the buy-back ratio is equal to 0.1 and releases it either to the grid when the buy-back ratio is equal to unity or directly supplies the house when there is a lack of PV production. In this particular case, 14% of the annual energy released by the battery is directly sold back to the grid.

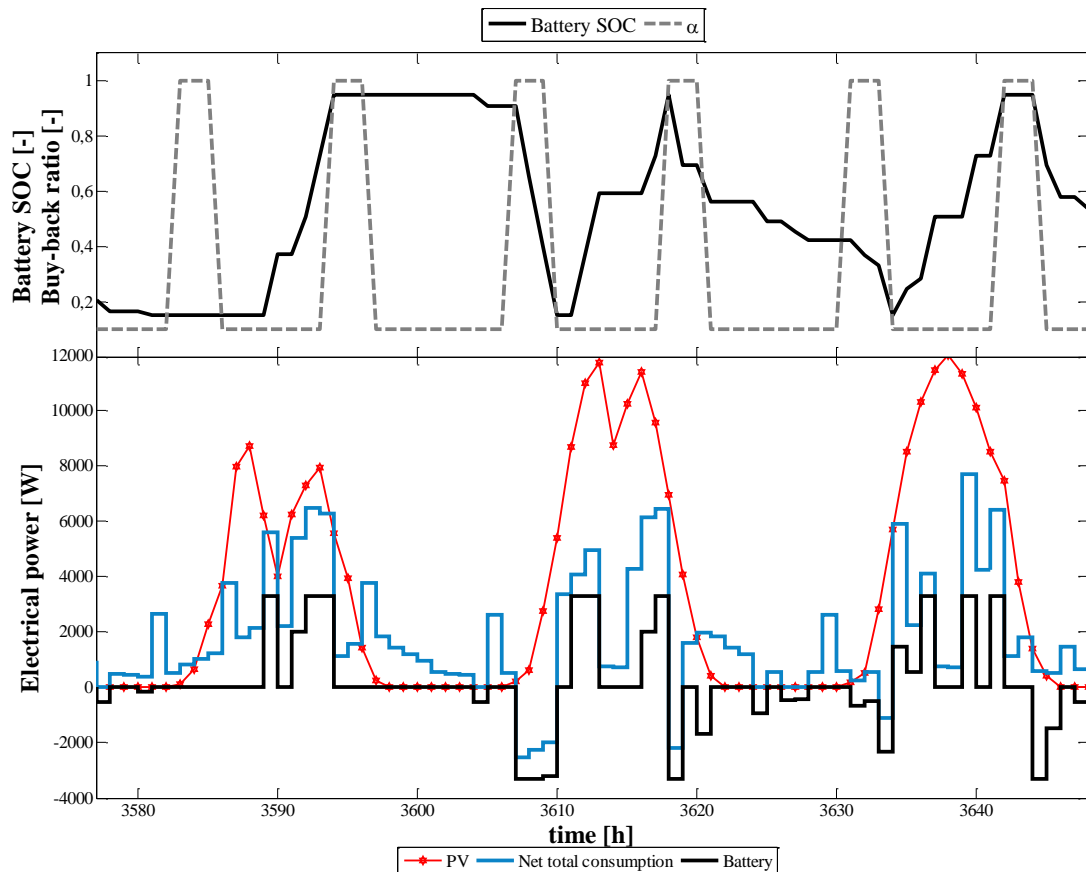


Figure 5.10 – Top: Battery state of charge and buy-back ratio profile for 3 days in the spring with south-oriented PVs, an annual PV load coverage of 100%, and a battery capacity of 14kWh. Bottom: Corresponding PV production, net electricity consumption and battery power.

5.4.4 Guidelines for system right-sizing

This section illustrates how cover factors and consumer pay-back times change with the size of the PV installation for different buy-back ratios and different storages. In the US, the average installation cost of PV panels was 3.27 \$ per watt peak in 2015 (National Renewable Energy Laboratory (NREL) (2015)). No significant scale benefits can be observed for an installed power in the range of 5kW_p to 10 kW_p. A federal tax credit incentive provided 30% reduction of the cost for residential PV systems (IREC 2012). The electricity retail tariff for residential consumers in Indiana was 0.11 \$/kWh. For the scenario with an electrical battery, investment costs were composed of 1500\$ for the inverter and the installation of the system, and of 429\$ per kWh of installed capacity. For the scenario with larger DHW tanks, the additional cost is about 350\$ per hundred liters. The case-study system of Section 5.4.1, with a DHW tank of 189L, is chosen as reference for this section. For this system, two control strategies are simulated: a strategy based on a conventional tracking of a prescribed indoor set point, referred to

as rule-based control (RBC), and the optimal control strategy proposed in this chapter, referred to as OPC. Three areas of PV panels are considered: 50%, 100% and 200% annual load coverage. For each of them, a comparison is performed between the reference case and the case-study system with either a water heater of 300L or three different battery sizes.

The impact of varying PV system size and storage type on the demand cover factor is presented in Figure 5.11 for a buy-back ratio of 0.01. Compared to the RBC reference, the increase in demand cover factor reaches up to 28%. Figure 5.12 illustrates the pay-back time reduction brought by the OPC formulation, compared to the RBC reference, for a buy-back ratio of 0.01. Reductions of 11% to 25% are observed depending on the load coverage and storage. With 50% PV load coverage, thermal storages lead to larger reduction in pay-back time, as the excess PV production to store in the battery is limited. For 100% PV load coverage, increasing the water heater volume from 189L to 300L decreases the pay-back time by a value close to the one obtained when using a 7kWh battery. For larger PV coverage, pay-back time reductions increase significantly with the capacity of the electrical storage. The use of electrical storage brings significant cost savings for the end-user. However, if the lifetime of the system is limited to 30 years for PVs and 10 years for an average domestic battery, none of the configurations with a battery investigated here are actually economical in the case of a buy-back ratio of zero. With the adopted assumptions on investment cost, pay-back times range from 15.4 years for the reference system to 37.3 years for the largest PV areas and battery storage. Conclusions may differ for time-varying buy-back ratios and retail tariffs.

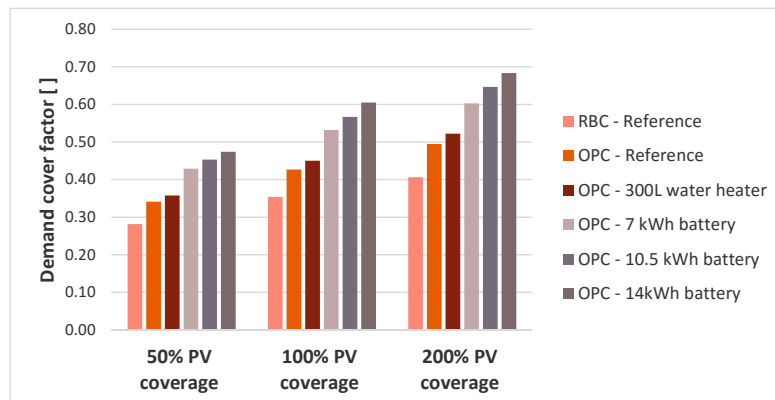


Figure 5.11 – Evolution of demand cover factor between the reference case (Section 5.4.1) with rule-based control (RBC) and optimal control (OPC) with the default systems, a water heater of 300L and three battery sizes for PV annual load coverages of 50%, 100% and 200% and a buy-back ratio of 0.01.

Figure 5.13 shows the reduction in CO₂ emissions for each case based on monthly average hourly data for the electricity production mix of RFC West subregion (OpenEI (2011)). These values were generated based on demand profiles of year 2008 and constitute the most comprehensive database available¹. With thermal storage only, the reductions reach 11% to 21%, whereas with additional electricity storage, the reductions increase to 22% to 46%.

As thermal storage offered by the building envelope and the water heater are naturally available in any house, a deeper analysis of the right sizing of PV panels with thermal storage only is proposed here after.

¹Using constant emission factors is only justified if a limited number of buildings is considered. Heat pumps and/or PV in a large number of buildings will influence the emission factor of central power generation.

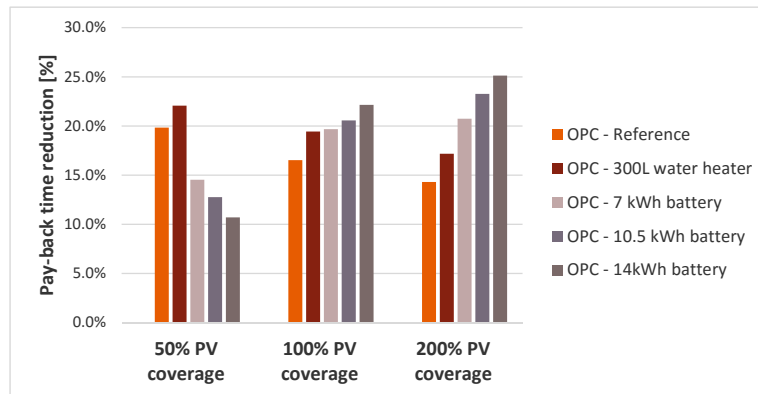


Figure 5.12 – Evolution of the pay-back time reduction with optimal control (OPC) of the default systems, a water heater of 300L and three battery sizes for PV annual load coverages of 50%, 100% and 200% and a buy-back ratio of 0.01 compared to the reference case.

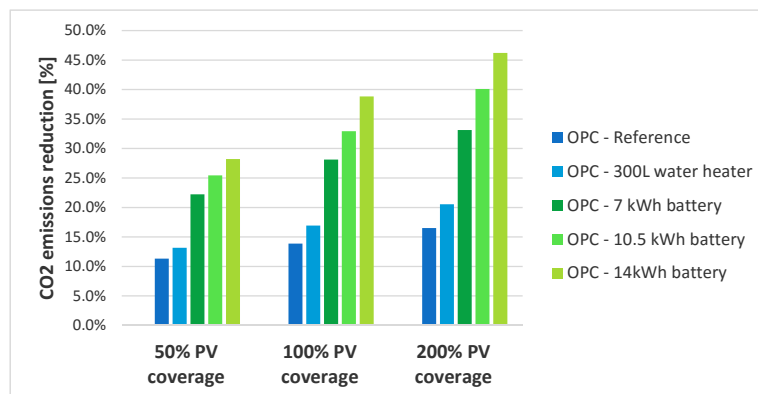
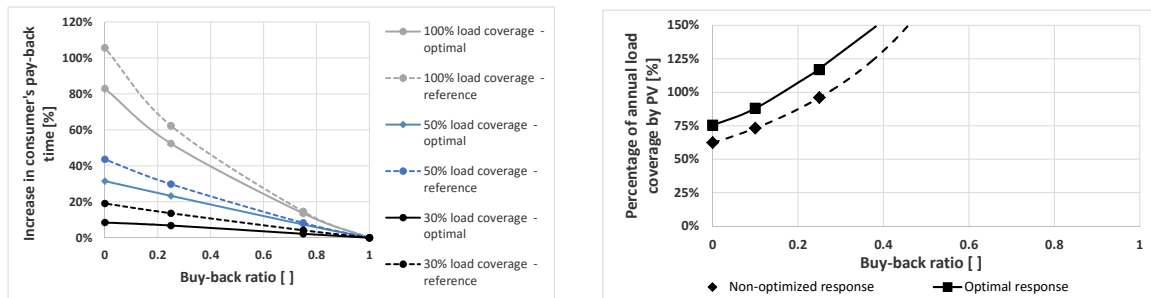


Figure 5.13 – CO₂ emissions reduction with optimal control (OPC) of the default systems, a water heater of 300L and three battery sizes for PV annual load coverages of 50%, 100% and 200% and a buy-back ratio of 0.01 compared to the reference case.

The total surface of PV panels was varied between 10% to 100% annual load coverage. As expected, for approximately the same total electricity consumption, the demand cover factor increases with the surface area of PV panels. However, the same tariff incentive promotes load shifting to different extents depending on the PV area. The largest load coverage by PV for a given buy-back ratio can be obtained from Equation (5.25). For this case study, Figure 5.14a compares the consumer's pay-back time for optimized and non-optimized load management as a function of the buy-back ratio for different PV areas. The pay-back time increases significantly with decreasing buy-back ratios, and especially for larger PV areas. For buy-back ratios decreasing from 1 to 0.25, the pay-back time for non-optimized load control increases by 14%, 30% and 62%, respectively, for 30%, 50% and 100% annual load coverage. Optimizing load profiles to match on-site PV production reduces this increase by 7% to 10%. Thus, for net-metering programs with buy-back ratios less than one and no other economic incentives, installing larger PV areas without increasing on-site storage capacity to promote load matching may become unprofitable. Given a life expectancy of about 30 years for PV panels, optimum sizing of PV panels, expressed in terms of percentage of the annual electricity consumption covered, can be derived

for each buy-back ratio. Results are illustrated in Figure 5.14b. For a buy-back ratio of 1, there is no theoretical limit, and a maximum of PV panels should be installed. For buy-back ratios less than 0.3, an optimum value arises. The maximum coverage goes down to 62% for non-optimized load profiles and 75% for optimized ones as the buy-back ratio approaches zero. These conclusions are closely linked to metering programs implemented in this study. The electricity supplier could promote other incentives in parallel, such as payoffs to prosumers who optimize on-site electricity consumption.



(a) Increase in consumer's pay-back time as a function of the buy-back ratio for three different load coverages (30%, 50%, 100%).

(b) Optimal load coverage by PV vs buy-back ratio.

Figure 5.14 – Determination of the influence of the buy-back ratio on the optimal load coverage by PVs.

5.5 Parametric studies

Several parameters are likely to influence the above results, such as system investment costs, retail electricity tariffs and electricity production mix. For example, significant differences exist between the different zones of the US. Average retail tariffs range from 0.069 to 0.34 \$/kWh (U.S. Energy Information Administration (EIA) (2013)). The impact of the buy-back ratio on the system pay-back time decreases with the increase in retail tariff and new optimal load coverage can be determined. Average CO₂ emissions in the U.S. vary between 369 to 789 kg/MWh of produced electricity (OpenEI (2011)). Depending on the electricity production mix, overconsumption entailed by load shifting may counterbalance reductions in emissions by increased on-site consumption of renewable energy. Projections regarding PV installation cost reach less than 1.5\$ per watt peak (U.S. Department of Energy (DOE) (2014)) and battery cost of 137\$/kWh (Brinsmead et al. (2015)) by 2035. Conclusions regarding the economic viability of thermal and electrical storage will be impacted.

In that regard, further analysis with thermal storage is carried out for different climate zones in the U.S., defined in International Code Council (ICC) (2009). Results are provided in Annex A.4.

5.6 Research outcome

A general method for optimal management of decentralized electricity production unit and HVAC system with storage in response to evolving metering programs is proposed. It is expected that future utility incentive programs will seek to minimize the excess electricity production delivered to the grid by promoting on-site consumption through the use of different metering tariffs. The proposed optimal

control formulation is very flexible, and can be applied to any type of storage systems (thermal or electrical) and of decentralized electricity production units, such as PV panels or μ -CHP units.

Given the variety of climates and electricity generation and prices investigated, general trends can be highlighted from the above results. With thermal storage capacity inherently available in most houses, composed of the thermal capacity of the building envelope and of the water tank for domestic hot water, it can be concluded that

- reducing buy-back ratios proves to be an effective way to promote load matching with on-site PV production. Surplus electricity production by PV delivered to the grid can be reduced by 10 to 30%.
- this potential tends to increase for climates with homogeneous PV production and temperature throughout the year.
- load matching is achieved through load shifting, which causes overconsumption as a side effect, due to increased heat transfer losses and degradation of system performance at part-load. The efficiency of load shifting is improved for well thermally-insulated houses, in particular for extreme climates.
- optimal load management helps reduce the impact of buy-back ratio and electricity retail tariff on the optimal sizing of a PV system. For heating-dominated climates, optimal load management allows increases of 30 to 80% in the optimal size of the system. The influence is the most substantial for locations with low PV potential and low electricity retail tariffs. The influence is less prominent for cooling-dominated zones.
- despite overconsumption of 3 to 9% engendered by load shifting, CO₂ reductions reach 6 to 46%.

To illustrate the flexibility of the proposed approach, the case of electrical storage was also considered. However, it was only investigated in the particular case of Indianapolis, IN. In that context, the additional cost savings brought by electrical storage are not sufficient for such systems to be economical. This conclusion is tightly bound to the low retail tariff in that state, and will vary according to local solar potential and retail tariff in place in other states. The proposed method easily extends to any other location, which is left for future work².

²For an insight on the economical viability of batteries in the European context, the reader is referred to the study of Quoilin et al. (2016).

6 Residential heat pump as flexible load for direct control service

This chapter is adapted from:

E. Georges, B. Cornélusse, D. Ernst, V. Lemort and S.Mathieu, " Residential heat pump as flexible load for direct control service with parametrized duration and rebound effect", *Applied Energy*, Vol. 187, pp 140–153, 2017.

6.1 Introduction

The increase in decentralized power generation and the integration of intermittent renewable energy sources in electrical distribution systems have entailed a rising interest in the use of load modulation services (Gellings (1985)). These services are provided by load aggregators which manage and trade the demand flexibility of electricity consumers.

This study takes the point of view of a load aggregator controlling a cluster of domestic heat pumps. The aggregator wants to offer direct control flexibility services. The services consist of an upward or downward modulation for a fixed number of periods followed by a constrained number of periods characterizing the rebound effect. The achievable power modulation amplitude is determined with respect to a reference baseline. This baseline is such that it minimizes the energy costs for the end-user. The activation of the flexibility is performed in three steps: (i) the modulation, (ii) a delay period with no deviations from the baseline consumption, and (iii) a payback period during which deviations in consumption occur to allow the heat pumps to return to their baselines. The amplitudes of the achievable modulations and of the deviations during the payback are well defined within the service.

The interest in quantifying the flexibility of heat pumps within a well-defined flexibility service resides in the opportunity to exchange it as a commodity in the electrical system and electricity markets. Different actors could resort to this flexibility service: an electricity retailer could use it either to balance its portfolio as a balance-responsible party or to adjust its consumption according to day-ahead spot market prices. In the electricity market, deviations from the positions stated to the system operator, in this case, the baselines, expose the market participant to a penalty based on the imbalance tariff. Therefore, the knowledge of the payback following the modulation is key information to activate the flexibility service. A system operator could rely on the service to relieve a congestion in a line or a transformer. The quantification of the payback resulting from the modulation allows the system

operator to activate the service without creating congestions further in time. Finally, a system operator could also rely on this service for balancing purposes (Mathieu et al. (2013), Mathieu et al. (2014)). Here again, the knowledge of the payback avoids the system operator reaching an unpredicted system imbalance following the activation of the modulation.

Relevant studies from the literature are summarized hereafter. Pavlak et al. (2014) investigate the potential of using the thermal mass of office buildings to minimize peak demand. A day-ahead multi-objective optimization is implemented to provide the modulation service at minimum cost for the end-user and minimum frequency regulation cost. The optimization also determines the optimal time period to activate the load modulation. The study is extended to a portfolio of office buildings in the study of Pavlak et al. (2015) and the possible additional benefits retrieved from synergies between the buildings are outlined. De Coninck and Helsen (2016) propose a bottom-up approach to determine the flexibility of buildings and heating, cooling and air-conditioning systems. Three optimal control problems are solved to determine, first, a cost-optimal baseline for the consumer, and then, the maximum upward and downward modulations available during a given time span of the day. Ali et al. (2015) propose a similar optimization scheme to the one presented by De Coninck and Helsen (2016) that is applied to residential demand response. The cost-optimal day-ahead prediction of the baseline is followed by an intra-day modulation with the introduction of "bonus" price incentives. A sensitivity study of the percentage of storage capacity allocated to the day-ahead and to the intra-day optimizations is carried out. The study also proposes a method to aggregate cost functions to optimize a cluster of systems and to model the price elasticity of such loads for unit commitment applications.

In light of the literature review, the first contribution of the present study lies in the investigation of a flexibility service with detailed models of thermostatically controlled loads. The second contribution is the characterization of the payback following the activation of the upward and downward power modulation service and of its influence on the achievable modulation amplitude for different periods of the day. The characterization of the payback is particularly useful for operational planning of the distribution network and real-time activation of the service by different actors. The methodology is therefore complementary to the methods presented by De Coninck and Helsen (2016) and Ali et al. (2015) by constraining the payback time and characterizing the rebound effect in terms of costs and energy volumes, and it differs from the study of Pavlak et al. (2014) in which the payback time is a result of the optimization scheme with a unique daily value. In this study, flexibility can be activated at any moment to tackle unpredicted issues in the electrical system.

The chapter is organized as follows. Section 6.2 defines the flexibility service. Models of the flexible thermal loads are provided in Section 6.3. Section 6.4 presents the two optimization problems to solve to obtain the baseline profiles and amplitudes of modulation. Section 6.5 presents the cluster of buildings representative of the Belgian residential building stock used to illustrate the method. Results are then presented in Section 6.6. Parametric studies are conducted to highlight the influence of the different parameters that characterize the service. Finally, Section 6.7 concludes the study.

6.2 Load modulation service

The mechanism considered in this chapter is a flexibility service consisting in the activation of a load modulation in a given period τ and a constrained rebound effect. The modulation service can be

activated during n consecutive periods. The activation is directly followed by a delay of l periods before a payback of k periods which compose the rebound effect. Within the delay, there is no deviation from the target consumption. During the payback, deviations in consumption are allowed for the system to return to its predefined state after the k periods. A graphical representation of the service is provided in Figure 6.1. The objective of the aggregator is to obtain the maximum modulation amplitude over the n periods, $\delta_\tau, \dots, \delta_{\tau+n-1}$, positive for an upward activation and negative for a downward activation, with minimum payback in the k periods. The dead band of l periods between activation and payback is introduced to mitigate and delay potential additional stresses on the electricity grid brought by the deviations inherent to the payback.

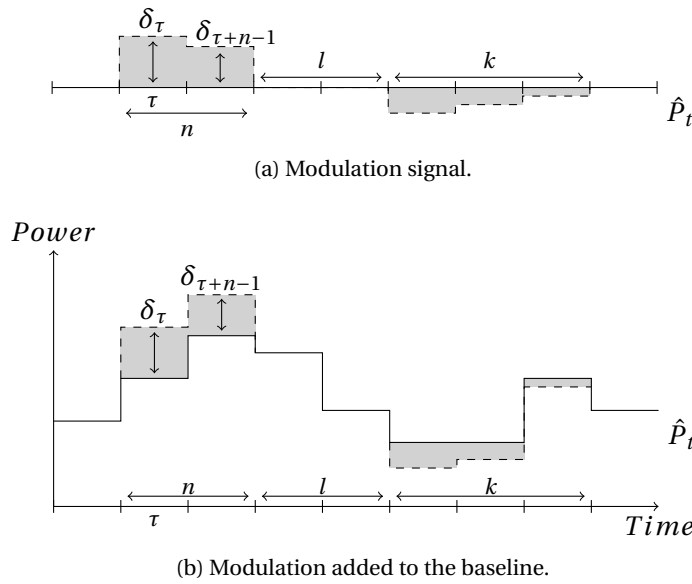
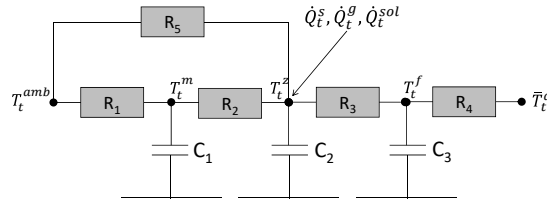


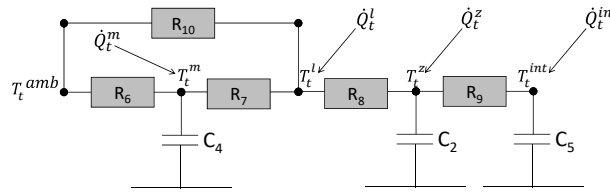
Figure 6.1 – Upward modulation during n periods with a payback of k periods delayed by l periods.

A modulation must be defined with respect to a reference consumption pattern (Goldberg (2010)). In this article, we take as reference a baseline \hat{P}_t that minimizes the consumer's electricity cost. This choice has two motivations. First, the use of flexible heat pumps should benefit the end-user. Minimizing the energy costs appears to be a good incentive for consumers to enroll in flexibility programs proposed by aggregators. The second motivation lies in the possibility for an aggregator to be a balance responsible party, which compels it to state its positions to the system operator prior to real-time. In this work, these baselines are computed by the aggregator and used as references to quantify the power modulations and resulting deviations.

The proposed flexibility service is the result of the aggregation of a set of houses equipped with heat pumps. A typical case is an electricity retailer using the flexibility of its clients to balance its own portfolio as a balance-responsible party. Another example is an aggregator proposing its services to a distribution system operator willing to relieve a congestion in a line or a transformer or to a transmission system operator for its secondary reserve. The aggregator proposes the service detailed in this section to another actor. Using flexibility for self-balancing would not require to define a flexibility service but only to directly optimize the consumption. The actual volume activated by the other actor may be less or equal to the total potential. The service provides all necessary information: the available potential of flexibility and the cost and deviations entailed by the activation of the service.



(a) Model I: model trained from detailed building simulation tools.



(b) Model II: model modified from ISO13790 model (Comité Européen de Normalisation (2008)).

Figure 6.2 – 5R3C Grey-box model structures.

With this information, the other actor is able to make a decision without having to directly manage each individual heat pump.

6.3 Buildings and heat pumps

The heat demand from the buildings can be determined using models containing different levels of details. Grey-box models are simplified models providing an accurate representation of the thermal response of a building with reduced computational requirements (Déqué et al. (2000)). The building thermal behavior is modeled by an equivalent thermal network consisting of thermal resistances, R in K/W, and lumped thermal capacitances, C in J/K. The RC parameters of the network can either be identified from validated models with higher level of details or imposed by normative definitions (Comité Européen de Normalisation (2008)). For the purpose of this study, two different single zone 5R3C models are used. They are illustrated in Figure 6.2. The first model structure, referred to as Model I, is the trained model presented in Section 3.2.1.1, and used to model typical retrofitted freestanding buildings. The second one, referred to as Model II, is a modification of the ISO13790 model, also detailed in Section 3.2.1.1. It is used for the large-scale application of the proposed method, when lack of available data prevents all buildings from being modeled with identified parameters.

Such models allow a straightforward linear state-space formulation of the governing differential equations as follows

$$\mathbf{x}_{t+1}^s = \mathbf{A}^s \mathbf{x}_t^s + \mathbf{B}^s \mathbf{w}_t^s + \mathbf{E}^s \dot{Q}_t^s \quad (6.1)$$

where \dot{Q}_t^s is the space-heating thermal power in period t . In Model I, the state vector \mathbf{x}_{t+1}^s is a three-

element vector composed of the indoor air temperature, T_t^z , the wall mass temperature, T_t^m , and the floor temperature, T_t^f . In Model II, the state vector \mathbf{x}_{t+1}^s is a three-element vector composed of the indoor air temperature, T_t^z , the massive external walls temperature, T_t^m and the massive internal walls temperature, T_t^{int} . \mathbf{w}_t^s is a four-element vector composed of the uncontrolled model inputs, i.e. the outdoor air temperature, T_t^{amb} , the yearly average outdoor air temperature, \bar{T}_t^{amb} , the solar gains, \dot{Q}_t^{sol} and the internal gains due to occupants and electrical appliances, \dot{Q}_t^g . In Model II, solar and internal gains are distributed amongst heat gains \dot{Q}_t^z , \dot{Q}_t^l , \dot{Q}_t^m and \dot{Q}_t^{int} on the different temperature nodes as described in Equations (3.12) to (3.15). The matrices \mathbf{A}^s , \mathbf{B}^s and \mathbf{E}^s are equivalent RC parameters of the state space model dependent on the house modeled.

Indoor thermal comfort for the occupants should be satisfied at any time, as imposed by the constraint

$$T_t^{min} \leq T_t^z \leq T_t^{max}. \quad (6.2)$$

The domestic hot water tank is modeled using a one-node capacitance model with homogeneous water temperature \mathbf{x}_t^w . Heat losses to the ambience are considered. The energy conservation law can be expressed by the state-space formulation

$$\mathbf{x}_{t+1}^w = \mathbf{A}^w T_t^w + \mathbf{B}^w \mathbf{w}_t^w + \mathbf{E}^w \dot{Q}_t^w \quad (6.3)$$

where \dot{Q}_t^w is the domestic hot water heating demand in period t and T_t^w is the water temperature in the tank constrained by

$$T^{min} \leq T_t^w \leq T^{max} \quad (6.4)$$

The input vector \mathbf{w}_t^w is composed of the outdoor air temperature and the mains water temperature. The matrices \mathbf{A}^w , \mathbf{B}^w and \mathbf{E}^w are parameters of the state space model dependent on the house modeled.

Variable-speed air-to-water heat pumps are used to cover the domestic hot water and heating needs of the houses. The choice of variable-speed technology is driven both by the higher efficiency at part-load and by the larger flexibility to perform load following. They are modeled using a linear empirical model based on the ConsoClim method and detailed in Section 3.2.2. The same model is used for space heating and domestic hot water, and it only differs by the temperature of the water supplied to the house and that of the water tank.

6.4 Optimization problems

This section presents the two optimal control problems which an aggregator solves in order to propose flexibility services. The first problem is to determine the electrical consumption of each building that minimizes energy costs in response to a forward retail price signal. This consumption profile, referred to as baseline consumption, is then used as an input for the second optimization problem. The latter determines the maximum upward or downward modulation amplitude that can be achieved from the baseline profile in a given time period.

In the following subsections, the thermal states transition model and the state constraints defined in

Section 6.3 are summarized by

$$\mathbf{x}_{t+1} = f(\mathbf{x}_t, \dot{W}_t^s, \dot{W}_t^w, \mathbf{w}_t) \quad (6.5a)$$

$$\mathbf{x}_t^{\min} \leq \mathbf{x}_t \leq \mathbf{x}_t^{\max} \quad (6.5b)$$

where \mathbf{x}_t is the vector of the state variables, and \dot{W}_t^s and \dot{W}_t^w are the optimization variables corresponding to the heat pump consumption for space heating and for domestic hot water heating, respectively. \mathbf{w}_t represents the set of time-dependent input parameters of the building model.

6.4.1 Baseline electricity consumption profile

The first optimization problem is solved in order to obtain a base consumption profile that minimizes the energy costs of the heat pump's owner. This baseline is denoted by \hat{P}_t and the corresponding states are denoted by $\hat{\mathbf{x}}_t$. This optimization problem is written as

$$\min \sum_{t \in \mathcal{H}} (\pi_t^+ P_t^+ - \pi_t^- P_t^-) dt \quad (6.6a)$$

subject to,

$$\hat{P}_t = P_t^+ - P_t^- \quad \forall t \in \mathcal{H} \quad (6.6b)$$

$$\hat{P}_t = \hat{W}_t^s + \hat{W}_t^w + \Gamma_t \quad \forall t \in \mathcal{H} \quad (6.6c)$$

$$\hat{\mathbf{x}}_{t+1} = f(\hat{\mathbf{x}}_t, \hat{W}_t^s, \hat{W}_t^w, \mathbf{w}_t) \quad \forall t \in \mathcal{H} \quad (6.6d)$$

$$\mathbf{x}_t^{\min} \leq \hat{\mathbf{x}}_t \leq \mathbf{x}_t^{\max} \quad \forall t \in \mathcal{H} \quad (6.6e)$$

$$0 \leq \hat{W}_t^s \leq \hat{y}_t \dot{W}_t^{s, \max} \quad \forall t \in \mathcal{H} \quad (6.6f)$$

$$0 \leq \hat{W}_t^w \leq (1 - \hat{y}_t) \dot{W}_t^{w, \max} \quad \forall t \in \mathcal{H} \quad (6.6g)$$

$$P_t^-, P_t^+ \geq 0 \quad \forall t \in \mathcal{H} \quad (6.6h)$$

$$\hat{y}_t \in \{0, 1\} \quad \forall t \in \mathcal{H} \quad (6.6i)$$

The duration of a period is given by dt , which for one quarter equals 0.25 h. \mathcal{H} is the optimization horizon composed of H periods. The amount of power bought from or sold to the grid in period t , P_t^+ and P_t^- , respectively at the prices π_t^+ and π_t^- in €/kWh, is given in Equation (6.6b). It is defined in Equation (6.6c) by the sum of the heat pump consumption for space heating, \hat{W}_t^s , or domestic hot water heating, \hat{W}_t^w , and of the exogenous consumption, Γ_t , corresponding to the net power consumed by other electric appliances or produced by decentralized electricity generation units. We assume $\pi_t^+ > \pi_t^-$. The case of an equality can be handled by removing constraint (6.6b) and using \hat{P}_t in the objective function. The fact that heat pumps cannot be used simultaneously for space heating and domestic hot water heating is modeled by a binary variable \hat{y}_t , which is equal to one if the heat pump is used for space heating and equal to zero for domestic hot water production.

6.4.2 Achievable modulation amplitude

The baseline consumption, \hat{P}_t , is given as input to a second optimization problem. The objective of the latter is to obtain the maximum upward modulation in a period τ over n consecutive periods,

with a payback effect over k periods and delayed from the modulation by l periods. The maximum modulation available in one house at a given period τ over n periods is denoted by δ_τ^* . In the case of an upward modulation, the corresponding optimization problem is written as:

$$\max \delta_\tau^* - \epsilon I^+ - \epsilon I^- \quad (6.7a)$$

subject to, $\forall t \in \mathcal{K}(\tau, n + l + k - 1)$:

$$P_t = \dot{W}_t^s + \dot{W}_t^w + \Gamma_t \quad (6.7b)$$

$$P_t = \hat{P}_t + \delta_t \quad (6.7c)$$

$$0 \leq \dot{W}_t^s \leq y_t \dot{W}_t^{s,max} \quad (6.7d)$$

$$0 \leq \dot{W}_t^w \leq (1 - y_t) \dot{W}_t^{w,max} \quad (6.7e)$$

$$\mathbf{x}_{t+1} = f(\mathbf{x}_t, \dot{W}_t^s, \dot{W}_t^w, \mathbf{w}_t) \quad (6.7f)$$

$$\mathbf{x}_t^{min} - \lambda \leq \mathbf{x}_t \leq \mathbf{x}_t^{max} + \lambda \quad (6.7g)$$

and,

$$\mathbf{x}_\tau = \hat{\mathbf{x}}_\tau \quad (6.7h)$$

$$\forall t \in \mathcal{K}(\tau, n - 1) : \delta_t \geq \delta_\tau^* \quad (6.7i)$$

$$\forall t \in \mathcal{K}(\tau + n - 1, l) : \delta_t = 0 \quad (6.7j)$$

$$\forall t \in \mathcal{K}(\tau + n + l - 1, k) : -I^- \leq \delta_t \leq I^+ \quad (6.7k)$$

$$-\sigma \leq \hat{\mathbf{x}}_{\tau+n+l+k} - \mathbf{x}_{\tau+n+l+k} \leq \sigma \quad (6.7l)$$

\mathcal{K} is the flexibility service horizon, composed of n periods of modulation followed by $l + k$ rebound periods. Equation (6.7c) defines the modulation that can be achieved with respect to the baseline. In constraint (6.7g), the parameter λ is used to relax the state constraint (6.6e) to improve the modulation potential. The initial condition of the state is given by equation (6.7h). Constraint (6.7i) expresses that the modulation amplitudes over the n consecutive periods should be greater than a common minimum value. Equality (6.7j) delays the payback effect by l periods after the modulation period. Variables I^+ and I^- are the maximum positive and negative deviations with respect to the baseline on the payback horizon. These deviations are penalized by a parameter ϵ set to 0.5. This choice is motivated in Section 6.6.3. Finally, equality (6.7l) ensures that the state at the end of the payback horizon is close enough to the one given by the baseline. Since the state transition only depends on the previous state and the power consumed by the heat pump, this condition ensures that there are no major deviations from the baseline after the payback horizon. The case of maximum downward modulation is obtained by replacing (6.7a) by $\min \delta_\tau^* + \epsilon I^+ + \epsilon I^-$ and (6.7i) by $\delta_t \leq \delta_\tau^* \forall t \in \mathcal{K}(\tau, n - 1)$.

In the proposed approach, the two optimization problems are solved consecutively, and the determination of the baseline profile is independent from the modulation. This choice is motivated by the opportunity to use such flexibility service for real-time applications when the baseline consumptions have already been stated on the day-ahead. One could carry out a combined optimization problem which would shape the baseline profile in order to obtain the maximum modulation amplitude in a

given time period while minimizing the energy costs.

6.5 Generation of the test cases

The method is applied to a cluster of buildings representative of the Belgian residential building stock. The characterization of the representative residential buildings in terms of geometry and envelope characteristics comes from the study of Gendebien et al. (2015). This study proposes a description of typical Belgian residential buildings with four building configurations, five construction time periods and various insulation levels of the envelope (Section 2.1.1). Geometrical and building envelope data are available in an *Excel* document and are straightforward to couple to building simulation and optimization tools. The four building configurations are freestanding, semi-detached and terraced houses, and apartments. Apartments in large buildings are often equipped with centralized heating production plants supplying all of them. The flexibility service therefore depends on a cluster of aggregated customers, for which the proposed method cannot be applied directly. For this reason, in the present work, only freestanding, semi-detached and terraced houses are considered. Among the representative buildings, 41% present sufficient envelope insulation levels to be potentially equipped with residential air-to-water heat pumps to supply both heating and domestic hot water needs. The selection criterion requires the maximum heating load of the building to be less than the largest residential single-stage heat pump capacity available on the market. For this set of buildings, the average heat pump nominal electrical power is 4.6 kW. Nominal conditions are defined based on normative values (Bureau of standardization (European Standard, 2007)) set to a 7°C outdoor temperature and a water temperature adapted to the house insulation level. Additional resistances of 3 to 5kW, depending on the house insulation level, are used as backups to cover the heat demand for space heating during the coldest days of the year.

The number of inhabitants in each house is drawn from a normal distribution of an average of three and a standard deviation of two with a maximum of five occupants. The exogenous consumption profiles associated with lighting and appliances, as well as the domestic hot water draw-off events, are obtained from the study of Georges et al. (2013) (see Section 2.1.2). Indoor temperature set point schedules are intermittent temperature profiles generated based on normal distribution laws for morning, midday and evening start-up times. All profiles have a weekly average indoor set point above 18°C. Occupancy profiles are derived from the latter. Indoor thermal comfort for occupants should be satisfied at all times. During the heating season, the indoor air temperature is constrained to deviate a maximum of 1K from the imposed set point during occupied periods of the daytime, and within 1K of the extreme limits of the daily set point during unoccupied periods. In the summer, the lower limit of the indoor air temperature is set to 1K below the imposed set point. The upper limit can vary, since no cooling system is considered.

Buildings are equipped with conventional hydronic radiators. The temperature of the water supplied to the radiator is adjusted according to the insulation level of each building. The radiators are assumed to be sized so that they are able to supply the thermal power required by the building at any time and the dependency of the emitted heat on the water supply temperature is not modeled. The domestic hot water tank lower limit in Equation (6.4) is imposed by sanitary constraints to 50°C, whereas the upper limit of 65°C is imposed by the heat pump design. The tank volume is adapted for each house based on a water consumption of 50 liters per person per day at 50°C, along with an additional safety

volume of 50 liters. It is therefore comprised between 100 and 300 liters. The supply temperature is set to 65°C, which underestimates the performance of the heat pump.

Ten percent of the buildings are also equipped with south or west-oriented PV panels with thirty-five degrees tilt angles and 18% average efficiency. The installed surface area is drawn from a discrete uniform distribution over an interval ranging from ten to thirty-five square meters.

6.6 Results

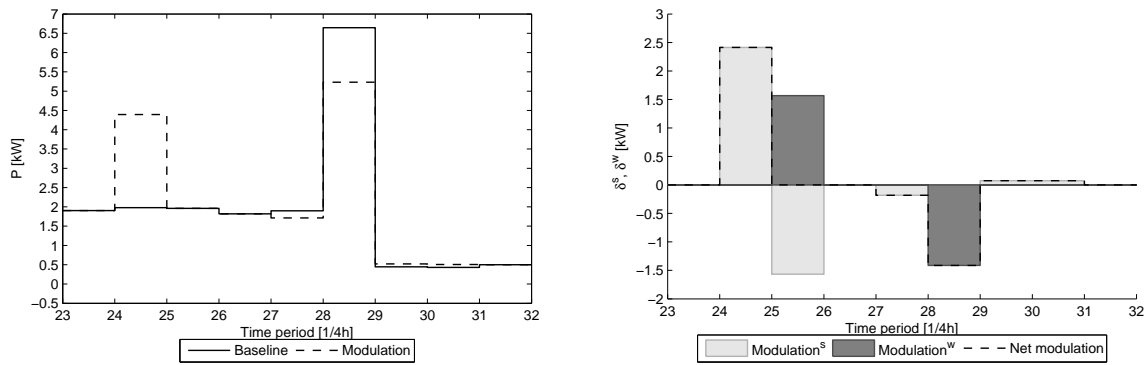
The test cases presented in Section 6.5 are simulated for three and a half days with a time step of fifteen minutes. The optimization results for the first two days serve the purpose of initializing the state variables and are discarded in the following analysis. The extra half day of simulation is used to avoid imposing terminal constraints on the states. The following results therefore focus on the third simulation day. Additional detailed results are available in Annex A.5.

The total modulation potential of an aggregated set of houses is the sum of the potential available for each house. A set of one hundred buildings offering the most cost-effective service is selected. These buildings are then used to perform parametric studies aiming to identify the influence on the modulation potential of each parameter defined within the service.

The optimization problem is a convex mixed integer linear programming problem (MILP) solved with the open-source MATLAB compatible toolbox YALMIP (Lofberg (2004)) coupled to CPLEX solver (ILOG (2013)). With a dual core i7 3GHz computer with 16GB RAM, the computation time for a baseline of one day for a single house takes a few seconds. It takes a few milliseconds to compute one modulation in one house in one time period τ with one set of modulation parameters n , l and k . Therefore, if an aggregator has a set of one hundred buildings, the computation of one hundred baselines takes about 8 minutes. For the given modulation parameters, calculating the available upward and downward modulations for the 96 periods of a day for all houses takes about 14 minutes.

6.6.1 Illustration on a single house

The proposed service is first illustrated in Figure 6.3 for a single house representative of houses built between 1991 and 2006 in Belgium, referred to as K45-level freestanding house in Section 3.1. An upward modulation is activated at period 24 for a single period. Delay and pay-back times are set to two and four periods respectively. Figure 6.3a shows an upward modulation amplitude of about 2.5kW from the baseline. As imposed by the delay parameter l , no deviation occurs during the next two periods. The amplitude of the following payback deviations are comprised within 1.5kW. Figure 6.3b presents the repartition of the heat pump modulation between space-heating mode and domestic hot water mode. The corresponding evolution of the zone and tank temperatures is shown in Figure 6.4. The upward modulation in period 24 is carried out by increasing the heat pump power in space-heating mode, causing the zone temperature to rise by about 0.5 °C. This entails a reduction in heat demand for space heating at period 25. To ensure no deviation from the baseline consumption over two periods following the modulation, the heat pump switches from space heating to domestic hot water mode. The water temperature increases by about 2°C, as illustrated in Figure 6.4b. A payback, contained within four periods, is observed from period 27 to 30. At period 31, both zone and tank

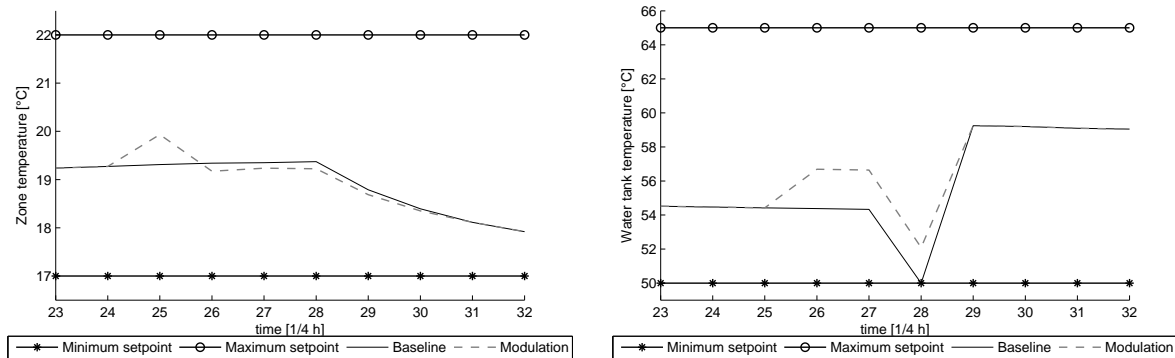


(a) Total power modulation.

(b) Space heating and domestic hot water power modulation.

Figure 6.3 – Power modulation of a freestanding house built between 1991 and 2006 for an activation in period 24, a delay of two periods and a payback on four periods.

temperatures have returned to their baseline level. It should be noted that the large temperature dead band illustrated in Figure 6.4a is due to a reduction of temperature set point from 21°C to 18°C overnight.



(a) Zone temperature.

(b) Tank temperature.

Figure 6.4 – Evolution of zone and water tank temperatures during an unoccupied period corresponding to an activation in period 24, a delay of two periods and a payback on four periods, for a freestanding house built between 1991 and 2006.

Heat pump power modulation in heating mode directly affects the thermal comfort of the occupants by deviating from the assumed comfortable baseline. ASHRAE standard 55 defines acceptable indoor air temperature variation rates that respect occupants' comfort (American Society of Heating, Refrigerating and Air-Conditioning Engineers (ASHRAE (1992))). The temperature variation should not exceed 2.2K during one hour period, and 1.1K during any quarter within that one hour period. Figure 6.5 shows the duration curve of temperature variations for upward and downward activations for the same building for a winter day. The temperature difference between the baseline profile and the modulation is represented by the curve labeled $|\hat{T}_t - T_t|$. The temperature difference between two consecutive time steps of the modulation profile is denoted $|T_t - T_{t-1}|$. The temperature variation within one hour period for the modulation profile is labeled $|T_t - T_{t-4}|$. This variation is always inferior to 2K. The temperature difference between two consecutive quarters and between the modulation and

the baseline always remain inferior to 1.1K. The comfort requirements imposed by the standard are therefore satisfied.

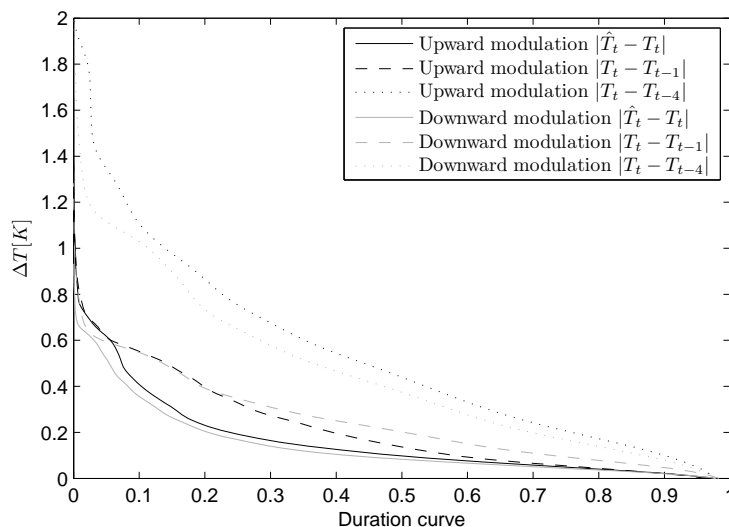


Figure 6.5 – Cumulative frequency density function of temperature differences between baseline and profile after activation and between two successive time steps of the modulation.

6.6.2 Choice of aggregated set of houses

In this section, the methodology is applied to all types of houses of the Belgian residential building stock that could potentially be equipped with heat pumps. Except for retrofitted freestanding houses built after 1971 for which detailed models are available, all other representative houses are simulated using Model II, as explained in Section 6.3. For those simulations, the modulation parameters are arbitrarily set to $n = 1$, $l = 0$ and $k = 5$.

In a first simulation set, each house, which represents a share of the building stock, is simulated once. Results are presented in Table 6.1 and expressed in terms of modulation amplitude and cost per activated volume per house. The cost is obtained by summing the deviations in consumption from the baseline entailed by the activation of the service, and is calculated with the imbalance tariff provided by the transmission system operator (Elia (2012c)). In order to obtain results per average house, the values obtained for each typical house are multiplied by its representative percentage in the building stock, and then summed. Based on the same weighting average technique, a distinction can be made between an average house, an average freestanding house, an average semi-detached house and an average terraced house. As seen in Table 6.1, the upward modulation potential reaches 2.9 kW per house and the downward modulation potential is 0.29 kW per house. The average cost is close to the average Belgian retail electricity tariff for an upward activation and more than double the retail tariff for a downward activation. Terraced houses present a higher potential than the average house for upward modulation, but a reduced downward modulation potential. Freestanding houses offer the highest downward modulation potential. Among freestanding houses built after 1971, some have undergone different levels of retrofitting to improve the insulation of their envelope, and others have been built to meet the legal insulation requirements (European Parliament (2010)). Such freestanding houses are represented by four typical building typologies based on the construction time-period, i.e., 1971-1990, 1991-2006 or after 2007, and based on the insulation level, i.e., heavy retrofit (HR) and light

retrofit (LR). They are referred to as retrofitted freestanding houses in the remainder of the chapter. To further illustrate the proposed method, and to introduce statistical distribution in terms of heat and hot water demand profiles, a second set of simulations focuses on the retrofitted freestanding houses only. To that end, a distribution of the four typical typologies of retrofitted freestanding houses is performed over one hundred houses, proportionally to their share in the building stock. Due to their higher insulation level, retrofitted freestanding houses present a limited upward modulation potential, but the largest downward modulation potential. For both modulations, the activation is the most economical for such houses, as insulation reduces overconsumption. For this reason, the parametric studies carried out in the remainder of the chapter focus only on this set of one hundred retrofitted freestanding houses. Their aggregated baseline consumption obtained for a day-night electricity tariff structure is illustrated in Figure 6.6 for a winter day, along with the corresponding outdoor temperature. The electricity demand profiles strongly depend on the ambient temperature, but also on the electricity retail tariff. The latter explains the peaks in consumption observed at around 7am, right before the transition to the day-time tariff. The consumption is 53.9 kWh per average house.

Table 6.1 – Modulation amplitude and activation cost per house.

Type of buildings	Mean modulation [kW]		Cost [€/kWh]	
	Up	Down	Up	Down
Average house - all types	2.90	0.29	0.27	0.69
Average Freestanding	2.10	0.42	0.27	0.70
Average Semi-detached	2.72	0.29	0.27	0.69
Average Terraced	3.95	0.14	0.26	0.57
Retrofitted freestanding	1.07	0.44	0.19	0.27

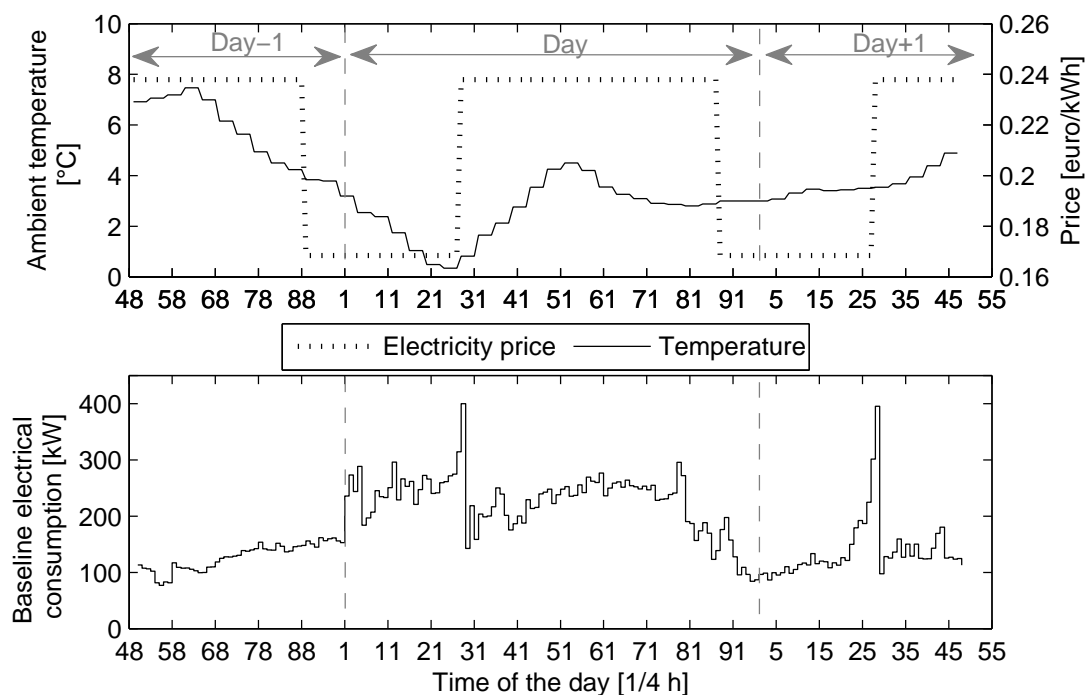


Figure 6.6 – Optimal baseline electricity consumption of one hundred retrofitted freestanding houses on January 24th and corresponding ambient temperature profile and electricity retail price profile.

6.6.3 Impact of power deviation amplitude limitation

The cost function presented in Equation (6.7a) is parametrized using the payback weight parameter ϵ . This parameter weighs the relative importance of the payback deviations compared to the modulation amplitude in the objective function (6.7a). For example, Figure 6.7 illustrates the impact of this parameter on the maximum modulation amplitude and the amplitude of the deviations for the four types of representative houses investigated and for an activation in period 18. Modulation service parameters n , l and k are set to one, zero and five periods respectively. For the four houses, as ϵ increases, the maximum modulation amplitude decreases. Houses built between 1971 and 1990 are the most impacted, particularly for downward activations. Indeed, the downward activation potential reaches zero for values of ϵ greater than 0.43 for lightly renovated houses and greater than 0.53 for heavily renovated houses. The upward activation potential tends towards zero for values of 0.7 and 0.88, respectively.

In the case of a downward activation, the reduction in achievable modulation amplitude with ϵ is explained as follows. The decrease in heat pump power consumption at a given time τ is usually followed by an increase in consumption during the payback time to return to the baseline. This increase in required power brings the heat pump closer to its full load operating conditions, which are characterized by a lower coefficient of performance for variable-frequency heat pumps. This therefore increases the amplitude of the deviations and is particularly marked for poorly insulated houses, for which the temperature in the zone drops quickly. An inverse trend is observed for upward activations. The increase in power consumption reduces the required power during the payback, which, for the same outdoor conditions, improves the system performance and reduces deviations. The fact that the influence of ϵ on the achievable modulation is stronger for downward modulations than for upward modulations comes from the chosen cost-optimal baseline. The minimization of energy costs tends to drive the temperature trajectory toward the low temperature set points during low price periods, reducing the downward activation potential, but increasing the flexibility for upward activations. For houses built after 1991, the better insulation of the envelope allows to switch the heat pump from heating mode to domestic hot water mode without compromising the occupants' comfort. This mode switch helps reduce the amplitude of the deviations and the influence of ϵ .

In the frame of the modulation service presented in this study, the most suitable service is obtained for a ratio of the modulation amplitude to the maximum deviation amplitude greater than one, i.e.

$$\frac{1}{96} \sum_{\tau=1}^{96} \frac{\sum_{i=1}^{100} \delta_i |_{\tau}}{\max(\sum_{i=1}^{100} I_i^+ |_{\tau}, \sum_{i=1}^{100} I_i^- |_{\tau})} > 1 \quad (6.8)$$

This ratio increases with ϵ , as illustrated in Figure 6.8b for the aggregated set of one hundred houses. However, the number of possible activations, represented by the mean modulation amplitude per house, decreases when increasing ϵ as shown in Figure 6.8a. Therefore, an empirical choice for ϵ corresponds to the value that maximizes the ratio of modulation to deviation (Equation (6.8)) while limiting the reduction in modulation amplitude. For downward modulations, the optimum is obtained for a value of ϵ equal to 0.52. For upward modulations, the optimum value is located around 0.55. One could also choose an empirical value for each type of house.

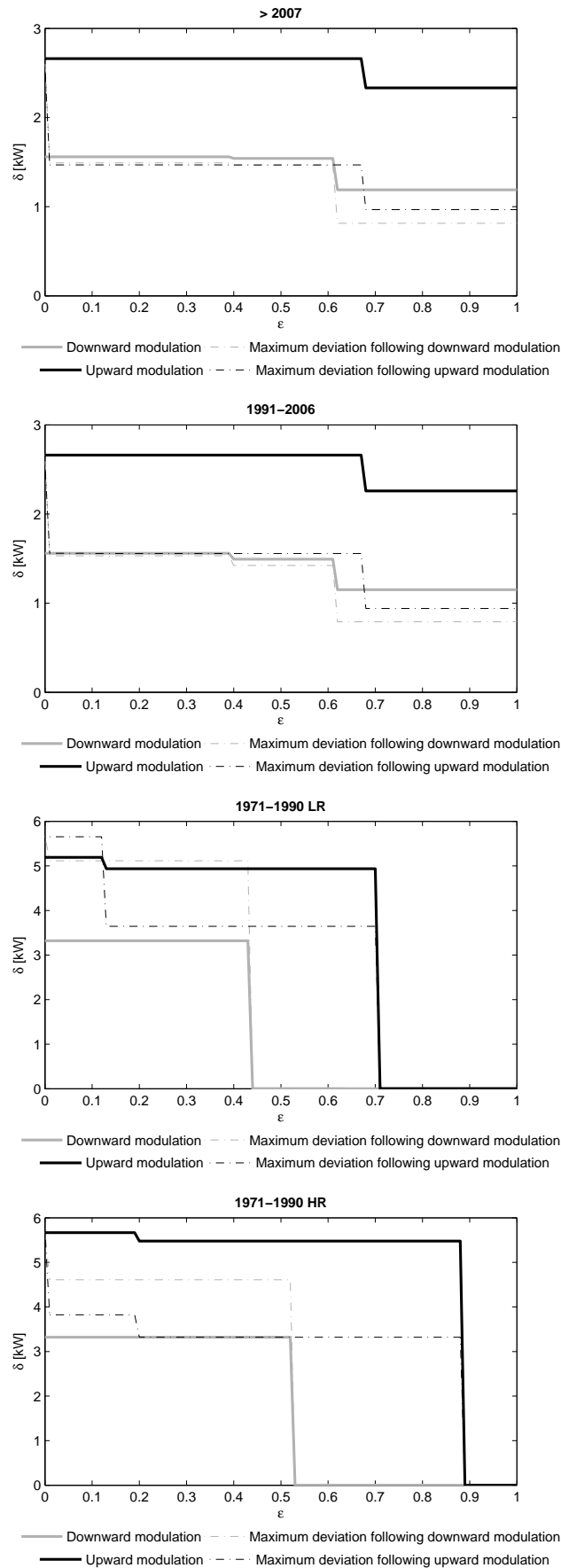
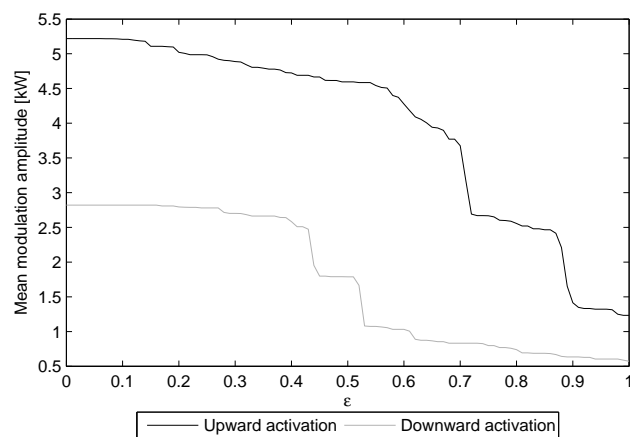
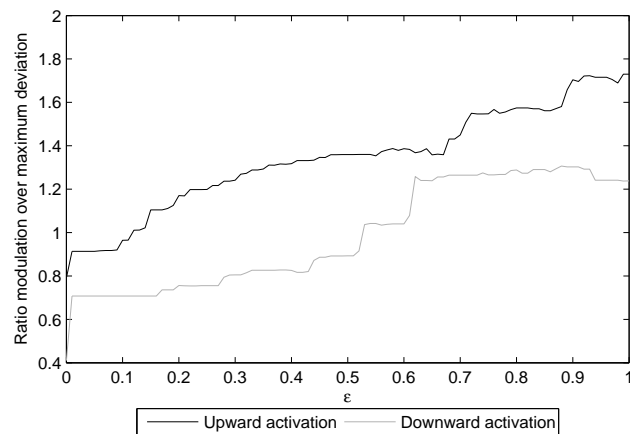


Figure 6.7 – Influence of ϵ on modulation amplitude and related deviations during payback, for $\tau = 18$, $n = 1$, $l = 0$ and $k = 5$.



(a) Mean modulation amplitude per house.



(b) Ratio of the modulation amplitude to the maximum deviation amplitude.

Figure 6.8 – Empirical choice of ϵ based on the maximization of the ratio of the modulation amplitude to the maximum deviations (Equation (6.8)).

6.6.4 Time constants of the modulation service

6.6.4.1 Payback length k

The maximum upward and downward modulations for the aggregated portfolio of one hundred freestanding houses are illustrated in Figure 6.9 for a winter weekday and three payback horizon lengths. The largest upward and downward modulations are obtained in periods 0 to 28, with maximum amplitudes reaching 370kW and 210kW, respectively. During that time frame, most of the flexibility is provided by space-heating consumption. The temperature profiles present a night setback where the set point is reduced and the allowed temperature range is wider. In addition, the modulation potential tends to follow the outdoor temperature profile. For the upward modulation, there is a maximum in periods 16 to 28. This phenomenon is due to the higher room temperature set point for the daytime, which allows a faster return to the baseline electricity demand of the house. In the case of downward modulation, the limitation of the heat pump capacity reduces the achievable downward modulation as

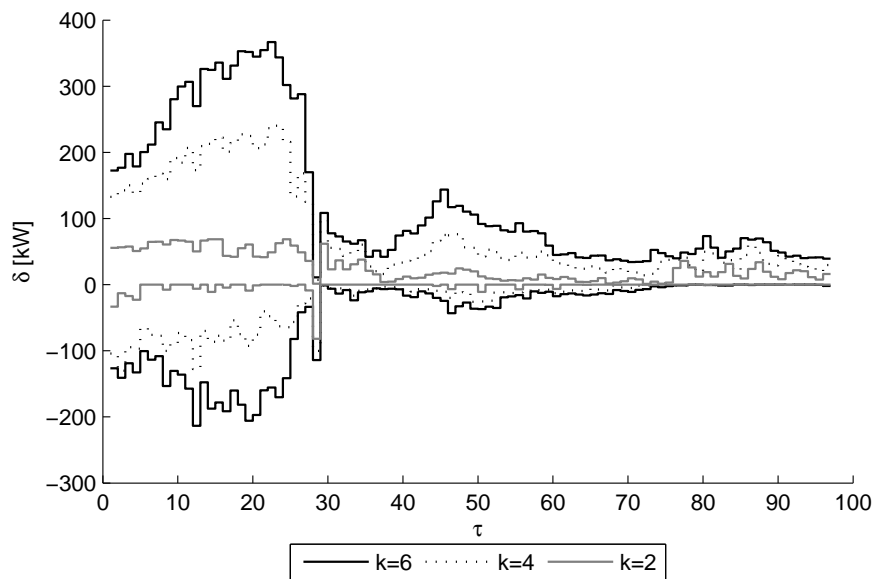


Figure 6.9 – Influence of the payback length on the modulation amplitude for each potential activation period on January 24th for 100 houses.

one gets closer to the set point transition. The upward peaks observed in periods 30 and 88 correspond to the start-up of heat pumps to produce domestic hot water after usual morning and evening water draw-off events. During the day, most of the upward and downward modulations are provided by space heating. Flexibility from the domestic hot water tank is mostly restricted by the high inertia of the water tanks, due to their good insulation. In addition to this inertia, major hot water draw-off events mainly happen in the morning and evening, which limits consumption needs. Within a day, the heat pump is mostly used for space heating, since the deadband of the room temperature is set to only 2°C. Consequently, and with the heat pump being limited to working in one mode at a time, consumption for domestic hot water is mostly concentrated in single periods to give more freedom for space heating. The potential of downward modulation gets close to zero for time periods between 88 and 95. This is explained by the fact that the optimization of the baseline drives the system toward minimizing the costs, and therefore, the temperatures hit their lower bound when the electricity tariff is high. In period 88, the night-tariff starts, but, due to the foreseen night temperature setback, the heat pump is slowed down, therefore reducing the downward modulation potential.

Figure 6.10 shows the impact of the payback length on the mean, minimum and maximum achievable modulation per average house. The mean upward and downward modulation amplitudes range from 0.05 to 1.24 kW and from 0.01 to 0.5 kW respectively for payback lengths of one to six periods. The average maximum modulation amplitude of the aggregated set is 3.8 and 1.9 kW respectively, whereas the maximum potential among the set reaches 9kW. For both upward and downward modulations, little improvement is observed in terms of mean and maximum modulation amplitudes when increasing the payback length from 5 periods to 6 periods. A payback duration of one hour and 15 minutes is thus chosen for the rest of the study.

Figure 6.11 illustrates the seasonal modification of the flexibility potential on the 24th of January, April, June and November. The difference in modulation observed between November and January lies in the higher outdoor temperature, which, combined to the nighttime setback, reduces the flexibility potential

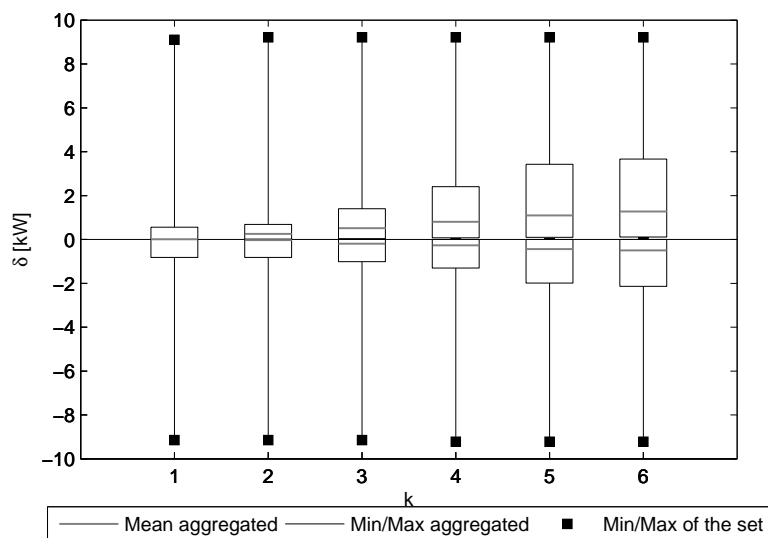


Figure 6.10 – Evolution of the minimum, maximum and mean modulation potentials per average house for the aggregated set of houses, and of the minimum and maximum modulation amplitudes among the set of houses with the payback length.

for space heating for time periods before period 20. The relative share of electricity consumption devoted to domestic hot water production increases in warmer seasons.

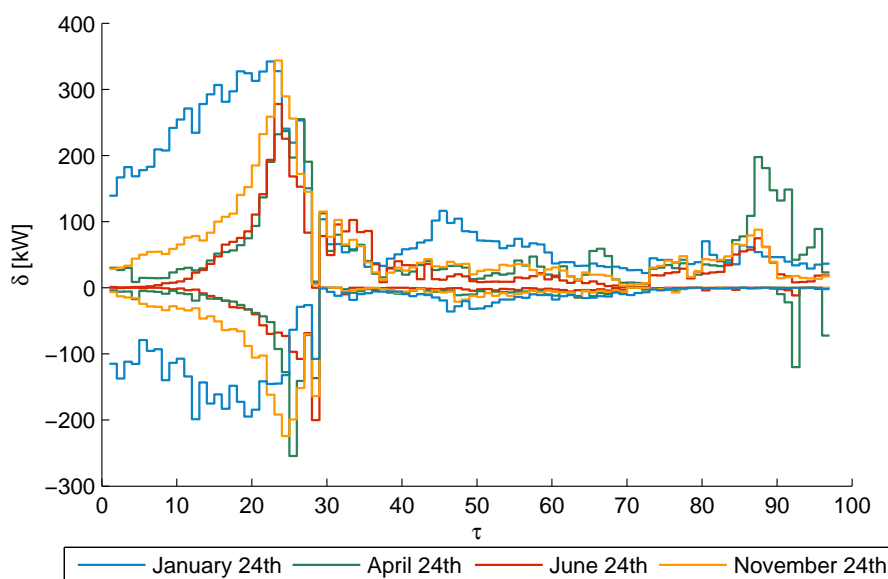


Figure 6.11 – Seasonal influence on the modulation for each activation period on January 24th for 100 houses.

6.6.4.2 Delay length l

The maximum upward and downward modulations for the aggregated portfolio of one hundred freestanding houses are illustrated in Figure 6.12 for a winter weekday, four delay lengths and a payback length of five periods. For all l , the largest upward and downward modulations are obtained

in periods 0 to 28, as explained in Section 6.6.4.1. As l increases from zero to one, a drastic reduction of the downward modulation potential is observed throughout the day, but most significantly for periods between 10 and 28. For upward activations, a decrease in potential is also observed during that time frame, but is not as strong. The decrease is due to the bounds on the water and indoor air temperatures and to the parametrized objective function, which limits the deviations. Indeed, if at the end of the modulation period, the temperatures have reached their upper or lower bounds, then preventing the heat pump from deviating from its baseline consumption during the next l periods may cause the system to cross the set point limits. Such situations are avoided by reducing the modulation potential and is particularly marked for time periods close to a set point transition, such as in periods 27 to 30.

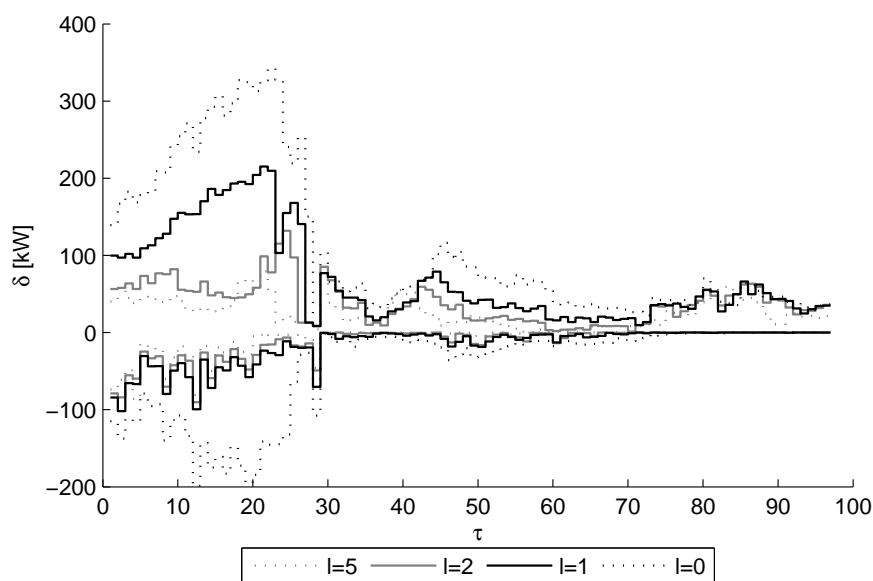


Figure 6.12 – Influence of the delay length before payback on the modulation amplitude for each potential activation period and a payback effect on five periods in January 24th for 100 houses.

The achievable upward modulation amplitude is further reduced when l increases from one to two. For this value, the average activation potentials for the set of houses decrease by 65% and 72% per house, respectively, for upward and downward modulations, as compared to no delay length. Beyond that value, the additional limitations of activation potential entailed by increased values of l are limited, as shown in Figure 6.13. Depending on the combination of flexibility service parameters l (0 to 8) and k (1 to 7), the mean upward modulation amplitude varies from 2.6 to 138 kW and the mean downward modulation amplitude from 0.4 to 51.4 kW for the aggregated set of houses (Annex A.5).

6.6.4.3 Modulation length n

The modulation potential achievable for any time period τ and three different modulation lengths is illustrated in Figure 6.14 for one hundred houses on a winter day. Payback and delay lengths are set to five and zero, respectively. As the modulation length increases from fifteen minutes to thirty minutes, the amplitude of activation drops significantly for all periods of the day.

For a modulation length greater than fifteen minutes, a larger modulation potential can be obtained by activating only a subset of heat pumps during each period of the modulation length n . Each group of

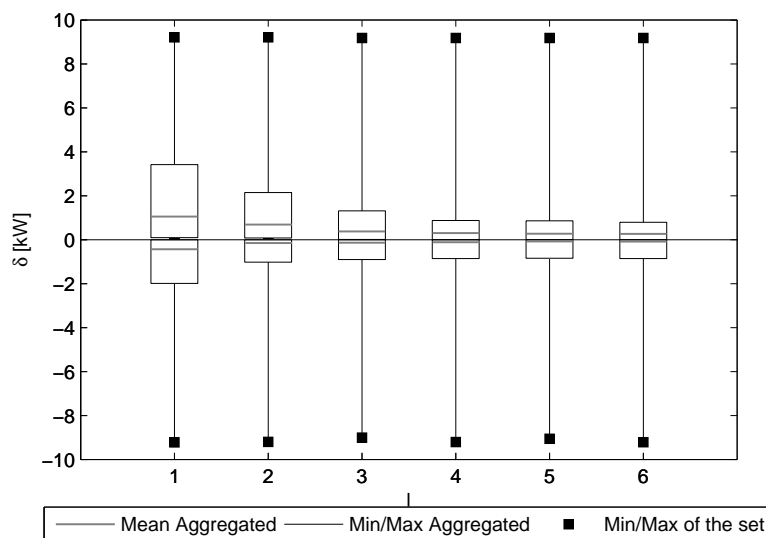


Figure 6.13 – Evolution of the minimum, maximum and mean modulation potentials per average house for the aggregated set of houses and minimum and maximum modulation amplitudes in the set of houses with the delay length l , for a payback over five periods.

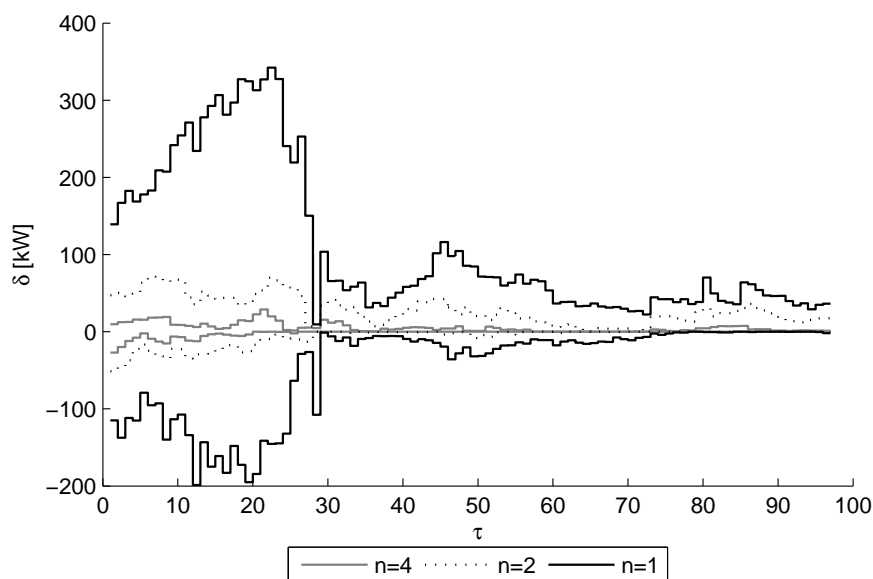


Figure 6.14 – Influence of the modulation length on the average modulation amplitude for each potential activation period on January 24th for 100 houses. Other parameters are set to $l = 0$ and $k = 5$.

heat pumps is activated in order to maximize the modulation amplitude in one of the n periods. This is referred to as asynchronous activation and is illustrated in Figure 6.15 for a delay length of thirty minutes. Compared to a synchronous activation of the whole set of heat pumps in each of the two periods, the activation of a subset of heat pumps on each period allows for an increase of the minimum upward activation amplitude by up to 110%. However, there exist time periods of the day where it remains more efficient to activate all heat pumps simultaneously during two consecutive periods, such as in period 31 for example. Figure 6.16 illustrates the number of heat pumps composing each activated subset for a desynchronized upward modulation.

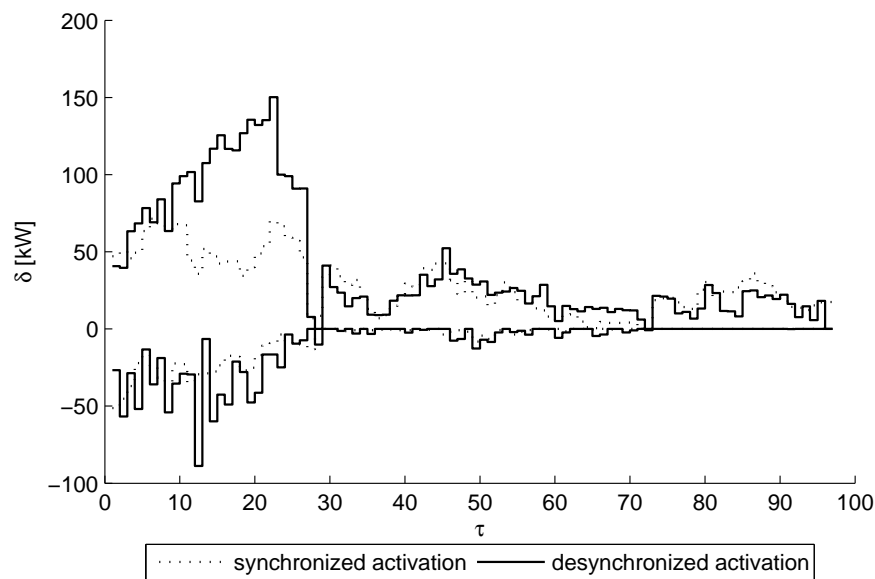


Figure 6.15 – Aggregated modulation amplitude for $n = 2$ for synchronous and asynchronous activations of heat pumps.

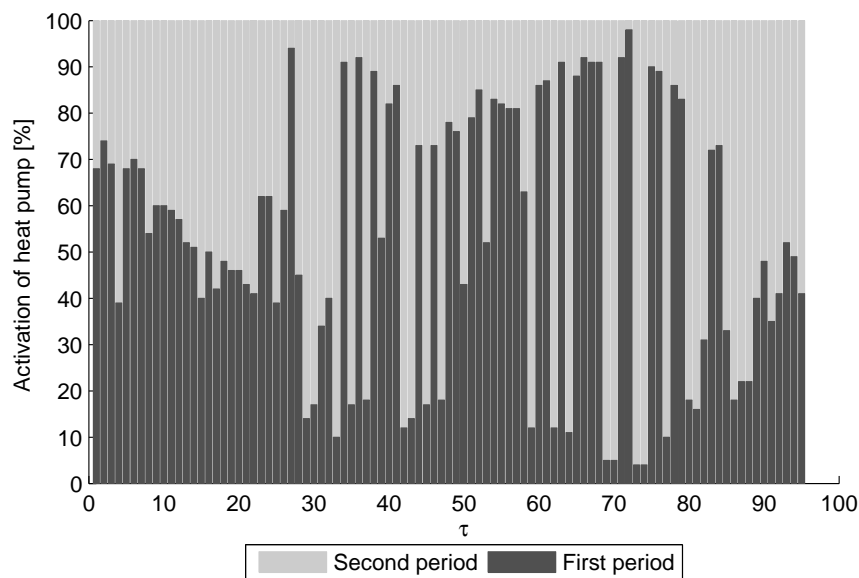


Figure 6.16 – Number of heat pumps activated in each of the two periods for asynchronous upward activations.

6.6.5 Deviations and overconsumption

Deviations in consumption from the specified baseline are traded on the imbalance market. In the frame of the flexibility service, it is useful to characterize them in duration, amplitude and associated costs. The volume of deviation is the sum of the absolute differences, during the payback periods, between the baseline consumption and the consumption after modulation. It is interesting to compare it to the energy volume activated by the modulation. For a given delay length, increasing the payback length increases both the achievable modulation amplitude and the relative proportion of deviations. An opposite trend is observed when increasing the delay length for a fixed payback. Depending on the

delay and payback lengths, the ratios of deviation over activated volume range from 39% to 123% for upward activations and from 27% to 123% for downward activations.

The activation of a modulation implies an overconsumption, defined as the net difference in energy consumed between the baseline consumption and the consumption with the modulation. The only exception lies in the case of a downward activation with a payback of one period, for which the total energy consumed is smaller than for the baseline. Similarly to the volume of deviation, the overconsumption can be expressed as a percentage of the energy volume activated by the modulation, and ranges from -4% to 83%. For a fixed delay length, overconsumption increases with the payback time. For each fixed payback time, there exists an optimum delay length that minimizes the ratio of overconsumption to activated volume.

6.6.6 Impact of state constraint relaxation

This section investigates the impact of varying parameter λ used in Constraint (6.7g) to relax the zone temperature bounds in order to increase the modulation potential of each building. In the above results, this parameter was set to zero. Results for the set of one hundred houses are presented in Figure 6.17 for a temperature variation ranging from zero to 1.5K. An additional deviation of 0.5K from the baseline limits allows for the doubling of both upward and downward modulation amplitudes. The increase is less significant for relaxations of 1K and 1.5K. A relaxation of 1K allows an increase of the upward modulation potential per house from about 1kW to 2.5kW and the downward modulation potential from about 0.5kW to 1.2kW.

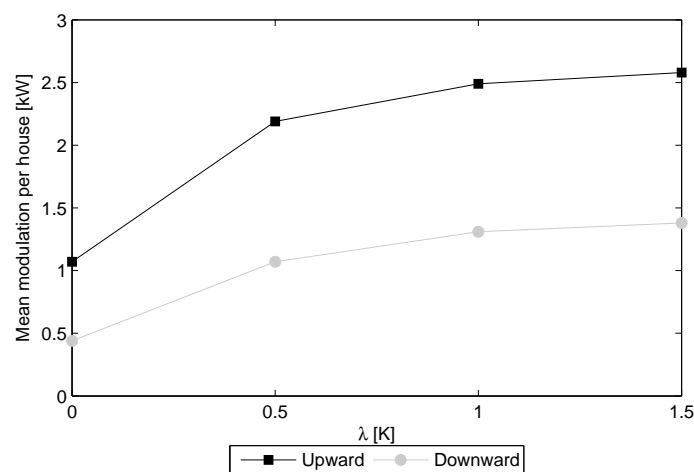


Figure 6.17 – Impact of zone temperature constraint relaxation on mean modulation potentials. The modulation parameters are set to $n = 1$, $l = 0$ and $k = 5$.

However, occupants willing to participate in such a service are more likely to feel thermal discomfort due to larger temperature variations. Figure 6.18 illustrates the duration curve for temperature difference between two consecutive time steps after modulation, with a delay length of zero and a payback over five periods. The temperature variations remain below 1.2K in 85 percent of the cases, regardless of the λ . It should be noted that when λ equals zero, the duration curve differs from the one of Figure 6.5, as the latter presented results for a single house only.

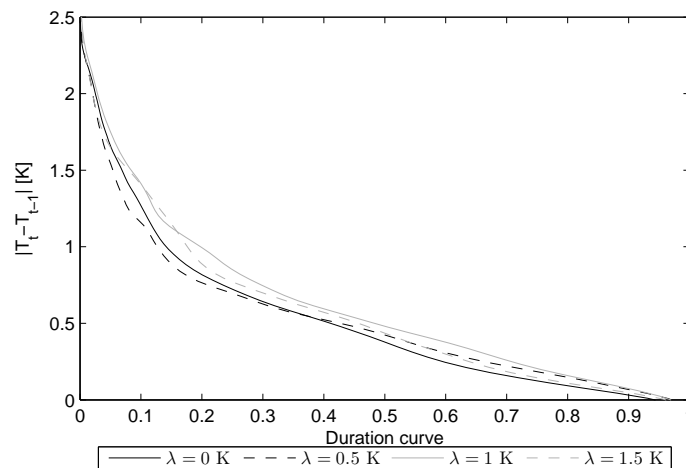


Figure 6.18 – Cumulative frequency density function of temperature differences during payback for four different relaxations of indoor zone temperature constraints in one hundred houses. The modulation service parameters are set to $n = 1$, $l = 0$ and $k = 5$.

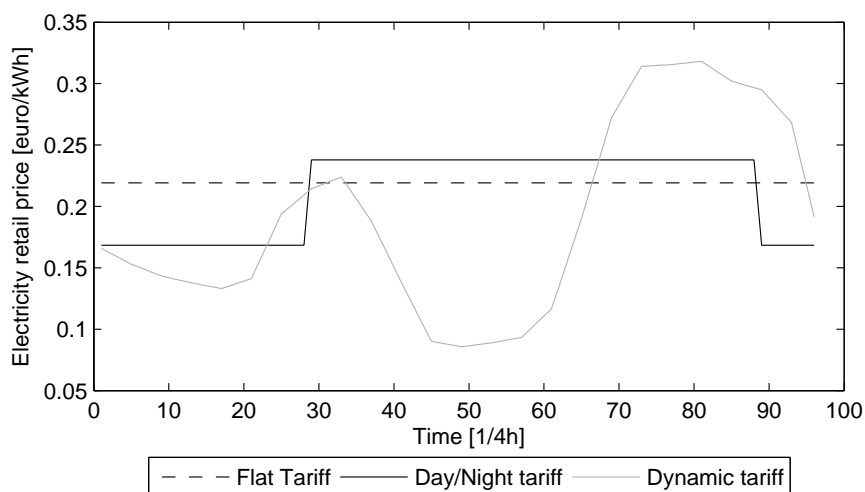
6.6.7 Influence of the tariff structure

Currently, in Belgium, residential customers can sign up for two types of tariff structures: flat and day/night retail tariffs. In the above sections, the retail tariff used to determine the cost-optimal baseline was the day/night structure. Tariff structures are expected to evolve toward dynamic pricing that reflects the availability of electricity in the market. Such tariffs present variable profiles that have been shown as suitable for demand response programs with heat pumps (Chapter 4). An example of a dynamic tariff is illustrated, along with flat and day/night tariffs, in Figure 6.19a.

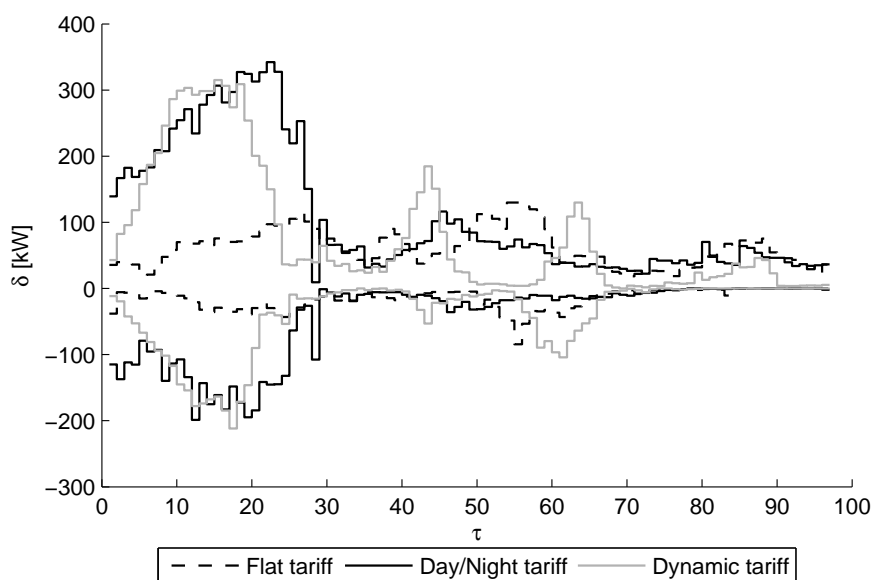
The cost of the optimized baseline consumption for a typical winter day is 11.33, 11.93 and 9.55 euros for the flat, day/night and dynamic tariffs, respectively. The impact of the tariff structure on the modulation potential is illustrated for one hundred houses for a typical winter day in Figure 6.19b. For this example, the modulation parameters are set to $n = 1$, $l = 0$ and $k = 5$. It appears that the flat tariff structure offers the lowest modulation potential. Compared to the day/night tariff, the dynamic structure allows for unlocking of the modulation potential in concentrated time periods, mostly before period 20, between periods 40 and 45 and from period 55 to 65. The dynamic tariff can therefore be tuned to maximize the modulation potential during critical time periods, such as during high imbalance or high day-ahead spot market prices, or to relieve a congestion. The average potential is the highest with the day/night tariff for both upward and downward modulations.

6.6.8 Illustration with the balancing market

The proposed service can be used to reduce the need for reserve to solve an imbalance at a given time period. However, the resulting cost savings depend on the imbalance tariff, which is unknown at the time of the activation of the modulation. The existence of a rebound effect inherent to TCLs may cause the modulation to become unprofitable. This is illustrated in Figure 6.20 for January 24th, 2012, with the corresponding historic imbalance prices. The service parameters are set to $n = 1$, $l = 0$ and $k = 5$.



(a) Electricity tariffs.



(b) Modulation amplitude.

Figure 6.19 – Impact of the electricity tariff structure on the modulation potential for the aggregated set of 100 houses. Modulation parameters are set to $n = 1$, $l = 0$ and $k = 5$.

For that specific day, it can be seen that most of the upward modulations performed with this set of one hundred houses are profitable. Most downward activations, contrariwise, are unprofitable. In particular, the activation of a downward modulation when the system imbalance is positive for several consecutive periods leads to an unprofitable activation. This strengthens the conclusion that providing downward modulations with TLCs is more challenging than an equivalent upward modulation. Results may differ as the number of considered houses increases, due to statistical effects of load diversity.

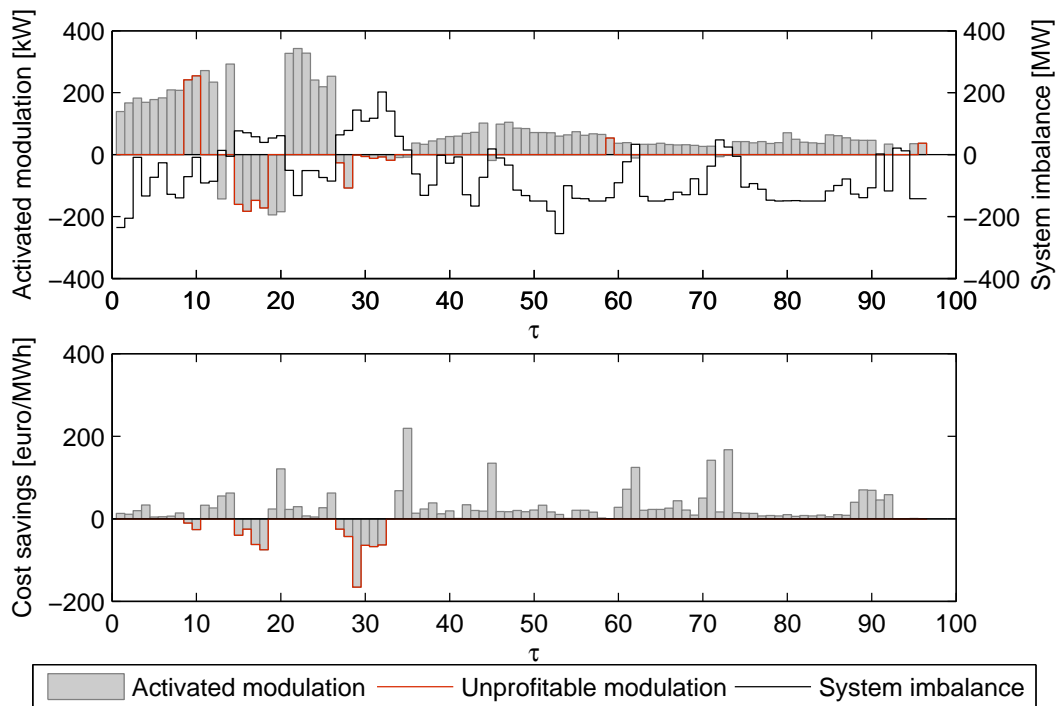


Figure 6.20 – Illustration of the potential cost savings for the activation of the modulation service by an aggregator on the imbalance market on January 24th, 2012. Modulation parameters are set to $n = 1$, $l = 0$ and $k = 5$.

6.7 Research outcome

This chapter presents a flexibility service provided by a load aggregator controlling domestic heat pumps. The heat pumps are used to supply both domestic hot water production and space-heating needs.

- *Method:* The flexibility service consists of the upward or downward activation of heat pumps at a certain time period and during a given number of periods. The activation is followed by a rebound effect with parametrized deviations from a baseline consumption over a fixed number of periods. This baseline is such that it minimizes the energy costs for the end-user. The rebound effect consists of a delay period with no deviations from the baseline consumption and a payback period during which deviations in consumption occur to allow the heat pumps to return to their baselines. A sequential optimization scheme is proposed to determine the modulation potential.
- *Case-studies:* The methodology is first applied to a cluster of houses representative of the Belgian residential building stock. The average modulation potential obtained for a modulation in one time period with no delay and a payback constrained over five periods is 2.9 kW and 0.29 kW per house for an upward modulation and a downward modulation, respectively. Retrofitted or well-insulated freestanding houses enable the most economical modulations, since insulating the building envelope reduces overconsumption. Such houses are then used to further investigate the influence of the parameters characterizing the modulation and rebound effect.
- *Parameters of influence:* An empirical choice of the weighting parameter between modulation

and deviation amplitudes is proposed based on the maximization of the ratio of these amplitudes. Given this choice of weighting parameter, the influence of the time constants of the modulation service is studied. The mean upward and downward modulation amplitudes range from 0.05 to 1.24kW and from 0.01 to 0.5kW, respectively, for paybacks of 15 minutes to one and a half hour. These values decrease by 65% and 72% per house, respectively, for upward and downward modulations for a delay length of thirty minutes, as compared to no delay length. Beyond two periods for the delay length, the average values remain almost unchanged. The limitation in modulation amplitude entailed by increased delay lengths is particularly marked for time periods during the day where the indoor temperature set point is close to a transition.

Results show that modulating a group of heat pumps in several consecutive time steps is less efficient than modulating only part of them in each time step. An asynchronous activation of the heat pumps increases the minimum modulation amplitude of the day by 110%. Sensitivity analyses of the modulation potential to the retail tariff structure are also presented. These analyses show that a tuned dynamic retail tariff structure can maximize the modulation potential during critical time periods, for example to relieve a congestion in the network or balancing the electrical system.

- *Application to the imbalance market:* The method is applied to solve an imbalance for a particular day in the winter. Given the imbalance tariff, results show that, for the given example, all upward modulations are profitable, whereas some downward modulations are not, hereby emphasizing the difficulty to perform downward modulations with TLCs. This is further investigated in Chapter 8.

A variant to the proposed service could be obtained by turning the sequential optimization problem into a combined optimization problem. This would allow to shape the baseline profile in order to obtain the maximum modulation amplitude in a given time period while minimizing the energy costs. This is investigated in Chapter 8.

7 A comparison of control strategies and thermal storage options

7.1 Motivations

In this chapter, a comparison of the three load modulation strategies proposed in Chapters 4 to 6 is performed. The objective is to homogenize the findings in terms of interactions between load modulation strategies and thermal characteristics of buildings and storage. Different thermal storage options are compared and ranked according to their suitability for an illustrative application.

7.2 Load modulation strategies

The proposed demand response program consists in triggering demand flexibility at a given time period, τ , and over set of consecutive periods, n . To that end, the three load modulation strategies, studied extensively in Chapters 4 to 6 can be implemented. Their adaptation to the example demand response program is summarized hereafter.

The investigated system is represented by a discrete state-space formulation. The state transition is summarized by

$$\mathbf{x}_{t+1} = f(\mathbf{x}_t, \mathbf{u}_t, \mathbf{w}_t) \quad (7.1)$$

where \mathbf{x} is the state space variable vector, \mathbf{u} is the vector of decision variables, i.e. the modular electric power, and \mathbf{w} is a vector of disturbances. The total electricity consumption of the consumer at time t , P_t , is composed of modular components, $u_{i,t}$, i.e., the consumption of systems that can be adjusted by the optimal load management scheme, and the exogenous consumption, Γ_t , i.e. the share of the electricity consumption that is not modifiable,

$$P_t = \sum_i u_{i,t} + \Gamma_t \quad (7.2)$$

A baseline consumption is obtained by minimizing the electricity costs for the flexible consumer for a given retail electricity price profile, π^+ ,

$$\min \sum_{t \in \mathcal{H}} \hat{P}_t \pi_t^+ \quad (7.3a)$$

with respect to the decision variables, on the optimization horizon \mathcal{H} , and subject to the following constraints

$$x_t^{min} \leq x_t \leq x_t^{max} \quad \forall t \in \mathcal{H} \quad (7.3b)$$

$$u_t^{min} \leq u_t \leq u_t^{max} \quad \forall t \in \mathcal{H} \quad (7.3c)$$

$$u_{i,t} + u_{j,t} \leq \max(u_{i,t}, u_{j,t}) \quad \forall t \in \mathcal{H} \quad (7.3d)$$

where Constraint (7.3c) specifies the upper and lower limits for power modulation of the modular components and Constraint (7.3d) ensures that two related decision variables are not activated simultaneously, as further explained in Section 7.4. The resulting baseline consumption profile is denoted \hat{P}_t .

From the baseline consumption, three mechanisms can be implemented to trigger load flexibility and increase the consumption during a given time interval. The first mechanism, referred to as **ADR#1**, consists in reducing the electricity retail tariff from time period τ over n periods. The objective for the end-users is to increase their consumption during that time period in order to lower their electricity costs for the rest of the day. The objective function is written as

$$\min \left(\sum_{t=\tau}^{\tau+n-1} P_t \pi_t^{DR} + \sum_{t=\tau+n}^H P_t \pi_t^+ \right) \quad (7.4)$$

subject to constraints (7.3b) to (7.3d), and where π^{DR} is the retail tariff used to trigger demand response.

The second method, referred to as **ADR#2**, is an optimal control formulation which promotes load matching between production and consumption. The net electricity flow, P_t^{net} , is the instantaneous difference between the power consumed and produced on site. If positive, the billing tariff is the retail tariff, π^+ . If negative, the excess production is bought back at a buy-back tariff, π_{bb} . One can therefore define a buy-back ratio $\alpha^{bb} = \pi^{bb} / \pi^+$. From a given time period τ and over n periods, the buy-back ratio is set to a value close to zero. The objective is to minimize the electricity cost for the end-user for a given net metering buy-back ratio, which can be expressed as

$$\min \sum_{t=\tau}^H \left(\max(P_t^{net}, 0) + \min(P_t^{net}, 0) \alpha^{bb} \right) \quad (7.5)$$

and subject to Constraints (7.3b) to (7.3d).

The third modulation strategy, **ADR#3**, consists in carrying out an upward modulation of the electrical consumption at a given time period τ over a number n of periods. The objective function translates as

$$\max I^{mod} \quad (7.6a)$$

subject to Constraints (7.3b) to (7.3d), and where

$$\delta_t \geq I^{mod} \quad \forall t \in \{\tau, \tau + n - 1\} \quad (7.6b)$$

The modulation profile, P_t , is defined from the baseline consumption by the decision variable δ_t

$$P_t = \hat{P}_t + \delta_t \quad \forall t \in \{\tau, \tau + n - 1\} \quad (7.6c)$$

After the n periods of upward modulation, a new consumption profile that minimizes the consumer's costs is determined based on Equation (7.3a).

7.3 Buildings and systems

7.3.1 Case-study buildings

The retrofitted freestanding houses studied in Chapter 6 and presented in Section 3.1 are used as test-cases in this chapter. These houses are characterized by two types of building geometries: a single-story building representative of freestanding houses built between 1971 and 1990 and a two-story building representative of freestanding houses built after 1991. For each geometry, two insulation levels are considered. Each house is equipped with a variable-speed air-to-water heat pump. Characteristics of the houses and systems are summarized in Table 7.1.

Table 7.1 – Buildings and heat pumps characteristics.

Year of construction	N# of floors []	Heated volume [m ³]	Ground floor area [m ²]	Average U value [W/m ² K]	Rated capacity [kW]	Nominal temperatures A/W [°C]	Auxiliary heater (-10°C) [kW]
2007-2014 (A)	2	457	75	0.31	6.5	7/45	3
1991-2006 (B)	2	457	75	0.46	8.0	7/45	3
1971-1990 (C)	1	423	148.5	0.77	12.0	7/65	5
Retrofit							
1971-1990 (D)	1	423	148.5	1.24	17.0	7/65	5

7.3.2 Storage options and sizing

Each house is equipped with a domestic hot water tank. Additionally, three thermal storage options are investigated for space heating (SH):

- storage in the building envelope,
- storage in a water tank following a parallel four-pipe configuration (Figure 7.1b): the heat pump supplies heat to the storage tank. The latter is used to supply the house.
- storage in a water tank following a parallel two-pipe configuration (Figure 7.2): the heat pump is connected to both the SH tank and the house. This configuration offers more flexibility to respond to variable retail tariffs, as illustrated in Figure 7.2. The tank is heated when the electricity price is low, and the stored heat is released to avoid consuming electricity when the retail price is high. However, since the heat pump can only supply one element at a time, this hydronic configuration can only be implemented for heating schedules that present temperature set backs during some periods, in order to avoid causing thermal discomfort to the occupants.

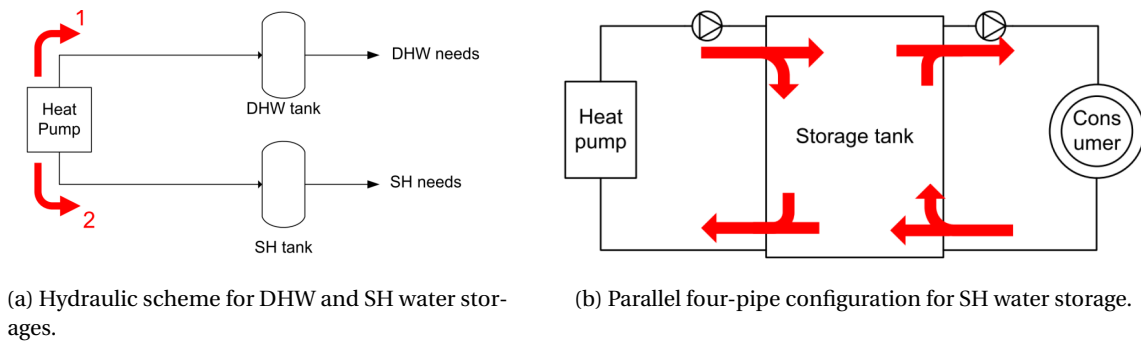


Figure 7.1 – Water tanks hydronic configurations.

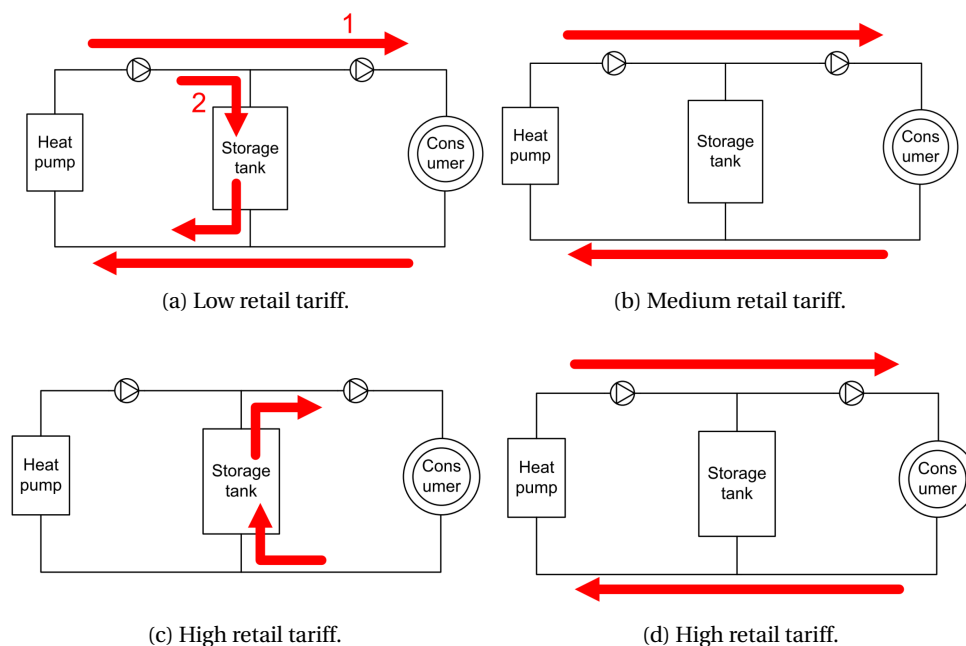


Figure 7.2 – Parallel two-pipe configuration - a) if the electricity retail tariff is low, the heat pump is used to supply the house directly if needed or to store heat in the storage tank. b) regardless of the retail tariff, the heat pump can be used to meet the house heating needs only. c) if the electricity retail tariff is high, the storage tank, provided that the water temperature is above the heating curve set point, is used to supply the house. d) if the electricity retail tariff is high, and the storage tank temperature level is too low to supply the house, then the heat pump is used to supply the house directly.

As illustrated in Figure 7.1a, both storage tanks for SH and DHW are installed in parallel, and the heat pump can only supply one of them at a time. Priority is always given to the DHW tank. Both DHW and SH tanks are modeled by one-node models with homogeneous water temperature.

DHW tank volumes are set to a default value of 250 liters, corresponding to a typical volume installed in dwellings with four inhabitants. For SH tanks, the sizing depends on the hydronic configuration. For a parallel four-pipe configuration, water tank storage for space heating are sized following the same method as in Chapter 4. Simulations are run for 10 days in the winter, spring and fall for both a reference consumption pattern without flexibility and a flexible consumption pattern. The optimal

tank volume is such that it maximizes cost savings while limiting overconsumption. Indeed, large tank volumes may allow more flexibility in the winter for example, but lead to excessive overconsumption during shoulder seasons. The minimum and maximum tank sizes are set to 300 and 1500 liters, respectively. For a parallel two-pipe hydronic configuration, the sizing is not as straightforward. The use of the storage tank is only relevant when combined to incentives to unlock flexibility and tends to depend on the application. In this case, the sizing is therefore discussed with the illustrative application in Section 7.5.

7.4 Problem constraints

Depending on the storage option for space heating, Constraints (7.3b) to (7.3d) translate as follows:

- for thermal storage in building envelope, the building zone temperature should remain within a dead band of 1K around the set point profile during occupancy hours and between the minimum and maximum daily set point for unoccupied hours. An intermittent heating strategy is chosen. The set point is set to 19°C during the night and unoccupied periods and to 21°C during occupied hours of the day.
- for the four-pipe SH tank configuration: the water temperature, $T^{w,s}$, is always maintained above the house heating curve temperature, T^{hc} :

$$T_t^{hc} \leq T_t^{w,s} \leq \min(T_t^{hc} + \Delta T_t^{A-pipe}, 65^\circ C) \quad (7.7)$$

where ΔT_t^{A-pipe} is set to 10K.

- for the two-pipe SH tank configuration: the water temperature has to be higher than the house heating curve temperature only when the tank is used to supply the house, which corresponds to y^s equals one:

$$T_t^{hc} y_t^s \leq T_t^{w,s} \leq \min(T_t^{hc} + \Delta T_t^{2-pipe}, 65^\circ C) \quad (7.8)$$

where ΔT_t^{2-pipe} is set to 10K. The tank can only be supplied during periods of active demand response or excess on-site electricity production.

- for both four-pipe and two-pipe configurations, the indoor temperature strictly follows the lower set point.
- the heat delivered to the house should not exceed the full load capacity of the heat pump and auxiliary heater combined or the limits imposed by the temperature in the tank and by the emission system.
- for DHW, the water tank temperature should remain within an imposed dead band of 50–57°C for houses A and B and 50–65°C for houses C and D. Indeed, for well thermally-insulated houses, the zone temperature fluctuations entailed by switching the heat pump mode from space heating to DHW production are limited. The latter can therefore occur more frequently than in poorly insulated houses, without compromising the occupants' comfort. In order to limit heat pump performance degradation, the maximum temperature in the tank can therefore be set to a lower level. For less thermally-insulated houses, the number of daily mode switches in heat pump mode can be reduced by increasing the maximum temperature level.
- the heat pump can only supply either the house, or the SH tank or the DHW tank at a time, which

introduces Boolean variables and turns the optimization problems into mixed-integer linear programs.

7.5 Case studies

The three load modulation strategies ADR#1, ADR#2 and ADR#3 are applied to mitigate voltage fluctuations entailed by photovoltaic (PV) production in distribution networks. The objective consists in minimizing the difference between the electricity consumption and the renewable production on a modulation interval $\{\tau, \tau + n - 1\}$. If positive, this difference is referred to as residual load. If negative, it is referred to as surplus production. The modulation strategies are first applied to each typical building A to D to compare the different storage options, and then extended to simulate the response of a set of buildings in a distribution feeder.

7.5.1 Ranking of thermal storage options

To propose a ranking of the thermal storage options with regards to the house insulation level and load modulation strategies, each association of house and thermal storage presented in Section 7.3.2 is simulated for two typical winter days and two typical days during shoulder seasons. The activation takes place at time period 49 and the modulation lasts over 10 consecutive periods. Simulations are performed for both intermittent and continuous heating schedules.

For this application, the SH water tank sizes that yield the highest flexibility are summarized in Table 7.2. As explained in Section 7.3.2, for the two-pipe configuration, the optimal tank volume is strongly dependent on the application. In this case, a good approximation of the optimal tank size can be obtained as follows:

$$V^{s,tank} = \frac{\delta^{mod} \Delta t^{OFF} \overline{COP}}{\rho c \Delta T} \quad (7.9)$$

where δ^{mod} is an average electrical power modulation amplitude, Δt^{OFF} is the time span during which the heat pump can stop working without violating the 2 K temperature dead-band on indoor zone temperature, \overline{COP} is the seasonal COP, ρ and c are the density and specific heat of water, and ΔT is the temperature difference between the nominal water temperature given by the heating curve and the average ambient temperature. For the application investigated here, δ^{mod} is a function of the installed PV capacity.

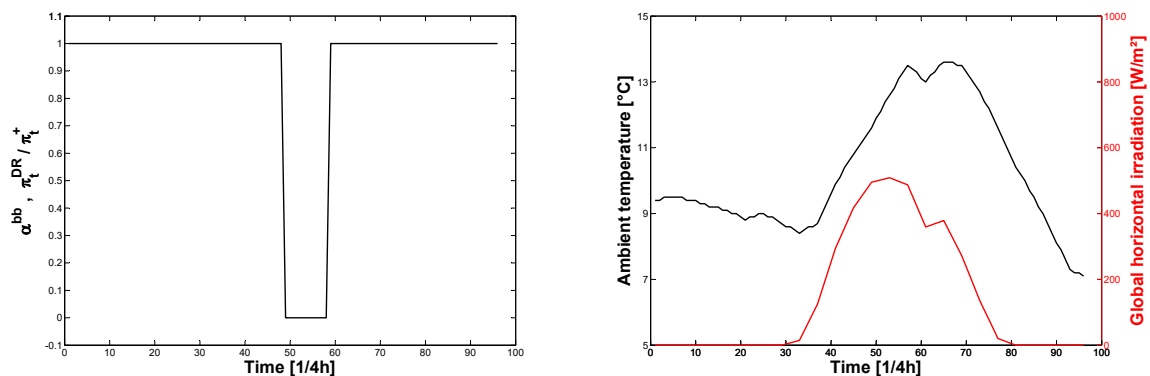
The incentive price signals used for strategies ADR#1 and ADR#2 are illustrated in Figure 7.3a. Figure 7.3b shows example ambient temperature and solar irradiation for a sunny spring day.

7.5.1.1 Intermittent heating strategy

Simulation results for test cases B1 to B3 and strategy ADR#2 are presented in Figure 7.4 for a sunny spring day. During the investigated time interval, the occupation profiles are such that the occupants leave the house at time period 53, which increases the allowed indoor temperature range between 18°C and 22°C. For all three storage options, both DHW production and SH contribute to demand

Table 7.2 – Water tank volumes.

House type - Storage option	DHW tank volume [m ³]	SH tank volume [m ³]	SH Tank configuration
A-1	0.25	/	/
A-2		0.6	Two-pipe
A-3		0.45	Four-pipe
B-1		/	/
B-2		0.45	Two-pipe
B-3		0.6	Four-pipe
C-1		/	/
C-2		0.25	Two-pipe
C-3		0.9	Four-pipe
D-1		/	/
D-2		0.25	Two-pipe
D-3		1.3	Four-pipe



(a) Price incentive signals ADR#1 (π_t^{DR}/π_t^+) and ADR#2 (α_t^{bb}). ADR#3 is a direct load control strategy. (b) Ambient temperature and solar irradiation on March 21st (Day 71).

Figure 7.3 – Incentive signals and weather conditions.

flexibility. During unoccupied periods, using the thermal envelope for demand flexibility allows the best match of PV production. The power consumption modulation from the baseline reaches up to about 3kW. Both the DHW tank and the zone can be preheated to meet comfort requirements imposed during occupied periods later in the day. For the two-pipe configuration, load matching is ensured either by DHW production, by direct space heating or by heat storage in the SH tank. The latter is heated during the last periods of the interval. This can be explained by two facts. First, the house can only be supplied either by the SH tank or directly by the heat pump, and not by both simultaneously. Secondly, the control strategy anticipates the use of the SH tank later in the day. In this case, the surplus electricity production is reduced by 46%. With the parallel four-pipe configuration, most of the flexibility is provided by the SH tank. Load matching is achieved during a concentrated time frame due to the limited storage capacity of both SH and DHW tanks and to the limited heating demand of the house during unoccupied hours. The surplus electricity production is reduced by 34%.

Figure 7.5 generalizes the findings of Figure 7.4 to houses A to D for the three control strategies. Results

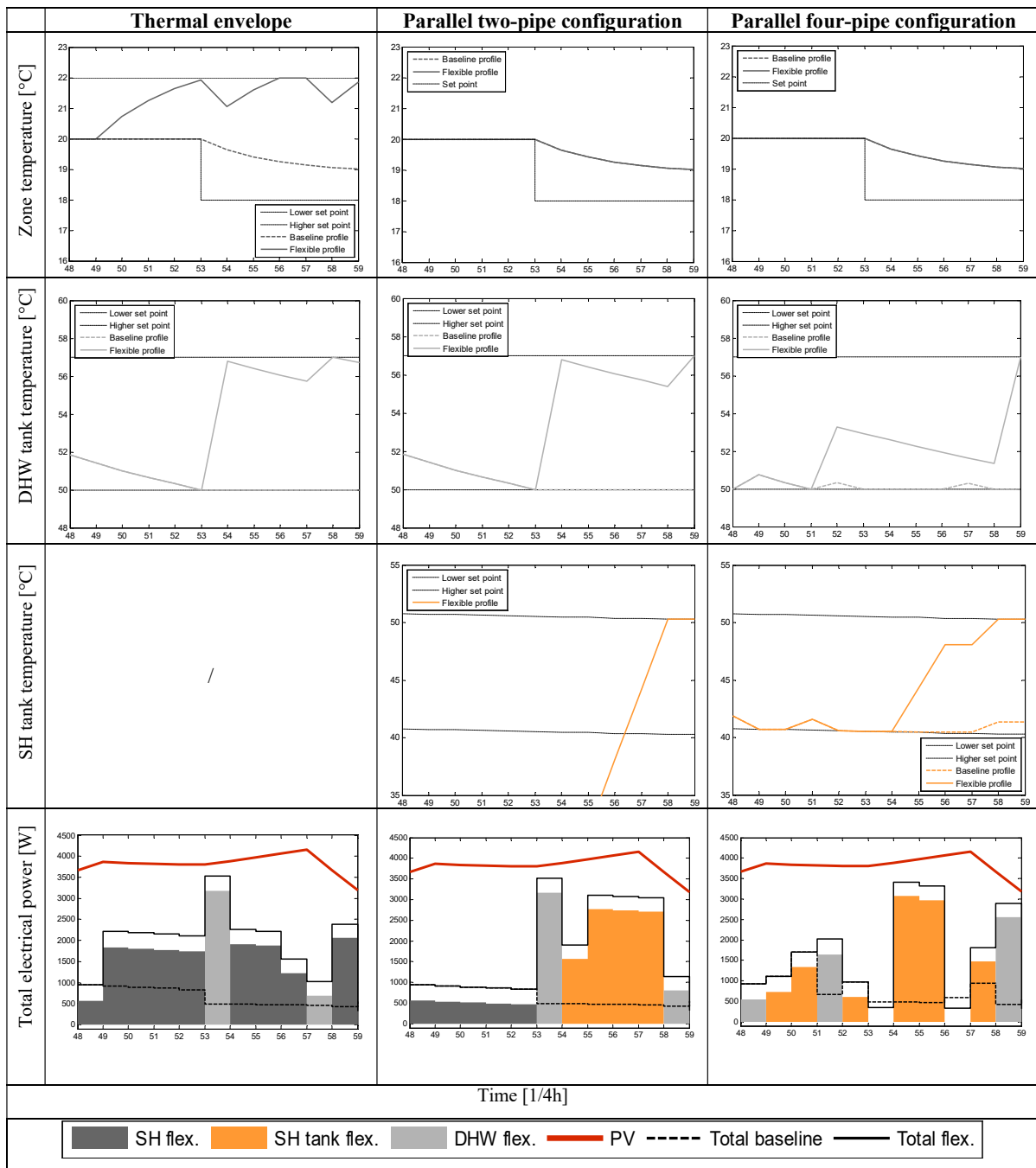


Figure 7.4 – Illustration of load modulation formulation ADR#2 for house B and three thermal storage options for a spring day (Day 71 – March 21st). Modulation starts in time τ equals 49 and lasts for 10 periods.

are presented in terms of average surplus production reduction and additional overconsumption and averaged over the four simulated days. The *overconsumption* is defined as the difference between the integrated daily electricity consumption of baseline and flexible profiles. The *additional overconsumption* is the share of overconsumption that does not occur during the modulation time interval. This metric allows to determine whether the additional heat stored during the modulation interval can be used effectively later in time.

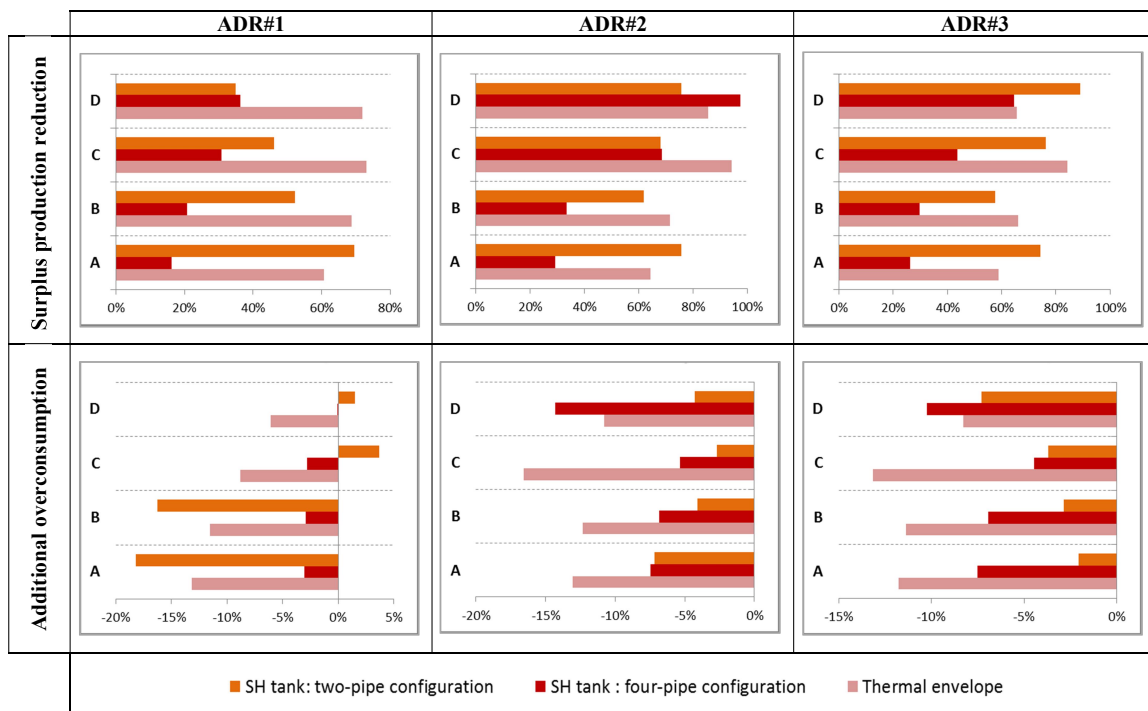


Figure 7.5 – Comparison of load modulation strategies ADR#1–3 and three storage options for an intermittent heating strategy.

The determination of the most suitable storage option for each house depends on the objective. If the latter is to reduce the surplus production, modulation strategy ADR#2 combined to thermal storage in the building thermal mass shows the best results. The electricity consumption profile is shaped to follow the PV production. The reduction in surplus production increases as the house insulation level decreases. A similar trend is observed with storage in space-heating water tank with parallel four-pipe configuration. In contrast, for the parallel two-pipe configuration of water tanks, the largest reduction in surplus production is obtained with modulation strategy ADR#3. As opposed to ADR#1 and ADR#2, ADR#3 does not anticipate future use of stored heat. Therefore, since the water temperature level in the storage tank is constrained to remain above the heating curve only when the tank is used to supply heat to the house, a significant share of surplus PV production can be reduced.

Results obtained with strategy ADR#1 show smaller reductions in surplus production than the two other modulation strategies. There are two underlying reasons. First, as opposed to ADR#2, there is no direct information regarding the amplitude of the PV power produced. Secondly, in contrast to ADR#3, the objective function aims at minimizing the electricity cost while including a prediction of the future use of stored heat, which reduced the possibility for excess storage. Reductions in surplus production obtained with all three control strategies range from 35% to 97%. The results obtained with ADR#1 provide some information regarding suitable coupling of storage options and house insulation levels:

- the parallel two-pipe hydronic configuration is best suited to provide load matching for well-insulated houses,
- the use of thermal mass as storage option is also preferable with well-insulated houses.

These conclusions are confirmed by the following analysis, that considers the mitigation of both surplus

production and additional overconsumption. For poorly-insulated houses such as house D, a coupling with water tanks in parallel four-pipe configuration allows to reduce the consumption after modulation by 14%. For houses B and C, the best storage option is the building thermal envelope. Residual load reductions of up to 71% and 94% are obtained for houses B and C, respectively. Depending on the modulation strategy, the heat stored during the modulation interval allows to reduce the electrical consumption after modulation by 9% to 17%. For well thermally-insulated houses such as house A, both thermal envelope and SH water tank with parallel two-pipe configuration are suitable storage options. Resulting reductions in surplus production range from 61% to 76%. The parallel two-pipe configuration outperforms the four-pipe configuration since the storage tank is only heated during the modulation interval instead of continuously throughout the day, which reduces ambient losses.

The performance of the parallel two-pipe configuration strongly depends on the sizing of the storage tank, particularly for poorly insulated houses such as houses C and D. Indeed, for such houses, the temperature reached in the water tank at the end of the modulation interval can be too low to successfully provide thermal comfort to the occupants later on, resulting in overconsumption.

7.5.1.2 Continuous heating strategy

Figure 7.6 shows the results for a continuous heating strategy. As explained in Section 7.3.2, the only two storage options considered for SH are building thermal mass and water tank with parallel four-pipe configuration. In terms of surplus production reduction, the use of thermal envelope outperforms the use of a water tank due to the larger storage capacity. However, for houses C and D, zone temperature variations when using thermal mass as storage option may compromise occupants' comfort. In contrast, the use of a water tank offers comparable flexibility potential and additional overconsumption reduction while guaranteeing thermal comfort.

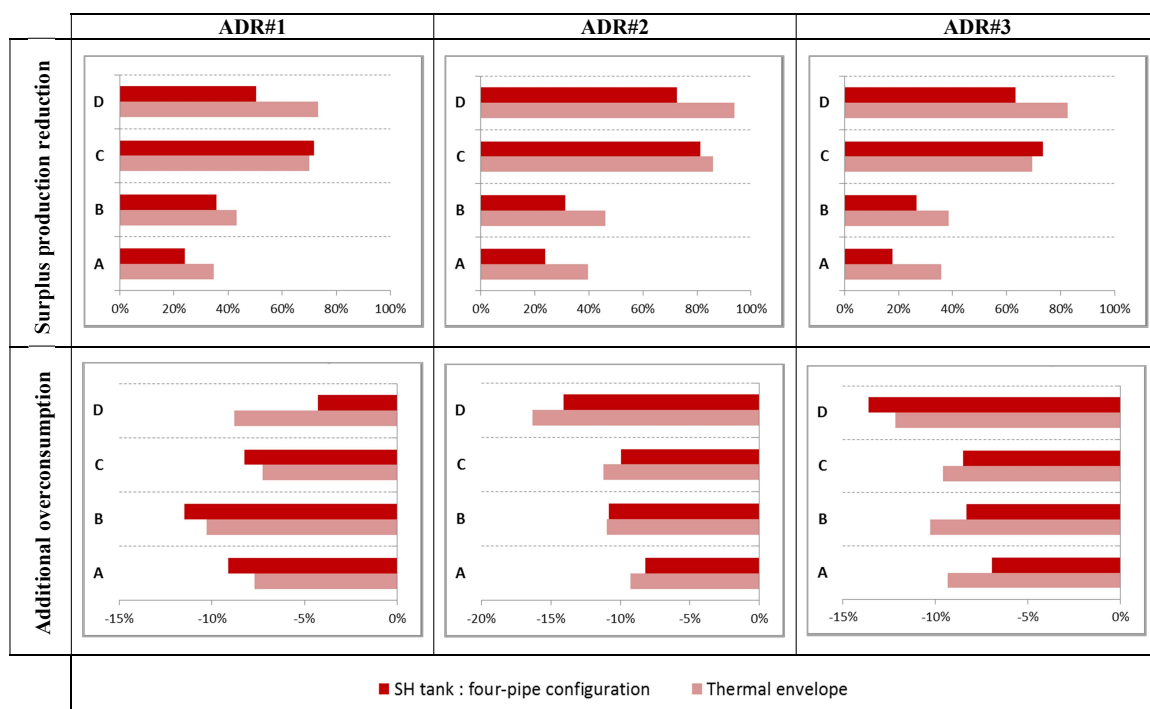


Figure 7.6 – Load modulation strategies ADR#1–3 for a continuous heating strategy.

7.5.1.3 Conclusion on storage ranking

The following ranking of storage options can be proposed:

- for well thermally-insulated houses, both storage in the building thermal mass and in a space-heating water tank with parallel two-pipe hydronic configuration are suitable options.
- for less thermally-insulated houses, the best option is the storage in a space-heating water tank with parallel four-pipe hydronic configuration.

7.5.2 Application to a semi-urban feeder

The methodology is applied to a typical semi-urban feeder in Belgium. The feeder has an average of 63 load points corresponding to 63 households, composed of freestanding buildings (Gonzalez et al. (2012)). Baetens (2015) has outlined the sensitivity of such feeders to high penetrations of distributed generation sources and heat pumps. For example, a penetration rate of PVs superior to 50% entails over-voltages, which could be reduced by load compensation. In this section, the potential of load compensation achievable with load modulation strategies ADR#1–3 is investigated.

The four typical houses presented above are distributed in the feeder according to their share in the Belgian residential buildings stock (Section 2.1.1). The number of inhabitants in each house is drawn from a normal distribution of average three and standard deviation of two with a maximum of five occupants. The exogenous consumption profiles associated to lighting and appliances, as well as domestic hot water draw-off events, are obtained from a previous study (Section 2.1.2). Indoor temperature set points schedules are intermittent temperature profiles generated based on normal distribution laws for morning, midday and evening start-up times. All profiles have a weekly average indoor set point above 18°C. Occupancy profiles are derived from the latter. Based on the results from Section 7.5.1, the best suited storage option that minimizes both surplus production and additional overconsumption is chosen for each of them. Additionally, 50% of the buildings are equipped with South, East or West-oriented PV panels with thirty-five degrees tilt angle and 18% average efficiency. The installed surface area is drawn from a discrete uniform distribution over an interval ranging from ten to forty square meters. PVs and heat pumps are distributed randomly over the 63 houses and may not coincide.

In a first step, for the results to be comparable, the random character of heating profiles, use of lighting and appliances, and of domestic hot water draw-off events is removed. Average profiles are used instead. Baseline consumption profiles for 10 and 20% penetration rates of heat pumps are illustrated in Figure 7.7 for a sunny spring day. Due to the intermittent heating strategy, the electrical power consumption with heat pumps tends to increase for time periods between 30–40 and 70–96. No significant improvement in load matching with PV production is observed when increasing the penetration rate of heat pumps. To cope with that, modulation strategies ADR#1 to #3 are implemented for 20% penetration rate of heat pumps. The resulting electrical profiles are illustrated in Figure 7.8 for a modulation interval starting in period τ equals 49 and lasting for 10 periods. With ADR#1, all end-users face a decrease in retail electricity tariff between period 49 and 58 and increase their electricity consumption. To avoid over-consumption due to increased heat losses, the consumption increase is the largest at the end of the modulation interval, which results in a loss of load diversity. This loss of load diversity is aggravated by the use of average instead of random profiles, as further discussed

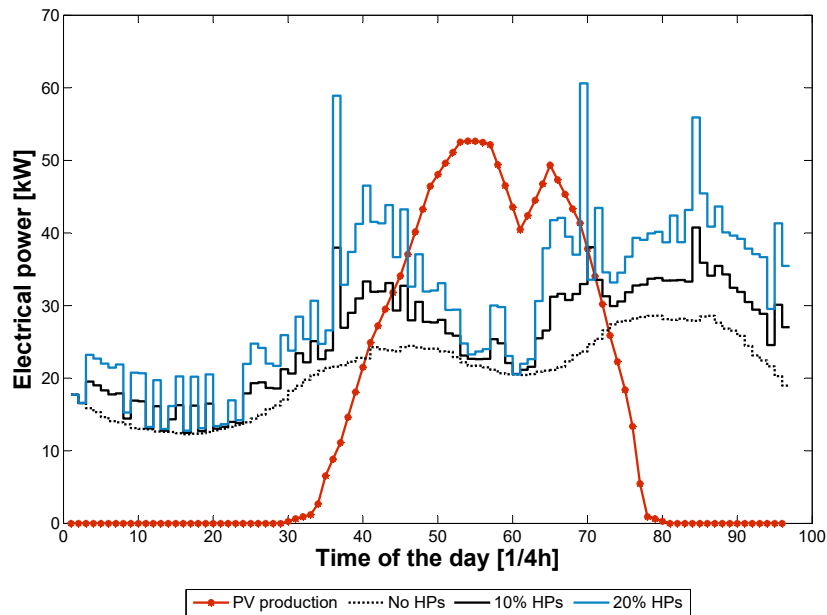


Figure 7.7 – Baseline electricity consumption profile in a semi-urban feeder with 50% PVs and 0, 10 % and 20% heat pumps for a spring day (Day 71 – March 21st) – no load modulation.

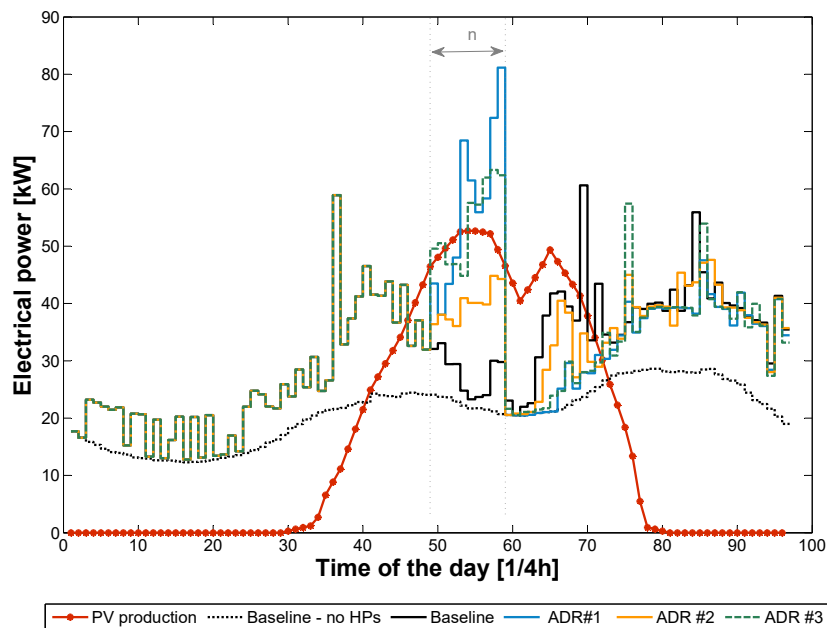


Figure 7.8 – Comparison of load modulation strategies ADR#1–3 implemented in a semi-urban feeder with 50% PVs and 20% heat pumps for a spring day (Day 71 – March 21st). The modulation interval is set to 10 periods of 15 minutes and starts in period 49.

hereafter. Since there is no limitation on the power modulation amplitude, surplus production may be turned into residual load, such as for period 53 to 58. For ADR#2, the PV power production provided as input to each home owner is the average PV production in the feeder. The initial surplus production of 56.9 kWh is reduced by 52%. Further reduction of surplus production could be obtained if each

end-user was given, for example, the maximum PV production in the feeder. However, using such an input in a decentralized optimization scheme could also lead to increased residual load. For ADR#3, all flexible end-users are encouraged to increase their consumption as much as possible over the modulation interval. Constraint (7.6b) requires all power increase on the interval to be larger than a minimum value. This minimum value is maximized in Equation (7.6a). The average resulting power modulation over the interval is less than with ADR#1, but the minimum modulation amplitude is greater.

As outlined in Chapter 6, the upward or downward activation of TCLs is followed by a rebound effect in the opposite direction in terms of consumption. As shown in Figure 7.8, the increase in consumption for periods 49–58 is directly followed by a decrease in consumption in periods 59–70. This decrease in consumption is particularly marked with ADR#1 and ADR#3, and might jeopardize grid operation. To mitigate this effect, one can resort to the methods proposed in Chapter 6.

The modulation length can be modified. Figure 7.9 illustrates the results obtained for a flexibility interval starting in period 40 and lasting over 31 periods. In this case, ADR#1 and #2 allow the reduction in surplus production that reach 41% and 44%, respectively. One major difference between the results obtained with modulation strategies #1 and #2 lies in the existence of power peaks at the end of the modulation interval. Compared to the baseline profile, the peak power demand increases by 144% and 65% with ADR#1 and ADR#2, respectively. Figure 7.10 shows the net total power modulation obtained with ADR#3. As the modulation interval increases from 10 to 31 periods, Constraint (7.6b) tends to flatten the modulation amplitude over the interval. The minimum modulation amplitude drops from 17.4 kW to 4.3 kW.

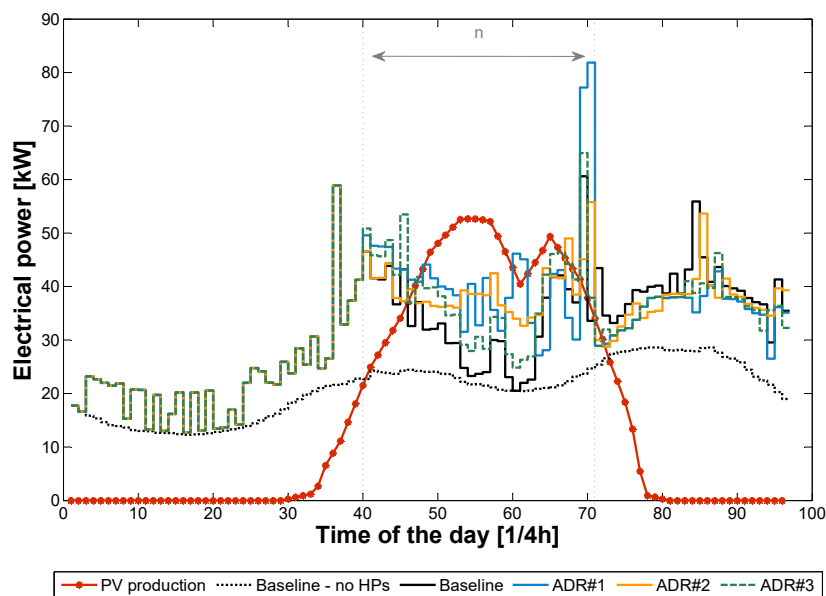


Figure 7.9 – Comparison of load modulation strategies ADR#1–3 implemented in a semi-urban feeder with 50% PVs and 20% heat pumps for a spring day (Day 71 – March 21st). The modulation interval is set to 31 periods of 15 minutes and starts in period 40.

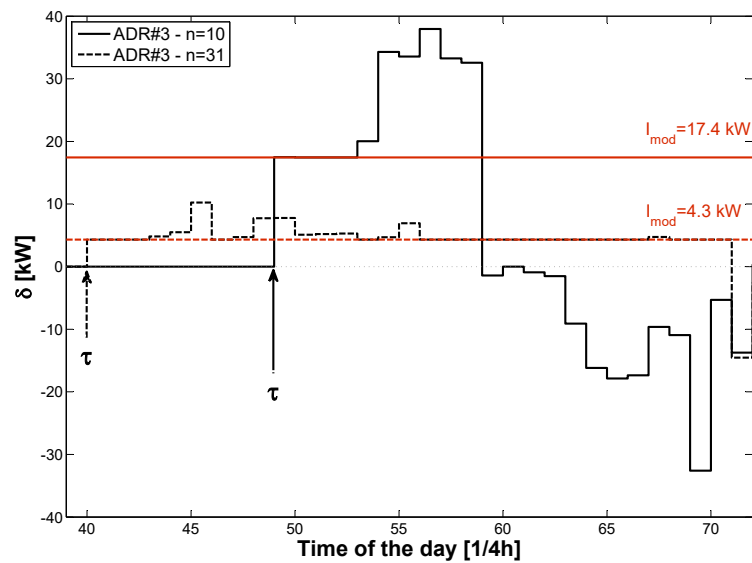
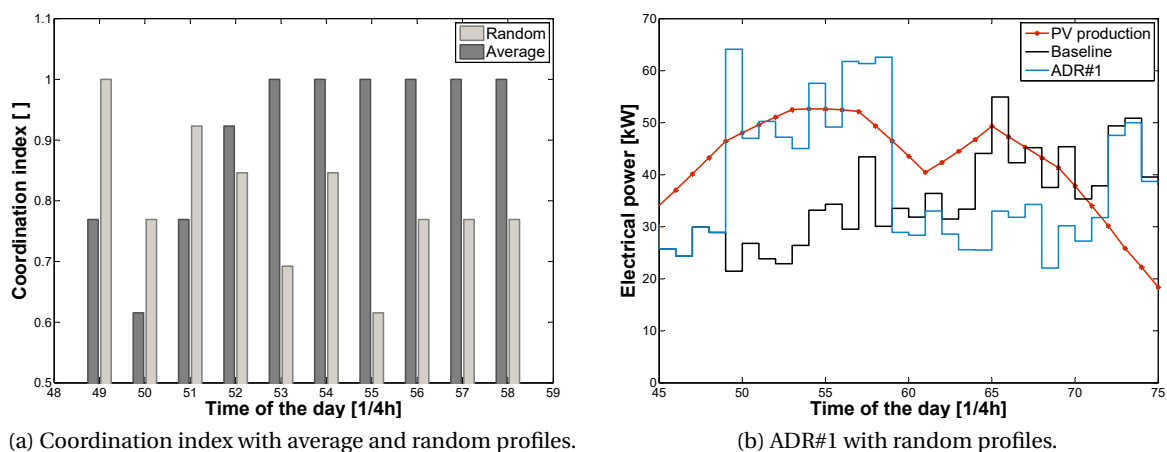


Figure 7.10 – Illustration of power modulation with ADR#3 for $n=10$ and $n=31$ – zoom on periods 40-70.

Finally, coordinated power peaks are naturally mitigated by the load diversity inherent to the different houses connected to a feeder. The different profiles detailed at the beginning of the section are therefore introduced in order to characterize the impact of load diversity on the outcome of modulation incentives. A new metric, the *coordination index*, is defined as the share of heat pumps increasing their consumption in each time step of the modulation interval. It is illustrated in Figure 7.11a for ADR#1 and 20% penetration of heat pumps. When using average heating profiles, the coordinated transition to a lower temperature set point in time period 53, combined to the low retail price tariff causes all heat pumps to increase their electricity consumption to store energy. With more diverse profiles, a coordinated response still occurs in time period 49, corresponding to the transition to a lower retail tariff. For the rest of the modulation interval, contrariwise, the percentage of heat pumps increasing their consumption varies. The resulting electrical power profile is shown in Figure 7.11b. Load diversity introduces a more homogenized power modulation over the interval and helps mitigate power peaks. However, a significant rebound effect is still observed for periods 59 to 72.



(a) Coordination index with average and random profiles.

(b) ADR#1 with random profiles.

Figure 7.11 – Influence of load diversity on power modulation ($\tau=49$, $n=10$).

7.6 Research outcome

In this chapter, a comparison of the three load modulation strategies proposed in Chapters 4 to 6 is performed. For each strategy, three storage options combining a DHW tank and either the thermal envelope of the building or a SH tank with two hydronic configurations are investigated for four typical Belgian houses characterized by different insulation levels. Among the options with a SH tank, one distinguishes two hydronic schemes: parallel two-pipe and parallel four-pipe. A ranking of storage options is proposed. It is concluded that

- for all types of houses and modulation strategies, the building structure offers the largest storage potential and the best mitigation of any potential bottleneck.
- however, as the house insulation decreases, greater indoor temperature fluctuations are observed, which can harm the occupants' comfort. In that case, the parallel-four pipe configuration with space-heating tank is the best alternative, for both intermittent and continuous heating strategies.
- for well-insulated houses, the parallel two-pipe hydronic configuration with space-heating tank is an interesting alternative to storage in the thermal mass. However, in the case of load matching with solar consumption, its benefit on an intra-day basis strongly depend on its sizing.

When comparing all three modulation strategies,

- control strategy ADR#1 is better suited for daily load shifting and reduction of electricity procurement costs than for the elimination of local bottlenecks.
- control strategy ADR#2 is the most versatile as it can be used both at the building scale or at larger scales, such as a district, by modifying the power production input. It is also better suited than the other strategies for load shaping applications.
- the implementation of a direct load control strategy (ADR#3) on each individual house without centralized input from the system operator yields a suboptimal response. This is further discussed in Chapter 8.

Finally, for the illustrative example investigated here, at the scale of a distribution feeder with 63 houses, if 50% of the houses are equipped with PV panels, a penetration rate of 20% heat pumps with appropriate thermal storage allows to reduce the residual load by 28 to 73.4%, depending on the control strategy and the modulation interval length. An upward modulation strategy shows good result for short interval lengths with relatively constant power production, whereas the load shaping strategy increases the residual load reduction by an extra 21% on longer modulation intervals.

**Load modulation strategies:
large-scale investigation**

Part IV

8 Large-scale assessment of the flexibility of residential heat pumps

8.1 Motivations

8.1.1 Centralized and decentralized control of thermostatically-controlled loads

As emphasized in Section 6.6.8, one drawback of thermostatically-controlled loads (TCLs) resides in the rebound effect that follows any load modulation. When applied to solve system imbalance, it has been shown that the cost associated to the rebound effect can potentially make the activation unprofitable. These results were obtained following a decentralized optimization approach in which each individual heat pump responds to an activation signal independently. To mitigate this rebound effect, a centralized optimization approach can be adopted. The method consists in pooling the heat pumps in order to meet a common power modulation objective. The optimal problem formulation can be expressed as follows:

- for each house, the baseline electrical consumption is obtained from Equation (6.6),
- the computation of the modulation potential from the baseline can be expressed as

$$\min \left| \sum_{i=1}^{n_{houses}} \delta_{\tau}^i - \delta^* \right| + \epsilon^* \sum_{t=\tau+1}^{\tau+n+l+k-1} \sum_{i=1}^{n_{houses}} \left| \delta_t^i \right| \quad (8.1)$$

where each house i is subject to Constraints (6.7b) to (6.7l). δ^* is the minimum targeted total modulation amplitude. ϵ^* is a parameter that weighs the relative importance of the mitigation of the rebound effect and the achievement of the expected modulation.

Both centralized and decentralized (see problem formulation in Chapter 6) optimization schemes are applied to one hundred freestanding houses. To limit the number of parameters of influence, houses geometry and thermal characteristics are chosen identical and correspond to houses built between 1991 and 2006 detailed in Chapter 3. Each house differs by occupancy and heating schedule profiles, use of lighting and appliances as well as by domestic hot water draw-off events. The simulation time step is set to 15 minutes. Modulation parameters presented in Chapter 6 are set to $n = 1$, $l = 0$, $k = 5$, and ϵ^* is set to 10. An example of results obtained with both decentralized and centralized optimization problems for an upward activation is illustrated in Figure 8.1. The modulation occurs in time period 43. With a decentralized optimization scheme, an upward modulation of 179.5 kW can be achieved by increasing the consumption of 99 heat pumps. One heat pump is unable to perform an upward

modulation at that given time period. The upward activation is directly followed by a payback period. The maximum deviation amplitude from the baseline reaches 82.3 kW. With a centralized optimization scheme, an upward modulation of 109.2 kW is achieved in time period 43 with 78 heat pumps. The 22 remaining heat pumps are activated upward in the next time period to mitigate deviations during the payback. No deviations from the baseline are observed.

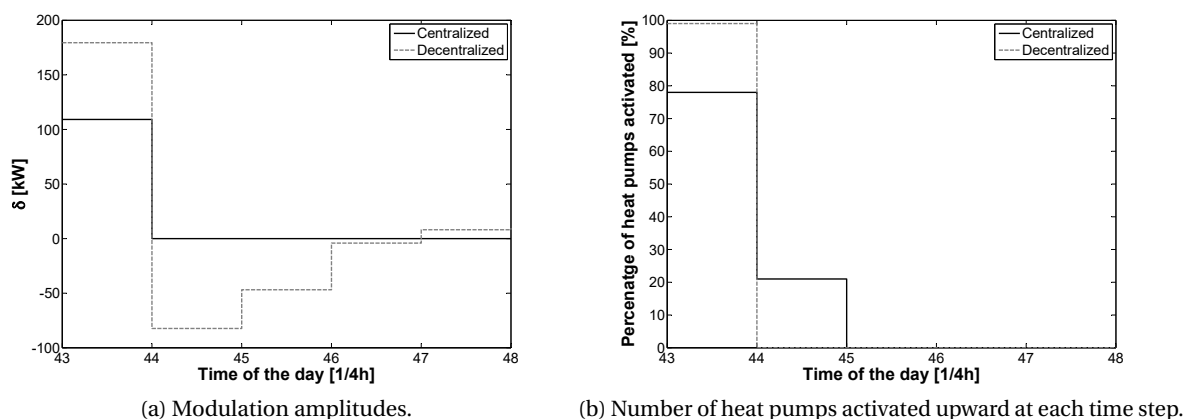


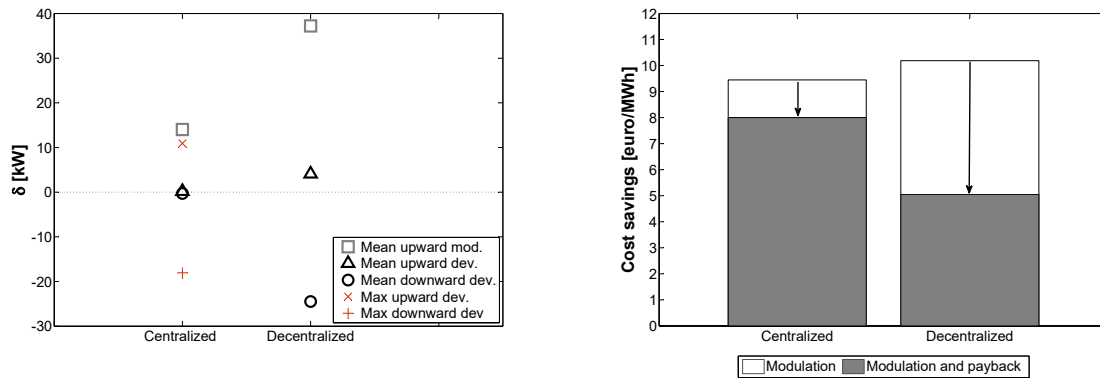
Figure 8.1 – Comparison of the results obtained with centralized and decentralized optimization schemes for an upward activation in period 43 with 100 houses. Modulation parameters are set to $n = 1$, $l = 0$ and $k = 5$.

Both approaches are implemented for all time periods τ on a winter day. Results in terms of average modulation amplitude and average cost savings for a load aggregator are shown in Figure 8.2. To mitigate the rebound effect, the centralized optimization reduces the average achievable upward modulation potential by 61%, compared to the decentralized approach. Average upward and downward deviation amplitudes are less than 500W. However, for some time periods, the rebound effect cannot be fully mitigated, as illustrated by the maximum deviation amplitudes shown in Figure 8.2a. Rebound effect mitigation directly impacts cost savings. The latter are calculated using historic imbalance prices. Cost savings per unit of activated volume retrieved on the modulation period τ is 8% greater with the decentralized approach, as shown in Figure 8.2b. However, when adding the costs induced by the payback period, the total cost savings decrease by 15% and 51% respectively with the centralized and decentralized approaches. The centralized control method therefore increases the profitability of the proposed balancing service. In that regard, centralized optimization schemes are further investigated in this chapter.

8.1.2 Aggregation of thermostatically-controlled loads

In a centralized optimization approach, as the number of houses increases, it becomes computationally expensive to model each end-user separately. In the literature, studies that investigate large-scale flexibility of domestic thermostatically-controlled loads (TCLs) resort to aggregated models.

Latiers et al. (2016) propose a linear aggregated model of "energy-controlled" loads such as batteries or electric water heaters. The model is based on the impulse response that represents the load variation from a baseline. RMS errors of less than 0.2% are found for aggregation of one hundred units. However,



(a) Average modulation amplitude (mod.) and deviations (dev.).

(b) Average cost savings for a load aggregator.

Figure 8.2 – Average results obtained with centralized and decentralized optimization problems for an upward activation with 100 houses. Modulation parameters are set to $n = 1$, $l = 0$ and $k = 5$.

the model does not easily extend to the modeling of thermal loads and associated losses.

In the study of Biegel et al. (2013), an equivalent lumped first-order RC analogy is used to model the thermal behavior of a set of heterogeneous houses. Model parameters, temperature limits and power constraints are set to the average values of the set. The authors point out the lack of accuracy that may arise from such modeling approach. Indeed, as shown by Hao et al. (2013), a distinction exists between the modeling of homogeneous and heterogeneous populations of TLCs. In the case of a *homogeneous* population of loads, with identical characteristics and boundary conditions, one can define a generalized battery model with a capacity equal to the average capacity of the set, and power limits set to the average over the set of loads. This is obviously no longer exact for a set of *heterogeneous* loads. In that case, a sufficient condition consists in modeling the general battery with power limits and capacity corresponding to the limiting case of the population of loads. Papaefthymiou et al. (2012) propose to model an aggregated set of buildings equipped with heat pumps as an equivalent storage plant. Similar loads are first pooled and modeled using detailed simulation tools. Comfort-driven simulations are performed in order to derive minimum and maximum temperature bounds, as well as power bounds for the aggregated model. In the aggregated model, temperature changes are modeled by a linear function of the electrical power variations of the heat pump. An aggregated model of residential buildings with heat pumps for demand-side management is proposed by Patteeuw and Helsen (2014). Each house differs by its characteristics and occupants' behavior. The number of inhabitants varies from one to six. First, each house is modeled separately in order to determine its warm-up and cool-down temperature curves. The obtained curves are then averaged over the set of buildings and used as lower bound for the unique aggregated model. Average internal heat gains are used as input to the model. For domestic hot water, there are as many equivalent tank models as the maximum number of inhabitants, i.e., six in that case. The actual lower bounds for the water storage tank temperatures are determined along with the average hot water demand. The aggregated model is validated against the results obtained when each house is modeled separately. Agreements within 5% are found in terms of energy consumption.

Although in line with the sufficient condition established by Hao et al. (2013), the aggregation methods

proposed by Papaefthymiou et al. (2012) and Patteeuw and Helsen (2014) still require to model each building separately in order to determine lower temperature bounds of the aggregated model. This may limit the ability of these methods to be extended to large-scale simulations, as it becomes challenging to obtain all information needed to model each building separately.

8.1.3 Research objectives

In light of the above analyses, one objective of this chapter is to investigate the flexibility potential of large sets of residential houses equipped with heat pumps based on a centralized control approach. To that end, reliable aggregated models that do not require modeling of each building a-priori are developed in Section 8.2. These models are then used for large-scale assessment of the flexibility of residential heat pumps based on centralized optimization approaches. A first application focuses on its impact on day-ahead market clearing prices (Section 8.3). The second application deals with the provision of power reserve (Section 8.4).

8.2 Load aggregation model

In Chapter 2, a method to cluster houses according to their similarities in terms of geometrical and thermal characteristics was presented. A tree-structure, composed of representative houses was developed. The proposed method did not take into account the aggregated modeling of diverse electrical demand profiles and occupants' behavior. The diversity of load profiles results in heterogeneous populations among similar houses of a cluster, which cannot be accurately modeled by average values. To reduce this heterogeneity, each cluster can be further divided based on occupancy-related constraints regarding space-heating and domestic hot water consumption.

The objective is thus to propose a method to aggregate buildings with similar constructive characteristics but different user consumption profiles with a minimum number of aggregated models, from the point of view of a load aggregator. To that end, the following inputs have to be provided to the load aggregator:

- house geometry and insulation level,
- heat pump nominal power and rated performance,
- desired temperature set point profile and allowed temperature dead band around the set point,
- DHW tank size,
- total number of occupants,
- hot water demand profiles, based either on average historical data, or on the definition of time periods of high demand probability.

8.2.1 Aggregation of space-heating demand

8.2.1.1 Generation of set point temperature profiles

Heating set point schedules can vary significantly from one building to another, depending on the occupants' behavior. Most profiles can be gathered under three conventional types of profiles:

- A *constant* daily set point profile,
- A *night set-back* profile, in which the set point temperature is lower during the night than during the day.
- An *intermittent* profile with a temperature set-back during the night as well as during hours of the day for which the building is unoccupied.

Some profiles, however, don't fit into any of these three standard categories and are completely *random*. They form a fourth category.

For the purpose of this work, temperature set point profiles are generated randomly for each building. First, a percentage of each type of profile is chosen randomly. Profiles are then generated with the following constraints:

- for *constant* profiles, the temperature level is drawn from a normal distribution of average 20°C and 1K standard deviation.
- for *night set-back* profiles, temperature levels are fixed to 18.5°C during the night and 21°C during the day. Time periods of the day that determine the beginning of day-time and night-time schedules are drawn from normal distributions. For weekdays (resp. weekends), the average start-up time is set to 6.5 am (resp. 7.5 am) with a standard deviation of 2 hours. The night-time schedule average start-up time is set to 10 pm with a two-hour standard deviation.
- for *intermittent* profiles, temperature levels for occupied and unoccupied periods are imposed to 21°C and 18.5°C respectively. Heating periods are divided in morning and afternoon/evening periods. Beginning and duration of occupancy periods are drawn from normal distributions, as explained for the night set-back profile. The afternoon heating start-up time is set to 5:30 pm with a one-and-a-half-hour standard deviation.
- for *random* profiles, a maximum of three different temperature levels is allowed within a day. Temperature levels have to be comprised between 18°C and 22°C. Temperature levels and start-up times are drawn from random distributions. Among the resulting profiles, some may therefore belong to one of the other three categories.

Occupancy profiles are directly derived from the set point profiles.

8.2.1.2 Clustering based on set point profiles

Three different methods to cluster buildings in terms of space heating needs are compared in this section. A first option consists in *averaging* the temperature set points of all buildings, resulting in a single aggregated model. A second method consists in associating the different profiles to the three conventional categories (constant, night set-back and intermittent heating schedules). This is referred to as *stratified* sampling. The association to a category is based on the number of temperature levels in the profiles. Profiles with one temperature level are evidently assigned to the constant profiles category. Profiles with two temperature levels are assigned to the night set-back category and profiles with three temperature levels are associated to the intermittent profile category. In a third method, it is proposed to associate the profiles either to one of the three conventional categories or to the "random" category. This method is referred to as *quota* sampling. The classification is based on the measure of the integrated temperature difference between each profile and a reference profile for each category. Similarities with the four categories of profiles are established as follows:

1. determine the number of temperature levels in the profile,
2. determine the similarity of the profile with one of the three conventional profiles.
 - in the case of one temperature level: assign the profile to the "constant" profiles category,
 - in the case two temperature levels: the profile could belong either to the "night set-back", or to the "intermittent" or to the "random" category. To choose the category, equivalent night set-back (T_t^{nsb}) and intermittent (T_t^{int}) profiles are built based on the temperature levels determined in the first step. The profile is then compared against those two reference profiles by the average integrated temperature difference, as follows:

$$\Delta^{nsb} = \frac{\sum_t |T_t - T_t^{nsb}|}{n} \quad (8.2a)$$

$$\Delta^{int} = \frac{\sum_t |T_t - T_t^{int}|}{n} \quad (8.2b)$$

where n is the number of periods. If the difference is larger than 1K, the profile is associated to the "random" profile category. If it is below that value, it is associated to the profile category with the minimum average integrated temperature difference.

- for three temperature levels: the procedure is identical to the case with two temperature levels. The category options for the profile are "intermittent" or "random". The principle is illustrated in Figure 8.3. For the example profile, the corresponding reference "intermittent" profile is such that the temperature is equal to the maximum temperature of the example profile during occupied periods and to the minimum temperature during unoccupied period. Transitions between temperature levels are smoothed to accommodate a larger panel of profiles. In this case, Δ^{int} is equal to 1.23, and the profile is thus associated to the "random" category.

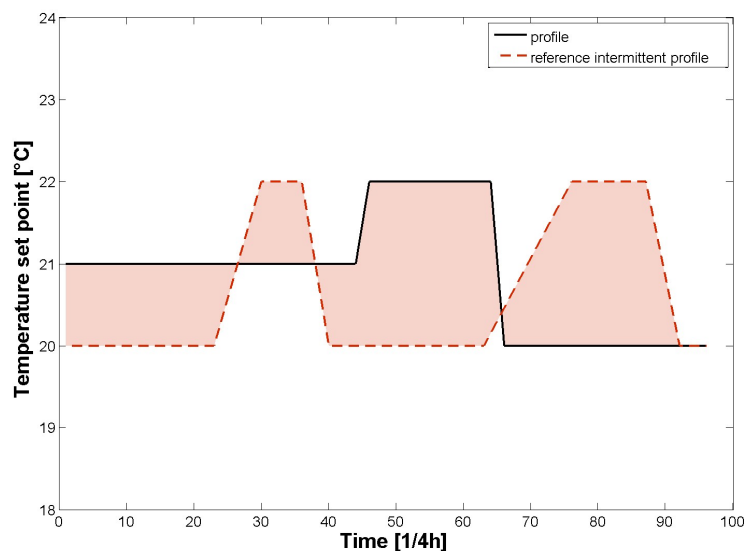


Figure 8.3 – Illustration of the method to classify set point profiles with three temperature levels.

Once distributed among the categories, all profiles in one cluster are averaged. Corresponding upper and lower temperature bounds are derived. These aggregated profiles are then used as temperature

bounds in the building model. Depending on the diversity of profiles, the number of aggregated models varies between one and four.

8.2.1.3 Validation

As proposed by Patteeuw and Helsens (2014), the accuracy of aggregated models can be determined from their ability to reproduce power profiles obtained in response to variable tariffs. To that end, the three clustering methods are applied to a set of one hundred buildings equipped with price-responsive heat pumps. First, each building is simulated separately by solving the optimal problem given in Equation (4.8) in order to obtain a reference consumption profile. The aggregated electricity consumption profile is the sum of the profiles obtained for each building. Secondly, aggregated models are derived following the three methods presented in Section 8.2.1.2, i.e. one model for the *averaging* method, three models for the *stratified sampling* method and one to four models with the *quota sampling* method. In this case, the selected one hundred profiles are quite diverse and four clusters are obtained with the last method. The same optimization problem (Equation (4.8)) is solved using those aggregated models. Results for the set of one hundred buildings are obtained by multiplying the results obtained with each aggregated model by the number of buildings that fall in each category.

Results for the three aggregation methods are illustrated in Figure 8.4. Figure 8.4a compares the aggregation of set points into four categories to the averaging into one profile. Figure 8.4b shows the aggregated power consumption profile obtained with one hundred models and the results obtained with the three aggregation methods. The RMS errors on the zone temperature obtained with the first, second and third methods are 0.43 K, 0.29 K and 0.09 K respectively. Corresponding normalized RMS errors on the electric power are 36.9%, 23.7% and 11.9%. Based on these results, it can be inferred that representing the set of buildings only with one model constrained by the average of the constraints of all the buildings results in a substantial loss of accuracy, due to the heterogeneity of the population of loads. Contrariwise, these results confirm the validity of the aggregation method based on the similarity in set point constraints. In particular, the improvement in accuracy brought by the use of a fourth model that gathers all "random" profiles is significant when comparing results obtained with stratified and quota sampling methods. Therefore, the quota sampling aggregation method is used in the remainder of the chapter.

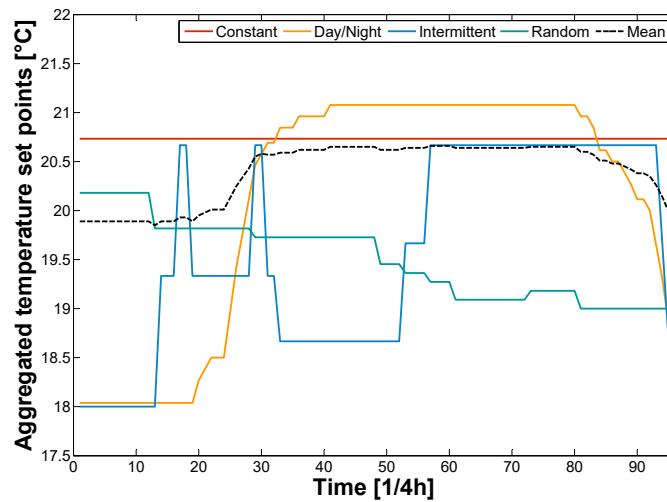
8.2.2 Aggregation of domestic hot water demand

8.2.2.1 Generation of DHW demand profiles

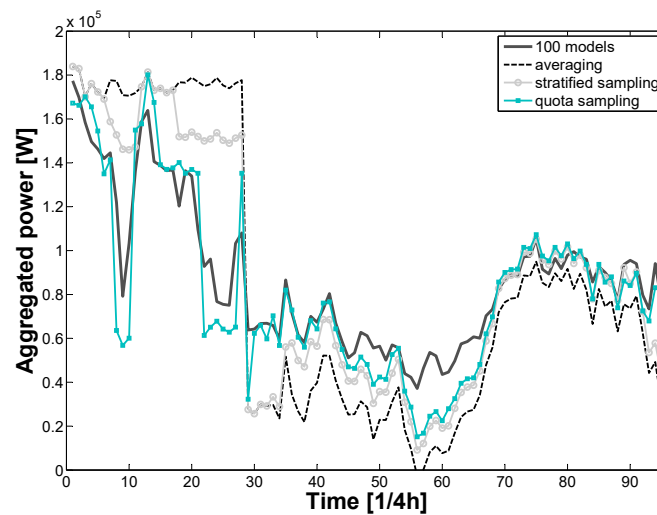
The domestic hot water profiles presented in Chapter 2 are used to simulate different water draw-off events for each building. They are modified to match the occupancy profiles generated in Section 8.2.1.1, in order to ensure that no DHW is used outside occupied periods of the day.

8.2.2.2 Clustering of DHW profiles

Different methods can be used to represent a cluster of domestic hot water tanks. The first method, referred to as *averaging* method, consists in modeling a single water tank with a volume equal to the average tank volume of the set of buildings and with the average DHW demand profile. The second



(a) Set points aggregation with the averaging method (mean) compared to quota sampling method with four categories (constant, day/night, intermittent and random).



(b) Total electrical power obtained with the averaging (1 model), stratified sampling (3 models) and addition of the "random" category with quota sampling (4 models).

Figure 8.4 – Comparison of the power consumption profiles obtained with three aggregation methods to those obtained with one model for each building.

method follows a *stratified sampling* method in which the population of loads is divided according to a given characteristic. In this case, as proposed by Patteeuw and Helsen (2014), water tanks can be clustered based on the number of occupants in the house. For each cluster, the aggregated tank model then consists in one tank of size and DHW demand profiles corresponding to the average values for the given number of occupants. The third method is based on *random sampling* techniques. Such sampling methods are used when the population is very large and random. In this case, it is proposed to determine a number of representative profiles, comprised between one and five. The choice of representative profiles is carried out in several steps:

1. Hourly DHW draw-off profiles are normalized with respect to the integrated daily value.
2. In order to capture relevant patterns, DHW draw-off events of volume inferior to one-tenth of the integrated daily usage are discarded. Other normalized DHW draw-off values are set to one.
3. A pairwise comparison of all normalized profiles is performed based on the computation of the RMS difference between them

$$RMSD_{i,j} = \sqrt{\frac{\sum_{t=1}^n (\dot{V}_{i,t}^* - \dot{V}_{j,t}^*)^2}{n}} \quad (8.3)$$

4. To each profile i is associated the profile j with the smallest $RMSD_{i,j}$. There can be more than one possibility, as illustrated in Figure 8.5. The resulting correspondence matrix is reduced to

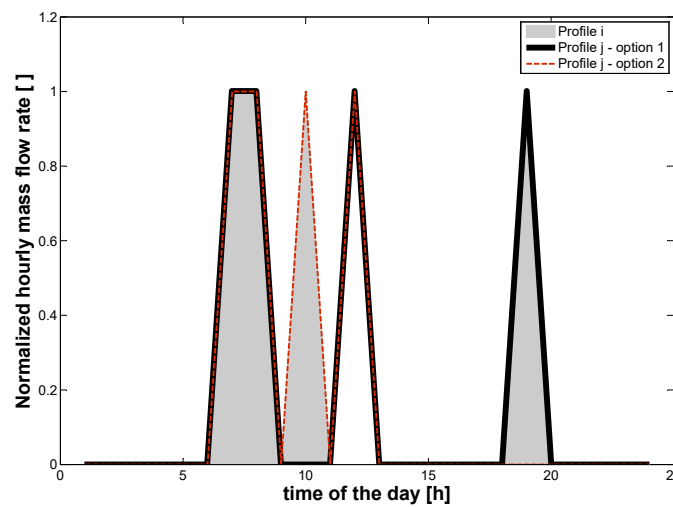


Figure 8.5 – Illustration of the process of pairwise comparison of normalized DHW flow rate profiles in the case of a profile i with two identical $RMSD_{i,j}$.

a column vector by replacing profiles with identical $RMSD_{i,j}$ by the profile with the largest number of occurrences in the matrix.

5. Resulting typical profiles are then ranked according to their occurrence in the vector. If there are more than five remaining profiles, the first five are chosen as representative profiles.
6. Profiles that did not fall into those five categories are redistributed in the category with the smallest RMSD.

An example of normalized representative DHW profiles obtained through the above procedure is provided in Figure 8.6. In this example, a set of 55 profiles is used. Five representative profiles are identified. They are compared to the average of the subset of profiles they represent.

These representative profiles are only used to distinguish the clusters and distribute the different profiles among them. As for space-heating set-point profiles, aggregated DHW use profiles are then given by the average of the profiles that fall in each category. Tank volumes, contrariwise, are set to the average value over the entire set of water tanks, regardless of the identified categories. Since heat pumps are used to supply both DHW and space heating, the validity of the proposed clustering method is verified in a combined exercise in the next section.

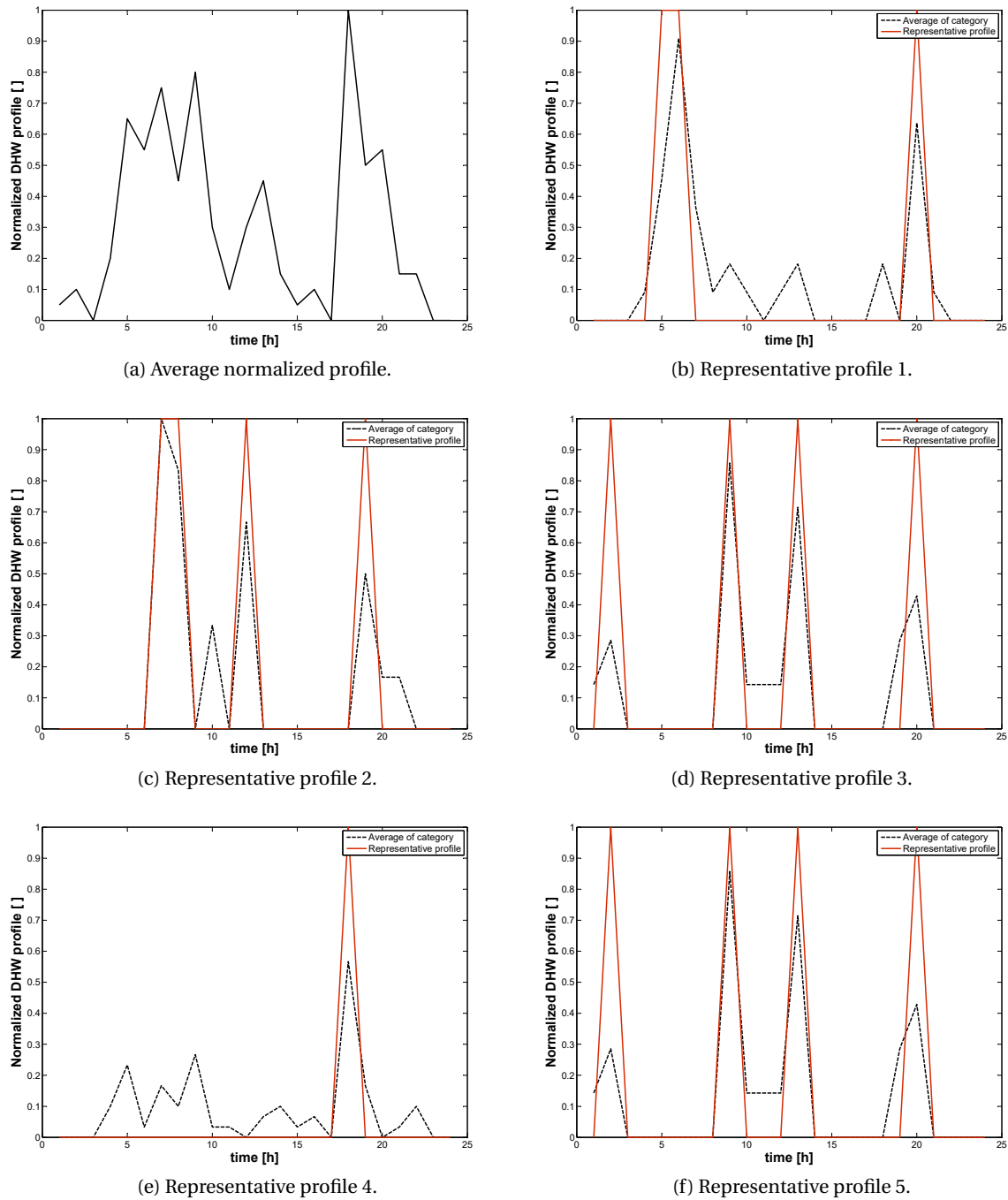


Figure 8.6 – Example of normalized representative DHW profiles obtained with the proposed method for a set of 55 profiles. Comparison between representative profiles and average profiles over each subset.

8.2.3 Aggregation of both space-heating and domestic hot water demands

The optimization problem solved to determine the validity of the proposed aggregation method is given by Equation (6.6). To each subset of buildings derived from the aggregation based on space-heating needs (quota sampling method) is associated one to five subsets of aggregated DHW tanks,

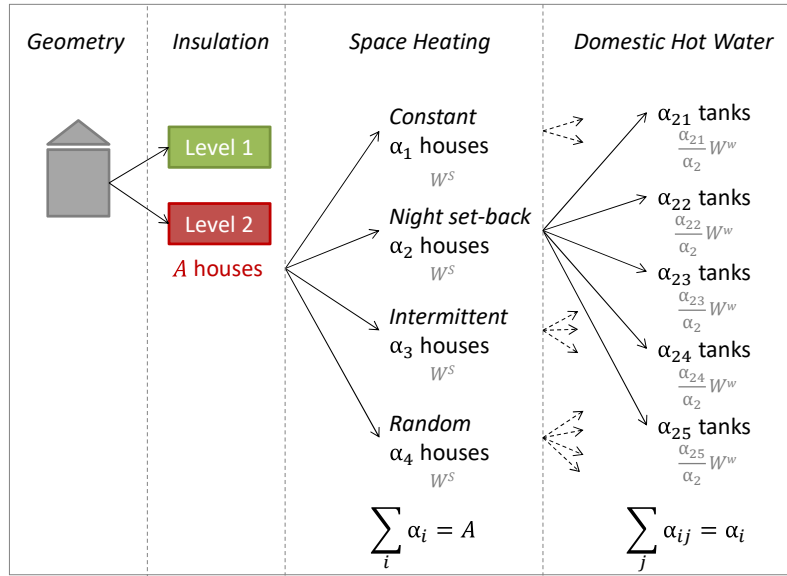


Figure 8.7 – Aggregation method of space heating and DHW needs.

as illustrated in Figure 8.7. One building model and one water tank represent the behavior of several of them. Since heat pumps are used to cover both space-heating and DHW needs, this has several implications in the context of the aggregation. First, within a decision time step, the heat pump is allowed to work in both space-heating and DHW modes simultaneously. The Boolean variable y of Constraints (6.6i) is therefore relaxed and can take values comprised between 0 and 1. Secondly, the aggregation of water tanks removes the existing diversity of temperature levels and tank sizes, which tend to lead to coordinated power peaks. To mitigate this effect, it is proposed to limit the heat pump power devoted to the domestic hot water production proportionally to the number of water tanks represented by each aggregated model, as indicated in Figure 8.7. Consequently, Constraints (6.6f), (6.6g) and (6.6i) can be replaced by

$$0 \leq W_t^s \leq y_t W_t^{s,max} \quad (8.4a)$$

$$0 \leq W_t^w \leq (1 - y_t) \frac{\alpha_{ij}}{\alpha_i} W_t^{w,max} \quad (8.4b)$$

$$0 \leq y_t \leq 1 \quad (8.4c)$$

where α_i is the number of houses aggregated in category i of space heating profiles and α_{ij} is the number of water tanks among those i houses aggregated in category j in terms of DHW draw-off profiles.

Finally, lower and upper temperature bounds in Equation (6.6e) should be set to the most restrictive values of the set (Hao et al. (2013)), such that

$$x_{i,t}^{min} = \max_{i=\{1..i^{max}\}} (x_{i,t}^{min}, \bar{x}_t^{min}) \quad (8.5)$$

and

$$x_{i,t}^{max} = \max \left(\min_{i=\{1..i^{max}\}} (x_{i,t}^{max}, \bar{x}_t^{max}), x_{i,t}^{min} \right) \quad (8.6)$$

where $\{1..i^{max}\}$ is the set of heating set-point categories.

The total number of aggregated models, n_C , is therefore equal to

$$n_C = \sum_i j_i^{max} \quad (8.7)$$

where j_i^{max} represents the number of models of DHW tanks for each house type i .

The total aggregated power over the set of buildings is the weighted average sum of power profiles for space-heating and DHW production obtained for each aggregated model, such that

$$P_t = \sum_{i=1}^{i^{max}} \left(\sum_{j=1}^{j_i^{max}} (W_{ij,t}^s + W_{ij,t}^w) \alpha_{ij} \right) = \sum_{k=1}^{n_C} (W_{k,t}^s + W_{k,t}^w) \alpha_k \quad (8.8)$$

8.2.4 Validation

The same set of one hundred buildings as in Section 8.2.1.1 is used to compare the three aggregation methods, i.e. averaging, stratified sampling and random sampling. Results are summarized in Table 8.1. Both stratified and random sampling methods show the smallest normalized RMS error on the electrical power consumption. The poorer performance of the averaging technique comes from the loss of load diversity which, despite the power limitation proposed in Equation (8.4b), results in power peaks, as shown in Figure 8.8. Both stratified and random sampling methods introduce a better load diversity and reduce the NRMSE on the electrical power by 3.8% and 4.7%, respectively, compared to the averaging method. The random sampling method allows to adapt the number of models from 4 to 20 depending on the diversity of DHW profiles. It yields slightly better results than the stratified sampling technique with 16 instead of 20 models.

Table 8.1 – Comparison of three aggregation techniques of DHW needs, combined to the "four-category" space-heating aggregation method for one hundred buildings.

	Averaging	Stratified Sampling	Random Sampling
Number of models	4	20	16
NRMSE \hat{P}_t	27.2%	23.4%	22.5%

To further outline the benefits of the random sampling over the stratified sampling method, five hundred buildings are simulated. The aggregation with both methods is performed on one hundred, three hundred and five hundred buildings for a day-night tariff structure. The random sampling method shows the lowest normalized RMS errors on the electrical power (Table 8.2). It also slightly outperforms the stratified sampling method by its ability to adapt the number of models according to the diversity inherent to the cluster of buildings. However, as the number of buildings increases, so do the diversity of DHW demand profiles and the number of models required to capture it.

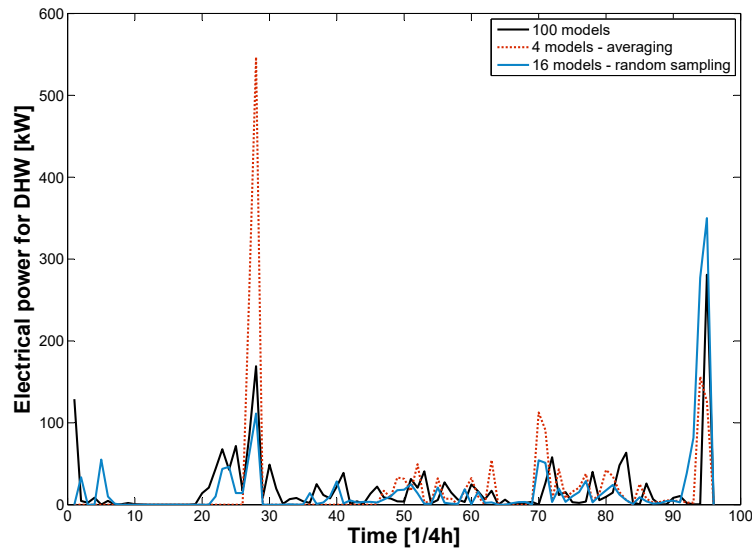


Figure 8.8 – Illustration of the averaging and random sampling aggregation techniques for DHW needs for one hundred buildings.

Table 8.2 – Illustration of aggregation methods for both SH and DHW needs. Comparison of stratified and random sampling methods for 100, 300 and 500 buildings.

Sampling		100 buildings	300 buildings	500 buildings
Stratified	Number of models	20	20	20
	NRMSE on \hat{P}_t	24.0%	23.8%	24.1%
Random	Number of models	17	20	20
	NRMSE on \hat{P}_t	22.0%	21.5%	23.2%

8.2.5 Generation of test-cases

For the large-scale assessment of the flexibility of heat pumps studied in the following sections, 40000 different buildings are considered. They are characterized by one type of building geometry, corresponding to the freestanding house presented in Section 3.1 with two different insulation levels, namely K30 and K45. The share of K30 and K45-level buildings is set to 25% and 75%, respectively.

40000 different daily appliances and lighting profiles are generated from the database presented in Chapter 2. Heating set point profiles are generated following the method proposed in Section 8.2.1.1. For each house, a random number of occupant is drawn from a normal distribution with an average of 3 occupants and a standard deviation of 2 occupants. For the DHW demand profiles, 100 typical profiles are available from the database presented in Chapter 2. A combination of those profiles is drawn randomly, according to the number of occupants. The water storage tank is sized to cover 50 liters of water per occupant, with an additional reserve volume of 50 liter, as explained in Chapter 6.

All buildings are equipped with air-to-water heat pumps used for both space-heating and DHW production. All heat emission systems are assumed to be conventional radiators.

8.3 Assessment of the impact of flexible heat pumps on day-ahead market prices

As shown in Chapter 4, the flexibility of heat pumps can be used to minimize electricity procurement costs of electricity retailers on the day-ahead market. In that chapter, such flexible units were not considered influential enough to affect market clearing prices and were thus modeled as *price-taker*. If this assumption is certainly verified at the scale of one single heat pump or even a few hundred heat pumps, *is it still valid for large penetration rates of flexible units?*

As pointed out by Papadaskalopoulos and Strbac (2013), the large-scale application of decentralized control schemes based on dynamic pricing may not optimally unlock demand flexibility and yield to concentrated power demand during low price periods. To cope with that, they propose a new day-ahead market mechanism that combines both a centralized market clearing optimization problem and a decentralized price-based approach. The method is based on the Lagrangian relaxation principle. It allows the decoupling of the optimization problem into sub-problems for each demand-side participant, hereby not requiring them to disclose their individual properties to the system operator. The method was applied to the participation of electric vehicles and heat pump systems in the UK context in a companion paper (Papadaskalopoulos et al. (2013)). In terms of modeling, demand-side models of buildings relied on the definition of typical building typologies distributed over the country, each of them being modeled separately. For the supply-side, a simplified representation based on linear marginal cost curves was used. For the considered case-study, with 30% penetration rates of heat pumps and electric vehicles, generation costs reduction reached up to 8%.

In light of this, the purpose of this section is to study the potential impact of large sets of flexible heat pumps on day-ahead market clearing prices in current and future energy contexts in a case-study applied to Belgium. To that end, the clustering method proposed in Section 8.2 is combined to a centralized optimization problem detailed hereafter. As opposed to the approach proposed by Papadaskalopoulos and Strbac (2013), the centralized optimization problem requires the full knowledge of all participants' properties by the system operator.

8.3.1 Day-ahead market clearing

8.3.1.1 Principle

Under the assumptions of

- a perfectly competitive market,
- with no market coupling,
- and no network constraints,

the day-ahead market clearing mechanism can be modeled by a merit order ranking problem of supply and demand electricity curves. Merit order ranking consists in aggregating supply ("sell") and demand ("buy") curves in increasing and decreasing price orders, respectively. The market clearing price is at the intersection of both curves, as illustrated in Figure 8.9. Market clearing is performed on an hourly basis for the day-ahead electricity market.

8.3. Assessment of the impact of flexible heat pumps on day-ahead market prices

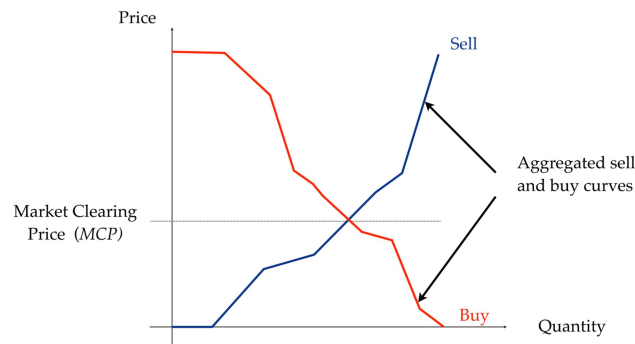
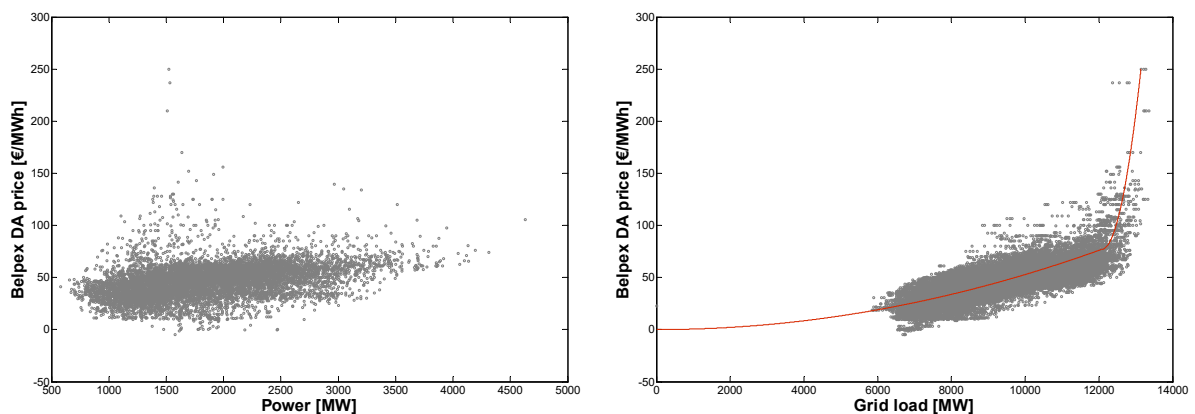


Figure 8.9 – Illustration of merit order principle for day-ahead market clearing mechanism (source: Cornélusse and Ernst (2014)).

8.3.1.2 The Belgian Day-Ahead Market

In Belgium, only 25 to 30 percent of the total electricity consumption is traded on the day-ahead market. As an example, hourly clearing prices are illustrated as a function of the amount of power traded in Figure 8.10a for year 2012. In general, clearing prices tend to increase with the amount of power traded. However, peak prices also arise for power exchange levels less than the maximum value, such that no strong correlation can be determined. These peak prices often correspond to peak power consumption periods in the winter.

Despite the small share of total power traded on the day-ahead market, there is a good correlation between day-ahead spot market prices and total grid load. A correlation curve is illustrated in red in Figure 8.10b for quarter-hourly power data. This correlation curve can be related to the merit order ranking of production plants in Belgium. In this approach, power plants are ranked by increasing production marginal costs. This is shown in Figure 8.11, in the case of low and high penetration of renewable energy sources.



(a) Market clearing price as a function of traded power.

(b) Market clearing price as a function of total grid load.

Figure 8.10 – Day-ahead market prices for year 2012 in Belgium.

A piece-wise linear interpolation of the market prices with respect to the total grid load, \hat{P} , is performed,

8.3. Assessment of the impact of flexible heat pumps on day-ahead market prices

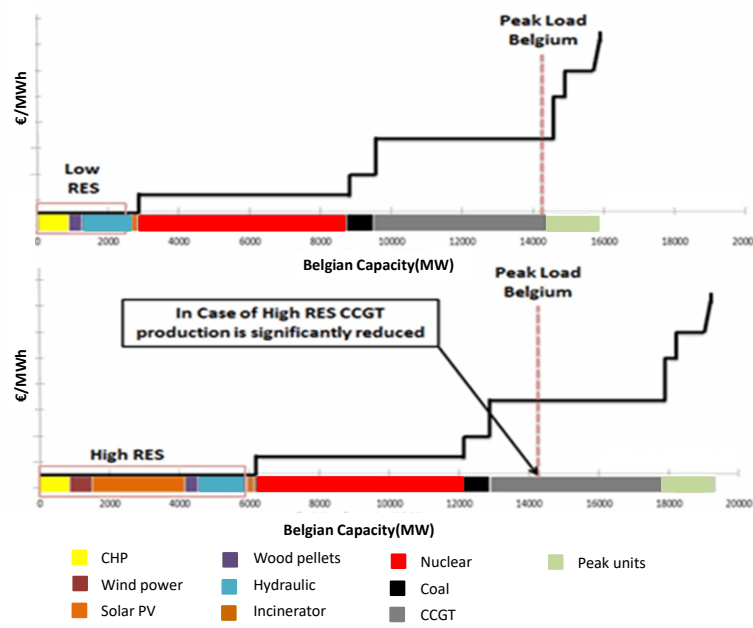


Figure 8.11 – Merit order ranking of power plants in Belgium (modified from Sia Partner (2013)).

based on data for year 2012, as follows:

$$\pi_t^{DA}(\hat{P}) = \begin{cases} 0 & \text{if } 0 \leq \hat{P} \leq P^R \\ 0.0030(\hat{P} - P^R) & \text{if } P^R \leq \hat{P} \leq P^R + P^{m,1} \\ \pi_t^{DA}(P^R + P^{m,1}) + 0.0084(\hat{P} - P^R - P^{m,1}) & \text{if } P^R + P^{m,1} \leq \hat{P} \leq P^R + P^{m,1+2} \\ \pi_t^{DA}(P^R + P^{m,1+2}) + 0.17(\hat{P} - P^R - P^{m,1+2}) & \text{if } \hat{P} > P^R + P^{m,1+2} \end{cases} \quad (8.9)$$

where

- P^R represents additional renewable energy sources that could arise in prospective scenarios, and is equal to zero in 2012.
- the 2012 production mix is divided in three categories: the first and second categories gather existing renewable sources and conventional plants, such as nuclear and CCGT plants. Their upper production limits are $P^{m,1} = 6000\text{MW}$ and $P^{m,2} = 6080\text{MW}$, respectively. Their sum is denoted by $P^{m,1+2}$. The third category gathers fast-response units used to cover peak load.
- it is assumed that power production levels of conventional plants can be continuously adjusted between 0 and $P^R + P^{m,1} + P^{m,2}$ (or $P^R + P^{m,1+2}$).

This simplified merit-order ranking is used in the following sections to model supply side bid curves in the day-ahead market context.

8.3.2 Optimization problem for the participation of heat pump aggregators in the day-ahead market

The optimization problem solved to assess the influence of flexible residential heat pumps on day-ahead market prices relies on the following assumptions:

8.3. Assessment of the impact of flexible heat pumps on day-ahead market prices

- 100% of the total grid load is traded on the day-ahead market,
- supply-side bid curves are modeled by Equation (8.9),
- heat pump load aggregators postulate that they can influence market prices by minimizing their procurement costs,

The objective function is given by

$$\min \sum_{t \in \mathcal{H}} \left(\hat{P}_t^0 + \sum_{i=1}^{n_C} (\hat{P}_{i,t} \alpha_i) \right) \pi_t^{DA} dt \quad (8.10a)$$

where

$$\pi_t^{DA} = C_{RES} \hat{P}_t^R + C_{m,1} \hat{P}_t^{m,1} + C_{m,2} \hat{P}_t^{m,2} + C_{peak} \hat{P}_t^{peak} \quad (8.10b)$$

subject to, $\forall i \in \{1, \dots, n_C\}, \forall t \in \mathcal{H}$,

$$\hat{\mathbf{x}}_{i,t+1} = f(\hat{\mathbf{x}}_{i,t}, \hat{W}_{i,t}^s, \hat{W}_{i,t}^w, \mathbf{u}_t) \quad (8.10c)$$

$$\hat{P}_{i,t} = \hat{W}_{i,t}^s + \hat{W}_{i,t}^w + \Gamma_{i,t} \quad (8.10d)$$

$$\mathbf{x}_{i,t}^{min} \leq \hat{\mathbf{x}}_{i,t} \leq \mathbf{x}_{i,t}^{max} \quad (8.10e)$$

$$0 \leq \hat{W}_{i,t}^s \leq \hat{y}_{i,t} \hat{W}_{i,t}^{s,max} \quad (8.10f)$$

$$0 \leq \hat{W}_{i,t}^w \leq (1 - \hat{y}_{i,t}) \hat{W}_{i,t}^{w,max} \quad (8.10g)$$

$$0 \leq \hat{y}_{i,t} \leq 1 \quad (8.10h)$$

and, $\forall t \in \mathcal{H}$, to

$$\hat{P}_t^0 + \sum_{i=1}^{n_C} (\hat{P}_{i,t} \alpha_i) = \hat{P}_t^R + \hat{P}_t^{m,1} + \hat{P}_t^{m,2} + \hat{P}_t^{peak} \quad (8.10i)$$

$$0 \leq \hat{P}_t^R \leq P_t^R \quad (8.10j)$$

$$0 \leq \hat{P}_t^{m,1} \leq P^{m,1} \quad (8.10k)$$

$$0 \leq \hat{P}_t^{m,2} \leq P^{m,2} \quad (8.10l)$$

$$\hat{P}_t^{peak} \geq 0 \quad (8.10m)$$

\mathcal{H} is the optimization horizon composed of H periods. \hat{P}^0 represents the total electrical power consumed by all the consumers connected to the grid other than houses equipped with heat pumps. Houses equipped with heat pumps are aggregated in n_C clusters according to the method proposed in Section 8.2, and α_i is the number of houses aggregated in each cluster i . The amount of power bought per average house of each cluster i in period t , $\hat{P}_{i,t}$ at the day-ahead market price π_t^{DA} , is defined in Equation (8.10d) as the sum of the heat pump consumption for space heating, $\hat{W}_{i,t}^s$, or domestic hot water heating, $\hat{W}_{i,t}^w$, and of the exogenous consumption, $\Gamma_{i,t}$. Variable $\hat{y}_{i,t}$, models the fact that the heat pump can be used to supply both DHW and space heating. It is equal to one if all heat pumps in a cluster are used for space heating and equal to zero if they all produce domestic hot water.

The spot market price π_t^{DA} , given by Equation (8.10b), is a piecewise linear function of the electricity consumption based on a merit-order ranking of the available production plants (Equation (8.10i)).

Constraints (8.10j) to (8.10m) express the production capacity of each plant in period t .

8.3.3 Case-studies in the Belgian context

The 40000 houses equipped with heat pumps presented in Section 8.2.5 are used to assess the impact of large penetration rates of heat pumps on clearing market prices. The diversity of their electricity demand profiles is assumed sufficient to represent different penetration rates of heat pumps, ranging from 10000 to one million. This assumption is verified in terms of the diversity of heating set-point and domestic hot water demand profiles. However, it does not accurately represent the diversity in terms of house geometries and insulation levels that arises as the number of heat pumps increases.

8.3.3.1 2012 Belgian context

In a first case-study, the electricity production mix of year 2012 is considered. The extra peak electricity consumption entailed by large penetration of heat pumps is met by additional fast-moving units, and it is assumed that this does not entail any extra investment. For each penetration rate of heat pumps, two scenarios are compared:

- a conservative scenario in which heat pump owners minimize their energy consumption ("no flex"),
- a flexible scenario ("flex") in which the flexibility of heat pumps is activated to minimize Equation 8.10a.

These scenarios are implemented for the cold season, from November through March. Resulting day-ahead market clearing prices are provided in Figure 8.12. In both cases, the use of less than one hundred thousand heat pumps has a negligible impact on the prices. For five hundred thousand heat pumps, a scenario with no activation of the flexibility results in an increased use of fast-moving units from 6.2% to 18.8% of the time. Activating the flexibility allows to limit this increase to 9.2% of the time and reduces average market prices by 11.7%. With one million heat pumps, the activation of flexibility reduces the use of peak production units by 17.1% compared to no flexibility. Average market prices are reduced by 16.5%.

Therefore, for an electricity production mix mainly composed of conventional CCGT and nuclear plants, it requires more than five hundred thousand flexible heat pumps to start influencing day-ahead clearing prices significantly. This corresponds to a penetration rate of heat pumps in the residential building stock greater than 10%. In 2012, the number of operating heat pumps in Belgium, including both office and residential buildings, reached about 16600 units only (Eurobserv'er (2013)). In that context, a price-taker assumption is therefore reasonable.

However, at the European scale, the number of operating units in 2012 was about 20.5 millions¹. As the percentage of renewable energy sources increases and electricity grids become more and more interconnected, the price-taker assumption may not be valid any longer.

¹This includes 15 million reversible units for both cooling and heating in Italy.

8.3. Assessment of the impact of flexible heat pumps on day-ahead market prices

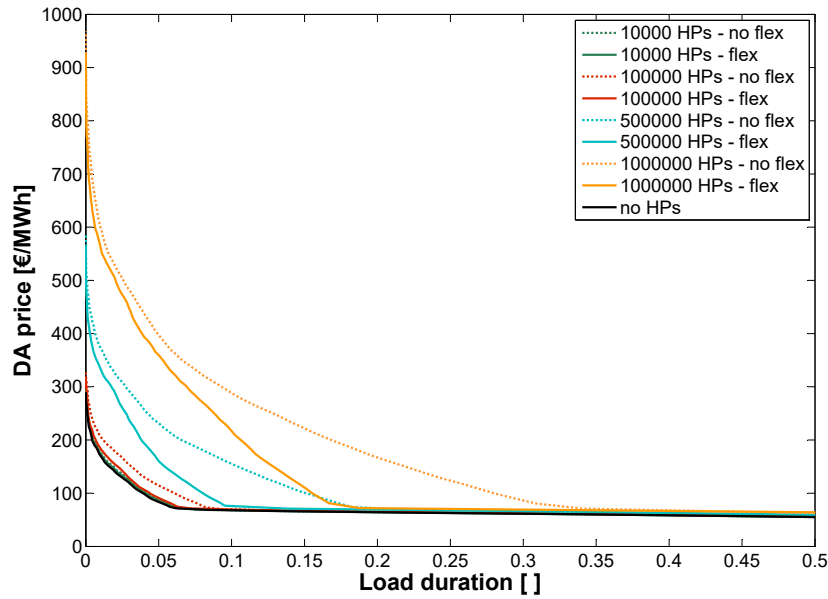


Figure 8.12 – Evolution of day-ahead market prices with high penetration of heat pumps. Comparison of scenarios with flexible heat pumps ("flex") and without activation of the flexibility of heat pumps ("no flex").

8.3.3.2 Increased share of renewable energy sources

In this second case-study, the electricity production mix is assumed to be composed of

- 35%² renewable energy sources composed of 30% PV panels and 70% wind turbines. Their marginal cost is set to zero. Historical data for Belgium in 2012 are used for the electricity generation by wind turbines, whereas the corresponding predictions are used for the solar PV generation (Elia (2012b)). All data are scaled up to reach a total of 35% penetration rate according to the following procedure.

The total annual electricity use, E_{tot} , depends on the number of heat pumps, n_{HP} , and is given by

$$E_{tot} = E_{tot}^{2012} + n_{HP}E_{HP} \quad (8.11)$$

where E_{HP} is the annual electricity use per house equipped with an air-to-water heat pump used for both space-heating and DHW production and approximated by the value obtained for a K45 building in Chapter 4. The share of the total electricity use covered by a given penetration rate of renewable sources, x_{RES} , is equal to

$$E_{RES} = x_{RES}E_{tot} \quad (8.12)$$

The share covered by each type of renewable energy source is then given by their respective

²corresponding approximately to the capacity factors for wind and solar PV.

8.3. Assessment of the impact of flexible heat pumps on day-ahead market prices

penetration rates:

$$E_{PV} = x_{PV} E_{RES} \quad (8.13)$$

and

$$E_{wind} = x_{wind} E_{RES} \quad (8.14)$$

The installed capacity, $ICap$, is determined from that of year 2012, according to the corresponding 2012 annual electricity generation, as follows:

$$ICap_{PV} = \frac{E_{PV}}{E_{PV}^{2012}} ICap_{PV}^{2012} \quad (8.15)$$

and

$$ICap_{wind} = \frac{E_{wind}}{E_{wind}^{2012}} ICap_{wind}^{2012} \quad (8.16)$$

2012 quarter-hourly generation profiles are then adjusted with these new installed capacities.

- 65% conventional plants: their marginal cost is kept identical to 2012. It is assumed that power production levels can be adjusted continuously. In practice, large amounts of renewable energy sources may prevent conventional base-load generation units from being used, and this assumption can no longer be fulfilled. However, this phenomenon cannot be captured by the simplified market model proposed here.
- A safety coefficient of 1.2 is added to the installed capacity of conventional plants.
- Peak time units: their marginal cost is kept identical to that of 2012.

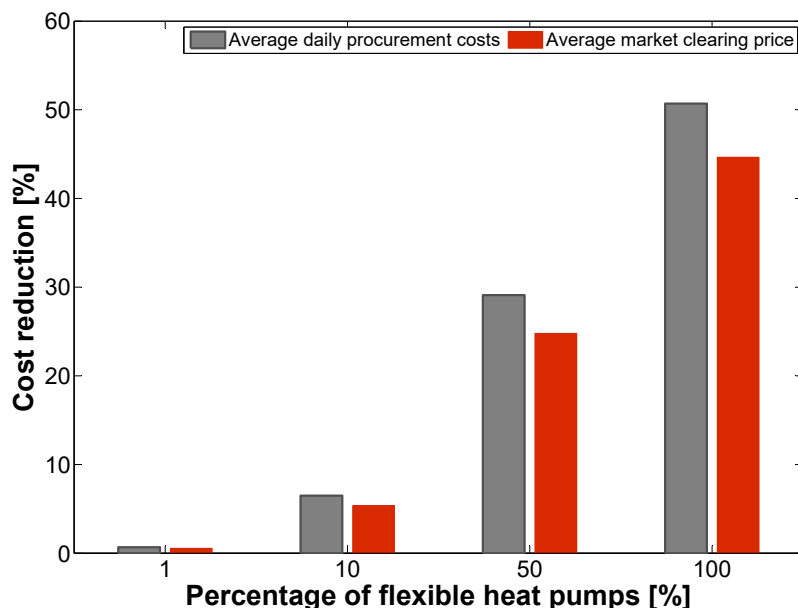


Figure 8.13 – Evolution of average market clearing prices and daily procurement costs with the percentage of flexible units for a prospective scenario with 35% renewable energy sources.

8.4. Application of load aggregation to the provision of ancillary services

The penetration rate of heat pumps in the residential building stock is set to 20%, which corresponds to around one million units. Among those heat pumps, the percentage of flexible systems is varied from 1 to 100%. The impact on DA market clearing prices is illustrated in Figure 8.13. Average clearing price reductions of 0.5 to 44.1% are obtained. In terms of average daily procurement costs, reductions of up to 51% are reached. Therefore, in future scenarios, the impact of the flexibility of heat pumps on day-ahead market clearing prices should be modeled. The price-taker assumption is no longer valid.

8.4 Application of load aggregation to the provision of ancillary services

8.4.1 Reserve mechanisms

To ensure grid balance and security of supply, different balancing mechanisms have been established by Transmission System Operators (TSOs). Power reserves are part of these mechanisms. In Europe, one distinguishes four types of power reserves (ENTSO-E (2015)):

- Frequency Containment Reserve (FCR) – also known as primary (or spinning) reserve: an automatic and decentralized mechanism that must be made fully available within 30 seconds. It is often constituted of power generators already operating. Its aim is to maintain balance within the high-voltage European interconnected system and prevent the frequency from further deviating from its nominal value.
- Frequency Restoration Reserves (FRR): one distinguishes the automatic (aFRR – also known as secondary reserve) and manual (mFRR – also known as tertiary reserve) Frequency Restoration Reserves. The capacities of secondary reserves must be made fully available within 30 seconds and be provided for 15 minutes. For tertiary reserves, they must be made available after 15 minutes, for an undetermined amount of time. Such reserves are used to solve regional imbalance and restore frequency.
- Replacement Reserves (RR) constitute slower power reserves activated manually after 15 minutes, and used to replace FRR for long term elimination of system imbalance.

In the frame of the secondary reserve, the amount of power that must be acquired on a yearly basis is determined by TSOs. In Belgium, the TSO distinguishes two actions within the provision of secondary reserves (Elia (2016)): *reservation* and *activation*. The reservation consists in contracting the defined amount of reserve from different providers. Reserve providers inform the TSO of the amount of reserve they can provide on a quarter-hourly basis, along with the opportunity costs associated to this reservation. Indeed, such power reservation prevents the use of those assets in other market segments. One day ahead, all parties enrolled in the provision of secondary reserve can offer an extra volume of reserve for the next day. In real-time, if needed, the reserve is activated by the TSO. To select the activated units, the TSO sorts the offers according to their activation prices until the contracted capacity is reached. Offers are sorted by ascending order in the case of an increase in electricity production, and descending order in the case of a diminution of electricity production. The remuneration is then performed according to a "pay as bid" approach. This principle of remuneration for the activation may no longer apply in the case of demand-side management. However, the definition of a new remuneration framework for the activation of power reserve goes beyond the scope of this work. In the following, only the problem of power reservation is considered.

8.4. Application of load aggregation to the provision of ancillary services

For year 2012, in Belgium, the contracted amount of reserve was imposed to 140 MW for both upward and downward capacities. The remuneration for the reservation was set to 32 €/MW/h.

8.4.2 Demand-side provision of reserve

Several studies focus on the use of demand response for ancillary services, and in particular, for the provision of reserve (Heffner (2008), Ma et al. (2013) and Mathieu et al. (2014)). As opposed to commercial and industrial consumers, residential demand response is not yet implemented in this context, but offers a promising potential through direct load control by third-party aggregator (O'Dwyer et al. (2012)). For example, the work of Zapata Riveros (2015) investigated the flexibility potential of residential micro-CHPs for grid balancing (self-balancing, passive balancing and bidding mechanisms). In particular, micro-CHPs were coupled to district heating networks to compensate uncertainties on renewable energy generation through stochastic programming techniques. The rescheduling was performed one day-ahead or in real-time, depending on the available generation forecast update and system imbalance data. It was shown that the micro-CHP units can provide flexibility services to the electricity system, but only moderate economic benefits were obtained.

Given their fast dynamics, heat pumps, provided that they are equipped with suitable communication devices, are well-suited to provide aFRR. However, as emphasized by ENTSO-E (2015), the rebound effect (see Chapter 6) that follows the activation of power modulations should be specified, if not fully mitigated. The available literature regarding the use of heat pumps for the provision of reserve is limited (Fischer and Madani (2017)) and based on demand-side models with little level of details. In light of the above, this section investigates the problem of power reservation with residential heat pumps, with a focus on the determination of reservation costs for future integration in the reserve market.

8.4.3 Optimization problem for the provision of reserve

The amount of reserve that can be provided by a set of heat pumps can be determined by an optimization problem. The objective is to unlock the flexibility offered by heat pumps to reduce electricity procurement costs in the day-ahead electricity market, while ensuring the provision of a contracted amount of reserve for real-time grid management. The optimization problem determines both the optimal electricity demand profile to be bought by load aggregators on the day-ahead market, referred to as the baseline consumption \hat{P}_t , and the costs associated to the reservation of given upward (R^+) or downward (R^-) capacities. In the following, as for Chapter 6, upward reserve refers to an increase of consumption, while downward reserve refers to a decrease (demand-side perspective). It is worthwhile to note that this definition is opposite to the traditional definition of upward and downward reserves from a power system perspective.

The reservation of upward power is illustrated in Figure 8.14. At each time period τ , a defined amount R^+ of power is reserved for one time period. If activated, the payback period is constrained over k periods. During the payback period, no further activation of reserve is allowed.

8.4. Application of load aggregation to the provision of ancillary services

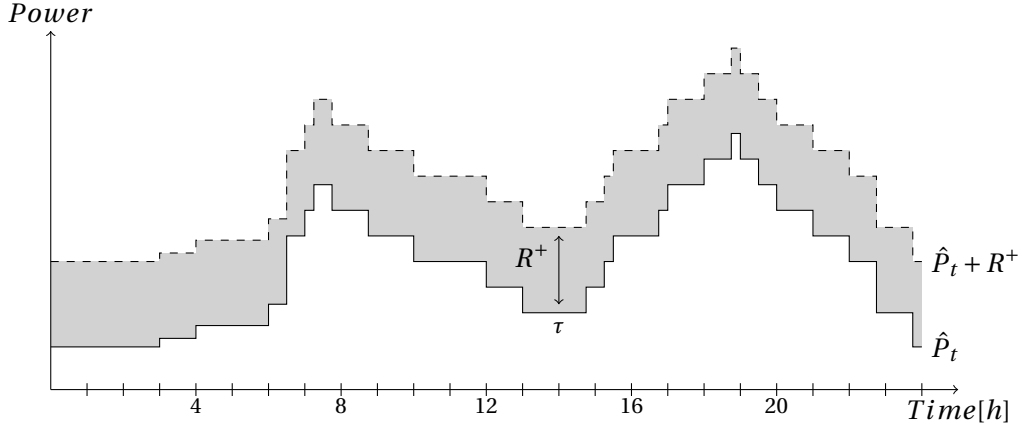


Figure 8.14 – Example provision of upward reserve (R^+).

For the allocation of upward reserve, the optimization problem can be formulated as

$$\min \sum_{t \in \mathcal{H}} \sum_{i=1}^{n_C} (\hat{P}_{i,t} \alpha_i) \pi_t^{DA} dt + \beta \sum_{\tau \in \mathcal{M}} \lambda_\tau \quad (8.17a)$$

subject to, $\forall i \in \{1, \dots, n_C\}, \forall t \in \mathcal{H}$,

$$\hat{\mathbf{x}}_{i,t+1} = f(\hat{\mathbf{x}}_{i,t}, \hat{W}_{i,t}^s, \hat{W}_{i,t}^w, \mathbf{u}_t) \quad (8.17b)$$

$$\hat{P}_{i,t} = \hat{W}_{i,t}^s + \hat{W}_{i,t}^w + \Gamma_{i,t} \quad (8.17c)$$

$$\mathbf{x}_{i,t}^{min} \leq \hat{\mathbf{x}}_{i,t} \leq \mathbf{x}_{i,t}^{max} \quad (8.17d)$$

$$0 \leq \hat{W}_{i,t}^s \leq \hat{y}_{i,t} \hat{W}_{i,t}^{s,max} \quad (8.17e)$$

$$0 \leq \hat{W}_{i,t}^w \leq (1 - \hat{y}_{i,t}) \hat{W}_{i,t}^{w,max} \quad (8.17f)$$

$$0 \leq \hat{y}_{i,t} \leq 1 \quad (8.17g)$$

and, $\forall i \in \{1, \dots, n_C\}, \forall \tau \in \mathcal{M}, \forall t^* \in \{0, \dots, k\}$, to

$$\mathbf{x}_{i,\tau,0} = \hat{\mathbf{x}}_{i,\tau} \quad (8.17h)$$

$$P_{i,\tau,t^*} = \hat{P}_{i,\tau+t^*} + \delta_{i,\tau,t^*} \quad (8.17i)$$

$$P_{i,\tau,t^*} = \hat{W}_{i,\tau,t^*}^s + \hat{W}_{i,\tau,t^*}^w + \Gamma_{i,\tau+t^*} \quad (8.17j)$$

$$\mathbf{x}_{i,\tau,t^*+1} = f(\mathbf{x}_{i,\tau,t^*}, \hat{W}_{i,\tau,t^*}^s, \hat{W}_{i,\tau,t^*}^w, \mathbf{u}_{\tau+t^*}) \quad (8.17k)$$

$$\mathbf{x}_{i,\tau+t^*}^{min} \leq \mathbf{x}_{i,\tau,t^*} \leq \mathbf{x}_{i,\tau+t^*}^{max} \quad (8.17l)$$

$$0 \leq \hat{W}_{i,\tau,t^*}^s \leq y_{i,\tau,t^*} \hat{W}_{i,\tau+t^*}^{s,max} \quad (8.17m)$$

$$0 \leq \hat{W}_{i,\tau,t^*}^w \leq (1 - y_{i,\tau,t^*}) \hat{W}_{i,\tau+t^*}^{w,max} \quad (8.17n)$$

$$0 \leq y_{i,\tau,t^*} \leq 1 \quad (8.17o)$$

$$\sum_{i=1}^{n_C} (\delta_{i,\tau,0} \alpha_i) \geq R^+ (1 - \lambda_\tau) \quad (8.17p)$$

$$-\sigma \leq \hat{\mathbf{x}}_{i,\tau+k+1} - \mathbf{x}_{i,\tau,k+1} \leq \sigma \quad (8.17q)$$

8.4. Application of load aggregation to the provision of ancillary services

Equations (8.17b) to (8.17g) are identical to Equations (8.10c) to (8.10h) in Section 8.3.2. The reserve service horizon is composed of one period of upward modulation in time period τ followed by k payback periods to allow the system to return to its baseline. Equation (8.17h) imposes the initial conditions of state variables. Equation (8.17i) defines the amount of reserve that can be provided with respect to the baseline consumption profile. For all periods in \mathcal{M} , the contracted amount of reserve is imposed by Constraint (8.17p). Beyond a certain value, the same amount of reserve may not be achievable for all periods of the day. Variables λ_τ serve the purpose of relaxing these constraints for such periods. In practice, load aggregators would not contract such amounts of reserve, but this allows to determine the maximum values that can be achieved. Finally, inequality (8.17q) ensures that the state at the end of the payback period is close enough to the one given by the baseline.

The cost entailed by the reservation of a contracted amount of power is given by the shadow price³ of Constraints (8.17p) (Ilak et al. (2014)).

The case of downward reserve is obtained by replacing Constraint (8.17p) by

$$\sum_{i=1}^{n_C} (\delta_{i,\tau,0} \alpha_i) \leq R^- (1 - \lambda_\tau) \quad (8.18)$$

The heat pump COP is expressed as a function of the ambient temperature and of the water supply temperature. However, for these problems to remain linear, water supply temperatures are set by the heating curve in space-heating mode, and approximated by an average water temperature in DHW mode, as discussed in Section 3.3.4. The influence of part-load conditions on heat pump performance is not modeled.

8.4.4 Illustration on a single house

The modification in baseline consumption entailed by power reservation is illustrated in Figure 8.15 for an example house. The payback period is set to 10 periods of 15 minutes. In this example, a minimum upward power reservation of 2000 W is contracted for all periods of the day. Due to the time varying electricity tariff, the baseline consumption profile without power reservation ($R^+ = 0$) increases during periods 25 to 30. To be able to provide upward reserve in those periods, the baseline consumption profile is modified ($R^+ > 0$) and increases in time periods 20 to 25. This modification in baseline profile yields a suboptimal control in terms of electricity costs. The latter increase by 0.5% in this case.

The imposed payback period also modifies the baseline consumption profile. This is illustrated in Figure 8.16 for the same case-study house. For this example, a power reservation of 2.75 kW is contracted in period 6. In the case of an activation of the power reserved, temperature levels increase in both the water tank and in the house. Due to the thermal inertia of those systems, the imposed payback period may not be long enough to return to the baseline state ($R^+ = 0$). This causes the baseline consumption profile with power reservation ($R^+ > 0$) to increase at the end of the payback horizon, i.e. in time period 16. However, as the duration of the payback period increases, this effect is less marked.

³The shadow price, or dual price, is a measure of the improvement in the objective function if the constraint is relaxed by one unit. A recall on duality in linear programming is available in Annex A.6

8.4. Application of load aggregation to the provision of ancillary services

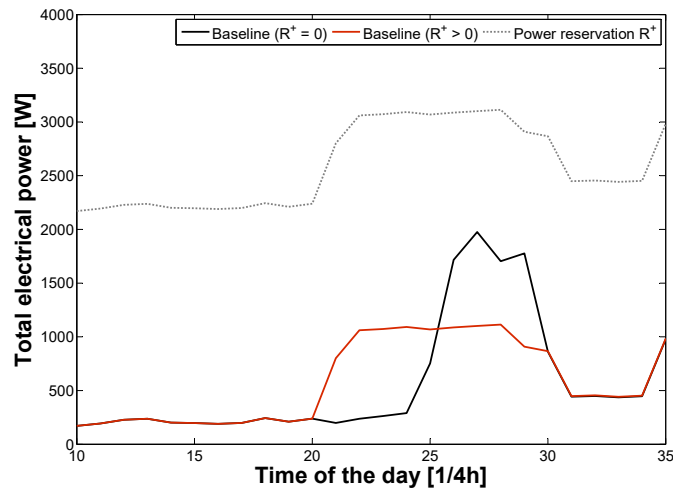


Figure 8.15 – Illustration of the influence of power reservation on baseline consumption profile.

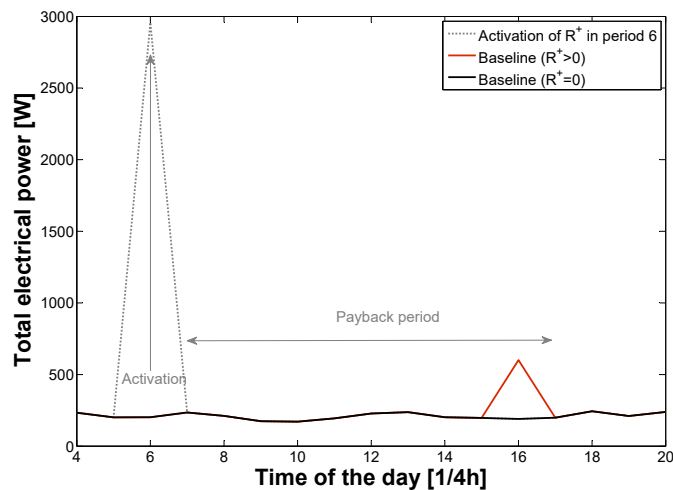


Figure 8.16 – Illustration of the influence of a fixed payback period on baseline consumption profile.

8.4.5 Application in the Belgian context

First, optimization problem (8.17) is solved for a flat day-ahead market price. The provision of upward and downward reserves are considered separately in order to quantify reservation costs and identify the bases which make them non zero. The same optimization problems are then solved with the set of 40000 houses described in Section 8.2.5 and with historical data for year 2012. Resulting costs and amounts of reserve are compared against historical data. Simulations are performed with a 15-minutes decision time step. Based on the conclusions drawn in Chapter 6, the pay-back period k should be greater than one hour, in order to limit its effect on the achievable modulation potential.

8.4.5.1 Reservation costs basis

The purpose of this section is to understand and identify the parameters of influence that impact the reservation costs resulting from optimization problems (8.17). Both upward and downward power reservations are considered. For the purpose of this analysis, the number of parameters of influence is

8.4. Application of load aggregation to the provision of ancillary services

limited by the following simplifications:

- 40000 houses are considered. House geometries and characteristics of the building envelope are those of the K45 house (Section 3.1). They differ by heating set point profiles and lighting and appliances consumption profiles.
- a number of 3 inhabitants per house is considered,
- the payback is arbitrarily set to 10 periods, i.e. 2.5 hours,
- the day-ahead market price is set to a constant value of 47€/MWh, corresponding to the average value for year 2012,
- the ambient temperature is kept constant and equal to 3°C,
- minimum and maximum temperature set points differ in each house but are kept constant throughout the day.

To initialize the state-space variables of the model, simulations are performed over two days with a room temperature imposed to the lower set point and a medium tank temperature of 57.5°C. The optimization problem is then solved over two identical consecutive days. Control (\mathcal{M}) and prediction (\mathcal{H}) horizons are set to $96 + k$ and 144 periods of 15 minutes, respectively. Results for the second optimization day are presented hereafter.

Upward reserve

For the provision of upward reserve, the amount of power reserved is varied between 0 and 135 MW. The maximum amount of reserve that can be provided uniformly for all periods of the day is 131 MW. Beyond that value, it is not possible to guarantee the same amount of reserve for each period of the day. The reservation of up to 100 MW can be achieved at zero marginal cost. For greater amounts of reserve, reservation costs increase, as illustrated in Figure 8.17. This increase is due to both the imposed payback period and the limited heat pump capacities. Indeed, imposing the payback period forces the system to return to its baseline state, as explained in Chapter 6. As the amount of power reserved increases, thermal inertia of systems maintains higher temperature levels. This causes the baseline consumption to increase, in order to comply with the fixed payback constraint. Increase in baseline consumption with the amount of reserve is illustrated in Figure 8.18. It reaches up to 2.2%.

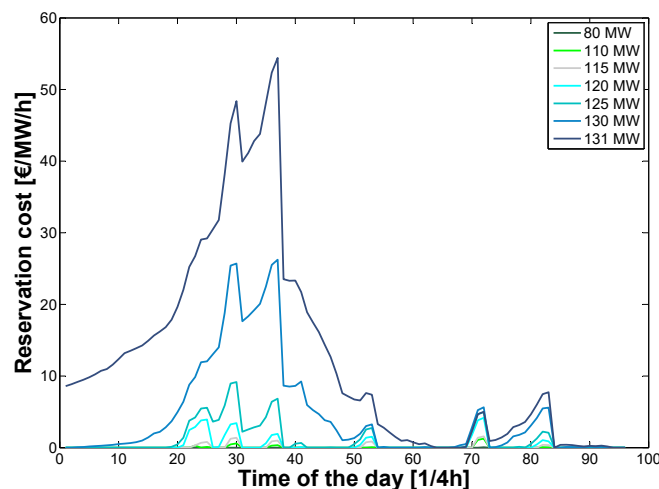


Figure 8.17 – Evolution of the price of reserve with the amount of upward power reserved for each period of the day.

8.4. Application of load aggregation to the provision of ancillary services

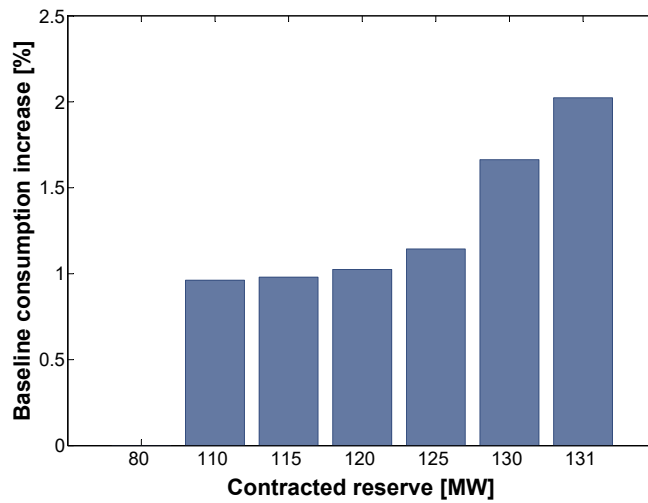
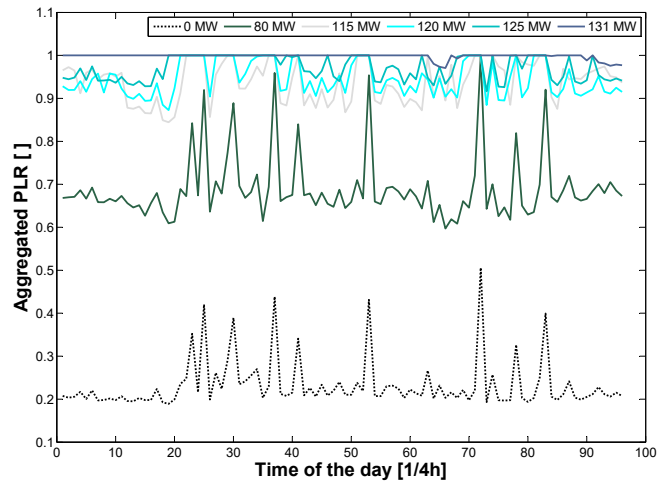
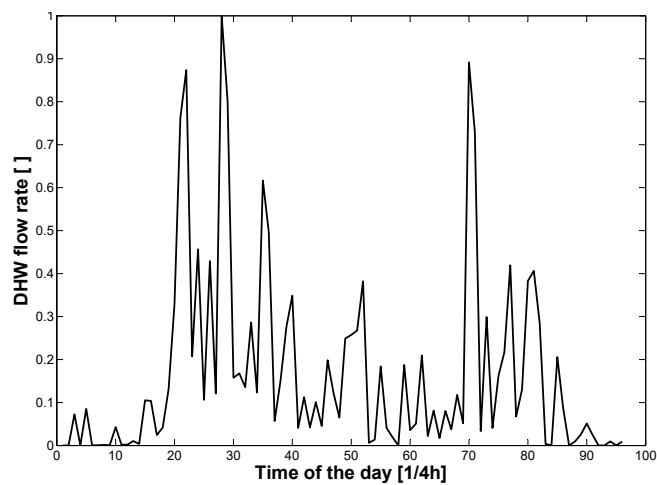


Figure 8.18 – Daily baseline consumption increase with the amount of contracted upward reserve.



(a) Heat pump part-load ratio for different amounts of activated reserve.



(b) Normalize aggregated daily DHW flow rate.

Figure 8.19 – Parameters of influence of reservation costs: heat pump capacity and DHW demand.

8.4. Application of load aggregation to the provision of ancillary services

The limitation of installed heat pump capacities partly explains the shape of the price profiles. For a given power reserved, the average heat pump part-load ratio over the aggregated set of 40000 units, PLR^{agg} is given by

$$PLR_t^{agg} = \frac{\sum_{i=1}^{n_c} (\dot{Q}_{i,t}^s + \dot{Q}_{i,t}^w) \alpha_i}{\sum_{i=1}^{n_c} (y_{i,t} \dot{Q}_{i,t}^{s,max} + (1 - y_{i,t}) \dot{Q}_{i,t}^{w,max}) \alpha_i} \quad (8.19)$$

Evolution of average heat pump part-load ratio with contracted reserve is illustrated in Figure 8.19a. When compared to Figure 8.17, it can be seen that reservation cost profiles present peaks when average heat pump consumption reaches full-load capacity. Such steep increases in heat pump consumption usually follow large domestic hot water demands (Figure 8.19b). For example, in time periods 30, 37, 53 and 72, the baseline consumption is greater than for the other periods of the day, even when no reserve is allocated. It should be noted that, despite the 40000 houses considered, the aggregated DHW demand profile obtained is not smooth. This is due to the reduced number of typical profiles available, and to the choice of 3 occupants in all houses.

Finally, neither the imposed payback period, nor the heat pump capacities explain the fact that reservation costs decrease with the time period of the day. This is due to the finite-horizon control scheme.

Downward reserve

For the provision of downward reserve, the amount of power reserved is varied between 0 and 50 MW. Reservation costs are illustrated in Figure 8.20. As opposed to the provision of upward reserve, it is impossible to reserve any downward capacity at zero marginal cost for all periods of the day. This results directly from the use of a flat day-ahead market price. Indeed, in this case, in order to minimize the baseline consumption cost if no capacity is reserved, the optimizer drives all temperatures towards their lower bounds. The reservation of any unit of downward capacity therefore requires higher temperature levels in the different storages, which increases the total consumption.

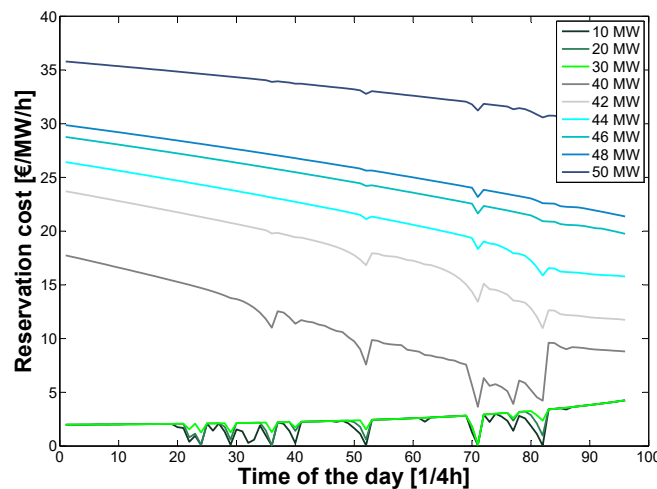


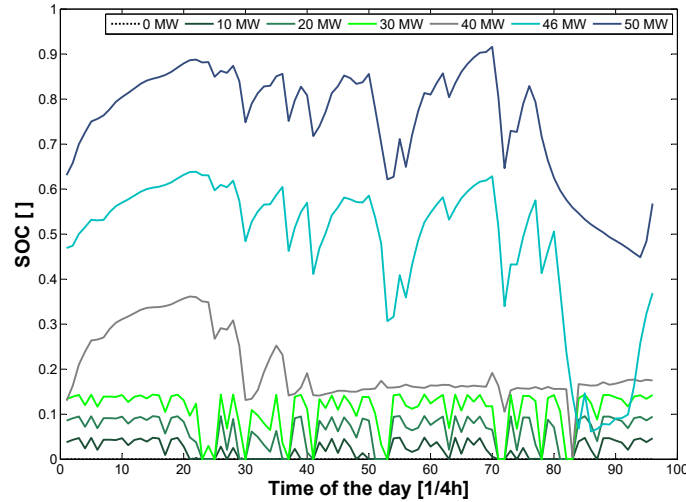
Figure 8.20 – Evolution of reservation costs with the amount of downward power reserve contracted.

8.4. Application of load aggregation to the provision of ancillary services

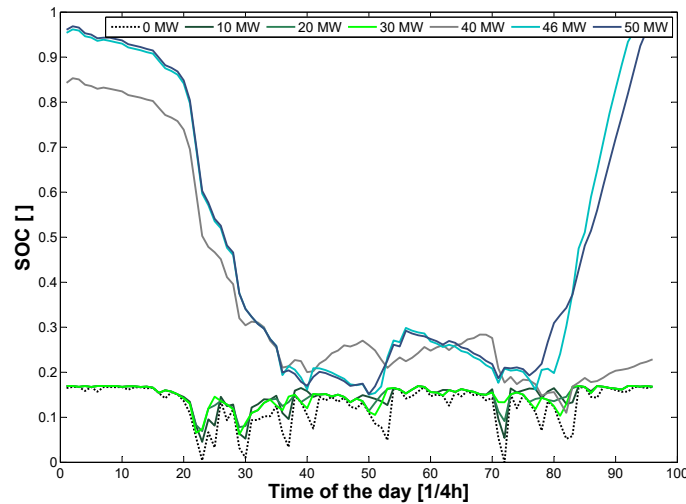
Temperature levels in water tanks or houses can be used to define aggregated state-of-charges (SOC^{agg}) as follows:

$$SOC_t^{agg} = \frac{\sum_{i=1}^{n_c} (T_{i,t} - T_{i,t}^{min}) \alpha_i}{\sum_{i=1}^{n_c} (T_{i,t}^{max} - T_{i,t}^{min}) \alpha_i} \quad (8.20)$$

where $T_{i,t}$ is either the water temperature in tank i , or the zone temperature of house i at time period t .



(a) Aggregated state-of-charge of houses based on zone temperature level.



(b) Aggregated state-of-charge of DHW tanks.

Figure 8.21 – Increase in aggregated state-of-charge with the amount of downward capacity reservation.

Aggregated state-of-charges in terms of water and zone temperatures are depicted in Figure 8.21. When no reserve is contracted, the zone temperature in each house is kept at the low set point, resulting in an aggregated state-of-charge of zero. The water temperature in the storage tanks is kept at the minimum level that can still satisfy upcoming DHW needs, which explains the variation in state-of-charge observed throughout the day. As the amount of contracted reserve increases, temperature levels

8.4. Application of load aggregation to the provision of ancillary services

increase as well. To minimize the consumption, the optimizer chooses to activate most heat pumps in space-heating mode preferentially, since the latter show better performance in that mode over DHW mode. However, for some time periods, downward reserve is provided by a reduction in consumption of heat pumps in DHW mode. This is the case for periods 30, 37 and 72 for example. Since these periods follow large DHW demand, the baseline power consumption is larger, which confers higher potential for downward activation. Therefore, for those periods, zone temperatures remain at the minimum level. Resulting increase in daily procurement costs reaches up to 13.2%.

8.4.5.2 Illustration with historical data

In light of the results of Section 8.4.5.1, the potential of provision of downward reserve is limited. Considering the provision of both upward and downward reserves simultaneously would therefore hamper the potential of providing upward reserve. The reservation of upward and downward capacities is therefore considered separately in this section. However, the method is straightforward to extend to the combined provision of upward and downward reserves.

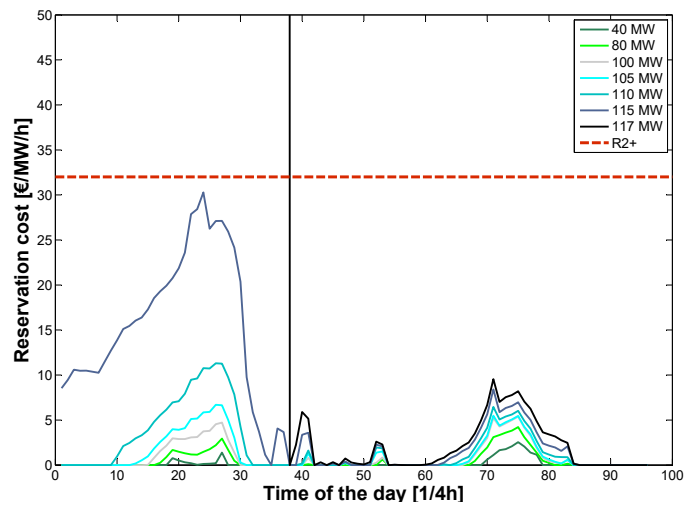
Optimization problems (8.17) is solved for several typical days with real data corresponding to year 2012. Results can be compared against historical data for the provision of secondary reserve. For year 2012, remuneration of capacity reservation was imposed by national regulations to 32 €/MW/h for both upward (R2+) and downward (R2-) reserve (Elia (2012a)). Reservation cost profiles are illustrated for a typical day in January in Figure 8.22.

For upward reserve, it is possible to provide up to 115 MW at 0 to 94% of the remuneration, depending on the period of the day. Above 115 MW, prices increase quickly, especially for time periods between 0 and 8 am, and it is not possible to guarantee the same amount of reserve for all periods of the day. Due to the significant increase in baseline consumption required for the allocation of downward reserve, it is possible to provide only around 30MW at competitive price. As shown in Figure 8.22b, the maximum amount of downward reserve that can be provided for all periods of the day is around 35 MW. Beyond that value, it is not possible to guarantee the same amount of reserve for all periods of the day, as illustrated with a power reservation of 43 MW for example.

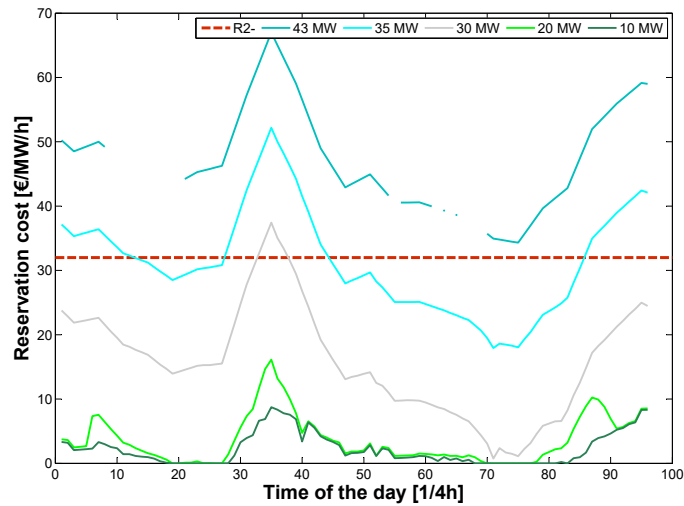
Reservation costs are presented for different days for the months of November through April in Figure 8.23a in the case of upward reserve. In all cases, an upward reserve potential of at least 100 MW can be guaranteed by the load aggregator. Resulting reservation costs range between 0 and 14 €/MW/h, and are much lower than the historical remuneration for the reservation. For downward reserve, the maximum capacity decreases as the average daily ambient temperature increases, as shown in Figure 8.23b. Most of the time however, providing the maximum amount of downward reserve is not competitive compared to the current remuneration.

Flexible heat pumps are therefore better suited for the provision of upward reserve. With 40000 units, it is possible to provide around 70% of the contracted upward volume during the winter season at significantly reduced costs, hereby decreasing system-level costs for the provision of secondary reserve by more than 50%. In the case of downward reserve, the potential for reserve provision varies between 10 and 45 MW depending on the time of the year.

8.4. Application of load aggregation to the provision of ancillary services

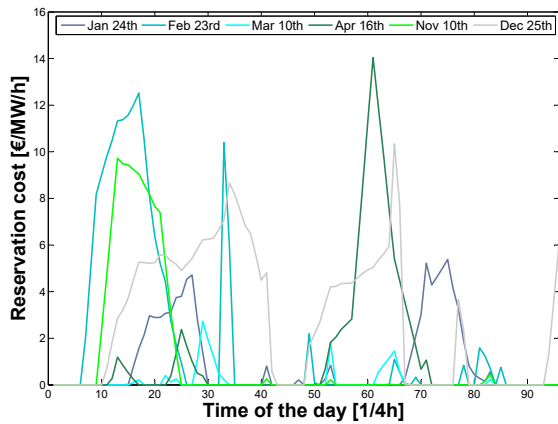


(a) Upward reserve.

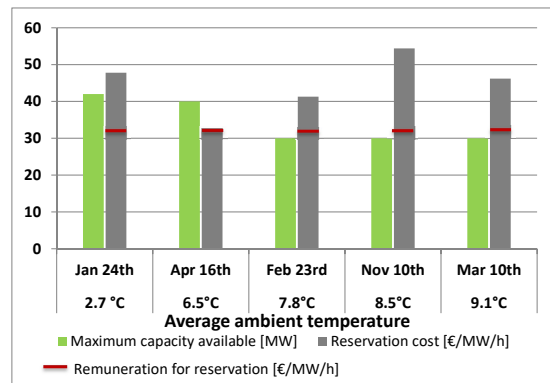


(b) Downward reserve.

Figure 8.22 – Reserve allocation price: daily profiles for January 24th, 2012. Comparison of the prices obtained with flexible heat pumps for different levels of power reserve to average historical prices for secondary reserve (R2+ for upward and R2- for downward).



(a) Upward reserve - reservation costs for 100MW.



(b) Downward reserve - maximum capacity and costs.

Figure 8.23 – Potential of power reserve for different months of the year.

8.4.5.3 Alternative optimization problem

The amount of power contracted must be guaranteed by the load aggregator. However, additional power reserves could be made available, depending on their competitiveness compared to other options available in the market. In that case, instead of imposing the contracted reserve capacity, one can impose an average remuneration, π^R . The problem then consists in determining the amount of upward reserve, R_t^+ , that can be provided at each time step, by solving

$$\min \sum_{t \in \mathcal{H}} \left(\sum_{i=1}^{n_C} (\hat{P}_{i,t} \alpha_i) \pi_t^{DA} \right) dt - \sum_{\tau \in \mathcal{M}} R_{\tau}^+ \pi^R d\tau \quad (8.21a)$$

subject to Constraints (8.17b) – (8.17q), where Constraints (8.17p) is replaced by

$$R_t^+ = \sum_{i=1}^{n_C} (\delta_{i,\tau,0} \alpha_i) \quad (8.21b)$$

$$R_t^+ \geq 0 \quad (8.21c)$$

The case of downward reserve is obtained by replacing Equation (8.21a) by

$$\min \sum_{t \in \mathcal{H}} \left(\sum_{i=1}^{n_C} (\hat{P}_{i,t} \alpha_i) \pi_t^{DA} \right) dt + \sum_{\tau \in \mathcal{M}} R_{\tau}^- \pi^R d\tau \quad (8.22)$$

and Constraint (8.21c) by $R_{\tau}^- \leq 0$.

Figure 8.24 illustrates the reserve capacities obtained when varying the remuneration from 4 to 300 €/MW/h. Results are presented for both upward (positive) and downward (negative) reserves in terms of minimum, average and maximum daily values. For both upward and downward reserves, increasing the remuneration increases daily average reserve capacities and reduces the gap between minimum and maximum daily values. The impact is more marked for the provision of downward reserve, since the reservation of additional units of reserve tends to be more costly than for upward reserve, as explained in Section 8.4.5.1.

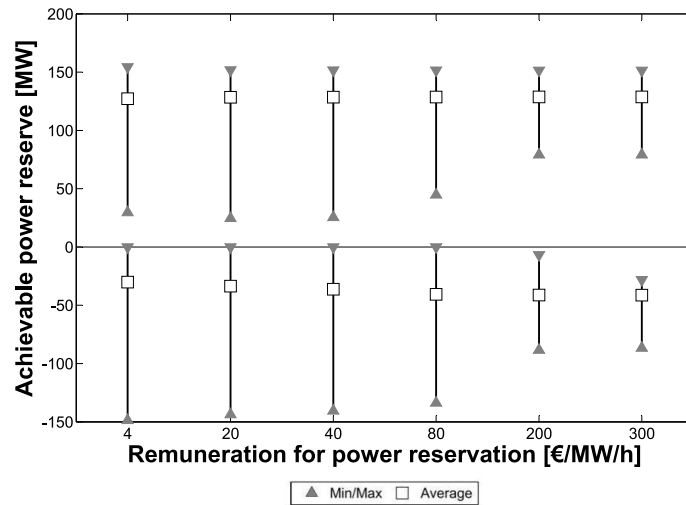


Figure 8.24 – Influence of remuneration for power reservation on achievable reserve capacities (Jan. 24th, 2012).

A parallel can be observed between this problem formulation and that proposed by Zapata Riveros (2015) for passive balancing with micro-CHPs. Indeed, the rescheduling in baseline electricity use could also be performed with remuneration prices set to the imbalance prices. The current approach could also be taken one step further by taking into account uncertainties on the system imbalance and resulting imbalance prices.

8.5 Research outcome

In this chapter, reliable physics-based aggregated models of heterogeneous sets of buildings for large-scale applications are developed. The proposed method determines the number of models needed to capture the diversity of the set in terms of occupant-related constraints. The clustering is thus based on similarities in consumption patterns to meet DHW and space-heating needs. The resulting number of models varies between one and twenty. For space-heating power consumption only, agreement within 12% error was found. The addition of DHW consumption increases the error to 20 – 25%. However, the time-evolution profile of power demand is well captured. As opposed to other methods available in the literature, the proposed method does not require the modeling of each building a-priori.

In the second part of the chapter, these aggregated models are used for large-scale assessment of the flexibility potential of residential heat pumps. The first application consists in investigating the impact of such flexible units on market clearing prices. To that end, a centralized optimization problem based on market clearing price settlement with flexible demand-side bid curves is proposed. The modeling of supply-side bid curves relies on a simplified merit-order approach. The problem is solved for a case-study applied to Belgium for a scenario corresponding to year 2012 and a prospective evolution scenario with 35% renewable energy sources. Under the assumptions of perfectly competitive market with one hundred percent of the power traded on the day-ahead segment, it is shown that

- for an energy mix composed of conventional nuclear and CCGT power plants, a price-taker assumption to model load aggregators with flexible heat pumps is reasonable.
- this is no longer true as the share of renewable sources increase. In that case, penetration rates of 1 to 20% of flexible heat pumps in the building stock yield 0.7 to 51% reduction in average daily procurement costs.

The second application focuses on the assessment of reservation costs for the provision of reserve with flexible heat pumps. A combined optimization problem that aims at the minimization of procurement costs on the day-ahead market while ensuring a certain amount of reserve is proposed. The bases that make reservation costs with TLCs non zero are explained. Both upward and downward provisions of reserve are considered for a case-study in the Belgian context. Results yield the following conclusions:

- the provision of upward reserve is limited by the ability of the system to return to its baseline state, and by limited heat pump capacities. The provision of up to 70% of the current contracted amount of reserve can be achieved with 40000 units during the winter at 43% of the cost.
- the provision of downward reserve yields significant increase in baseline consumption, limiting the potential for downward reserve and increasing reservation costs. As the amount of contracted reserve increases, the latter becomes non competitive compared to current reserve market prices. However, this conclusion may change in future electricity production context with large shares

of renewable energy sources.

Demand-side flexibility of residential consumers for real-time balancing therefore seems to constitute an affordable solution. It is however subjected to the availability of proper regulatory framework, aggregators and adapted smart metering schemes.

It should finally be noted that the above analysis was conducted with a perfect foresight hypothesis. Both the baseline and the modified consumption profiles for balancing and/or reserve allocation would be impacted by taking uncertainty into account, which might in turn modify the magnitude of the results.

Conclusions **Part V**

Conclusion

The literature review presented in **Chapter 1** highlighted that the fast spread of distributed power generation and the expected electrification of residential systems represent additional challenges for the management of the electricity grid and entail growing need for flexibility.

This was further illustrated in **Chapter 2** with an introductory case-study applied in the Belgian context and focusing on the impact of large-scale penetration of heat pumps and PV panels. Three metrics proposed in the literature were used to highlight the impact of large penetration rates of such systems on the overall grid operation costs: the load factor, the peak-to-valley ratio and the power ramping rate. For penetration rates of heat pumps ranging from 10 to 50% of the residential building stock, it was shown that the average yearly peak demand increased by 9 to 47%. Peak-to-valley ratios increased by up to 27%. In addition to heat pumps, large penetration rates of PV panels gave rise to a well-known mismatch between midday peak solar production and evening consumption peak. Excess power production supplied to the grid increased the need for upward and downward power ramping capabilities of centralized generation units. For example, it was shown that with 25% penetration rates of heat pumps and PVs, power level differences between two successive hours entailed downward modulation of the supply-side up to three times greater than in the absence of those systems.

However, the use of heat pumps for space conditioning and domestic hot water production also turns residential consumers into potential flexible loads. In order to reduce system costs and ensure security of supply, load management of such systems for peak shaving, valley filling and load matching through load shifting is essential. In that context, the general objective of this research work was *to determine efficient and scalable load modulation strategies of those systems and to assess the associated flexibility potential at different scales*. Several underlying research questions were stated in Section 1.4. The following sections summarize how those questions were addressed and highlight the contributions of this PhD thesis.

C.1 Modeling and control framework

One objective of this PhD work was to develop a consistent modeling and control framework for demand-side management applications. **Chapter 3** set the basis of the proposed modeling framework. Its main focus was on the implementation of both detailed and reduced-order (grey-box and black-box) models of building physics, and on the linear modeling of water tanks and residential air-to-water heat pumps. Additional models were developed in **Chapter 5**, including moisture balance in buildings, electrical batteries and PV panels.

In terms of control strategies, both rule-based (**Chapter 4**) and model predictive control methods were investigated. At the scale of a single building, a decentralized control approach was followed (**Chapter 4 – 7**). In that approach, each building was controlled separately in response to system-level inputs. For large-scale investigation of the flexibility potential, centralized control schemes were proposed (**Chapter 8**). In that case, all systems were pooled and controlled in order to meet a common objective.

To deal with the resulting large-scale optimization problems, reliable aggregated models were required. To that end, **Chapter 8** presented an aggregation method based on the clustering of heterogeneous loads in semi-homogeneous subsets. Similarities between loads were determined based on

C.2. Price-based load shifting and analysis of overconsumption

occupant-related constraints for space-heating and domestic hot water needs. The resulting number of aggregated models varied between one and twenty, depending on the diversity of the initial set of loads modeled. For the modeling of space-heating power use only, agreement within 12% error was found. The addition of domestic hot water use increased the error to 20 – 25%. Nevertheless, the time-evolution profile of the power demand remained well captured. As opposed to other methods available in the literature, the proposed method did not require the modeling of each building a-priori.

Finally, model-based predictive control allows to tackle unpredicted disturbances such as changes in weather forecast or occupants' behavior. To illustrate this, a closed-loop scheme with feedback from a detailed emulator of the real building was implemented in **Chapter 4** based on state observation with Kalman filtering.

The modeling and control framework developed in this thesis was used to propose general methods for optimal load management of flexible residential loads summarized in the next sections.

C.2 Price-based load shifting and analysis of overconsumption

A second research question aimed at determining the flexibility potential offered by price-based load shifting and at characterizing the resulting overconsumption and its impact on the economics of different market actors.

In that regard, **Chapter 4** proposed different control strategies based on both heuristic laws and optimal control methods at the scale of a building. It was shown that load shifting could be successfully achieved by incentive programs relying on dynamic electricity retail tariffs reflecting day-ahead electricity market prices. With such tariffs, consumers could shift their consumption in time to minimize their electricity bill, which in turn, reduced suppliers' procurement costs. To quantify the flexibility of residential consumers, new metrics were introduced and considered both consumer's and supplier's standpoints. In particular, a new flexibility index was proposed, that determined the percentage of consumption shifted towards low price periods, while penalizing overconsumption. Different tariff structures were compared in the Belgian context: day/night, real-time and prospective multiplicative real-time pricing with increased share of renewable energy sources. Additionally, different house insulation levels, heat emission systems, storage options and heating schedules were investigated. Annual simulation results showed flexibility indexes ranging from 53.7 to 95.2% for storage in the building structure with conventional radiators. Flexibility indexes increased for well thermally-insulated buildings and were the largest with an intermittent heating strategy. Floor heating systems increased the energy volume shifted from peak to off-peak periods by 12 to 57%, depending on the house thermal insulation level. From a consumers' standpoint, load shifting entailed overconsumption of 2.8 to 22.6%, due to increased heat transfer losses and degradation of heat pump performance. With a single-speed heat pump, performance degradation at part-load represented up to 28% of the total electricity consumption and could be reduced by the use of variable-speed technology. Despite the overconsumption, consumers' cost savings reached between 5% and 44%.

In **Chapter 5**, a novel general method for optimal management of decentralized electricity production and HVAC systems with storage in response to evolving metering programs was proposed. In that chapter, load shifting for load matching was triggered by the use of a buy-back ratio, defined as the

ratio of sale price of surplus electricity production to retail electricity tariff. The proposed optimization problem aimed at minimizing the excess electricity production delivered to the grid depending on the buy-back ratio. The optimal load management methodology was applied to a case study consisting in a typical U.S. house equipped with a reversible heat pump, an electric water heater, a battery and PV panels. Results showed that imposing a tariff lower than the retail tariff for the excess electricity generated proved to be a good incentive to promote load matching. For the considered case-study, the yearly percentage of demand directly covered by on-site generation increases by 3 to 28%, depending on the available storage capacity, bringing between 6.4 and 27.5% additional cost savings. However, as the buy-back ratio decreased, overconsumption reached up to 3.3%. A breakdown of the sources of overconsumption was proposed, including heat losses through building envelope and water tank walls, and COP degradation. The proposed method also allowed to provide guidelines for the right-sizing of a PV system depending on the buy-back ratio.

C.3 Direct load control and characterization of the rebound effect

Flexibility can also be harvested through direct load control. The third research question was therefore devoted to the definition of a new flexibility service that could be provided by a load aggregator controlling domestic heat pumps. In addition, the impact on the flexibility service of the rebound effect inherent to direct load control with TLCs was analyzed thoroughly.

The flexibility service proposed in **Chapter 6** consisted of the upward or downward activation of heat pumps from their baseline consumption at a certain time period and during a given number of periods. The activation was followed by a rebound effect with parametrized deviations from the baseline over a fixed number of periods. The modulation potential was obtained from a sequential optimization problem. The baseline was such that it minimized the energy costs for the end-user. The rebound effect was composed of a delay period with no deviations from the baseline consumption and a payback period during which deviations in consumption occurred to allow the heat pumps to return to their baselines. The detailed characterization of the payback and the investigation of its impact on the achievable modulation amplitude constitutes a contribution to the current state-of-the-art in the field.

Example results in the Belgian context indicated that mean upward and downward modulation amplitudes ranged from 0.05 to 1.24 kW and from 0.01 to 0.5 kW, respectively, for paybacks of 15 minutes to one and a half hour. These values decreased by 65% and 72% per house, respectively, for upward and downward modulations, for a delay length of thirty minutes, as compared to no delay length. Beyond two periods for the delay length, the average values remained almost unchanged. The limitation in modulation amplitude entailed by increased delay lengths was particularly marked for time periods during the day where the indoor temperature set point was close to a transition. A sensitivity analysis of the modulation potential to the retail tariff structure was also presented. This analysis showed that a tuned dynamic retail tariff structure can maximize the modulation potential during critical time periods, for example to relieve congestion in the network or balance the electrical system. Finally, it was shown that the rebound effect has a significant impact on the potential application of such flexibility services for balancing purposes, as it can cause the activation of the service to be unprofitable or postpone the imbalance issue to a later time.

C.4 Choice of storage option

The three load modulation strategies proposed in Chapters 4 – 6 were compared in an application of load matching at the scale of a district with distributed electricity production in **Chapter 7**. Different thermal storage options were considered, including the building structure and two hydraulic configurations with space-heating water tanks and domestic hot water tanks. A ranking of the most suitable storage options with regard to the building insulation level and modulation strategy was performed. Results showed that for all types of houses and modulation strategies, the building structure offered the largest storage potential and the best mitigation of local bottlenecks. However, as the house insulation decreased, greater indoor temperature fluctuations and overconsumption were observed. In that case, the use of an additional storage tank in a parallel-four pipe configuration was the best alternative. For well-insulated houses, the parallel two-pipe hydraulic configuration was an interesting alternative to storage in the building structure.

C.5 Large-scale applications

In **Chapter 8**, it was shown that centralized control schemes in which the electricity use of all systems is optimized jointly to meet a common objective allows for better mitigation of both overconsumption and rebound effect. The aggregated models developed in the frame of this work were thus used to investigate two large-scale applications relying on centralized optimization problems.

In the literature, a price taker assumption is often made when investigating the flexibility potential of price-responsive heat pumps. The first large-scale application considered in this work therefore aimed at demonstrating whether this assumption is still reasonable as the number of flexible units increases. The resulting research question was therefore to determine the impact of large-scale implementation of retail-price-based load shifting strategies on day-ahead market prices. To that end, supply-side bid curves were modeled by a simplified merit-order approach. Two scenarios were considered in the Belgian context: a scenario with the electricity production mix of year 2012 and a prospective scenario with a 35% share of renewable energy sources. Under the assumptions of a perfectly competitive market with one hundred percent of the power traded on the day-ahead segment, the following conclusions were drawn. In the 2012 scenario, for less than 10% penetration rates of flexible heat pumps in the building stock, a price-taker assumption to model load aggregators with flexible heat pumps was reasonable. For the second scenario, a penetration rate of 20% heat pumps was considered. Among those heat pumps, the percentage of flexible units was varied between 1% and 20%. This resulted in 0.7 to 51% reduction in average daily procurement costs.

The second application was based on the direct control service proposed in Chapter 6 and applied to the provision of secondary reserve in the Belgian context. The sequential optimization problem solved in the decentralized approach was combined into a centralized optimization problem that aimed at the minimization of procurement costs on the day-ahead market, while ensuring the provision of a certain amount of reserve. One contribution of this work was to identify the bases that make the reservation costs non zero with thermostatically-controlled loads. It was shown that constrained rebound effect and limited heat pump capacity both increase reservation costs in the case of upward reserves, whereas overconsumption plays a major role in reducing the potential provision of downward reserves. During the winter, the provision of up to 70% of the current contracted amount of upward

reserves (140MW) could be achieved with 40000 units at 44% of the costs. For downward reserve, as the amount of allocated power increased, the latter became non competitive compared to market prices. However, this conclusion may change in the future electricity production context with a large share of renewable energy sources.

C.6 General conclusions

The present work proposed a comprehensive assessment of the flexibility potential offered by TLCs, and in particular, by heat pumps. The proposed modulation strategies have shown promising outcomes of residential demand-side flexibility for use in the frame of operational planning or real-time balancing by system operators. However, in the current conjuncture, the financial benefits retrieved by flexible consumers are limited. Furthermore, the challenges inherent to unpredictable occupant behavior, while out of the scope of the present study, certainly need to be addressed in future work. Nevertheless, this work constitutes a useful tool for future market agents such as load aggregators, as well as for energy planning and assessment of energy policies.

Limitations and recommendations for future work

The load modulation strategies proposed in the present work were based on predictive optimization schemes assuming perfect prediction of all disturbances. In practice, one challenge associated to the use of TLCs for demand-side management lies in the accurate prediction of the baseline consumption. Indeed, between day-ahead predictions and real-time consumption, different sources of uncertainties may arise, due to unpredicted changes in occupant behavior and weather conditions. An insight of the impact of such uncertainties on changes in baseline consumption was provided in Chapter 4 at the scale of one building. This should be further extended to a detailed large-scale uncertainty analysis. Resulting deviations from predicted baseline consumption could be correlated to the diversity of the modeled set of loads. To that end, the aggregation method proposed in Chapter 8 could be coupled to a more diverse set of building geometries and insulation levels available in the building stock description presented in Chapter 2. Moreover, in line with the results presented in Chapter 8, one could assess the impact of such uncertainties on the ability of flexible loads to provide balancing services.

Regarding the general load management scheme for load matching presented in Chapter 5, future work could consist of implementing the method at the level of a district by including detailed modeling of the actual distribution grid. This would allow one to quantify the effect of different methods on the elimination of local bottlenecks.

One limitation of the approach proposed in Chapter 6 is that, if load modulation is activated in one period, no further activation can be performed before the end of the rebound period. The possibility of additional activations during the rebound period should be investigated and extended to the problem of provision of secondary reserves proposed in Chapter 8.

As highlighted in Chapter 8, price-induced flexibility must be investigated while taking into account the impact of such flexibility on day-ahead market prices themselves. The assumptions behind the modeling of market prices and supply-side "bid" curves used in this work are too limiting to fully capture this effect, particularly in the case of large penetration rates of renewable energy sources.

To address this, the methods and models developed in this work could be included into detailed interaction models between market actors and unit-commitment of power plants.

The question of the retribution of flexible consumers and other market actors such as load aggregators in the case of centralized control schemes also needs to be addressed.

Finally, practical implementation of the proposed methods requires the use of communication devices. In that context, there is a need to identify relevant monitoring data and suitable communication devices to control the systems. Attention should be given to consumers' privacy concerns.

Ultimately however, the present study provides the basis for which this future work can be constructed upon.

List of Symbols

List of Acronyms

BRP	Balance responsible party
CCGT	Combined Cycle Gas Turbine
COP	Coefficient of performance
CS	Cost savings
DHW	Domestic hot water
DSM	Demand-side management
DSO	Distribution System Operator
FI	Flexibility index
HP	Heat pump
HVAC	Heating, Ventilation and Air-Conditioning
OC	Overconsumption
PLR	Part-load ratio
PV	Photovoltaic
RES	Renewable energy sources
RMS	Root mean square
SH	Space heating
SLP	Synthetic load profile
TCL	Thermostatically-controlled load
TOU	Time-of-Use
TSO	Transmission System Operator
VS	Volume shifted

Nomenclature

Chapter 3

Symbols

A	surface area [m ²]
c	specific heat [J/(kg.K)]
C	thermal capacitance [J/K]
g	solar factor
h	heat transfer coefficient (convection/radiation) [W/m ²]
H	number of periods in the prediction horizon \mathcal{H}
\mathcal{H}	prediction horizon
m	mass [kg]
M	number of periods in the control horizon \mathcal{M}
\mathcal{M}	control horizon
P	electrical power [W]
\dot{Q}	heat transfer capacity [W] (or q heat transfer capacity per surface area [W/m ²])
R	thermal resistance [K/W]
T	temperature [K]
u	decision variable
U	heat transfer coefficient (U-value) [W/m ²]
w	disturbance
\dot{W}	compressor electrical power [W]
x	state variable

Subscripts and Superscripts

amb	ambient
avg	avg
c	convective
d	direct
f	floor
fl	full load
gl	glazing
h	heating
in	indoor/inlet
inf	infiltration
int	internal
l	light
m	massive
op	opaque
out	outdoor/outlet
r	radiative
rat	rated

<i>sol</i>	solar
<i>surr</i>	surroundings
<i>su</i>	supply
<i>t</i>	time
<i>tot</i>	total
<i>w</i>	wall, water
<i>win</i>	window
<i>z</i>	zone

Chapter 4

Symbols

<i>A</i>	surface area [m ²]
<i>C</i>	thermal capacity [J/K]
<i>E</i>	energy consumption [J]
<i>g</i>	solar factor
<i>h</i>	heat transfer coefficient (convection/radiation) [W/m ²]
<i>H</i>	number of periods in the prediction horizon \mathcal{H}
\mathcal{H}	prediction horizon
<i>K</i>	Kalman filter gain
<i>m</i>	mass [kg]
<i>M</i>	number of periods in the control horizon \mathcal{M}
\mathcal{M}	control horizon
<i>P</i>	electrical power [W], covariance matrix in Kalman filter implementation
<i>Q</i>	process noise in Kalman filter implementation
\dot{Q}	heat transfer capacity [W] (or <i>q</i> heat transfer capacity per surface area [W/m ²])
<i>R</i>	thermal resistance, measurement noise in Kalman filter implementation
<i>S</i>	innovation covariance
<i>T</i>	temperature [K]
<i>u</i>	decision variable
<i>U</i>	heat transfer coefficient (U-value) [W/m ²]
<i>w</i>	disturbance
<i>x</i>	state variable

Greek symbols

π	price [€/kWh]
-------	---------------

Subscripts and Superscripts

<i>amb</i>	ambient
------------	---------

<i>avg</i>	average
<i>bh</i>	back-up heater
<i>c</i>	convective
<i>cons</i>	consumption
<i>d</i>	daily
<i>DA</i>	day-ahead
<i>em</i>	emitter
<i>f</i>	floor
<i>fl</i>	full load
<i>gl</i>	glazing
<i>h</i>	heating
<i>hf</i>	heating floor
<i>HP</i>	heat pump
<i>in</i>	indoor/inlet
<i>inf</i>	infiltration
<i>int</i>	internal
<i>l</i>	light
<i>m</i>	massive
<i>op</i>	opaque
<i>out</i>	outdoor/outlet
<i>r</i>	radiative
<i>rad</i>	radiator
<i>rat</i>	rated
<i>ref</i>	reference
<i>ret</i>	retail
<i>sol</i>	solar
<i>sp</i>	set point
<i>surr</i>	surroundings
<i>su</i>	supply
<i>t</i>	time
<i>tot</i>	total
<i>w</i>	wall
<i>win</i>	window
<i>z</i>	zone

Chapter 5

Symbols

<i>C</i>	thermal capacity [J/K], investment cost [USD]
<i>E</i>	energy [J]
<i>f</i>	fraction
<i>h</i>	enthalpy [J]

H	prediction horizon
L	system lifetime [year]
m	mass [kg]
M	control horizon
P	electrical power [W]
\dot{Q}	heat transfer capacity[W]
R	thermal resistance [K/W]
S	savings
T	temperature [K]
u	decision variable
w	disturbance
x	state variable
Y	thermal capacity or COP

Greek symbols

α	buy-back ratio
π	electricity price [USD/kWh]
Γ	exogenous consumption [W]

Subscripts and Superscripts

a	air
abs	absorbed
adp	apparatus
amb	ambient
avg	average
bb	buy-back
bp	bypass
bt	bottom
c	cooling
$cond$	condensation
$cons$	consumption
$conv$	convective
ex	exhaust
f	floor
fl	full load
in	indoor/inlet
inf	infiltration
l	latent
m	mass flow rate
net	net
occ	occupant
out	outlet
PV	photovoltaic

<i>rad</i>	radiator
<i>rat</i>	rated
<i>ret</i>	retail
<i>s</i>	sensible
<i>su</i>	supply
<i>sol</i>	solar
<i>sp</i>	set point
<i>T</i>	temperature
<i>t</i>	time
<i>tp</i>	top
<i>trans</i>	transmitted
<i>w</i>	wall, water
<i>wb</i>	wet bulb
<i>WH</i>	water heater
<i>win</i>	window
<i>z</i>	zone

Chapter 6

Parameters

H	Number of periods in the horizon
\mathcal{H}	Optimization horizon $\{1, \dots, H\}$
n	Number of modulation periods
l	Number of delay periods before payback
k	Number of payback periods
$\mathcal{K}(\tau, (n-1) + l + k)$	Flexibility service horizon $\{\tau, \tau + 1, \dots, \tau + (n-1) + l + k\}$
$\mathbf{A}^i, \mathbf{B}^i, \mathbf{E}^i$	Parameters of state-space model
C	Thermal capacitance [J/K]
dt	Period duration [s]
COP_t	Heat pump coefficient of performance
ϵ	Penalty for the payback imbalance
Γ_t	Exogenous power consumed [W]
$\dot{Q}_t^g, \dot{Q}_t^{sol}$	Internal heat gains, solar gains [W]
π_t^+	Buying price of electricity [€/kWh]
π_t^-	Selling price of electricity [€/kWh]
R	Thermal resistance [K/W]
σ	State deviation tolerance from baseline
λ	State constraint relaxation
$T^a mb_t$	Ambient temperature [K]
T_t^{su}	Water supply temperature [K]
\mathbf{w}_t	State-space model parameters
\mathbf{x}^i	Initial state

Variables

δ_t	Modulation amplitude
δ_τ^*	Minimum modulation amplitude over n periods
I^+	Maximum positive deviation after a modulation
I^-	Maximum negative deviation after a modulation
P_t	Total consumption [W]
P_t^+	Power bought from the grid [W]
P_t^-	Power sold to the grid [W]
\dot{Q}_t	Heat pump thermal capacity [W]
T_t	Temperature [K]
\dot{W}_t	Compressor electrical power consumption [W]
\mathbf{x}_t	State variable
y_t	Heating mode

Powers are taken as positive when consumed and negative when produced. A positive modulation corresponds to an increase in consumption. Variables obtained for the baseline are denoted with a $\hat{\bullet}$.

Superscripts

<i>amb</i>	ambient
<i>g</i>	gain
<i>int</i>	internal
<i>l</i>	light
<i>m</i>	massive
<i>n</i>	nominal
<i>s</i>	space heating
<i>sol</i>	solar
<i>su</i>	supply
<i>w</i>	water
<i>z</i>	zone

Chapter 7

For this chapter, the reader is referred to the nomenclature of Chapter 4 through Chapter 6.

Chapter 8

For this chapter, the reader is referred to the nomenclature of Chapter 6.

Bibliography

- Air-conditioning, Heating and Refrigeration Institute (AHRI). 210/240 - standard for performance rating of unitary air conditioning and air-source heat pump equipment, 2008.
- M. Ali, A. Alahäivälä, F. Malik, M. Humayun, A. Safdarian, and M. Lehtonen. A market-oriented hierarchical framework for residential demand response. *International Journal of Electrical Power & Energy Systems*, 69:257–263, 2015.
- K. Allacker. *Sustainable building: The Development of an Evaluation Method*. PhD thesis, KU Leuven, 2010.
- American society of heating, refrigerating and air-conditioning engineers (ASHRAE). Standard 116 - methods of testing for rating seasonal efficiency of unitary air conditioners and heat pumps, 1983.
- American Society of Heating, Refrigerating and Air-Conditioning Engineers (ASHRAE). Standard 55 : Thermal environmental conditions for human occupancy, 1992.
- American society of heating, refrigerating and air-conditioning engineers (ASHRAE). Handbook of fundamentals. 2013.
- Architecture et Climat and Service public de Wallonie. Efficacité énergétique des bâtiments tertiaires - les radiateurs.
- A. Arteconi, N. Hewitt, and F. Polonara. Domestic demand-side management (DSM): Role of heat pumps and thermal energy storage (TES) systems. *Applied Thermal Engineering*, 51(1):155–165, 2013.
- A. Arteconi, D. Patteeuw, K. Bruninx, E. Delarue, W. D'haeseleer, and L. Helsen. Active demand response with electric heating systems: impact of market penetration. *Applied Energy*, 177:636–648, 2016.
- P. Bacher and P. Delff. Iea common exercise 4: ARX, ARMAX and grey-box models for thermal performance characterization of the test box. Technical report, Report-2014-08, Technical University of Denmark, 2014.
- P. Bacher and H. Madsen. Procedure for identifying models for the heat dynamics of buildings. Technical report, Technical University of Denmark, 2010.
- B. Baeten, T. Confrey, S. Pecceu, F. Rogiers, and L. Helsen. A validated model for mixing and buoyancy in stratified hot water storage tanks for use in building energy simulations. *Applied Energy*, 172: 217–229, 2016.

- R. Baetens. *On Externalities of Heat Pump-based Low-Energy Dwellings at the Low-Voltage Distribution Grid*. PhD thesis, KUL, 2015.
- R. Baetens, R. De Coninck, J. Van Roy, B. Verbruggen, J. Driesen, L. Helsen, and D. Saelens. Assessing electrical bottlenecks at feeder level for residential net zero-energy buildings by integrated system simulation. *Applied Energy*, 96:74–83, 2012.
- R. Barth, H. Brand, P. Meibom, and C. Weber. A stochastic unit-commitment model for the evaluation of the impacts of integration of large amounts of intermittent wind power. In *International Conference on Probabilistic Methods Applied to Power Systems (PMAPS)*, pages 1–8. IEEE, 2006.
- B. Biegel, P. Andersen, T. S. Pedersen, J. Stoustrup, L. H. Hansen, et al. Electricity market optimization of heat pump portfolio. In *2013 IEEE International Conference on Control Applications (CCA)*, pages 294–301. IEEE, 2013.
- B. Biegel, M. Westenhof, L. H. Hansen, J. Stoustrup, P. Andersen, and S. Harbo. Integration of flexible consumers in the ancillary service markets. *Energy*, 67:479–489, 2014.
- T. Bohlin. Special issue on grey box modelling. *International journal of adaptive control and signal processing*, 9(6):461–464, 1995.
- A. Bolher, R. Casari, E. Fleury, D. Marchio, and M. J. Méthode de calcul des consommations d'énergie des bâtiments climatisés ConsoClim. Technical report, Ecole des Mines (Paris), 1999.
- M. Brandemuehl, S. Gabel, and I. Andersen. HVAC2 toolkit: A toolkit for secondary HVAC system energy calculations. *American Society of Heating, Refrigerating and Air Conditioning Engineers*, 1993.
- J. E. Braun. Reducing energy costs and peak electrical demand through optimal control of building thermal mass. *ASHRAE transactions*, 96(2):876–888, 1990.
- J. E. Braun and N. Chaturvedi. An inverse gray-box model for transient building load prediction. *HVAC&R Research*, 8(1):73–99, 2002.
- BRG Building Solutions. The european heating product markets (update 2013). Technical report, 2013.
- T. Brinsmead, P. Graham, J. Hayward, E. Ratnam, and L. Reedman. Future energy storage trends: an assessment of the economic viability, potential uptake and impacts of electrical energy storage on the NEM 2015-2035, 2015.
- K. Bruninx, D. Patteeuw, E. Delarue, L. Helsen, and W. D'haeseleer. Short-term demand response of flexible electric heating systems: The need for integrated simulations. In *2013 10th International Conference on the European Energy Market (EEM)*, pages 1–10, May 2013. doi: 10.1109/EEM.2013.6607333.
- Bureau of standardization. EN14511 - 2 (2008): Air conditioners, liquid chilling packages and heat pumps with electrically driven compressors for space heating and cooling - part 2: test conditions, European Standard, 2007.
- J. Cai and J. E. Braun. Efficient and robust training methodology for inverse building modeling. In *Fifth National Conference of IBPSA-USA*, 2012.

- J. A. Candanedo and A. K. Athienitis. Application of predictive control strategies in a net zero energy solar house. In *26th Conference on Passive and Low Energy Architecture*, 2009.
- CEEME. Personal communication. Technical report, Centre of expertise in economic modeling of ENGIE, 2015.
- Centre Scientifique et Technique du Bâtiment (CSTB). Caractérisation de l'inertie thermique des bâtiments. Technical report, CSTB Marne-la-Vallée, France, 2012.
- Comité Européen de Normalisation. *EN ISO 13790: Energy Performance of Buildings: Calculation of Energy Use for Space Heating and Cooling (ISO 13790: 2008)*. CEN, 2008.
- B. Cornélusse and D. Ernst. ELEC0018-1 - marché de l'énergie. Technical report, University of Liège, Belgium, 2014.
- Z. Csetvei, J. Østergaard, and P. Nyeng. Controlling price-responsive heat pumps for overload elimination in distribution systems. In *2011 2nd IEEE PES International Conference and Exhibition on Innovative Smart Grid Technologies (ISGT Europe)*, pages 1–8. IEEE, 2011.
- W. Cyx, N. Renders, M. Van Holm, and S. Verbeke. IEE TABULA-typology approach for building stock energy assessment. *Mol, Belgium: VITO*, 2011.
- K. Dallmer-Zerbe, D. Fischer, W. Biener, B. Wille-Hausmann, and C. Wittwer. Droop controlled operation of heat pumps on clustered distribution grids with high PV penetration. In *2016 IEEE International Energy Conference (ENERGYCON)*, pages 1–6. IEEE, 2016.
- U. I. Dar, I. Sartori, L. Georges, and V. Novakovic. Advanced control of heat pumps for improved flexibility of net-zero towards the grid. *Energy and Buildings*, 69:74–84, 2014.
- R. De Coninck. *Grey-Box Based Optimal Control for Thermal Systems in Buildings—Unlocking Energy Efficiency and Flexibility*. PhD thesis, 2015.
- R. De Coninck and L. Helsen. Quantification of flexibility in buildings by cost curves—methodology and application. *Applied Energy*, 162:653–665, 2016.
- R. De Coninck, R. Baetens, B. Verbruggen, J. Driesen, D. Saelens, and L. Helsen. Modelling and simulation of a grid connected photovoltaic heat pump system with thermal energy storage using modelica. In *8th International Conference on System Simulation in Buildings*, pages 1–21, 2010.
- R. De Coninck, R. Baetens, D. Saelens, A. Woyte, and L. Helsen. Rule-based demand-side management of domestic hot water production with heat pumps in zero energy neighbourhoods. *Journal of Building Performance Simulation*, 7(4):271–288, 2014.
- R. De Coninck, F. Magnusson, J. Åkesson, and L. Helsen. Toolbox for development and validation of grey-box building models for forecasting and control. *Journal of Building Performance Simulation*, 9(3):288–303, 2016.
- P. Denholm and M. Hand. Grid flexibility and storage required to achieve very high penetration of variable renewable electricity. *Energy Policy*, 39(3):1817–1830, 2011.

- F. Déqué, F. Ollivier, and A. Poblador. Grey boxes used to represent buildings with a minimum number of geometric and thermal parameters. *Energy and Buildings*, 31(1):29 – 35, 2000.
- O. Dumont, C. Carmo, R. Dickes, E. Georges, S. Quoilin, and V. Lemort. Hot water tanks: How to select the optimal modelling approach? *Proceedings of Clima2016 Conference*, 2016.
- Dynasim AB. Dynamic modeling laboratory (dymola) – user’s manual version 5.3a.
- Elia. Secondary reserves, 2012a. URL http://www.elia.be/~media/files/elia/grid-data/balancing/secondary_reserves.pdf.
- Elia. Generated energy, 2012b. URL <http://www.elia.be/en/grid-data/data-download>.
- Elia. Imbalance prices, 2012c. URL <http://www.elia.be/en/grid-data/balancing/imbalance-prices>.
- Elia. Ancillary services, 2016. URL <http://www.elia.be/en/suppliers/purchasing-categories/energy-purchases/Ancillary-services>.
- M. Ellis, H. Durand, and P. D. Christofides. A tutorial review of economic model predictive control methods. *Journal of Process Control*, 24(8):1156–1178, 2014.
- EnergyVille. Linear project: Demand response for families. Technical report, 2014.
- ENTSO-E. Impact of merit order activation of automatic frequency restoration reserves and harmonised full activation times. Technical report, 2015.
- Eurobserv’er. Heat pumps barometer, 2013.
- European Commission. Best practices on renewable energy self-consumption. Technical Report COM(2015) 339 final, 2015.
- European Parliament. 2010 energy performance of buildings directive, 2010.
- A. Faruqui, R. Hledik, and J. Palmer. *Time-varying and dynamic rate design*. Regulatory Assistance Project, 2012.
- D. Fischer and H. Madani. On heat pumps in smart grids: A review. *Renewable and Sustainable Energy Reviews*, 70:342–357, 2017.
- A. Floss and S. Hofmann. Optimized integration of storage tanks in heat pump systems and adapted control strategies. *Energy and Buildings*, 100:10–15, 2015.
- C. W. Gellings. The concept of demand-side management for electric utilities. *Proceedings of the IEEE*, 73(10):1468–1470, 1985.
- S. Gendebien, E. Georges, S. Bertagnolio, and V. Lemort. Methodology to characterize a residential building stock using a bottom-up approach: a case study applied to belgium. *International Journal of Sustainable Energy Planning and Management*, 4:71–88, 2015.
- E. Georges, S. Gendebien, S. Bertagnolio, and V. Lemort. Modeling and simulation of the domestic energy use in belgium following a bottom-up approach. In *Proceedings of the CLIMA 2013 11th REHVA World Congress & 8th International Conference on IAQVEC*, 2013.

- E. Georges, P. Garsoux, G. Masy, D. De Maere, V. Lemort, et al. Analysis of the flexibility of belgian residential buildings equipped with heat pumps and thermal energy storages. In *Proceedings of CLIMA2016 Conference*, 2016.
- M. Goldberg. Measure twice, cut once. *Power and Energy Magazine, IEEE*, 8(3):46–54, 2010.
- C. Gonzalez, J. Geuns, S. Weckx, T. Wijnhoven, P. Vingerhoets, T. De Rybel, and J. Driesen. LV distribution network feeders in belgium and power quality issues due to increasing PV penetration levels. In *2012 3rd IEEE PES Innovative Smart Grid Technologies Europe (ISGT Europe)*, pages 1–8. IEEE, 2012.
- S. Gottwalt, W. Ketter, C. Block, J. Collins, and C. Weinhardt. Demand side management—a simulation of household behavior under variable prices. *Energy Policy*, 39(12):8163–8174, 2011.
- R. Halvgaard, N. K. Poulsen, H. Madsen, and J. B. Jørgensen. Economic model predictive control for building climate control in a smart grid. In *2012 IEEE PES Innovative Smart Grid Technologies (ISGT)*, pages 1–6. IEEE, 2012.
- H. Hao, B. M. Sanandaji, K. Poolla, and T. L. Vincent. A generalized battery model of a collection of thermostatically controlled loads for providing ancillary service. In *2013 51st Annual Allerton Conference on Communication, Control, and Computing (Allerton)*, pages 551–558. IEEE, 2013.
- K. Hedegaard, B. V. Mathiesen, H. Lund, and P. Heiselberg. Wind power integration using individual heat pumps—analysis of different heat storage options. *Energy*, 47(1):284–293, 2012.
- G. Heffner. Loads providing ancillary services: Review of international experience. *Lawrence Berkeley National Laboratory*, 2008.
- E. Hirst. Bulk-power ancillary services for industrial customers. 1999.
- S. Holloway. An annual performance comparison of various heat pumps in residential applications. Master’s thesis, Purdue University, 2013.
- P. Ilak, S. Krajcar, I. Rajšl, and M. Delimar. Pricing energy and ancillary services in a day-ahead market for a price-taker hydro generating company using a risk-constrained approach. *Energies*, 7(4): 2317–2342, 2014.
- I. ILOG. Cplex optimization studio, 2013.
- International Code Council (ICC). International energy conservation code (iecc), 2003.
- International Code Council (ICC). International energy conservation code (iecc), 2009.
- International Energy Agency. Transition to sustainable buildings strategies and opportunities to 2050. Technical report, France, 2013.
- International Energy Agency (IEA). Task 40/annex 52: Towards net zero energy solar buildings load match and grid interaction in NZEB with high-resolution data, 2014.
- A. Janssens, E. Van Londersele, B. Vandermarcke, S. Roels, P. Standaert, and P. Wouters. Development of limits for the linear thermal transmittance of thermal bridges in buildings. In *10th Thermal Performance of the Exterior Envelopes of Whole Buildings Conference (ASHRAE)*, 2007.

- R. Judkoff, J. Neymark, and B. Polly. *Building Energy Simulation Test for Existing Homes (BESTEST-EX)*. National Renewable Energy Laboratory, 2011.
- R. Kamyar and M. M. Peet. Optimal thermostat programming and optimal electricity rates for customers with demand charges. In *2015 American Control Conference (ACC)*, pages 4529–4535. IEEE, 2015.
- S. Kärkkäinen. Integration of demand-side management, distributed generation, renewable energy sources and energy storages. *Report Task XVII of International Energy Agency Demand-Side Management Program*, 1:77, 2008.
- F. Karlsson. *Capacity control of residential heat pump heating systems*. PhD thesis, Chalmers University of Technology, Sweden, 2007.
- Y.-J. Kim, L. K. Norford, and J. L. Kirtley. Modeling and analysis of a variable speed heat pump for frequency regulation through direct load control. *IEEE Transactions on Power Systems*, 30(1):397–408, 2015.
- B. Kirby and E. Hirst. Load as a resource in providing ancillary services. 1999.
- K. Klein. Review of metrics describing the grid interaction and flexibility of buildings. personal communication, 2016.
- N. Kumar, P. Besuner, S. Lefton, D. Agan, and D. Hilleman. Power plant cycling costs. *Contract*, 303: 275–3000, 2012.
- M. Kvasnica. *Model Predictive Control*. Institute of Information Engineering, Automation, and Mathematics, Slovak University of Technology in Bratislava, 2014.
- L. Laret. *Contribution au développement de modèles mathématiques du comportement thermique transitoire de structures d’habitation*. PhD thesis, 1981.
- A. Latiers, F. Glineur, E. De Jaeger, B. Martin, et al. On decentralized control of small loads and energy rebound within primary frequency control. In *PSCC 2016*, 2016.
- J. Lofberg. Yalmip: A toolbox for modeling and optimization in matlab. In *2004 IEEE International Symposium on Computer Aided Control Systems Design*, pages 284–289. IEEE, 2004.
- J. P. Lopes, N. Hatziargyriou, J. Mutale, P. Djapic, and N. Jenkins. Integrating distributed generation into electric power systems: A review of drivers, challenges and opportunities. *Electric power systems research*, 77(9):1189–1203, 2007.
- A. Loudon. Summertime temperatures in buildings without air conditioning. Technical report, Building Research Station Current Paper, 47/68, 1968.
- O. Ma, N. Alkadi, P. Cappers, P. Denholm, J. Dudley, S. Goli, M. Hummon, S. Kiliccote, J. MacDonald, N. Matson, et al. Demand response for ancillary services. *IEEE Transactions on Smart Grid*, 4(4): 1988–1995, 2013.
- Y. Ma, A. Kelman, A. Daly, and F. Borrelli. Predictive control for energy efficient buildings with thermal storage. *IEEE Control system magazine*, 32(1):44–64, 2012.

- J. M. Maciejowski. *Predictive control: with constraints*. Pearson Education, 2002.
- G. Masy. *Definition and validation of a simplified multi-zone dynamic building model connected to heating system and HVAC unit*. PhD thesis, 2008.
- G. Masy, E. Georges, C. Verhelst, V. Lemort, and P. André. Smart grid energy flexible buildings through the use of heat pumps and building thermal mass as energy storage in the belgian context. *Science and Technology for the Built Environment*, 21(6):800–811, 2015a.
- G. Masy, I. Rehab, P. Andre, E. Georges, F. Randaxhe, V. Lemort, and J. Lebrun. Lessons learned from heat balance analysis for holzkirchen twin houses experiment. *Energy Procedia*, 78:3270–3275, 2015b.
- S. Mathieu, D. Ernst, and Q. Louveaux. An efficient algorithm for the provision of a day-ahead modulation service by a load aggregator. In *Innovative Smart Grid Technologies Europe (ISGT EUROPE), 2013 4th IEEE/PES*. IEEE, 2013.
- S. Mathieu, Q. Louveaux, D. Ernst, and B. Cornélusse. A quantitative analysis of the effect of flexible loads on reserve markets. In *Proceedings of the 18th Power Systems Computation Conference (PSCC)*. IEEE, 2014.
- P. Meibom, J. Kiviluoma, R. Barth, H. Brand, C. Weber, and H. V. Larsen. Value of electric heat boilers and heat pumps for wind power integration. *Wind Energy*, 10(4):321–337, 2007.
- M. Miara, D. Günther, Z. L. Leitner, and J. Wapler. Simulation of an air-to-water heat pump system to evaluate the impact of demand-side-management measures on efficiency and load-shifting potential. *Energy Technology*, 2(1):90–99, 2014.
- MIT Energy Initiative Symposium. Managing large-scale penetration of intermittent renewables, 2012.
- J. W. Mitchell and J. E. Braun. *Principles of heating, ventilation, and air conditioning in buildings*. Wiley New York, 2013.
- J. D. Mondol, Y. G. Yohanis, and B. Norton. Optimising the economic viability of grid-connected photovoltaic systems. *Applied Energy*, 86(7):985–999, 2009.
- National Renewable Energy Laboratory (NREL). The open PV project, 2015. URL <https://openpv.nrel.gov/>.
- G. R. Newsham and B. G. Bowker. The effect of utility time-varying pricing and load control strategies on residential summer peak electricity use: a review. *Energy Policy*, 38(7):3289–3296, 2010.
- P. Ngendakumana and G. Liebecq. Les facteurs de réponse simplifiés de paroi. Technical Report PNG860215-01, University of Liege, Belgium, 1986.
- K. M. Nielsen, P. Andersen, and T. S. Pedersen. Aggregated control of domestic heat pumps. In *2013 IEEE International Conference on Control Applications (CCA)*, pages 302–307. IEEE, 2013.
- S. Nykamp, A. Molderink, V. Bakker, H. A. Toersche, J. L. Hurink, and G. J. Smit. Integration of heat pumps in distribution grids: Economic motivation for grid control. In *2012 3rd IEEE PES Innovative Smart Grid Technologies Europe (ISGT Europe)*, pages 1–8. IEEE, 2012.

- C. O'Dwyer, R. Duignan, and M. O'Malley. Modeling demand response in the residential sector for the provision of reserves. In *2012 IEEE Power and Energy Society General Meeting*, pages 1–8. IEEE, 2012.
- B. W. Olesen. Lecture 2c on floor heating, 2009.
- OpenEI. Hourly energy emission factors for electricity generation in the united states, 2011. URL <http://en.openei.org/datasets/dataset/hourly-energy-emission-factors-for-electricity-generation-in-the-united-states>.
- S. N. Palacio, K. F. Valentine, M. Wong, and K. M. Zhang. Reducing power system costs with thermal energy storage. *Applied Energy*, 129:228–237, 2014.
- P. Palensky and D. Dietrich. Demand side management: Demand response, intelligent energy systems, and smart loads. *IEEE transactions on industrial informatics*, 7(3):381–388, 2011.
- D. Papadaskalopoulos and G. Strbac. Decentralized participation of flexible demand in electricity markets—part i: Market mechanism. *IEEE Transactions on Power Systems*, 28(4):3658–3666, 2013.
- D. Papadaskalopoulos, G. Strbac, P. Mancarella, M. Aunedi, and V. Stanojevic. Decentralized participation of flexible demand in electricity markets—part ii: Application with electric vehicles and heat pump systems. *IEEE Transactions on Power Systems*, 28(4):3667–3674, 2013.
- G. Papaefthymiou, B. Hasche, and C. Nabe. Potential of heat pumps for demand side management and wind power integration in the german electricity market. *IEEE Transactions on Sustainable Energy*, 3(4):636–642, 2012.
- D. Patteeuw and L. Helsen. Residential buildings with heat pumps, a verified bottom-up model for demand side management studies. In *9th International Conference on System Simulation in Buildings*, 2014.
- D. Patteeuw, K. Bruninx, A. Arteconi, E. Delarue, W. D'haeseleer, and L. Helsen. Integrated modeling of active demand response with electric heating systems coupled to thermal energy storage systems. *Applied Energy*, 151:306–319, 2015a.
- D. Patteeuw, G. Reynders, K. Bruninx, C. Protopapadaki, E. Delarue, W. D'haeseleer, D. Saelens, and L. Helsen. CO₂-abatement cost of residential heat pumps with active demand response: demand- and supply-side effects. *Applied Energy*, 156:490–501, 2015b.
- G. S. Pavlak, G. P. Henze, and V. J. Cushing. Optimizing commercial building participation in energy and ancillary service markets. *Energy and Buildings*, 81:115–126, 2014.
- G. S. Pavlak, G. P. Henze, and V. J. Cushing. Evaluating synergistic effect of optimally controlling commercial building thermal mass portfolios. *Energy*, 84:161–176, 2015.
- S. Quoilin, K. Kavvadias, A. Mercier, I. Pappone, and A. Zucker. Quantifying self-consumption linked to solar home battery systems: Statistical analysis and economic assessment. *Applied Energy*, 182:58–67, 2016.
- G. Reynders, T. Nuytten, and D. Saelens. Potential of structural thermal mass for demand-side management in dwellings. *Building and Environment*, 64:187–199, 2013a.

- G. Reynders, T. Nuytten, and D. Saelens. Robustness of reduced-order models for prediction and simulation of the thermal behavior of dwellings. In *Proceedings of BS2013: 13th conference of international building performance simulation association, Chambéry, France*, 2013b.
- P. Rivière. *Performances saisonnières des groupes de production d'eau glacée*. PhD thesis, École Nationale Supérieure des Mines de Paris, 2004.
- A. Rudd. Expert Meeting: Recommended Approaches to Humidity Control in High Performance Homes, 2013.
- Sia Partner. The belgian electricity market: overview, analysis of today's issues and suggestions to fix it. Technical report, 2013.
- D. Six, J. Desmedt, D. Vahnoudt, and J. Bael. Exploring the flexibility potential of residential heat pumps combined with thermal energy storage for smart grids. In *21th International Conference on Electricity Distribution, Paper*, volume 442, 2011a.
- D. Six, J. Desmedt, D. Vahnoudt, and J. Bael. Exploring the flexibility potential of residential heat pumps combined with thermal energy storage for smart grids. In *21th International Conference on Electricity Distribution*, volume 442, 2011b.
- S. Stinner, R. Streblow, and D. Muller. Operation flexibility of building energy systems with thermal storages. In *Building simulation Conference 2015*, 2015.
- P. Stratmann. Ways to trigger demand side flexibility: a case example for dynamic pricing. Technical report, European Sustainable Energy Week, Brussels, 2014.
- G. Strbac. Demand side management: Benefits and challenges. *Energy policy*, 36(12):4419–4426, 2008.
- G. Strbac, C. K. Gan, M. Aunedi, V. Stanojevic, P. Djapic, J. Dejvises, P. Mancarella, A. Hawkes, D. Pudjianto, S. Le Vine, et al. Benefits of advanced smart metering for demand response based control of distribution networks. *ENA/SEDG/Imperial College report on Benefits of Advanced Smart Metering (Energy Networks Association)*, 2010.
- Synergrid. Synthetic load profiles. Technical report, 2012. URL <http://www.synergrid.be/index.cfm?PageID=16896>.
- T. Tran, K. Ling, and J. M. Maciejowski. Economic model predictive control-a review. In *Proceedings of International Symposium on Automation and Robotics in Construction*, pages 9–11, 2014.
- U.S. Department of Energy (DOE). Photovoltaic system pricing trends historical, recent, and near-term projections, 2014.
- U.S. Energy Information Administration (EIA). Policies for compensating behind-the-meter generation vary by state, 2012.
- U.S. Energy Information Administration (EIA). 2013 retail power marketers sales- residential, 2013. URL http://www.eia.gov/electricity/sales_revenue_price.
- J. Van Roy, R. Salenbien, D. Vanhoudt, J. Desmedt, and J. Driesen. Thermal and electrical cover factors: Definition and application for net-zero energy buildings. 2013.

- D. Vanhoudt. Lab test results of an active controlled heat pump with thermal energy storage for optimal integration of renewable energy. In *International renewable energy storage conference*, pages 12–14, 2012.
- N. Venkatesan, J. Solanki, and S. K. Solanki. Residential demand response model and impact on voltage profile and losses of an electric distribution network. *Applied energy*, 96:84–91, 2012.
- C. Verhelst, F. Logist, J. Van Impe, and L. Helsen. Study of the optimal control problem formulation for modulating air-to-water heat pumps connected to a residential floor heating system. *Energy and Buildings*, 45:43–53, 2012.
- P. Vinter. Dong energy—towards the intelligent utility network. In *CIREN Seminar on Smart Grids for Distribution*, pages 1–4. IET, 2008.
- V. Vittal. The impact of renewable resources on the performance and reliability of the electricity grid. *The Bridge*, 40(1):5–12, 2010.
- E. Vrettos, K. Lai, F. Oldewurtel, and G. Andersson. Predictive control of buildings for demand response with dynamic day-ahead and real-time prices. In *European Control Conference (ECC), Zürich, Switzerland*, 2013.
- D. Wang, S. Parkinson, W. Miao, H. Jia, C. Crawford, and N. Djilali. Online voltage security assessment considering comfort-constrained demand response control of distributed heat pump systems. *Applied Energy*, 96:104–114, 2012.
- D. Wang, S. Parkinson, W. Miao, H. Jia, C. Crawford, and N. Djilali. Hierarchical market integration of responsive loads as spinning reserve. *Applied energy*, 104:229–238, 2013.
- P. Wang, J. Huang, Y. Ding, P. Loh, and L. Goel. Demand side load management of smart grids using intelligent trading/metering/billing system. In *2011 IEEE PowerTech*, pages 1–6. IEEE, 2011.
- S. Weitemeyer, D. Kleinhans, T. Vogt, and C. Agert. Integration of renewable energy sources in future power systems: The role of storage. *Renewable Energy*, 75:14–20, 2015.
- J. Widén, E. Wäckelgård, and P. D. Lund. Options for improving the load matching capability of distributed photovoltaics: Methodology and application to high-latitude data. *Solar Energy*, 83(11):1953–1966, 2009.
- J. H. Yoon, R. Baldick, and A. Novoselac. Dynamic demand response controller based on real-time retail price for residential buildings. *IEEE Transactions on Smart Grid*, 5(1):121–129, 2014.
- J. Zapata Riveros. *Facilitating the integration of renewable energy through combined-heat-and-power flexibility*. PhD thesis, KU Leuven, 2015.
- Y. Zhang and G. Augenbroe. Right-sizing a residential photovoltaic system under the influence of demand response programs and in the presence of system uncertainties. In *Building simulation*, 2014.

Annexes

A.1 Chapter 2 - Additional material

The wall composition for each age class of the tree-structure presented in Chapter 2 are provided in Figure A.1.1. U-values and thermal capacitances are listed in Figure A.1.2.

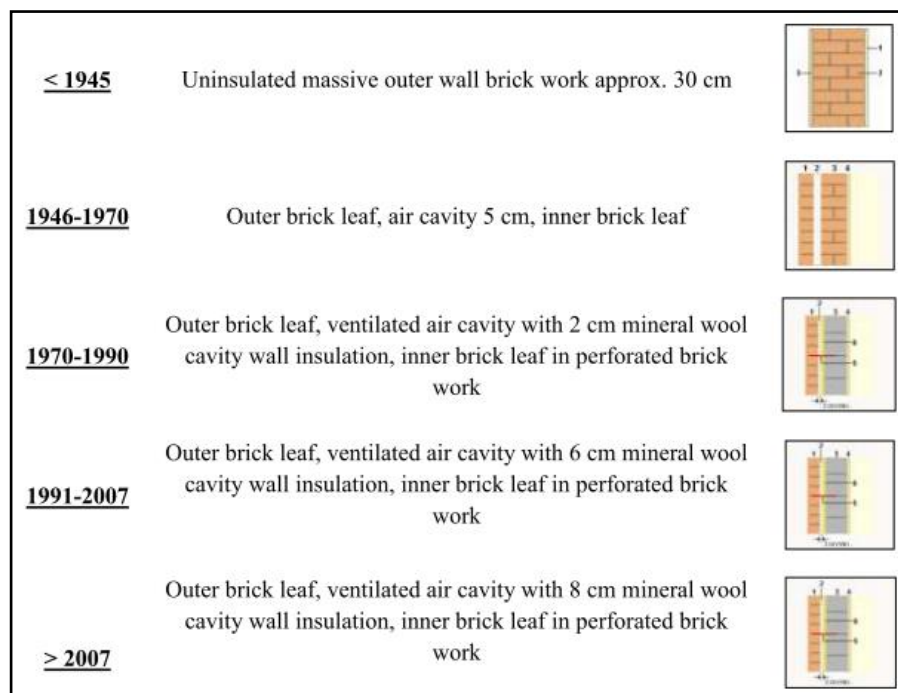


Figure A.1.1 – Wall composition per age class.

For thermal bridges, Janssens et al. (2007) conducted a study on the development of limits for the linear thermal transmittance of thermal bridges in buildings. They provided typical U-values increase to be added to the average thermal transmittance per type of dwelling for Belgium. The following assumptions are made to apply them to the different buildings:

- For buildings with totally uninsulated walls (before 1970) thermal bridging were not taken into account.
- For retrofitted buildings, values of 0.15, 0.10, 0.08 and 0.07 W/m^2K were applied respectively for apartments, terraced houses, semi-detached houses and detached houses.

A.1. Chapter 2 - Additional material

Conduction coefficient of heat transmission		U_{wall} [W/m ² K]		$U_{windows}$ [W/m ² K]		U_{roof} [W/m ² K]		U_{floor} [W/m ² K]		U_{door} [W/m ² K]
		NI**	WI**	NI	WI	NI	WI	NI	WI	Mean
Insulation										
Source		Tabula (value before renovation), LEHR (added insulation thickness for renovated elements of houses constructed before 1990), EPB 2010 (for renovated elements of houses constructed after 1990)								
YOC*	< 1945	2.25	0.59	5	2.75	4.15	0.44	3.38	0.77	3.3 3.3
	45-70	1.56	0.53	5	2.75	3.33	0.43	3.38	0.77	3.3
	70-90	0.98	0.44	3.5	2.75	0.77	0.3	1.14	0.43	3.3
	90-07	0.49	0.4	3.5	2	0.43	0.3	0.73	0.4	3.3
	> 08	0.4		2		0.3		0.4		3.3

* YOC: year of construction

** NI/WI: not insulated/with insulation

Capacity		K_{wall} [kJ/m ² -K]		K_{roof} [kJ/m ² -K]		K_{floor} [kJ/m ² -K]	
		NI	WI	NI	WI	NI	WI
Insulation							
Source		Tabula (wall composition), LEHR (added insulation thickness for renovated elements of houses constructed before 1990)					
YOC	< 1945	453.6	472.1	30.9	43.8	235.2	236.4
	1945-1970	483.9	502.4	42.6	55.5	235.2	236.4
	1970-1990	394.2	412.7	44.7	57.5	347.5	348.7
	1990-2007	396.2	414.8	46.7	50.9	348.1	349.2
	> 2008	397.3		50.3		348.4	

Figure A.1.2 – Coefficient of heat transmission and thermal capacitance.

- For buildings built or retrofitted after 2012, values of 0.04, 0.02, 0.01 and 0.005 W/m^2K were applied respectively for apartments, terraced houses, semi-detached houses and detached houses.

Infiltration rates were imposed to those provided in Cyx et al. (2011), and shown in Figure A.1.3.

Infiltration rate at 50Pa [m ³ /hm ²]					
Initial walls					Walls insulated after retrofit
Time period	Freestanding house	Semi-detached house	Terraced house	Apartment	All type
<1971	18	18	14.9	14.9	6
1971-1990	17.1	16.3	14.1	14.1	6
1991-2007	12	12	10	10	6
2008-2002	6.1	6.3	6	6	6
>2012	/	/	/	/	2.5

Figure A.1.3 – Infiltration rates.

A.2 Chapter 3 - Model Identification

For the multi-zone dynamic building model proposed by Masy (2008), the parameters identification process is based on the admittance method, first presented by Loudon (1968). The admittance of a wall is defined as its capacity to store and restore energy over a 24h cycle and can be expressed as the ratio of the heat flux variation over the temperature variation over that period. The identification process depends on the boundary conditions:

- For isothermal boundary conditions, Masy (2008) defines the wall isothermal transmittance (K_T) and admittance (A_T) respectively as "the ratio of the indoor side heat flux variation to the outdoor side temperature variation for a constant indoor temperature" and "the ratio of the indoor side heat flux variation to the indoor side temperature variation for a constant outdoor temperature", for a given solicitation period. They can be expressed as functions of the lumped thermal resistance and capacitance of the wall as follows:

$$K_T = \frac{1}{(1-\theta)R + \theta R + \theta(1-\theta)R^2\phi C j\omega} \quad (\text{A.1})$$

$$A_T = -\frac{1 + (1-\theta)R\phi C j\omega}{(1-\theta)R + \theta R + \theta(1-\theta)R^2\phi C j\omega} \quad (\text{A.2})$$

The parameters are tuned to reproduce the magnitude of the isothermal admittance and transmittance over the 24h period.

- For boundary with imposed heat flux, the adiabatic admittance is defined as the ratio of the indoor side heat flux variation to the indoor-side temperature variation for an imposed outdoor-side heat flux and for a given solicitation period. It can be expressed as

$$A_q = -\frac{\phi C j\omega}{1 + \theta R\phi C j\omega} \quad (\text{A.3})$$

The parameters are tuned to reproduce the magnitude and angle of the adiabatic admittance computed for the 24h period.

Further details regarding the identification method can be found in the work of Masy (2008) and Ngendakumana and Liebecq (1986).

A.3 Chapter 4

A.3.1 2030 cost scenario - Energy mix and RES share

The high cost levels observed at night on the RTP2030 price curve in Figure 4.1b can be partly explained by the significant share of solar energy considered in the energy mix, as shown in Figure A.3.1, and by a possible suboptimal planning of maintenance operations (CEEME (2015)).

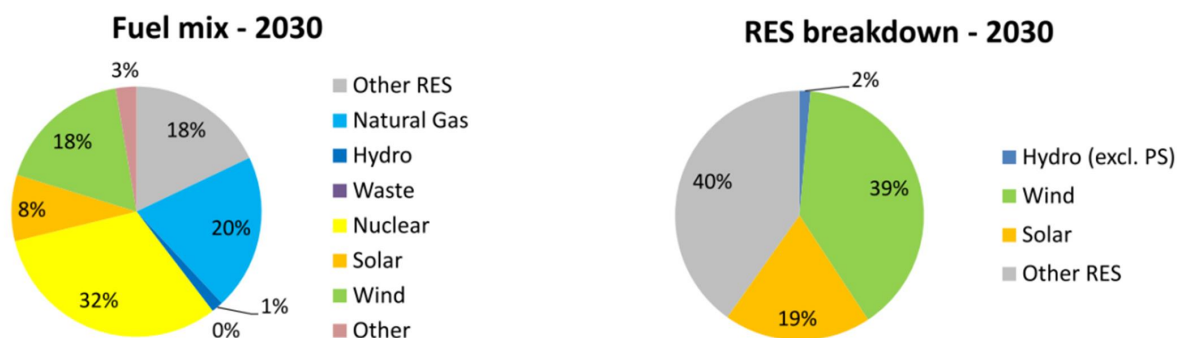


Figure A.3.1 – 2030 prospective scenario (CEEME (2015)): energy mix and breakdown of renewable energy sources (RES).

A.3.2 Dialog Matlab – Dymola

The dialog framework set up between *Matlab* and *Dymola* is performed using *dymosim* executable file. The latter is generated by Dymola and allows to perform continuous simulations with the model implemented in Dymola in different environments (Dynasim AB).

To simulate the system in Matlab using *dymosim.exe*, one can resort to the *dymosim.m* function and to the file *alist.exe*, provided with the Dymola "Mfiles":

```
[s, n]= dymosim(exp,x0,p)
with
exp[1,1]= StartTime
exp[1,2]= StopTime
exp[1,3]= Communication step size OR
exp[1,4]= Number of communication intervals
exp[1,5]= Relative scalar tolerance
exp[1,6]= Integration algorithm
x0: Initial values of states
p: Actual values of parameters
```

The simulation requires two input files, *dsin.txt* containing variables and parameters, as well as *dsu.txt* containing the input signals for a model with external inputs.

The following command lines help create those input files and retrieve results for the continuous simulation:

```
dymosim - i :
generates Dymosim input file - dsin.txt
```

```
!alist - b name.txt name :
writes in Matlab binary format
```

```
tsave('name', s, n) :
saves the numeric matrix "s" and the string-matrix "n" as trajectory on file "name.mat".
```

```
!alist - a name name.txt :
writes in ASCII format (default)
```

A.4 Chapter 5 - Parametric studies for the U.S.

Several parameters are likely to influence the results obtained in Chapter 5, such as system investment costs, retail electricity tariffs and electricity production mix. For example, significant differences exist between the different zones of the US. Average retail tariffs range from 0.069 to 0.34 \$/kWh (U.S. Energy Information Administration (EIA) (2013)). The impact of the buy-back ratio on the system pay-back time decreases with the increase in retail tariff and new optimal load coverage can be determined. Average CO₂ emissions in the U.S. vary between 369 to 789 kg/MWh of produced electricity (OpenEI (2011)). Depending on the electricity production mix, overconsumption entailed by load shifting may counterbalance reductions in emissions by increased on-site consumption of renewable energy. Projections regarding PV installation cost reach 1.5\$ per watt peak (U.S. Department of Energy (DOE) (2014)) and battery cost of 137\$/kWh (Brinsmead et al. (2015)) by 2035. Conclusions regarding the economic viability of thermal and electrical storage will be impacted.

In that regard, further analysis with thermal storage is carried out for different climate zones in the U.S, defined in International Code Council (ICC) (2009).

Climate zone characteristics in terms of retail electricity price, heating degree days (HDD) and sun irradiation are summarized in Table A.4.1. The same house geometry is considered, but insulation levels are adapted to the different locations, as detailed in (Holloway (2013)). To avoid system oversizing (Mitchell and Braun (2013), HVAC systems are sized using average maximum values provided in the “Climatic design information” of the ASHRAE Handbook of Fundamentals (American society of heating, refrigerating and air-conditioning engineers (ASHRAE) (2013)). For zones 2 to 5, the rated capacity in heating is obtained from its equivalent in cooling. For zone 1, the need for a heating system occurs very occasionally, and it seems more suitable to install a simple air-conditioning unit and an electric heater rather than a reversible heat pump. For zone 6, the design rated capacities are computed in heating mode. Rated capacities and auxiliary heater powers are summarized in Table A.4.2.

Table A.4.1 – Climate zones - electricity price, annual heating degree days and solar irradiation.

Zone	State	City	Electricity price (U.S. EIA 2013) [c\$/kWh]	HDD18.3	Solar irradiation		
					σ [W/m ²]	μ [W/m ²]	RSD* μ/σ
Zone 1	Hawaii	Honolulu	36.98	0	184	259	1.4
Zone 2	Texas	Houston	11.35	807	164	246	1.5
Zone 3	California	Bakersfield	16.19	1164	200	296	1.5
Zone 4	Washington	Seattle	8.7	2614	133	221	1.7
Zone 5	Indiana	Indianapolis	11.07	2929	160	242	1.5
Zone 6	Minnesota	Minneapolis	11.81	4151	151	234	1.5

*RSD – relative standard deviation

Figure A.4.1 shows the breakdown of annual electricity consumption for each climate zone. As expected, the share in consumption related to heating needs increases from zone 1 to zone 6. The electricity consumption for cooling represents 19 to 41% of the annual consumption for zone 3 to zone 1 and is the lowest for zone 4. Electricity consumption for DHW production varies between 20 and 30% of the annual consumption for all zones. This breakdown of the consumption is a key for a correct

Table A.4.2 – Design rated heating and cooling capacities.

City	Heating [kW]	Auxiliary heater [kW]	Cooling [kW]
Honolulu	10.8	1.5	10.4
Houston	12.5	1.5	12.1
Bakersfield	12.1	0.0	11.7
Seattle	7.4	3.0	7.2
Indianapolis	11.7	5.0	11.3
Minneapolis	26.0	5.0	25.1

interpretation of the following results.

Figure A.4.2 illustrates the evolution of the supply cover factor with the buy-back ratio for the different climate zones. For each zone, the PV system is sized to cover 50% of the annual electricity consumption.

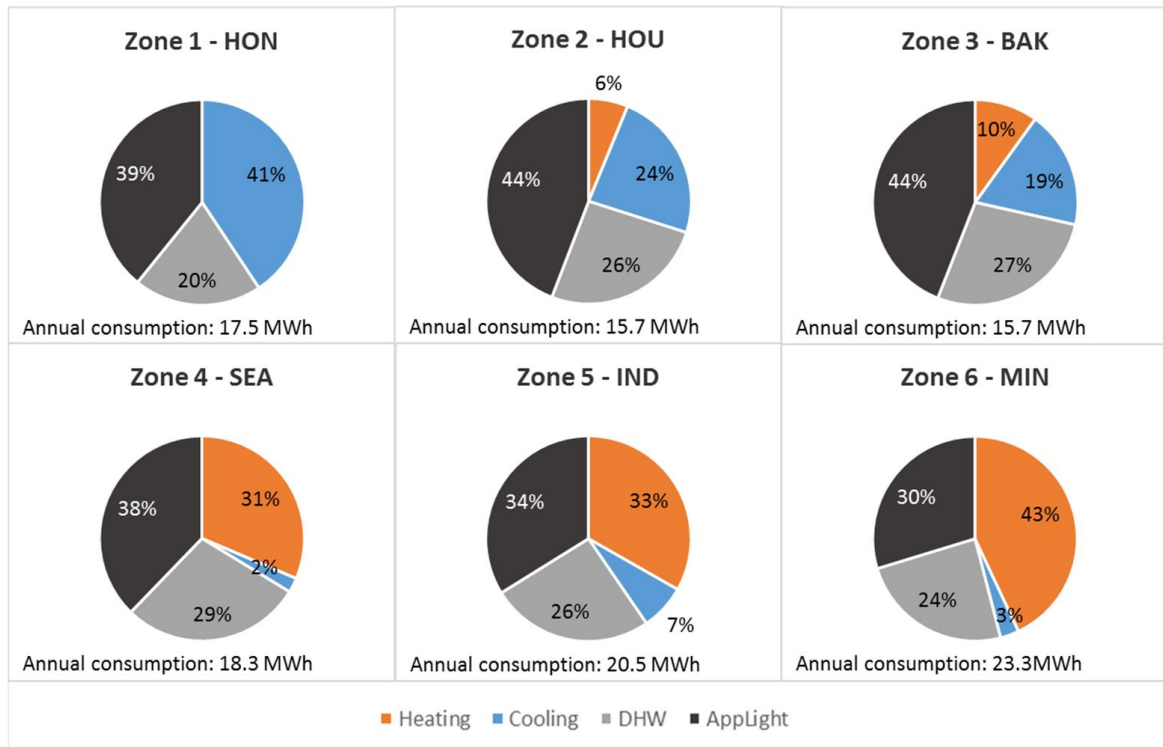


Figure A.4.1 – Breakdown of annual electricity consumption.

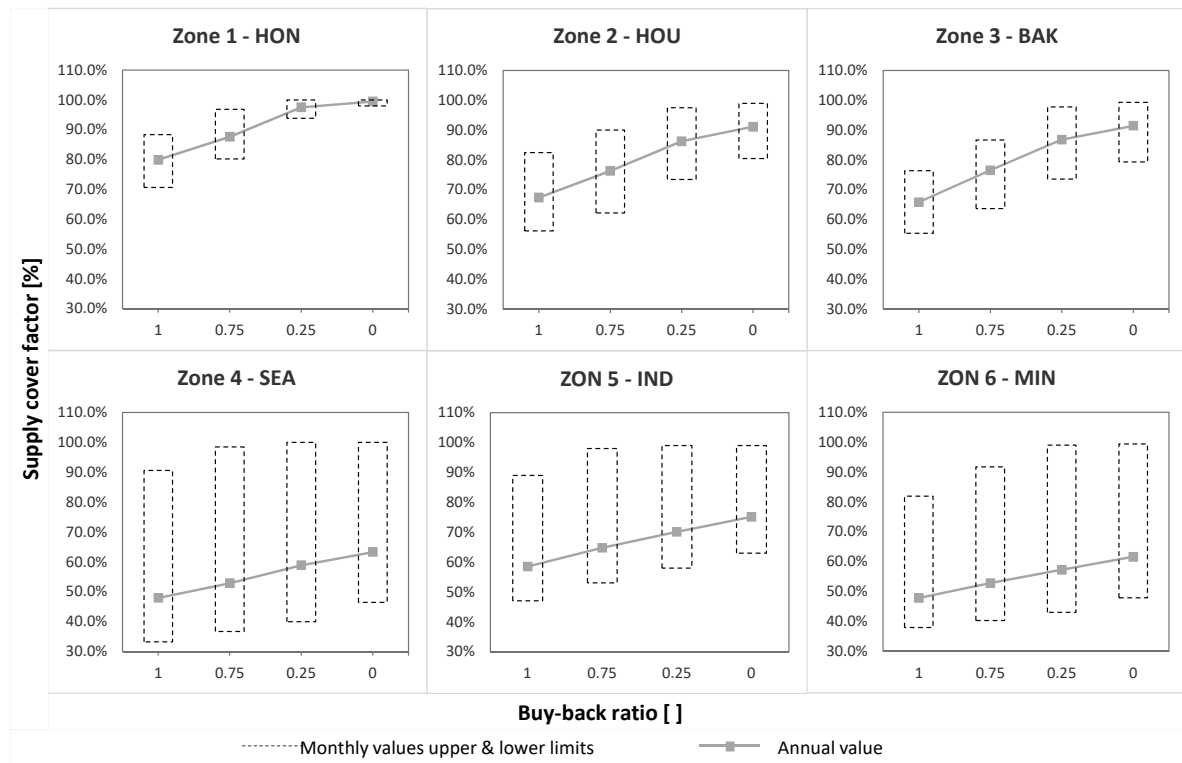


Figure A.4.2 – Evolution of the supply cover factor with the buy-back ratio for all climate zones for 50% annual load coverage by PV panels.

For each buy-back ratio, the square marker corresponds to the value of supply cover factor calculated on a yearly basis, whereas the dashed box represents the range of variation for monthly values. For zone 1, the annual supply cover factor increases by 20% when reducing the buy-back ratio from 1 to 0. For a buy-back ratio close to zero, almost all monthly supply cover factors converge to 100%. The reasons for that lie in the fact that Honolulu has a relatively small temperature variation as well as a quite homogenous PV production throughout the year, as indicated by the low relative standard deviation (RSD) of solar irradiation (Table A.4.1). Cooling needs therefore naturally tend to coincide with PV production. The trends observed for zone 2 and 3 are similar and the annual increase in supply cover factor reaches up to 25%. As opposed to zone 1 to 3 for which the monthly variation in supply cover factor values remain within 10% of the average annual value, zone 4 has the widest variation throughout the year. This can be explained by the large RSD for solar irradiation, and the small cooling demand. Indeed, in the summer, load matching is achieved mostly through DHW production, whose potential for load flexibility is limited by the size of the tank, its high level of insulation and the fixed daily hot water consumption. In the winter, contrarily, the load matching potential comes primarily from the flexible space heating load, which in itself accounts for 31% of the annual electricity demand. For zone 4 to zone 6, increases in annual supply cover factors of around 15% can be reached when reducing the buy-back ratio from 1 to 0.

Although reducing the buy-back ratio seems to be a suitable incentive to promote load matching between the household electricity consumption and the on-site PV production, it also causes the pay-back time of the PV system to increase. The optimal PV sizing method illustrated in Section

5.4.4 is here generalized to the different climate zones. Figure A.4.3 indicates the optimal sizing of the PV system for given buy-back ratios. Two cases are distinguished: the non-optimized response, corresponding to a set-point driven conventional control (RBC) of the system and the optimal response (OPC), where load matching results from the optimal predictive scheme. For zone 1 and zone 3, load coverage larger than 100% of the annual electricity consumption can be achieved regardless of the buy-back ratio with both RBC and OPC load management strategies. In the case of zone 1, this is due to the combined effects of a high electricity retail price, large annual PV production per installed square meter, and significant load matching potential, as discussed above. A similar explanation can be given for zone 3. For zone 2, differences in results between RBC and OPC can be observed. Indeed, with RBC, an optimal load coverage less than 100% is obtained for a buy-back ratio below 0.5, whereas, it is only observed for buy-back ratios below 0.25 in the case of OPC. For a buy-back ratio close to 0, an optimal load control allows a doubling of the optimal installed PV capacity compared to RBC. Zone 4 has the lowest PV production per installed square meter and the lowest electricity retail price. Therefore, installing PV panels without optimizing the electricity consumption to match the on-site production does not ensure return on investment over the lifetime of the system. With optimal load management, optimal load coverage of 30 to 80% can be reached. For zone 6, optimal load coverages of less than 100% are observed for buy-back ratios below 0.5. In that case, the OPC strategy allows to increase the optimal load coverage by PV from 33 to 90%.

Load matching through load shifting entails overconsumption of 3 to 9 percent depending on the climate zone. One should ensure that benefits in terms of reduction of CO₂ emissions are still retrieved. Table A.4.3 presents the average CO₂ emissions for electricity generation per zone and the annual emissions for domestic consumption, per house, with conventional control.

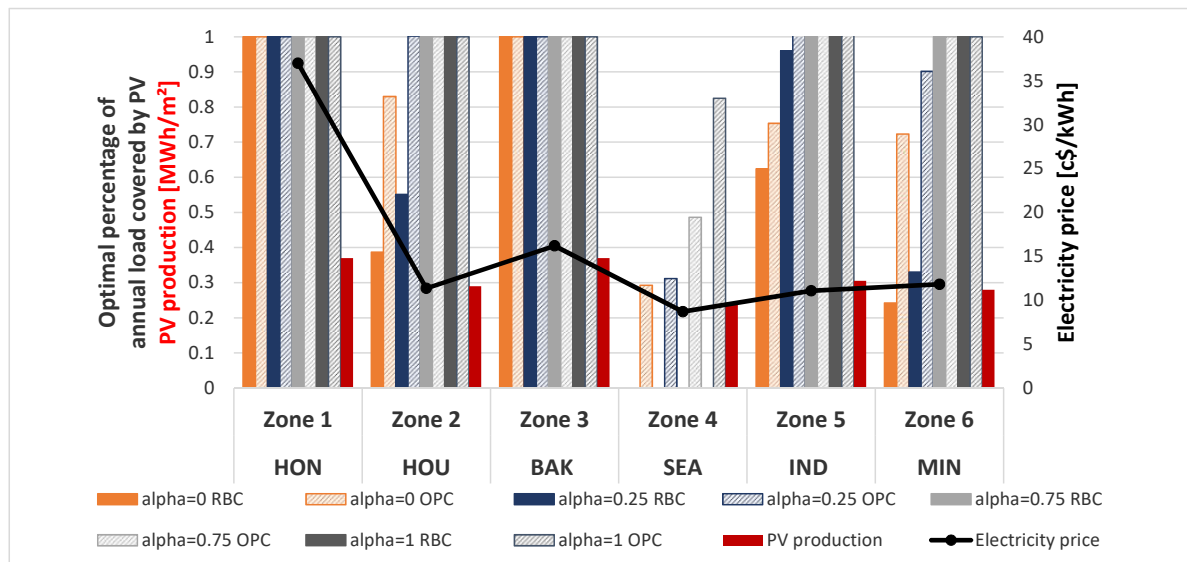


Figure A.4.3 – Optimal load cover factor by PV panels for different buy-back ratios per climate zone with conventional control (RBC) and optimal predictive control (OPC).

Table A.4.3 – Electricity generation – average CO₂ emissions per MWh (OpenEI (2011)). Domestic electricity consumption – annual CO₂ emissions.

	Zone 1	Zone 2	Zone 3	Zone 4	Zone 5	Zone 6
Electricity generation: CO ₂ emissions [kg/MWh]	727	578	369	395	758	789
Domestic consumption: Annual CO ₂ emissions [t] per house with 50% load load coverage by PV (RBC)	8.2	6.3	4.5	5.5	11.4	14.3

Figure A.4.4 illustrates the additional reduction in CO₂ emissions that can be achieved with OPC compared to RBC. For a fixed installed capacity of the PV panels, reduction in CO₂ emissions tends to decrease with decreasing buy-back ratios, but remains greater than zero. The steepness of the decrease is directly linked to overconsumption. The latter tends to increase for lower buy-back ratios, since larger heat transfer losses occur and the system may operate in less favorable conditions. For a fixed buy-back ratio, the reduction decreases with increasing size of PV system, since the supply cover factor tends to decrease. For zone 1, however, a maximum exists for about 50% load coverage since below this value and regardless of the buy-back ratio, the annual supply cover factor tends to 100%. Reductions in CO₂ emissions are largest in zone 2, 5 and 6, due to higher CO₂ emissions inherent within the electricity generation mix. Although this number is high for Honolulu as well, the combined effects of large overconsumption (up to 8%) and inherently high supply cover factors limit the effect on CO₂ emissions reduction.

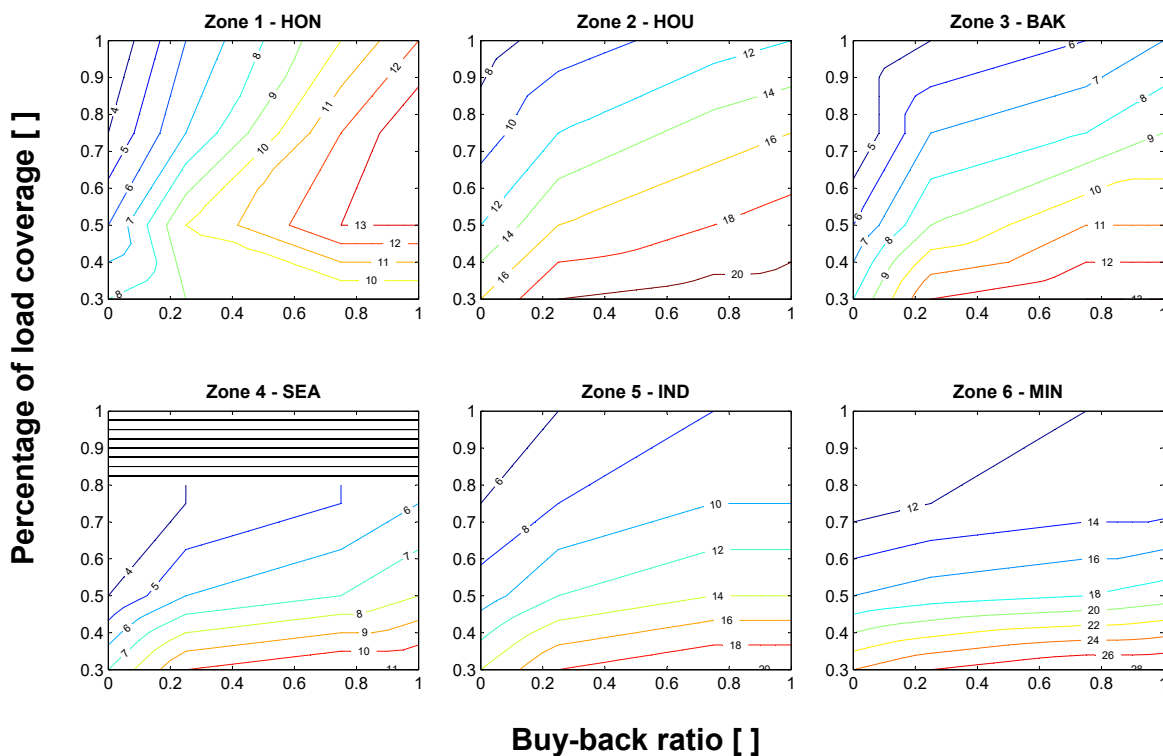


Figure A.4.4 – Additional CO₂ emissions avoided, in kilogram per installed square meter of PV panels, with OPC compared to RBC.

A.5 Chapter 6 - additional results

Table A.5.1 – Influence of the delay and payback lengths on deviations following an activation for January 24th 2012 for 100 houses.

(a) Upward activations.

		Activated volume [kWh] / Deviation [kWh]						
		k						
		1	2	3	4	5	6	7
1	0	1.09	0.68	0.73	0.68	0.63	0.64	0.62
	1	1.09	1.04	0.78	0.80	0.54	0.48	0.49
	2	1.11	1.10	0.74	0.84	0.84	0.52	0.43
	3	1.14	1.15	0.78	0.89	0.93	0.51	0.39
	4	1.14	1.18	0.83	0.93	0.97	0.50	0.43
	5	1.16	1.20	0.88	0.96	0.98	0.81	0.44
	6	1.18	1.19	1.05	0.98	1.02	0.90	0.44
	7	1.23	1.21	1.15	1.00	1.04	0.99	0.45
	8	1.21	1.22	1.16	1.02	1.06	1.04	0.46

(b) Downward activations.

		Activated volume [kWh] / Deviation [kWh]						
		k						
		1	2	3	4	5	6	7
1	0	1.04	0.98	0.39	0.46	0.36	0.35	0.35
	1	1.06	0.93	0.72	0.46	0.49	0.29	0.31
	2	1.05	0.93	0.76	0.47	0.50	0.51	0.29
	3	1.05	0.98	0.77	0.48	0.51	0.52	0.27
	4	1.07	0.98	0.79	0.50	0.53	0.54	0.52
	5	1.07	0.93	0.74	0.52	0.53	0.54	0.53
	6	1.05	0.89	0.76	0.53	0.55	0.56	0.54
	7	1.23	1.21	1.15	1.00	1.04	0.99	0.55
	8	1.21	1.22	1.16	1.02	1.06	1.04	0.57

Table A.5.2 – Influence of the delay and payback lengths on overconsumption due to the activation of the flexibility service for January 24th 2012 for 100 houses.

(a) Upward activations

		Overconsumption [kWh] / Activated volume [kWh]						
		k						
l		1	2	3	4	5	6	7
	0	0.08	0.39	0.37	0.41	0.44	0.43	0.43
	1	0.09	0.15	0.34	0.33	0.48	0.54	0.52
	2	0.10	0.16	0.35	0.31	0.30	0.48	0.57
	3	0.13	0.17	0.33	0.30	0.29	0.50	0.62
	4	0.12	0.18	0.32	0.30	0.30	0.52	0.58
	5	0.14	0.20	0.32	0.31	0.32	0.35	0.58
	6	0.15	0.22	0.29	0.32	0.33	0.35	0.59
	7	0.19	0.24	0.30	0.35	0.35	0.37	0.60
	8	0.17	0.26	0.32	0.36	0.36	0.37	0.61

(b) Downward activations

		Overconsumption [kWh] / Activated volume [kWh]						
		k						
l		1	2	3	4	5	6	7
	0	-0.04	0.02	0.63	0.54	0.69	0.72	0.72
	1	-0.05	0.07	0.17	0.51	0.48	0.83	0.79
	2	-0.05	0.07	0.21	0.51	0.49	0.50	0.84
	3	-0.05	0.02	0.23	0.50	0.49	0.49	0.90
	4	-0.06	0.01	0.23	0.49	0.48	0.49	0.52
	5	-0.06	0.07	0.30	0.48	0.49	0.51	0.52
	6	-0.05	0.11	0.29	0.47	0.47	0.48	0.51
	7	-0.11	0.07	0.32	0.47	0.46	0.48	0.49
	8	-0.02	0.10	0.32	0.46	0.46	0.47	0.47

Table A.5.3 – Impact of the electricity tariff structure on the minimum, mean and maximum modulation potentials for the aggregated set of one hundred houses. Modulation parameters are set to $n = 1$, $l = 0$ and $k = 5$.

(a) Upward activations

Tariff	Modulation amplitude [kW]		
	<i>min</i>	<i>mean</i>	<i>max</i>
Flat	18.4	61.3	130.1
Day/Night	9.5	107.4	342.4
Dynamic	0	78.2	315.3

(b) Downward activations

Tariff	Modulation amplitude [kW]		
	<i>min</i>	<i>mean</i>	<i>max</i>
Flat	0	15.7	84.3
Day/Night	0	43.9	198.7
Dynamic	0	37.8	211.8

A.6 Recall on linear programming

A.6.1 Duality in linear programming

A linear programming problem consists in a problem that aims at maximizing or minimizing a linear function subject to linear constraints. The function to maximize/minimize is referred to as the *cost function* or *objective function*.

The generalized form of the maximization problem can be written as

$$\max \mathbf{c}^T \mathbf{x} \quad (\text{A.4a})$$

subject to constraints

$$\mathbf{Ax} \leq \mathbf{b} \quad (\text{A.4b})$$

$$\mathbf{x} \geq 0 \quad (\text{A.4c})$$

The dual problem of the generalized maximization problem is

$$\min \mathbf{b}^T \mathbf{y} \quad (\text{A.5a})$$

subject to constraints

$$\mathbf{A}^T \mathbf{y} \geq \mathbf{c} \quad (\text{A.5b})$$

$$\mathbf{y} \geq 0 \quad (\text{A.5c})$$

The *duality theorem* states that if x is feasible for the primal, and y is feasible for the dual,

$$\mathbf{c}^T \mathbf{x} \leq \mathbf{b}^T \mathbf{y} \quad (\text{A.6})$$

and that, if one of the primal or dual has a finite optimum, they both do, and both optima are identical.

In addition, the *complimentary slackness theorem* states that, assuming x and y to be the feasible solutions of the primal and dual problems, respectively, then

1. If $x_j > 0$, then the j th constraint in the dual problem is binding,
2. If the j th constraint in the dual is not binding, then $x_j = 0$,
3. If $y_i > 0$, then the i th constraint in the primal is binding,
4. If the i th constraint in the primal is not binding, then $y_i = 0$.

These relations can make the resolution of one problem straightforward to obtain from its complementary problem.

Dual variables provide useful information regarding the primal problem. They are also referred to as

dual prices or shadow prices. The *shadow price* of a constraint can be interpreted as a measure of the improvement in the objective function if the constraint is relaxed by one unit.

A.6.2 Solving linear programs

The solver used in this work is Cplex (ILOG (2013)). Among others, this solver can handle linear, quadratic and mixed-integer programming problems. To solve linear problems, Cplex uses the *Simplex* algorithm. The latter is a robust and self-initiating method that can solve any feasible linear program.

The method solves both primal and dual problems. There are several underlying reasons to that:

- the dual provides useful information on the primal problem, such as the shadow price,
- it is sometimes easier to find an initial feasible point for the dual problem,
- the dual problem might be easier to solve, for example in the case of a primal problem with a large amount of constraints but few variables.

A.7 Electronic annex

Example of codes developed in this thesis will be made available at

https://github.com/EmelineGeorges/PhDthesis_code

Curriculum Vitae

Emeline Georges

EDUCATION PhD candidate, University of Liège

Topic: Modulation Strategies of Residential HVAC Systems for Demand Side Management

Master of Science in Electromechanical Engineering, University of Liège, June 2012

Specialization: Energy Systems

Topic: Organic Rankine Cycle Systems

Bachelor of Science in Chemical Engineering, Mechanical Engineering minor, University of Liège, June 2010

RESEARCH EXPERIENCE

Applied Thermodynamics, University of Liège – FNRS PhD candidate

Liège, Belgium
Oct 2013 – Present

Ray W. Herrick Laboratories, Purdue University, USA – Visiting Scholar

West-Lafayette, IN,
USA
Feb - Oct 2014

Applied Thermodynamics, University of Liège – Teaching Assistant

Liège, Belgium
Oct 2012 – Sep 2013

Ray W. Herrick Laboratories, Purdue University, USA – Visiting Scholar

West-Lafayette, IN,
USA
Feb - Jul 2012

List of Publications

Legend

Bibliometric indicators linked to the journal (for those whose ISSN has been indicated by the author)

• **IF = Impact factor** Thomson ISI. Are indicated : IF of the year of publication and IF of the last edition of JCR (**last**), « ? » if not known by ORBi yet ; « - » if non-existent.

• **IF5** : idem as IF but for a 5 year period (new indicator since 2009).

• **EigenF = EigenFactor** (see : <http://www.eigenfactor.org/>).

• **Article Infl. = Article Influence** : EigenFactor divided by the number of articles published in the journal.

→ More information ? <http://orbi.ulg.ac.be/rpt#rev>

Bibliometric indicators linked to the article


• **ORBi viewed** = total number of visualizations of a reference on ORBi (of which X internally within the ULg).


• **ORBi downloaded** = total number of downloads of the full text via ORBi, including requests copy.

• **SCOPUS®** = number of citations picked up by SCOPUS®.

→ More information ? <http://orbi.ulg.ac.be/rpt#art>

(Warning : According to disciplines, some bibliometric indicators may not be relevant)






 etc: full text of the document available in Open Access



 etc: full text of the document available in restricted access

1. Published books, as author, co-author or editor

2. Books chapters, as author or co-author










3. Articles accepted in journals with committee (peer reviewed)

- 1)  **Georges, E.**, Cornélusse, B., Ernst, D., Lemort, V., & Mathieu, S. (2017). Residential heat pump as flexible load for direct control service with parametrized duration and rebound effect. *Applied Energy*, 187, 140-153.
<http://hdl.handle.net/2268/203636>
ORBi viewed: **277** (28 ULg) ; downloaded: **155** (11 ULg) — SCOPUS®: **0**
IF 2017: ?; last: **5.746**; IF5: **6.222** — EigenF 2017: ?; last: **0.058** — Article Infl. 2017: ?; last: **1.2**
- 2)  **Georges, E.**, Braun, J., & Lemort, V. (2016, August). A general methodology for optimal load management with distributed renewable energy generation and storage in residential housing. *Journal of Building Performance Simulation [=JBPS]*.
<http://hdl.handle.net/2268/200920>
ORBi viewed: **45** (13 ULg) ; downloaded: **13** (4 ULg) — SCOPUS®: **0**
IF 2016: ?; last: **1.807**; IF5: **2.089** — EigenF 2016: ?; last: **0.001** — Article Infl. 2016: ?; last: **0.6**
- 3)  Dumont, O., Carmo, C., **Georges, E.**, Quoilin, S., & Lemort, V. (2016). Economic assessment of electric energy storage for load shifting in positive energy building. *International Journal of Energy and Environmental Engineering*.
<http://hdl.handle.net/2268/204724>
ORBi viewed: **37** (6 ULg) ; downloaded: **9** — SCOPUS®: **0**
- 4)  Masy, G., **Georges, E.**, Verhelst, C., Andre, P., & Lemort, V. (2015). Smart Grid Energy Flexible Buildings through the use of Heat Pumps and Building Thermal Mass as Energy Storage in the Belgian context. *Science and Technology for the Built Environment*, 21(6), 800-811.
<http://hdl.handle.net/2268/185768>
ORBi viewed: **104** (19 ULg) ; downloaded: **312** (10 ULg) — SCOPUS®: **5** (3 self citations excluded)
IF 2015: -; last: -; IF5: **0.102** — EigenF: — Article Infl.:
- 5)  Bell, I., Quoilin, S., **Georges, E.**, Braun, J. E., Groll, E. A., Horton, T., & Lemort, V. (2015). A generalized moving-boundary algorithm to predict the heat transfer rate of counterflow heat exchangers for any phase configuration. *Applied Thermal Engineering*, 79.
<http://hdl.handle.net/2268/180104>
ORBi viewed: **90** (8 ULg) ; downloaded: **11** (6 ULg) — SCOPUS®: **8** (4 self citations excluded)
IF 2015: **3.043**; last: **3.043**; IF5: **3.269** — EigenF 2015: ?; last: **0.027** — Article Infl. 2015: ?; last: **0.7**

- 6) Gendebien, S., **Georges, E.**, Bertagnolio, S., & Lemort, V. (2014, December). Methodology to characterize a residential building stock using a bottom-up approach: a case study applied to Belgium. *International Journal of Sustainable Energy Planning and Management*.
 <http://hdl.handle.net/2268/178418>
 ORBi viewed: **65** (26 ULg) ; downloaded: **345** (7 ULg) — SCOPUS®: **5** (3 self citations excluded)
- 7) **Georges, E.**, Declaye, S., Dumont, O., Quoilin, S., & Lemort, V. (2013, May 12). Design of a small-scale organic Rankine cycle engine used in a solar power plant. *International Journal of Low Carbon Technologies*.
 <http://hdl.handle.net/2268/149519>
 ORBi viewed: **181** (31 ULg) ; downloaded: **539** (17 ULg) — SCOPUS®: **4** (3 self citations excluded)

4. Articles accepted in journals without committee (non-peer reviewed)

5. Articles accepted in conference proceedings

- 1) **Georges, E.**, & Lemort, V. (2016). Load modulation strategies of residential heat pumps for demand-response programs with different thermal storage options. *Proceedings of the 4th International High Performance Buildings Conference at Purdue*.
 <http://hdl.handle.net/2268/207417>
 ORBi viewed: **0** ; downloaded: **0**
- 2) **Georges, E.**, Cornélusse, B., Ernst, D., Louveaux, Q., Lemort, V., & Mathieu, S. (2016). Direct control service from residential heat pump aggregation with specified payback. *Proceedings of the 19th Power Systems Computation Conference (PSCC)*.
 <http://hdl.handle.net/2268/194522>
 ORBi viewed: **196** (31 ULg) ; downloaded: **243** (9 ULg) — SCOPUS®: **0**
- 3) **Georges, E.**, Garsoux, P., Masy, G., De Maere D'Aertrycke, G., & Lemort, V. (2016). Analysis of the flexibility of Belgian residential buildings equipped with Heat Pumps and Thermal Energy Storages. *Proceedings of CLIMA2016 Conference*.
 <http://hdl.handle.net/2268/200346>
 ORBi viewed: **36** (5 ULg) ; downloaded: **31** (3 ULg) — SCOPUS®: -
- 4) Masy, G., Rehab, I., Andre, P., **Georges, E.**, RANDAXHE, F., Lemort, V., & Lebrun, J. (2015). Lessons Learned from Heat Balance Analysis for Holzkirchen Twin Houses Experiment. *Energy Procedia*.
 <http://hdl.handle.net/2268/182956>
 ORBi viewed: **70** (20 ULg) ; downloaded: **6** (6 ULg) — SCOPUS®: **0**
- 5) **Georges, E.**, Braun, J. E., Groll, E., Horton, W. T., & Lemort, V. (2014). Impact of net metering programs on optimal load management in US residential housing - a case study. *Proceedings of 9th International Conference on System Simulation in Buildings*.
 <http://hdl.handle.net/2268/178419>
 ORBi viewed: **68** (16 ULg) ; downloaded: **432** (6 ULg) — SCOPUS®: -
- 6) **Georges, E.**, Masy, G., Verhelst, C., Andre, P., & Lemort, V. (2014). Smart Grid Energy Flexible Buildings through the use of Heat Pumps in the Belgian context. *3rd International High Performance Buildings Conference at Purdue*.
 <http://hdl.handle.net/2268/170847>
 ORBi viewed: **122** (22 ULg) ; downloaded: **79** (14 ULg) — SCOPUS®: -
- 7) **Georges, E.**, Gendebien, S., Dechesne, B., Bertagnolio, S., & Lemort, V. (2013). IMPACT OF THE INTEGRATION OF VARIOUS HEATING TECHNOLOGIES ON THE ENERGY LOAD PROFILES OF THE BELGIAN RESIDENTIAL BUILDING STOCK. *Proceedings of IRES 2013 conference*.
 <http://hdl.handle.net/2268/159588>
 ORBi viewed: **80** (26 ULg) ; downloaded: **127** (13 ULg) — SCOPUS®: -
- 8) Gendebien, S., **Georges, E.**, Prieels, L., & Lemort, V. (2013). Experimental performance characterization of a new single room ventilation device with heat recovery. *Proceedings of the 34th AIVC conference*.
 <http://hdl.handle.net/2268/156859>
 ORBi viewed: **146** (40 ULg) ; downloaded: **244** (32 ULg) — SCOPUS®: -
- 9) **Georges, E.**, Gendebien, S., Bertagnolio, S., & Lemort, V. (2013). Modeling and simulation of the domestic energy use in Belgium following a bottom-up approach. *Proceedings of the CLIMA 2013 11th REHVA World Congress & 8th International Conference on IAQVEC*.
 <http://hdl.handle.net/2268/147390>
 ORBi viewed: **260** (94 ULg) ; downloaded: **10** (10 ULg) — SCOPUS®: -

- 10) Declaye, S., **Georges, E.**, Bauduin, M., Quoilin, S., & Lemort, V. (2012). DESIGN OF A SMALL-SCALE ORGANIC RANKINE CYCLE ENGINE USED IN A SOLAR POWER PLANT. *Proceedings of Heat Powered Cycles Conference 2012*.



<http://hdl.handle.net/2268/135302>

ORBi viewed: **310** (21 ULg) ; downloaded: **11** (1 ULg) — SCOPUS®: -

6. Oral presentations in conferences with scientific selection committee

- 1) Lemort, V., **Georges, E.**, Gendebien, S., & Garsoux, P. (2016, January 26). *Evolution of the energy load profiles of the Belgian residential building stock with new heating technologies for demand side management*. Paper presented at BERA 1st Seminar on Demand Response, Brussels, Belgium.



<http://hdl.handle.net/2268/192397>

ORBi viewed: **35** (9 ULg) ; downloaded: **7** — SCOPUS®: -

- 2) Dumont, O., Carmo, C., Dickes, R., **Georges, E.**, Quoilin, S., & Lemort, V. (2016). *Hot water tanks : how to select the optimal modelling approach?* Paper presented at Conference CLIMA 2016.



<http://hdl.handle.net/2268/199778>

ORBi viewed: **37** (4 ULg) ; downloaded: **19** (1 ULg) — SCOPUS®: -

- 3) Dumont, O., Carmo, C., **Georges, E.**, Quoilin, S., & Lemort, V. (2016). *Economic assessment of energy storage for load shifting in Positive Energy Building*. Paper presented at Conference ECOS 2016.

<http://hdl.handle.net/2268/191568>

ORBi viewed: **75** (8 ULg) — SCOPUS®: -

7. Patents
